

ABSTRACT

Title of Dissertation: CAPILLARY PUMPED LOOP PERFORMANCE
INVESTIGATION THROUGH FLOW
VISUALIZATION

Kimberly Reneè Wrenn, Doctor of Philosophy, 2004

Dissertation directed by: Associate Professor Keith E. Herold
Department of Mechanical Engineering

Capillary pumped loops (CPLs) are two-phase thermal control devices which, like heat pipes, use surface tension forces to circulate a cooling fluid from an evaporator to a condenser. The pressure difference for fluid circulation is developed in the pores of a wick structure located in the evaporator. Unlike heat pipes, CPLs separate the liquid and vapor flows such that counterflow is eliminated. A key failure mode of a CPL is called deprime. This is where the liquid feed to the capillaries is interrupted, resulting in the loss of the meniscus from the pores of the wicking material. CPLs are used in both terrestrial and space cooling applications. Therefore performance in micro-gravity is of interest

to the satellite community, particularly the recognition of events that precede CPL deprime.

Visualization in an Experimental Water Capillary Pumped Loop (VIEW-CPL) was designed and built to investigate the operation of a CPL in a micro-gravity environment through the use of a capillary evaporator with a window for flow visualization. The experiment flew on the Middeck of the Space Shuttle Columbia in November 1996. VIEW-CPL was instrumented with a video camcorder and sensors for measuring the loop pressure and temperature at various locations. The data that was collected from the micro-gravity and ground tests provide significant insight into the physics of CPL operation.

Heat transfer models of the VIEW-CPL operating modes of pressure prime and start-up were developed and compared to test data. Video recordings of bubbles on the liquid side of the capillary evaporator were collected during both ground and micro-gravity testing. The movement of the bubbles corresponded with low frequency temperature fluctuations in the range of 0.003 to 0.01 Hz. An analysis is presented that explains the observed phenomena through pressure changes in the evaporator resulting from a partially dry wick. Understanding the source of the temperature oscillations is a necessary step for predicting the potential for evaporator deprime and impact on system performance.

CAPILLARY PUMPED LOOP PERFORMANCE INVESTIGATION
THROUGH FLOW VISUALIZATION

by

Kimberly Renee Wrenn

Dissertation submitted to the Faculty of the Graduate School of the
University of Maryland, College Park in partial fulfillment
of the requirements for the degree of
Doctor of Philosophy
2004

Advisory Committee:

Associate Professor Keith E. Herold, Chair
Professor Marino di Marzo
Professor Richard McCuen
Associate Professor Tien-Mo Shih
Assistant Professor Bao Yang

©Copyright by
Kimberly Renee Wrenn
2004

DEDICATION

To my grandmothers, Lorraine Worden and Cecelia Kolos, for their constant prayers and faithful support in all of my endeavors. You are wonderful role models from whom I have inherited my persevering nature.

ACKNOWLEDGEMENTS

This thesis would not have materialized without the support and guidance from the engineering community at the University of Maryland, the Thermal Branch at Goddard Space Flight Center, Swales Aerospace, and most importantly my family. I thank my devoted husband, Colin Wrenn, for supporting me from the beginning to the very end; for helping me with manufacturing drawings, flying to Houston with me on my first airplane trip and especially for not allowing me to give up. I thank my parents Gail and Bob Kolos for making me the person I am today and for continuously reminding me of how proud they are of my accomplishments. I thank my brother Chris Kolos for his support and solutions that pulled me out of some challenging moments. I am grateful to all of my family members for their prayers, especially Cecelia Kolos, Erskine and Lorraine Worden, and Mary Wrenn. A special thanks to Diane Kolos, Tom Kolos, and Linette Kolos for their contributions to the VIEW-CPL hardware.

I am extremely appreciative of my advisor, Dr. Keith Herold, whose support and guidance was vital from the proposal through the final edit of the thesis. I also extend my appreciation to Dr. Richard McCuen, for planting the grad school seed and for teaching me not to let opportunities pass by, but to grab them and make something wonderful happen. I am grateful to my mentor, Mr. David Wolf, for insight into two-phase systems and for selflessly giving of his time to listen and advise.

In addition to the corporate contribution of Swales Aerospace, I appreciate the individual efforts of Ed Kroliczek, Marc Kaylor, Heimo Gangl, Stuart Whitelock, and Vladimir Kriznik during the VIEW-CPL fabrication. Also from Swales Aerospace, I acknowledge Mike Morgan, Stan Kos, Pete Weinberger, and Paul Barcomb, whose support was crucial for completing the thesis and defense. From the Thermal Branch at NASA Goddard Space Flight Center I am grateful to Ted Swanson for supporting me from the time of my Master's work through VIEW-CPL, to Bob Meloy for electrical design support, and Jim Dye for assembling the VIEW-CPL electronic controls. I am thankful for the hard work of the STS-80 crew, especially Dr. Tamara Jernigan and Capt. Kent Rominger who operated VIEW-CPL in space. Also to the staff at NASA Johnson Space Flight Center who helped me compile the documentation to prepare VIEW-CPL for flight, including Anne Vaughan, Vanessa Ellerbe, Jacqueline Prewitt, Tim Heimann, Kathleen Kilpatrick, and Steven Stenzel. Finally, I thank Mr. Richard Kadunc and those from the IN-STEP program office at NASA Headquarters who saw the value in the VIEW-CPL experiment and guided me along the route from proposal through flight.

TABLE OF CONTENTS

List of Figures	viii
List of Tables	xvi
List of Nomenclature	xx
1.0 Introduction	1
1.1 Thesis Overview	1
1.2 CPL Technology	1
1.3 Research Motivation	5
1.4 Investigation Objectives	7
2.0 Background and Literature Review	9
2.1 CPL Description	9
2.1.1 Capillary evaporator	9
2.1.2 Condenser	18
2.1.3 Reservoir	19
2.2 CPL Functionality	24
2.2.1 Operating features	24
2.2.2 Typical testing modes	34
2.3 CPL Experiments and Applications	35
2.3.1 Flight experiments	37
2.3.2 Visualization experiments	39
2.3.3 Space applications	42
2.3.4 Enhancements	44
3.0 VIEW-CPL Design	45
3.1 Shuttle Interfaces	46
3.2 CPL Design	53
3.2.1 Evaporator design	57
3.2.2 Condenser and subcooler design	64
3.2.3 Micro-gravity reservoir	83
3.2.4 Transport lines	89
3.3 Electrical Components and Data Acquisition	94
3.3.1 Electronic control box and power distribution	95
3.3.2 Circuit protection	103
3.3.3 Data acquisition system	106
3.4 Johnson Space Center (JSC) Supplied Equipment ..	112
3.5 System Preparation Procedures	112

4.0 VIEW-CPL Test Plan and Analysis	117
4.1 Payload Commands (Astronaut Instructions)	118
4.2 Test Plan Objectives and Expected Observations During Testing	118
4.3 Analysis of Pressure Prime	126
4.4 Start-up Analyses	135
4.4.1 Sensible heating of the evaporator	136
4.4.2 Vapor line clearing	141
4.4.3 Cold-shock analysis	156
4.5 Steady-state Operation	158
4.5.1 Operating with a partially dry wick	159
4.5.2 Fluid pumping axially in the wick	168
4.6 Deprime and Bubble Life Cycle	170
4.6.1 Radial dry-out of the wick during deprime	172
4.6.2 Pressure drop change due to slowed circulation	174
4.6.3 Bubble life cycle	175
5.0 VIEW-CPL Test Results and Discussion	185
5.1 Pressure Prime Test Results	185
5.1.1 Indications of noncondensable gas	192
5.1.2 Data comparison to pressure prime model	195
5.1.3 Heat loss from the reservoir	200
5.2 Observations of VIEW-CPL Start-up	200
5.2.1 Sensible heating	203
5.2.2 Heat loss from the evaporator	214
5.2.3 Vapor line clearing observations	217
5.3 Steady-State Operations	223
5.4 Observations of Bubble Growth in the Evaporator Core	229
5.5 Comparison of Micro-gravity and Ground Results	235
6.0 Conclusions	237
6.1 General Observations	237
6.2 Micro-gravity Observations	238
6.3 Noncondensable Gas	239
6.4 Heat Transfer Effects	240
6.5 Bubble Oscillations	241
6.6 Water and Wick Contact Angle	242
7.0 Recommendation for Future Research	244
7.1 Enhanced design	244
7.1.1 Instrumentation	244
7.1.2 CPL enhancements	245
7.1.3 Control	246

7.2 Visualization in Loop Heat Pipes	247
Appendix A: Typical Testing Modes for CPLs	248
Appendix B: VIEW-CPL As-Built Materials	250
Appendix C: Electronics	256
Appendix D: Verification Documents	268
Appendix E: Uncertainty Analysis	279
E.1 Resolution from the PGSC Interface Unit (PIU)	279
E.2 Temperature measurements	280
E.3 Pressure measurements	281
E.4 Electrical measurements	283
E.5 Vapor volume measurements	284
E.6 NCG calculation	285
Appendix F: Obtaining Data from Video	286
F.1 Downloading video frames	286
F.2 Measuring bubbles	287
Appendix G: VIEW-CPL Temperature Measurements and Corrections	290
G.1 Temperature sensor circuits	290
G.2 Temperature sensor calibration and sensitivity	290
G.3 Resistor drift correction	292
G.4 Temperature correction routine	301
Appendix H: VIEW-CPL Data Acquisition Software	303
H.1 Pseudo-code	303
H.2 Subroutine definitions	305
H.3 QuickBasic code for VIEW-CPL data acquisition	307
H.4 VIEW-CPL data acquisition user's manual	333
Appendix I: Explanation of Voltage Drops in Data	339
Appendix J: Information about On-orbit Testing	342
References	349

LIST OF FIGURES

1.1	Generic schematic of a capillary pumped loop (CPL)	3
1.2	Generic schematic of a loop heat pipe (LHP)	3
1.3	Generic schematic of a heat pipe (HP)	3
1.4	Generic schematic of a loop heat pipe with a secondary wick as the thermal and hydraulic connection between the evaporator and reservoir	4
2.1	Schematic of a typical two-port capillary evaporator	15
2.2	Schematic of a three-port capillary evaporator, also known as a capillary starter pump	15
2.3	Pressure-enthalpy diagram for VIEW-CPL steady-state operating cycle at 15 W and evaporator temperature of 51.1°C. The lower plot is an exploded view of the line at 13 kPa in the top plot	30
2.4	Time line of CPL and LHP development, testing and applications	36
3.1	VIEW-CPL configuration during operations in the Space Shuttle Middeck	45
3.2	VIEW-CPL capillary pumped loop structure, shown without the protective shroud, payload control box and insulation that covers all tubing, the evaporator, and the reservoir	55
3.3	Rendering of the VIEW-CPL experiment with protective shroud, support brackets, and electronics box	56
3.4	VIEW-CPL capillary evaporator with Lexan window for flow visualization capabilities	58
3.5	Cross-section of conducting tube assembly used to increase the resistance to conduction from the evaporator block to the liquid feed line	61
3.6	VIEW-CPL copper-finned condenser with polyethylene insert	65

3.7	Schematic of VIEW-CPL air-cooled condenser with fans and duct	67
3.8	Fan performance and system curves for the VIEW-CPL air-cooled condenser. Volume flow rate reflects rate available from two fans	67
3.9	Geometrical characteristics of a square fin	72
3.10	Condensation film coefficient and condensing length as a function of net evaporator power (total power minus heat loss to ambient) for VIEW-CPL	76
3.11	Water temperature profile in the condenser for net evaporator power of 5, 25, and 75 W	77
3.12	Air-cooled subcooler attached to VIEW-CPL liquid line	81
3.13	Flow path of air used to cool the electronics box, reservoir, thermoelectric cooler heat sink, and the liquid-line subcooler	82
3.14	Two-phase, temperature controlled reservoir for VIEW-CPL with internal polyethylene wick for restricting vapor flow through the liquid feed line	84
3.15	Internal wick structure for the VIEW-CPL reservoir made from porous polyethylene with 20 μm pore radii	85
3.16	Reservoir temperature drop based on the percentage of the condenser that is filled with vapor during the VIEW-CPL start-up along with the energy required to restore the reservoir to its initial temperature (50°C). Perfect mixing is assumed between the reservoir fluid and the incoming liquid from the vapor line and condenser (25°C).	89
3.17	Predicted steady-state pressure drop components for VIEW-CPL	91
3.18	VIEW-CPL predicted pressure drop during start-up as a function of power contributing to evaporation. Capillary limit for water is calculated for a 0° contact angle. For contact angles greater than 0°, the capillary limit is calculated using Eq. 2.1	93

3.19	VIEW-CPL electrical layout with auxiliary equipment connections	95
3.20	Location of heaters, AD590 temperature sensors, and thermostats on the VIEW-CPL hardware	96
3.21	VIEW-CPL payload control box (PCB) switch layout	97
3.22	PGSC and PIU functional process	106
3.23	Voltage divider circuit for monitoring 28 V bus	111
3.24	VIEW-CPL manufacturing and verification processing flow diagram	114
3.25	Schematic of water charging station for VIEW-CPL	115
4.1	Control volumes for the pressure prime model (see Figure 1.1 for details on loop components)	127
4.2	Results of pressure prime model using VIEW-CPL inputs from Table 4.8 (assuming no noncondensable gas) . .	134
4.3	Predicted effect of overall conductance on the duration of the pressure prime	135
4.4	Prediction from pressure prime model with heat transfer coefficient modified for effect of noncondensable gas	136
4.5	Two-dimensional finite element grid for the VIEW-CPL transient conduction analysis	138
4.6	Normalized wick temperature predicted for the VIEW-CPL heater combinations. Temperature traces were selected from the warmest node at the wick/stainless steel interface (refer to Figure 4.5) for each given heater combination	139
4.7	Normalized evaporator temperatures predicted at node 30 (refer to Figure 4.5) for VIEW-CPL heater combinations	140
4.8	Control volumes for the pressure surge model (see Figure 1.1 for details on loop components)	142
4.9	Pressure surge prediction for 35 W on VIEW-CPL	

evaporator	150
4.10 Temperature prediction during pressure surge as the vapor / liquid interface moves from the VIEW-CPL evaporator to the vapor line. The vapor temperature decreases to within 0.1 K of the internal reservoir temperature after the oscillations are damped	151
4.11 Pressure surge prediction during the movement of the vapor / liquid interface from the VIEW-CPL evaporator grooves into the vapor line for 35 W heater power. Pressure decreases with the corresponding decrease in temperature of the vapor space as the vapor transfers heat to the wall of the vapor line	153
4.12 Predicted pressure surge results for VIEW-CPL geometry and available evaporator power combinations	155
4.13 Control volume for vapor flow through a dry portion of the VIEW-CPL wick	163
4.14 Temperature profile in the liquid control volume inside the wick core (refer to Figure 4.13)	164
4.15 Length of bubble resulting from a dry portion of the wick at powers ranging from 15 to 75 W and for condensation heat transfer coefficients of 500 and 3000 W/m ² -K	164
4.16 Comparison of approximated core temperature profile with the profile determined from integrating the energy balance over the length of the core	166
4.17 Axial transport of liquid water at 50°C in the VIEW-CPL wick as a function of contact angle	168
4.18 Schematic of heat transfer within the capillary evaporator	173
4.19 Two options for the positioning of the grooved polyethylene insert inside the condenser	176
4.20 Schematic of a pressure profile for VIEW-CPL normal operations	177
4.21 Proposed pressure profile due to the loss of meniscus in the capillary evaporator	177

4.22	Description of bubble life cycle and changing boundary conditions between the bubble and the adjacent liquid	179
4.23	Plot of liquid temperature and heat transfer rate at bubble interface inside the core of the evaporator	180
4.24	Prediction of evaporator temperature and bubble volume for VIEW-CPL operating at 30 W with a dry portion of wick. A bubble volume prediction is provided for a water and polyethylene contact angle of 0° and 89.3°	183
5.1	Example of pressure prime during flight testing of VIEW-CPL	186
5.2	Example of pressure prime of VIEW-CPL during ground testing of VIEW-CPL before flight	187
5.3	Example of pressure prime of VIEW-CPL during ground testing of VIEW-CPL after flight	188
5.4	Amount of noncondensable gas in VIEW-CPL system calculated from the partial pressure exerted by the gas	193
5.5	Predicted noncondensable gas bubble volume based on mass diffusion into a semi-infinite pool of water	195
5.6	Comparison of temperature predictions to test data for VIEW-CPL flight pressure prime PRIME-1	198
5.7	Results from a one-dimensional conduction analysis on the temperature lag from the reservoir heater location to temperature sensor	199
5.8	Example of start-up during flight testing of VIEW-CPL	204
5.9	Example of start-up during pre-flight testing of VIEW-CPL . .	205
5.10	Example of a start-up during post-flight testing of VIEW-CPL	206
5.11	Comparison of predicted and observed time for fluid in the VIEW-CPL evaporator to boil after heater power is turned on	207
5.12	Effect of noncondensable gas concentration on evaporator saturation temperature	210

5.13	Predicted normalized temperatures for the evaporator core and wick outer diameter at the measured time of observed start-up in the VIEW-CPL flight tests. Temperature differences called out on the plot correspond to the gradient between the outer diameter of the wick to the core at the time when either evaporation or boiling is observed in the evaporator core or vapor grooves	211
5.14	Comparison of predicted evaporator temperatures with VIEW-CPL flight data (temperature sensor T6) at the time of start-up	213
5.15	Comparison of predicted evaporator temperatures with VIEW-CPL data for pre-flight, flight, and post-flight start-up tests	214
5.16	Least squares fit to the flight data to determine heat loss ($UA = 0.54$ W/K) from the VIEW-CPL evaporator by the lumped capacitance analysis. Data from LOW-2 and Preship S40-1 were used to check the correlation. They were not included in the sample for least squares determination of the UA value	216
5.17	Plot of the time required to move the vapor front from the beginning (exiting evaporator) to the end of the vapor line (inlet of condenser) measured during VIEW-CPL flight and ground (pre-ship) tests. Note that the curve fits overlap for the flight and pre-ship data of the vapor front exiting the evaporator	218
5.18	Pressure surge analysis for VIEW-CPL compared to start-up data for flight test S35-1. Vapor volume required to displace all liquid from the vapor grooves is 4.95 cc and volume to displace all liquid from the vapor line is 29.11 cc	219
5.19	Comparison of predicted (open symbols) to measured (solid symbols) time required to move the vapor front from the beginning to the end of the vapor line during the VIEW-CPL flight tests. The curve fit to the predicted times is a dashed line while the curve fit to the actual data is a solid line	222
5.20	Example of VIEW-CPL steady operations during ground testing before flight	226

5.21	Example of VIEW-CPL operations with power changes during ground testing after flight	227
5.22	Fluctuation in core bubble volume and temperatures during VIEW-CPL flight test S35-1	230
5.23	Comparison of flight data from test S35-1 to the bubble volume and evaporator temperature predictions made using the theory of vapor back-flow through a dry portion of the evaporator. Matching the model to the test data was achieved by setting the contact angle between water and polyethylene at 89.3°	231
5.24	Example of a CPL deprime (at 20:06) after apparently steady-state operations for approximately 20 minutes. Test data is from ground testing of VIEW-CPL after flight	232
C.1	VIEW-CPL wiring diagram for electronics attached to the CPL	256
C.2	Payload control box (PCB) wiring diagram for VIEW-CPL . . .	258
C.3	On/off temperature control profile	263
C.4	Location of fuses within the VIEW-CPL fuse plug connector .	266
C.5	DB 25 connector and corresponding channels for VIEW-CPL PGSC Interface Unit (PIU)	267
D.1	UMCP-VER-001-VCPL: VIEW-CPL proof pressure test and leak check (3 pages)	268
D.2	UMCP-VER-003-VCPL: VIEW-CPL initial pressure prime . .	271
D.3	UMCP-VER-005-VCPL: VIEW-CPL thermal switch and reservoir temperature controller verification (5 pages) . .	272
D.4	UMCP-VER-006-VCPL: VIEW-CPL surface temperature measurement on Sept. 13, 1996	277
D.5	VIEW-CPL weight, dimensions, and center of gravity	278
F.1	Example of measuring bubbles from photographs downloaded from the VIEW-CPL experiment	289

G.1	AD590 temperature transducer circuit as used in the VIEW-CPL experiment	290
G.2	Steady VIEW-CPL resistance calculations from the reservoir AD590 panel meter and T8 temperature measurement	297
G.3	Pre-flight, flight, and post-flight curve fits to VIEW-CPL resistance data from the reservoir T8 AD590 circuit	299

LIST OF TABLES

2.1	Comparison of ammonia and water for CPL systems operating at 50 and 100°C	12
2.2	Slope of the vapor pressure curve calculated from Eq. 2.8 at T=20 and 50°C	17
3.1	VIEW-CPL and shuttle interfaces	47
3.2	VIEW-CPL acoustic measurement data	52
3.3	Hardware or designs previously used in experiments flown in the shuttle and ground based designs	53
3.4	Characteristic dimensions of components in the VIEW-CPL evaporator	59
3.5.	Parameters used to estimate the cool-down time for the uninsulated VIEW-CPL evaporator transferring heat via convection with ambient Middeck cabin air	64
3.6	Characteristic dimensions of components in the VIEW-CPL condenser	65
3.7	Loss coefficients for determining pressure drop for flow through the VIEW-CPL finned condenser system	69
3.8	External conductance calculations through VIEW-CPL condenser components on a per unit length basis	73
3.9	Subcooler fan operating conditions	83
3.10	Reservoir fluid inventory calculation	86
3.11	Transport line dimensions and associated fittings	90
3.12	Summary of dimensions from CPL components	93
3.13	Power distribution for VIEW-CPL with 30 VDC power supply	102
3.14	μMAC-1050 channel assignment	107

3.15	Manufacturer's accuracy data for the pressure transducers .	110
3.16	Heater power measurements using the PIU compared to expected values	111
3.17	Equipment supplied by NASA Johnson Space Center for VIEW-CPL use on STS-80	113
4.1	Procedures for preparing VIEW-CPL testing	119
4.2	Procedures for concluding VIEW-CPL testing	119
4.3	VIEW-CPL test objectives and procedures	120
4.4	Description of pressure prime procedures used on the VIEW-CPL experiment	123
4.5	Segments of the start-up period in VIEW-CPL testing	125
4.6	Effective flow resistance in VIEW-CPL components	129
4.7	Governing equations for the pressure prime control volumes	132
4.8	Inputs to the pressure prime model representing VIEW-CPL	133
4.9	Conservation equations of energy, momentum, and mass for the pressure surge control volumes	145
4.10	Frictional (β) and inertial coefficients (α) from Eq. 4.25 for liquid flow in VIEW-CPL geometry	147
4.11	Initial conditions and volumetric summary for VIEW-CPL pressure surge calculation.	149
4.12	Conservation equations of energy, momentum, and mass for the vapor leak through the wick	161
5.1	Measured and predicted duration of VIEW-CPL pressure prime times	197
5.2	Heat loss from the reservoir in the shuttle cabin during flight testing	200

B.1	VIEW-CPL Inorganic Materials List	250
B.2	VIEW-CPL Polymeric Materials List	253
C.1	Brand names and sources for electronic components	260
C.2	VIEW-CPL heater specifications for evaporator and reservoir	262
C.3	Reservoir temperature controller specifications	262
C.4	Components attached to power supplies and corresponding power consumption	264
C.5	Fuse sizing for electronics in VIEW-CPL	265
E.1	Measurement uncertainties for data from the VIEW-CPL experiment	280
E.2	Summary of uncertainty in heater power measurements . . .	284
F.1	Example bubble measurements	289
G.1	Slope calibration factors for the AD590 temperature sensors used in the VIEW-CPL experiment	292
G.2.	VIEW-CPL T8 resistance curve-fit coefficients and goodness-of-fit statistics	299
G.3	Comparison of resistance values from the VIEW-CPL AD590 circuits	302
I.1	Voltage drop associated with powered components during shuttle operations	340
I.2	Measured voltage drop during ground operations	340
J.1	Summary of on-orbit testing of VIEW-CPL on STS-80	342
J.2	Summary of evaporator core at the beginning of on-orbit tests	343

J.3	Initial state of the evaporator prior to start-up for on-orbit testing	345
J.4	Location of initial bubble growth for on-orbit testing (continued on next page)	346
J.5	Initial start-up period for on-orbit testing.	348

LIST OF NOMENCLATURE

ACPL	Advanced Capillary Pumped Loop
AD	Analog Device
CAPL	Capillary Pumped Loop Flight Experiment (-1, -2, -3)
CCPL	Cryogenic Capillary Pumped Loop
CPL	Capillary Pumped Loop; a two-phase heat transport system
CSR	Customer Support Room
CV	Control Volume
EHD	Electrohydrodynamic
EMC	Electromagnetic compatibility
EMI	Electromagnetic interference
ESA	European Space Agency
GAS can	Get Away Special Canister; canisters available for testing in the cargo bay of the Space Shuttle
GSFC	NASA Goddard Space Flight Center, Greenbelt, Maryland
HP	Heat Pipe
HPP	Heat Pipe Performance Experiment
HPSTM	High Power Spacecraft Thermal Management
HST	Hubble Space Telescope
IDD	Interface Definition Document
IN-STEP	In-Space Technology Experiments Program
JSC	NASA Johnson Space Center, Houston, Texas
KSC	NASA Kennedy Space Center, Florida
LED	Light Emitting Diode
LHP	Loop Heat Pipe
MH	Main Heaters
MUP	Middeck Utility Panel
NA	Not Available
NASA	National Aeronautics and Space Administration

NCG	Noncondensable gas
NICMOS	Near Infrared Camera and Multi-Object Spectrometer
NTU	Number of Transfer Units
OD	Outer Diameter
OMS	Orbiter Maneuver System
OSMQ	Office of Safety and Mission Quality
PCB	Payload Control Box
PGSC	Payload and General Support Computer
PIU	PGSC Interface Unit
PN	Part Number
PS	Power Supply
PSDP	Payload Safety Data Packages
RCS	Reaction Control System
RH	Reservoir Heater
SSP	Space Shuttle Program
STS	Space Transportation System (Space Shuttle)
SVS	Snappy Video Snapshot
TEC	Thermoelectric cooler
UHMW	Ultra-High Molecular Weight
UMCP	University of Maryland at College Park
VDC	Volts Direct Current
VEG	Vaporization enhancement groove
VIEW-CPL	Visualization in an Experimental Water - Capillary Pumped Loop
VIU	Video Interface Unit
WSTF	White Sands Test Facility

Variables

A	Area (m^2)
A/R	Area ratio (dimensionless)
Bi	Biot number (dimensionless)
c	Specific heat (J/kg-K), flow resistance ($1/\text{m-s}$)
C_D	Drag Coefficient (dimensionless)
C_f	Friction Coefficient (dimensionless)
d	Diameter (m)
dB, dBA	Decibel, decibel from A-weighted filtered frequency response
D_h	Hydraulic diameter (m)
dz	Axial differential length (m)
E	Energy (J)
f	Moody friction factor (dimensionless)
$F_{x,p}$	Pressure force (N)
G	Mass flux ($\text{kg/m}^2\text{-s}$)
g	Gravitational acceleration (m/s^2)
h	Heat transfer coefficient ($\text{W/m}^2\text{-K}$), enthalpy (kJ/kg)
H	Ratio of the convective heat transfer coefficient and the thermal conductivity ($1/\text{m}$)
IO	Input / output signal
j	Correlation coefficient for Nusselt number in finned tube banks
J_0	Bessel function of the first kind of order 0
k	Thermal conductivity (W/m-K)
K	Loss coefficient for pressure drop (dimensionless)
k_p	Permeability (m^2)
L	Length (m)
L_c	Corrected fin length for non-adiabatic fin tip (m)
m	Mass (kg)
\dot{m}	Mass flow rate (kg/s)

Nu	Nusselt number (dimensionless)
P	Pressure (saturation or local) (kPa)
Pe	Peclet number (dimensionless)
Po	Poiseuille number (dimensionless)
Pr	Prandtl number (dimensionless)
Q	Heat transfer rate (W)
r	Radius (m)
R	Ideal gas constant (8.314 kJ/kmol-K), resistance (ohms)
Re	Reynolds number (dimensionless)
r_p	Radius of pore (m)
s	Space between fins (m)
St	Stanton number (dimensionless)
T	Temperature (saturation or local) ($^{\circ}\text{C}$ or K)
t	Time (s), thickness (m)
t^*	Dimensionless time
u	Velocity (m/s)
U	Overall heat transfer coefficient ($\text{W}/\text{m}^2\text{-K}$)
UA _{pL}	Conductance per unit length ($\text{W}/\text{m-K}$)
v	Specific volume (m^3/kg), velocity (m/s)
V	Volume (m^3), voltage (V), velocity (m/s)
w	Width (e.g. heat exchanger depth) (m)
W	Work rate (W)
x	Quality (dimensionless), Axial distance (m)
y	Distance from tube wall (m)
z	Axial distance (m)

Greek letters

α	Thermal diffusivity coefficient (m^2/s), geometric coefficient for inertial terms in momentum balance ($1/\text{m}$), void fraction (dimensionless)
β	Geometric coefficient for frictional terms in momentum balance ($1/\text{m}^4$)
δ	Liquid thickness (m)
Δ	Denotes difference in variable (i.e., ΔP is pressure difference)
ε	Porosity, volume void fraction
η	Efficiency (e.g., η_f is fin efficiency)
θ	Contact angle ($^\circ$)
λ	Latent heat of vaporization (kJ/kg)
μ	Dynamic viscosity ($\text{Pa}\cdot\text{s}$)
ν	Specific volume (m^3/kg)
ρ	Density (kg/m^3)
σ	Surface tension (N/m^2)
τ	Shear stress (Pa)
Y	Bubble growth rate (m^2/s)
ν	Kinematic viscosity (m^2/s)
ϕ^2	Two-phase multiplier (dimensionless)
X_{tt}	Martinelli Nelson parameter (dimensionless)

Subscripts

∞	Bulk temperature (e.g. ambient air temperature T_∞)
1, 2, 3	Control volume designators
b	Bubble
cap	Capillary
c, cond	Pertaining to the condenser
dec	Deceleration

e, evap	Effective, Pertaining to the evaporator
ext	External
f	Pertaining to the fin
fin	Pertaining to the fin
fg	Denotes difference between liquid and vapor values
fr	Frictional
i	Interface, inner (e.g., inner radius)
l, L	Liquid
liq	Pertaining to the liquid transport line
lo	Liquid only
m	Measured
max	Maximum
min	Minimum
ms	Measured from supply (e.g., voltage)
o	Outer (e.g., outer radius), overall (e.g. η_o overall efficiency), initial (e.g. initial temperature T_o)
p	Pertaining to a pore
s	Solid
sat	Saturation
SH	Superheat
ss	Stainless steel
sys	Pertaining to CPL system
t	Total (e.g., A_t is total surface area of a fin)
v	Vapor
vap	Pertaining to vapor transport line
w, wall	Pertaining to the wall

Superscripts

–	Average
---	---------

1.0 INTRODUCTION

1.1 Thesis Overview

VIEW-CPL (Visualization in an Experimental Water - Capillary Pumped Loop) refers to a space shuttle flight experiment based on a capillary pumped loop (CPL). It was flown on space shuttle Columbia during the STS-80 mission from November 19 through December 7, 1996. The goal of VIEW-CPL was to develop an understanding of the physics of the fluid flow inside a CPL evaporator in a micro-gravity environment. VIEW-CPL had a window in the evaporator that allowed observation and video recording of the life cycle of bubbles. The window allowed confirmation of theories on the system-level impact of bubbles on the liquid side of the CPL. Of particular interest was the ability of the evaporator to continue operating with vapor in the liquid core. The VIEW-CPL results provide insight into the physics that allowed operation with a bubble in the evaporator.

1.2 CPL Technology

CPL technology is currently under development as an option for transporting thermal energy within a spacecraft (i.e., thermal management). A CPL system is a two-phase flow loop that uses heat input and surface tension forces to circulate a cooling fluid in a closed loop. In place of a mechanical pump, the pressure difference required to circulate the fluid comes from a capillary pressure rise across the meniscus separating the vapor and liquid phases in a fine pore wick located in the evaporator. Figure 1.1 is a generic schematic of a

CPL system. The loop heat pipe (LHP) and the heat pipe (HP) are related to the CPL; they are shown in Figures 1.2 and 1.3, respectively.

In operation, the working fluid inside the CPL, LHP, or HP evaporator absorbs energy from a source, such as an electronics assembly, and is vaporized. The vapor flows to the condenser, where the heat is rejected, and liquid flows back to the evaporator to complete the loop. In CPL and LHP systems, liquid and vapor transport lines connect the evaporator and condenser and provide separate paths for the working fluid to circulate through the system. Both CPL and LHP systems are similar to heat pipes in that all three use capillary forces to move the working fluid and all are passive energy transport devices. A primary difference is that the heat pipe has counter flowing vapor and liquid. The separation of the liquid and vapor transport lines is a key advantage of a CPL (and LHP) over a heat pipe since the separation eliminates liquid entrainment which limits heat pipe capacity.

Thus, the major advantage of both CPL and LHP systems over a heat pipe is that they can transport energy over a longer distance for the same system mass. Operating at the same temperature and with the same fluid a CPL can transport 1.13 kW over 5 m for a heat transport capability of 5.7 kW-m with a mass of 2.5 kg [Wrenn, 2002a and 2002b] while a system of heat pipes of the same mass can transport 1.13 kW for only 2.8 m for a heat transport capability of only 3.2 kW-m [Swales, 2004]. The transport capability advantage is primarily

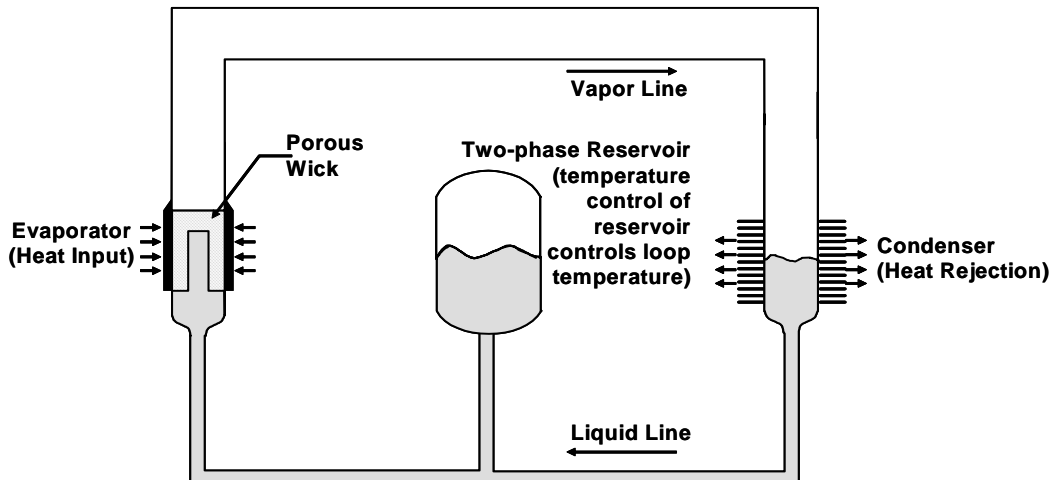


Figure 1.1 Generic schematic of a capillary pumped loop (CPL).

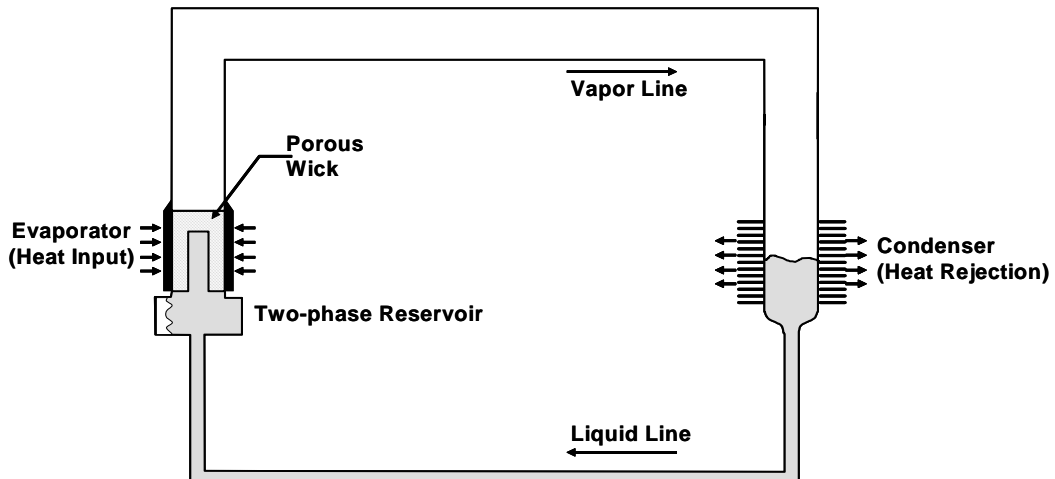


Figure 1.2 Generic schematic of a loop heat pipe (LHP).

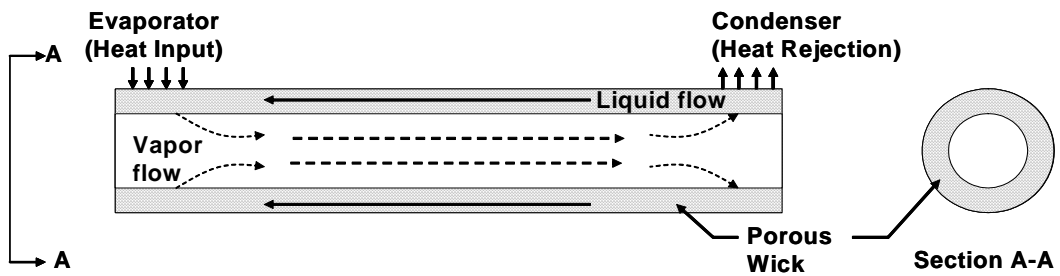


Figure 1.3 Generic schematic of a heat pipe (HP).

due to increased pumping capability of the small pored wick along with the reduced pressure drop due to the separation of the vapor and liquid phases. The latter avoids entrainment and counter-flow viscous losses.

The difference between CPL and LHP systems is the combined thermal/hydraulic connection between the evaporator and the reservoir. In the CPL, the reservoir is physically separated from the evaporator. In the LHP, the reservoir is connected to the evaporator, either by co-location (as in Figure 1.2) or by a secondary wick that provides the thermal and hydraulic link between the components, as shown schematically in Figure 1.4. The disadvantage associated with the co-location of the reservoir and evaporator in the LHP is packaging on the spacecraft. In designs that do not use co-location, the reservoir

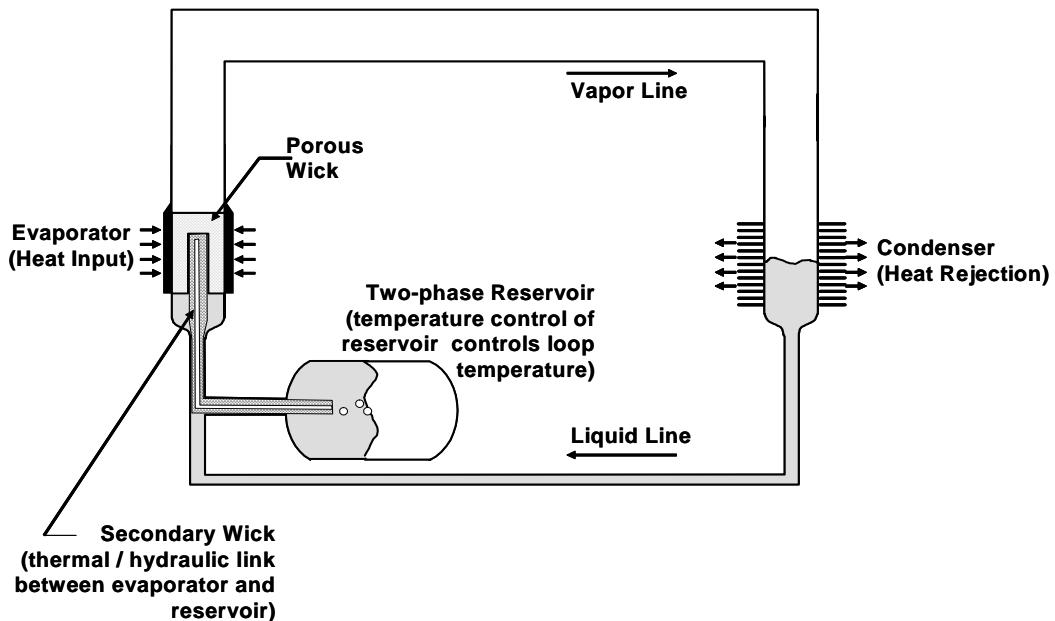


Figure 1.4 Generic schematic of a loop heat pipe with a secondary wick as the thermal and hydraulic connection between the evaporator and reservoir.

can be placed away from the heat source in areas of the spacecraft that have more volume available.

The LHP's link between the reservoir and evaporator has advantages. One being immediate start-up by ensuring that the wick is always wetted with fluid (i.e., self-priming), and another being control of bubbles inside the wick by moving them to the reservoir where they will not affect liquid flow to the wick. Both the CPL and LHP need to manage bubbles inside the evaporator core. The choice between using a CPL and a LHP is dependent upon the cooling application. For the VIEW-CPL experiment, the CPL was chosen because it facilitated the visualization of the fluid flow inside the evaporator during both normal operation and during events that can lead to deprime.

Deprime is a CPL or LHP circulation failure mode where a gas or vapor bubble appears on the suction side of the evaporator preventing normal capillary pumping operation. An evaporator is said to deprime when the liquid feed to the capillaries is interrupted by such a gas or vapor bubble, resulting in the loss of the meniscus from the pores of the wick material. Depriming stops the transport of energy. Since other systems depend on the CPL to transport energy, a deprime often impacts other subsystems.

1.3 Research Motivation

CPL technology was pioneered at NASA Lewis Research Center with the development of a water-based CPL by Stenger [1966]. Since then, CPL technology has undergone extensive development at NASA Goddard Space

Flight Center (GSFC) and by various aerospace contractors [Ku, 1993]. Several flight experiments and numerous engineering models have been tested to demonstrate the capability of CPL systems for space applications. Yet, the physics of CPL operation is not completely understood and additional testing of CPL components is required to achieve the expectations of CPL technology for routine spacecraft thermal management applications and to continue development of advanced CPL technology.

The need for flow visualization studies on CPL components arises from the desire to completely understand CPL physics. Physical observation of processes in the evaporator provides data for verification of theories on CPL operation. Visualization in the evaporator is key to studying both start-up phenomena and deprime phenomena. Effective CPL start-ups are necessary for successful operation. The quantity (if any) of vapor introduced into the liquid core during start-up and the effects on subsequent operations are both of interest. The causes of deprime and the ability of the evaporator to withstand vapor bubbles before deprime occurs is also of particular interest, especially for investigating CPL robustness. An important goal in studying start-up and deprime phenomena is the ability to predict and consequently prevent failure of CPL systems.

To support application, CPL technology must reach a high level of confidence through extensive testing and the complete understanding of CPL physics. Flow visualization experiments have been used to examine fluid flow phenomena during CPL ground operation (as discussed in Chapter 2).

Experiments for observing the capillary evaporator in a CPL have been designed and tested at NASA/GSFC and at the University of Maryland (among others) with very informative results. However, without micro-gravity testing, these results cannot be automatically applied to spacecraft designs. Comprehensive testing of CPL systems in micro-gravity is necessary to enable a complete description of the effectiveness of CPL technology for use in satellite thermal management.

1.4 Investigation Objectives

The goal of this study is to observe and to characterize CPL systems in typical operation. This includes a detailed description of CPL operational modes and a focus on defining CPL operational characteristics that lead to deprime. A typical sequence of CPL operation modes included in this study is as follows: (1) pressure priming, (2) start-up, (3) standard operation, (4) deprime, and (5) re-priming.

The ability to prevent deprime can be achieved by recognizing events that cause the liquid-vapor meniscus in the evaporator, which creates the pressure rise for circulating the fluid, to leave the porous wick material. “Re-priming” techniques are also investigated to allow CPL operation to quickly resume after a deprime event has occurred. The results from both 1-g and micro-gravity testing of a water CPL with flow visualization capability in the evaporator are used in determining the sequence of events leading to a CPL deprime.

Visualization In an Experimental Water Capillary Pumped Loop (VIEW-CPL) was designed to investigate the operation of a CPL in micro-gravity and 1-g

environments through the use of a capillary evaporator with a window for flow visualization. VIEW-CPL flew in the Space Shuttle Middeck as part of NASA's In-Space Technology Experiments Program (IN-STEP). The goal of the flight experiment was to develop a complete understanding of CPL physics in a micro-gravity environment through flow visualization of a CPL evaporator.

The VIEW-CPL experiment provided recorded data on the life cycle of bubbles on the liquid side of an operating CPL system and observations of the ability of the capillary evaporator to continue pumping with vapor in the liquid core. This was accomplished by recording key system variables during operation including temperatures, pressures, and power levels and by making a video recording through the transparent evaporator window. The video images are interpreted together with the operating data to fully understand the bubble dynamics.

This research advances the state-of-the-art of CPL technology in the following ways:

- 1) VIEW-CPL is the first test of a water CPL in space.
- 2) VIEW-CPL provided the first visualization of a CPL evaporator during operation in micro-gravity.
- 3) The results increase understanding of the consequences of a vapor bubble in the liquid core of the evaporator during CPL operation.

2.0 BACKGROUND AND LITERATURE REVIEW

2.1 CPL Description

A typical CPL system consists of a capillary evaporator, a condenser, a reservoir, liquid transport lines, and vapor transport lines, as previously shown in Figure 1.1. The evaporator is the heart of a CPL system; it provides the pumping action necessary to move the working fluid. Heat applied to the evaporator causes the liquid to evaporate from a meniscus between the liquid and vapor phases in the evaporator wick. The vapor transport lines carry the vapor to a condenser section where the latent heat is removed and the fluid is condensed. For a typical spacecraft application, a condenser removes the heat by radiation to space. The liquid then flows back to the evaporator and through the wick to start the process again.

2.1.1 Capillary evaporator

Evaporator pump. The system pumping head is provided by capillary action in a porous wick material that extends the length of the evaporator housing. The effective radii of the wick pores are on the order of 1 to 10 μm , and thus, the surface tension in the meniscus provides a pressure increase from liquid to vapor (across the meniscus) and prevents the vapor from flowing back into the liquid core of the evaporator. The points of lowest and highest absolute pressure are located on the liquid and vapor sides of the meniscus, respectively. The magnitude of the pressure rise is related to the radius of the pores, r_p , the contact

angle between the fluid and the solid, θ , and the surface tension of the fluid, σ by [Carey, 1992]

$$\Delta P_{cap} = P_{vap} - P_{liq} = \frac{2\sigma \cos\theta}{r_p} \quad (2.1)$$

For a particular working fluid, note that the maximum pressure rise is achieved when the wick is perfectly wetted ($\theta=0^\circ$) and the meniscus has the same radius of curvature as the wick pore size.

The actual pressure rise across the meniscus, ΔP_{cap} , adjusts to balance the system pressure drop, ΔP_{sys} . The system pressure drop, ΔP_{sys} , includes the capillary pressure developed in the condenser, $\Delta P_{cond-cap}$, plus the viscous pressure losses in the evaporator (wick and vapor grooves), condenser and transport lines [Stenger, 1966].

$$\Delta P_{cap} = \Delta P_{sys} = \Delta P_{cond-cap} + \Delta P_{wick} + \Delta P_{grooves} + \Delta P_{cond} + \Delta P_{liq} + \Delta P_{vap} \quad (2.2)$$

In order for the working fluid to circulate, the system pressure losses must be lower than the maximum capillary pressure rise created by the capillary action (see Eq. 2.1).

Working fluid characteristics. One of the key factors in designing a successful CPL system is a good working fluid choice. The ideal CPL working fluid has the following properties: high latent heat, high surface tension, moderate vapor pressure, and low vapor viscosity [Stenger, 1966]. The high latent heat allows for the transfer of large amounts of energy while maintaining

minimal flow rates. Referring to Equation 2.1, it is seen that a high surface tension provides a greater pressure difference to circulate the fluid through the loop. For example, an ammonia system with a 10 μm wick can create a pressure rise up to 0.5 psi. Due to the higher surface tension of water, CPL systems using water as the working fluid can achieve a pressure rise up to 1.5 psi using the same wick. The relatively low capillary pressure rise from the wick leads directly to the need to keep frictional losses to a minimum. The low vapor viscosity serves to reduce the viscous pressure drop in the CPL system. The moderate vapor pressure provides a balance between high vapor density which reduces vapor velocity and the wall thickness of the pressure vessel.

Ammonia is a good fluid for CPLs operating at 50°C (typical of spacecraft cooling systems) because it has all of the properties mentioned above. However, ammonia is toxic and has a pungent odor. Water is also a good fluid for such systems, provided that the system is protected from freezing. For a quantitative comparison between the two fluids, an example calculation was performed where the diameter of the transport lines and condenser were sized to match the capillary pressure rise available from a 10 μm wick. Table 2.1 summarizes the results for ammonia and water at both 50 and 100°C for a 1 kW system with 10 m transport lines that sees an equivalent sink of 200 K. At 50°C, ammonia results in a lighter system with less volume, while water is better at 100°C. The evaporator pressure drop was neglected in the system sizing.

Table 2.1 Comparison of ammonia and water for CPL systems operating at 50 and 100°C.

Fluid	Ammonia	Water	Ammonia	Water
Saturation Temperature [°C]	50	50	100	100
Capillary Pressure Rise [kPa]	3.20	13.59	1.16	11.78
Condenser Pressure Drop [kPa]	-0.39	-1.74	-0.29	-0.30
Transport Line Pressure Drop [kPa]	-2.80	-2.37	-0.87	-11.48
System Pressure Drop [kPa]	-3.20	-4.11	-1.16	-11.78
Transport Line Volume [cc]	93	180	151	87
		92% larger	73% larger	
Transport Line Mass [kg]	1.71	2.17	2.48	1.61
		27% heavier	55% heavier	

Wick characteristics. The ideal wick material has the following properties:

(1) small pores, (2) high permeability and porosity, (3) low thermal conductivity, (4) high melting and deformation temperatures, and (5) chemical compatibility with the working fluid [Ku, 1997]. The wick materials used in CPL evaporators contain small pores with an effective pore radius, r_p , typically in the range of 2 to 20 μm . A smaller pore radius provides a greater capillary pumping pressure, but also increases the pressure drop as the liquid flows through the wick due to a decrease in the wick permeability, k_p . Permeability is a measure of flow resistance in the wick material and is defined by the Darcy law approximation of viscous effects [Arpaci and Larsen, 1984]

$$\frac{dP}{dr} = -\frac{\mu_l}{k_p} V_l \quad (2.3)$$

where V_l is the superficial velocity and the flow is assumed to be one-dimensional radial flow through the annular wick. Upon integration, the viscous pressure drop through the wick is

$$\Delta P = -\frac{\mu_l}{k_p} \ln\left(\frac{r_o}{r_i}\right) \frac{\dot{m}}{\rho_l 2\pi L} \quad (2.4)$$

Thus, a low permeability (typical of small pore wicks) increases the pressure drop through the wick. Porosity, ϵ , is the ratio of void volume to the total volume of a wick structure. Assuming that the porous material is a random array of particles, McKetta and Cunningham [1985] reason that a tortuosity factor can be approximated by $1 / \epsilon$. They then use the Hagen-Poiseuille law to develop a relationship for permeability to average pore radius and porosity

$$k_p = \frac{(\bar{r}_p \epsilon)^2}{8} \quad (2.5)$$

Therefore, as pore diameters decrease the porosity must be increased to maintain comparable permeability. Note that Equation 2.5 uses the average pore radius which is smaller than the effective pore radius, a measure of the largest pore in the wick structure which is defined on the next page.

Other important properties include thermal conductivity, melting and deformation temperatures, and chemical compatibility. Low thermal conductivity is desirable for CPL wicks because it minimizes the heat transfer to the liquid core. High melting point and deformation temperatures allow welding of CPL components (i.e., CPL system assembly) without damaging the wick. Finally, chemical compatibility with working fluids is essential to prevent the formation of non-condensable gas and to maintain the wick structure.

The CPL wicks considered in this study were made from ultra high molecular weight (UHMW) porous polyethylene. The porous polyethylene is formed from a sintering process that fuses polyethylene particles under controlled thermal conditions [Porex, 1989]. The effective pore radius in CPL wick material is typically measured using the bubble point method [McKetta and Cunningham, 1985] as the minimum pressure required to push a gas bubble through a wetted wick (with contact angle $\theta = 0^\circ$) according to

$$r_p = \frac{2\sigma}{\Delta P} \quad (2.6)$$

The effective pore radius for the UHMW porous polyethylene wick that was used in the VIEW-CPL experiment was $13.7 \mu\text{m}$, with a porosity (ϵ) of 50% and a permeability of $6.2 \times 10^{-13} \text{ m}^2$ [Nguyen, 1996]. An average pore size of $4.5 \mu\text{m}$ is implied from Eq. 2.5. The contact angle between water and polyethylene for the wicks used in VIEW-CPL is unknown because the wicks were bubble-point tested in alcohol which has a 0° contact angle with polyethylene. Since water does not readily wet plastics, the contact angle is expected to be larger than 0° but less than 90° based on previous experience of operating a water CPL with the same type of wick material [Kolos et al., 1996]. The thermal conductivity is calculated as 0.49 W/m-K , based on the parallel conductance of liquid water, $k_l = 0.60 \text{ W/m-K}$ [Incropera and DeWitt, 1990], and solid polyethylene, $k_s = 0.38 \text{ W/m-K}$ [Callister, 1991]

$$k_{wick} = k_l \epsilon + k_s (1 - \epsilon) \quad (2.7)$$

Polyethylene has a melting point of 120°C, which makes it difficult to weld components containing polyethylene wick materials.

Evaporator design. A typical two-port capillary evaporator is shown in Figure 2.1. Subcooled liquid enters the evaporator and flows through the core and into the wick. The liquid must be subcooled in order to prevent vapor generation in the evaporator core. Heat applied to the evaporator housing is transferred to the working fluid in the wick causing vaporization. Vapor grooves channel the vapor to the exit of the evaporator.

A three-port evaporator [Yun et al., 1996], also known as a capillary starter pump, is shown in Figure 2.2. In this design, the evaporator has three ports: (1)

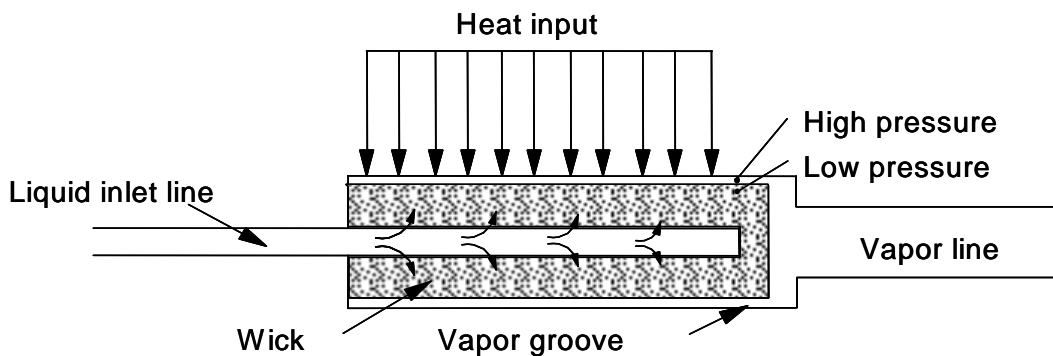


Figure 2.1 Schematic of a typical two-port capillary evaporator.

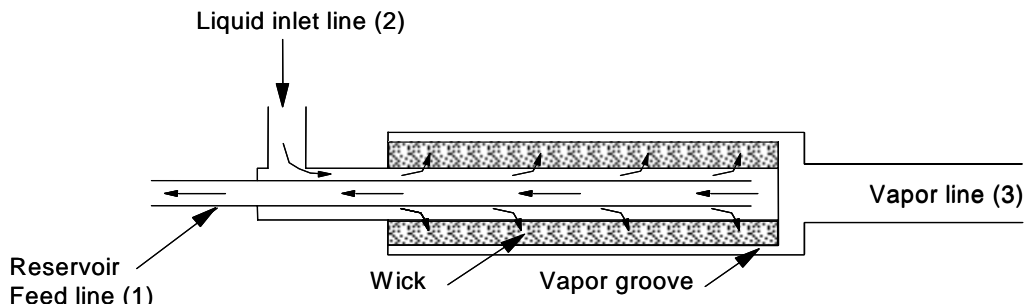


Figure 2.2 Schematic of a three-port evaporator, also known as a capillary starter pump.

a connection to the reservoir, (2) a liquid line port, and (3) a vapor port. The reservoir connection is a small diameter tube, called a bayonet tube, that is inserted inside the core of the wick. The liquid inlet line allows liquid to flow around the bayonet tube into the evaporator core. The vapor port is at the exit of the vapor grooves in the same fashion as the two-port evaporator. The benefit of the three port design is that during start-up cool liquid en route to the reservoir is forced through the core of the evaporator; the cool liquid can collapse any vapor bubbles that may be present in the liquid core of the evaporator. Start-up issues are discussed in detail in Section 4.4.

Subcooling requirements. It has long been recognized that subcooling the liquid entering the evaporator is important to prevent deprime [Schweickart et al., 1987]. Without sufficient subcooling, the liquid can evaporate before reaching the evaporator wick and subsequently block the liquid supply to the evaporator. By convention, the amount of liquid subcooling is defined as the temperature difference between the evaporator inlet and the saturated vapor exiting the evaporator. Since pressure rises across the meniscus, the saturation temperature of liquid in the evaporator core is lower than the saturation temperature of the vapor exiting the evaporator. The importance of the meniscus pressure rise in interpreting the subcooling is a function of the slope of the vapor pressure curve which can be calculated from the Claypreon equation [Moran and Shapiro, 1988]

$$\left(\frac{dP}{dT} \right)_{sat} = \frac{\lambda}{T_{sat} v_{fg}} \quad (2.8)$$

The required amount of subcooling entering the wick is equal to the pressure rise across the meniscus times the inverse of the vapor pressure curve. For ammonia, where the slope of the vapor pressure curve at 20°C is relatively high, a 500 Pa difference in saturation pressure results in a 0.02 K difference across the meniscus. This difference is small compared to the 2.87 K temperature difference for 500 Pa pressure difference in a water system which has a lower slope. These properties are summarized in Table 2.2.

Table 2.2 Slope of the vapor pressure curve calculated from Eq. 2.8 at T = 20 and 50°C.

	v_{fg} (m ³ /kg)	λ (J/g)	dP/dT (Pa/K)
T = 20°C			
Ammonia	0.1475	1186	27440
Water	57.78	2453	144.8
T = 50°C			
Ammonia	0.06160	1051	52780
Water	12.04	2382	612.4

When the CPL is transporting energy, the temperature of the liquid returning to the CPL evaporator must be below the saturation temperature of the evaporator vapor by a minimum temperature difference associated with the pressure drop specified in Eq. 2.2 or the liquid may flash in the evaporator core leaving the CPL susceptible to deprime. Heat leaks from the evaporator to the liquid line compound the situation by increasing the liquid line temperature. The effect of heat leaks are more significant when the evaporator is exposed to a

small heat load. The small flow rate resulting from the low power allows axial conduction from the higher temperature liquid in the evaporator core to the fluid in the liquid inlet. The Peclet number (Pe) provides a measure of the relative importance of energy transfer due to bulk motion of the fluid and axial conduction; the rule of thumb is that axial conduction can be neglected for situations where Pe is above 100 [Kays and Crawford, 1980]. For a heat load of 15 W, the VIEW-CPL liquid line Peclet number is 11, indicating conduction from the evaporator may be significant. Under such low power conditions, the subcooling must compensate to allow the CPL to operate.

Non-condensable gas and vapor in the evaporator. Non-condensable gas (NCG) and/or vapor bubbles located in the evaporator core can cause the CPL to deprime if the bubbles grow and block the flow of liquid to the evaporator wick. An experimental study by Antoniuk and Pohner [1994] demonstrated that the lifetime of vapor bubbles, injected into an evaporator core containing subcooled liquid with dissolved NCG, was longer than the lifetime of vapor injected into a gas-free system. One conclusion from their study was that bubbles formed from vapor back-flow through the wick (into the liquid core with dissolved gases) would be enriched in NCG by diffusion from the liquid. These bubbles would collapse at a much slower rate as compared to pure vapor bubbles, due to gas diffusing back into the liquid.

2.1.2 Condenser

For a spacecraft, a condenser rejects heat by radiating to space. Two

typical condenser designs used in spacecraft are heat pipe heat exchangers and direct condensation radiators. In the heat pipe heat exchanger, the vapor from the CPL can flow in smooth walled tubes or through the grooves of an integral heat pipe extrusion [Chalmers et al., 1986; Butler and Hoang, 1991]. Heat pipes move the latent heat from the condenser section to the radiator. With the direct condensation radiator, the vapor flows through smooth walled tubing that is mounted directly to the facesheet of a radiator. Grooved tubing can increase the heat transfer area and enhance heat transfer [Braun, 1990]. Both types of condensers reject heat by radiating to space.

The condenser is sized to ensure that, while it is in its hottest environment, it can condense all of the vapor flowing from the highest heat load applied to the evaporator and still provide sufficient subcooling to counter balance both parasitic heat gains and evaporator inlet subcooling requirements.

Since VIEW-CPL operates in a 1 atm environment the heat is rejected through forced convection instead of radiation. The condenser is a smooth walled tube separated into four internal segments using an insert. Fins are attached to the outside of the tube to increase surface area and allow the condenser to be packaged in a smaller volume. Section 3.2.2 contains details on the VIEW-CPL condenser design.

2.1.3 Reservoir

The role of the reservoir in a CPL system is to control the evaporator temperature (i.e. to control the heat rejection temperature). The user controls

the temperature of the reservoir by controlling the power to the reservoir heater. Since the reservoir contains both vapor and liquid, control of the temperature also controls the pressure. The reservoir controls the loop pressure by supplying or accepting liquid. This, in turn, controls the evaporator temperature through the working fluid properties. The reservoir feed line connects the reservoir to the liquid line of the CPL system. Distribution of the liquid between the reservoir and CPL is regulated by the pressure balance between the reservoir and liquid line; changes to the CPL system alter the balance and allow flow into and out of the reservoir.

Temperature set-point regulation. The reservoir contains both liquid and vapor phases so that the system pressure can be controlled by controlling the saturation temperature. Typically, the reservoir operates at a temperature above the ambient, such that heaters are required to maintain a controlled temperature. In the CPL literature, this is referred to as cold-biasing the reservoir. Cold-biasing can be achieved in a spacecraft system by (1) mounting the reservoir on a radiator or (2) by building a shroud around the reservoir that is cooled by the CPL liquid transport line carrying fluid returning from the condenser to the evaporator [Ku, 1997].

The evaporator saturation temperature during steady-state operation is determined by the evaporator pressure, which is equal to the reservoir pressure minus the viscous pressure drop between the evaporator and the reservoir. With high vapor pressure fluids, the viscous pressure drop is small compared to the

absolute pressure of the reservoir so that the evaporator temperature is very close to the reservoir temperature. In low vapor pressure systems, such as those with water as the fluid (VIEW-CPL), the viscous pressure drop can result in a more noticeable evaporator temperature difference.

CPL conductance modes. A CPL can be operated as a constant conductance device, if the reservoir is completely filled with liquid, but is normally operated as a variable conductance device. This means that the evaporator temperature stays approximately constant as the evaporator heat load varies over a wide range. In order for the reservoir to control the CPL operating temperature, there must be both liquid and vapor present in the reservoir, and the condenser must be partially filled with liquid [Ku, 1993]. The reservoir must be sized correctly if it is to control the operating temperature independent of evaporator heat loads and condenser temperatures. As the CPL operating conditions change (either heat load and/or sink temperatures), the portion of the condenser area blocked by liquid increases or decreases to achieve an energy balance. Hence, the conductance is variable. If more heat is applied to the evaporator, the vapor area of the condenser will increase in size to allow the additional heat rejection. If the condenser sink temperature decreases, which could occur when spacecraft orbits change, the condenser vapor area will decrease in size to allow the conductance to shift and balance the change in temperature. In both of these examples, the amount of liquid in the main loop (evaporator, condenser, and transport lines) varies and the reservoir allows liquid

to flow in or out to account for the variation in the liquid inventory. To ensure proper temperature regulation over the full range of possible operating conditions, the reservoir must be sized so that liquid and vapor are present for the following two extreme cases: (1) no heat load (in this case the CPL is fully flooded with liquid, and the amount of liquid in the reservoir is a minimum) and (2) maximum heat load at maximum condenser temperature (maximum amount of liquid in reservoir).

If the reservoir becomes filled with liquid, the CPL switches to constant conductance mode. Constant conductance refers to the inability to adjust the condenser vapor volume because there is no volume available in the reservoir. Once the CPL has made the transition to constant conductance mode, the reservoir no longer controls the evaporator temperature which will adjust to follow the operating conditions. A CPL system can be designed to transition between variable and constant conductance modes by sizing the reservoir to be filled with liquid during certain operating conditions [Clayton et al., 1997]. Allowing the system to switch to constant conductance is one method of assuring that there will always be liquid in the condenser (because there is no volume to displace liquid into the reservoir) and vapor will not be permitted to pass through the condenser and into the liquid inlet of the evaporator.

Design requirements. A CPL reservoir should meet the following requirements for proper operation: (1) discharge only liquid into the CPL, (2) exhibit temperature stability (i.e. have sufficient heater power and/or thermal

mass to avoid temperature excursions due to liquid inflow), (3) have a low pressure drop during liquid exchanges between the reservoir and CPL system while minimizing pressure oscillations, and (4) minimize liquid expulsion time [Butler and Hoang, 1991; Buchko, 1992; Hoang and Ku, 1996]. The CPL reservoir is always connected to the liquid transport line. On Earth, gravity fed reservoirs can ensure that only liquid exits the reservoir. In space, however, a wick structure (discussed in Section 3.2.3) is necessary to prevent vapor from exiting the reservoir and entering the liquid line. The wick structure also ensures that liquid is fed to the reservoir heater locations to enhance temperature control. Stable temperature control involves maintaining the reservoir saturation temperature at the desired set-point through the use of heaters. It is important to design the internal wick structure to ensure that liquid is available for evaporation in the heated region to prevent over-temperature conditions.

The reservoir connecting line must be sized to allow fluid to easily transfer between the reservoir and the loop during rapid changes in the evaporator heat load or condenser sink conditions. On the other hand, flow restriction in the reservoir line helps damp out pressure oscillations often seen in CPL systems. These conflicting requirements make CPL design interesting. Hoang and Ku [1995] provide a mathematical formulation for analysis of CPL component designs for minimizing fluid oscillations.

Cold shock. As liquid flows into the reservoir from the CPL liquid line, the temperature of the inflow is normally colder than the saturation temperature of the

fluid inside the reservoir due to subcooling in the condenser. The inflow of cold liquid tends to condense some of the vapor in the reservoir, which lowers the pressure and pulls in more cold liquid. If the reservoir heaters cannot maintain the reservoir temperature, the reservoir experiences a failure mode called “cold shocking” [Cullimore, 1991]. A cold shocked reservoir often leads to CPL deprime because liquid in the evaporator core flashes due to a sudden decrease in loop pressure [Antoniuk, 1995]. The displacement of liquid from the evaporator core to the reservoir, created by the large change in vapor volume inside the reservoir, thus interrupts the liquid feed to the capillaries.

2.2 CPL Functionality

This section describes the functionality of CPL systems in terms of typical operating characteristics and testing modes.

2.2.1 Operating features

The fundamental purpose of a CPL is to circulate fluid from the evaporator to the condenser to transfer energy. There are both beneficial and limiting features that come naturally with the CPL configuration. The two-phase reservoir allows precise control of the operating temperature, but requires electrical power and appropriate ambient conditions to maintain its temperature set-point. The volume of the reservoir allows collection of NCG (provided NCG can be swept into the reservoir) thus removing evaporator sensitivity to NCG. The reservoir can be used to fill the loop with liquid, an operation known as pressure priming. Since the reservoir is not co-located or connected to the evaporator with a

thermal/hydraulic link (as it is with an LHP) the pressure prime is a procedure that must occur prior to CPL start-up but can also be used to recover from an evaporator deprime. Because the evaporator uses capillary action, it is a self-regulating device that only moves the amount of liquid that is needed to keep the evaporator cool. There is no need for a by-pass line or auxiliary pumping during transient conditions (e.g. start-up, heat load variations, sink temperature changes, shut-down). The evaporator wick also permits the CPL to exhibit a diode function [Ku, 1997], allowing heat transfer from the evaporator to the condenser but not from the condenser to the evaporator, because there is no wick in the condenser to provide circulation. But the evaporator is sensitive to vapor on the liquid side of the capillaries; oscillatory temperature fluctuations and deprime can occur when vapor is in the evaporator core. The above mentioned features are discussed further in the following paragraphs.

Pressure prime. In a shut down mode, the CPL contains both liquid and vapor phases. Before the CPL can operate, liquid must saturate the pores of the polyethylene wick structure inside the evaporator (i.e. it must be primed). This is done by forcing liquid out from the reservoir into the remainder of the loop. This procedure is called a pressure prime.

A pressure prime results in filling of the CPL evaporator, condenser, and transport lines with liquid from the reservoir. Increasing the temperature of the reservoir drives liquid out of the reservoir until the remainder of the CPL is filled with liquid [Ku, 1994]. The pressure prime ensures that there is no vapor in the

evaporator core and liquid lines that could block the flow of liquid to the evaporator wick [Hoang, 1997]. Pressure priming a CPL requires considerable time because the energy stored in any vapor in the loop must be transferred out of the loop as heat. The temperature difference that drive this heat transfer results from compression heating of the vapor as the reservoir liquid fills the loop.

Start-up. The start-up phase begins after the pressure prime. This phase consists of heating the evaporator to reservoir temperature. In a test environment, the heat is supplied by heaters; in an actual application the heat is supplied by the instrument or equipment requiring the cooling. In both cases, the energy is transferred through the evaporator walls to the working fluid where it raises the temperature up to saturation. The time required to initiate boiling inside the evaporator depends upon the heat load, the initial state of the fluid in the evaporator and other evaporator characteristics such as available nucleation sites [Cullimore, 1991].

During the start-up phase, several dynamic events can occur in the CPL system. First, a certain amount of superheat is necessary for nucleate boiling to initiate [Cullimore, 1991; Hoang and Ku, 1996] and bubble formation during boiling can involve significant local effects including pressure spikes. A pressure spike associated with flashing of superheated liquid in the evaporator can sometimes exceed the capillary limit of the wick, thus allowing vapor to penetrate the wick and flow into the liquid core [Antoniuk, 1995; Hoang and Ku, 1996; Ku, 1997]. These pressure spikes are more prominent when the CPL system is

largely filled with liquid (such as after a pressure prime where the evaporator, condenser and transport lines are completely filled with liquid) because there are no vapor bubbles near-by that can be readily compressed to absorb the energy.

Hoang and Ku [1996] describe the calculation of the pressure spike (ΔP) as a function of superheat (ΔT_{SH}) and the bubble radius (r). The growth of the vapor bubble is described in terms of the superheat and fluid properties by

$$\gamma = r \frac{dr}{dt} = \frac{\pi}{2} \left(\frac{\Delta T_{SH} \sqrt{k_l \rho_l c_{p,L}}}{\rho_v \lambda} \right)^2 \quad (2.9)$$

Using the inertial and frictional coefficients between the wick and reservoir line, α_r and β_r , and the rate of bubble increase, γ , the pressure spike is

$$\Delta P = \alpha_r \rho_l \left(4\pi \frac{\gamma^2}{r} \right) + \beta_r \rho_l (4\pi \gamma r) \quad (2.10)$$

Once the pressure spike has occurred and the initial vapor bubble begins to expand, the pressure must overcome the inertial force of the liquid in the vapor grooves, vapor transport line, condenser, and reservoir connecting line [Cullimore, 1991]. During the clearing of the vapor grooves, the liquid is displaced along the path of least resistance which, depending upon the CPL design, can be backwards through the wick to the reservoir. This would push warm liquid into the evaporator core and leave the core susceptible to bubble initiation and growth from the beginning of operations. The backflow stops after the vapor grooves are cleared and the liquid/vapor interface is established along

the length of the wick. Cullimore [1991] describes the start-up of pumping as the point at which the vapor grooves are cleared, since it is the time where liquid must flow forward through the wick.

The largest pressure differences in the system typically occur during the start-up process. In order to clear the vapor grooves in a fully flooded CPL, the vapor must displace the liquid from the vapor transport line and move it to the reservoir. At the on-set of evaporation inside the evaporator, the liquid inside the vapor grooves and vapor transport lines must be displaced at a volumetric flow rate equal to the expansion rate of the vapor. As the vapor line clears, the liquid is pushed through the vapor line at a velocity equal to the velocity of the vapor front leaving the evaporator. The displacement results in a liquid mass flow rate described by

$$\dot{m}_l = \frac{\rho_l}{\rho_v} \frac{\dot{Q}_e}{\lambda} \quad (2.11)$$

This mass flow rate is much greater than that achieved at steady-state for the same power and results in temporarily large evaporator pressures, typically called pressure surge [Cullimore, 1991; Hoang and Ku, 1996]. The higher pressure is sustained as long as it takes to displace the liquid from the vapor line and condenser to the reservoir.

Steady operations. A detailed thermodynamic analysis of steady-state CPL operations is provided by Ku [1994]. The analysis presented is valid for the operation of a variable-conductance CPL within the capillary limit of the wick

[refer to Eqs. 2.1-2.3] (i.e., operations resulting in deprime are not included). In the present study, the model formulated by Ku was used to size the liquid and vapor transport lines in the VIEW-CPL experiment (see Section 3.2.4). An example of the thermodynamic state of the working fluid around VIEW-CPL is presented in the following paragraph.

Once the flow begins in the evaporator, the saturation pressure inside the evaporator is not exactly the same as the saturation pressure of the reservoir. The pressure drop in the lines due to the flow of the liquid slightly decreases the saturation pressure (and therefore temperature) on the liquid side of the evaporator. Figure 2.3 is an example of the predicted steady-state pressure drop combined with temperature data collected from VIEW-CPL super-imposed on the pressure-enthalpy (P-h) diagram of water. The condition shown is for a net evaporator power of 15 W with the reservoir controlled at 51°C. Due to the capillary pressure rise within the wick, the evaporator outlet pressure is higher than the reservoir ($P_5 > P_1$). For the example based on water in Figure 2.3, the corresponding temperature difference between the evaporator and reservoir is only 0.1 K since the viscous pressure drop at 15 W is small.

For a system operating at a temperature near the triple point, the effect of the pressure drops becomes more critical since the lowest pressure (P_3 in Figure 2.3) must be greater than the triple point pressure to maintain operation. A related factor is that the shape of the vapor pressure curve implies that operation near the triple point results in larger temperature differences between the

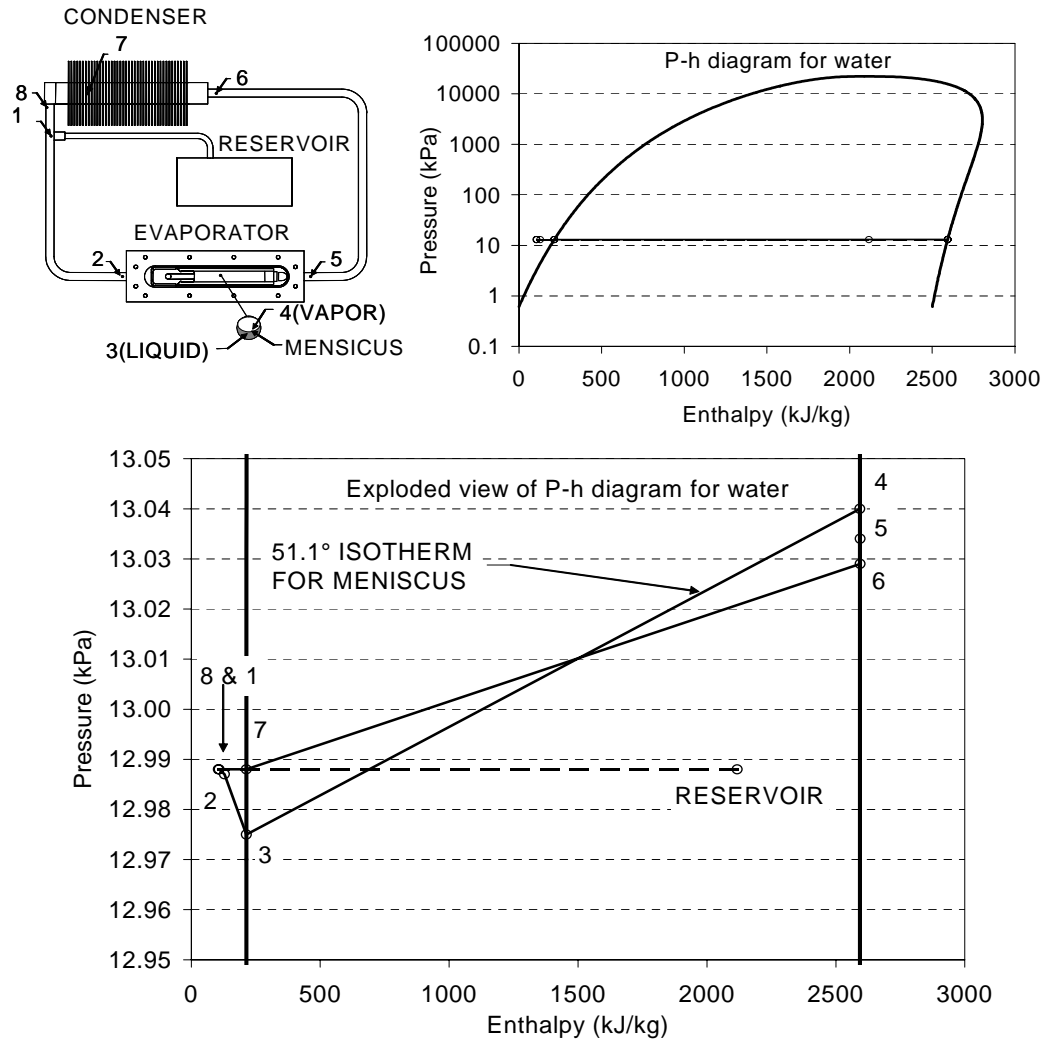


Figure 2.3 Pressure-enthalpy diagram for VIEW-CPL steady-state operating cycle at 15 W and evaporator temperature of 51.1°C. The lower plot is an exploded view of the line at 13 kPa in the top plot.

evaporator and reservoir. Those concerns contributed to the decision to operate VIEW-CPL at a nominal temperature of 50°C, well away from the triple point of water (0.01°C).

Pressure and temperature oscillations. High frequency (1 Hz) pressure oscillations have been observed in CPL systems [Ku et al., 1993; Ku and Hoang,

1995, O'Connell et al., 1995]. A mass-spring-dashpot model has been developed that attributes the oscillations to amplification of thermal disturbances in the CPL system [Hoang and Ku, 1995]. The perturbation from steady-state results in flow oscillations between the vapor space in the CPL and the vapor space inside the reservoir. The model is primarily used to determine the system conditions under which the disturbance is amplified and the pressure oscillations exceed the capillary limit of the wick. Oscillation of the differential pressure across the capillary evaporator has been observed in numerous ground tests performed on ammonia CPLs [Ku et al., 1986b; Ku, 1993]. In a flow visualization experiment using ammonia, the differential pressure oscillations were recorded and corresponded to visual observations of radial liquid motion in and out of the wick [Ku et al., 1993]. During the same testing, deprime of the evaporator was normally preceded by large amplitude and high frequency pressure oscillations.

Oscillations during deprime were observed in the condenser during testing of a water CPL at the University of Maryland [Kolos et al., 1996]. During some deprimes, the condenser showed a spatial oscillation of the liquid/vapor interface. In one case when the evaporator began to deprime at low heat load, the fluid in the condenser did not flow but instead oscillated. This was observed visually when small non-condensable gas bubbles in the condenser vibrated without flowing through the condenser. At high heat loads, the onset of deprime from vapor in the evaporator core was predicted by the advancing and receding of the vapor/liquid interface in the condenser. At heat loads nearing the capacity of the

condenser, wavy annular flow was observed moving along the wall of the condenser, which also made the condensed liquid slug at the liquid/vapor interface oscillate.

Although high frequency (1 Hz) pressure oscillations were also observed in the VIEW-CPL experiment, the present study focuses on low frequency oscillations (0.003 to 0.01 Hz) in temperature measurements and visual observations as described by Kolos and Herold [1997]. For VIEW-CPL the evaporator bubble oscillation occurred at 0.003 Hz and the corresponding evaporator inlet temperature fluctuated by 5 K during each cycle. The power range over which the oscillatory behavior was observed was 20 to 40 W. In a separate study, similar amplitudes and frequency were measured by Lin et al. [1994] (fluid not disclosed in reference) with low frequency temperature oscillations having 0.0055 Hz and 8 K amplitude during low power operations at 50 W.

Low frequency oscillations have been observed since the early testing of CPLs. Low frequency temperature oscillations that were observed in CPL-2 (an early ammonia CPL breadboard tested in the 1980s) were attributed to conduction from the evaporator body to the liquid inlet and possible non-condensable gas generation due to brazing materials at the liquid inlet [Kiper et al., 1988]. Kiper presents a model based on conduction and convection at the inlet and predicts an unstable region where undamped oscillations can exist. His results come close to predicting the CPL-2 temperature fluctuations with an

amplitude of 2 K and frequency of 0.0005 Hz. The results of Kiper's work do not apply directly to the VIEW-CPL observations because of the careful design to reduce heat conduction into the liquid line.

Deprime. The failure to pump liquid comes from loss of the meniscus from the pores of the wicking material. If a single pore dries out, vapor back-flow occurs through the wick which can lead to deprime of other pores and system deprime. In ground testing, deprime has been caused by factors such as high liquid evaporator-inlet temperatures, condenser failure, presence of non-condensable gas, and reservoir set-point fluctuations [Ku et al., 1993; Ottenstein et al., 1993]. Some investigators have observed temperature oscillations in the evaporator inlet prior to deprime [Antoniuk and Pohner, 1994]. In some cases, deprime could not be traced to a particular cause [Ku, 1993]. In addition to the types of deprime already known, any deprime phenomena inherent in micro-gravity, such as elimination of stratified flow, need to be investigated. The important factor in studying deprime phenomena is the ability to predict and consequently prevent failure of the CPL system.

Diode function. The CPL diode function refers to the transfer of heat in one direction, from the evaporator to the condenser, and not the reverse. This function is inherent in the design because there is no wick in the condenser to pump vapor toward the evaporator. The diode function is a beneficial feature to prevent heat input to the condenser (e.g., during a spacecraft maneuver that places the condenser in view of the Sun) from being transferred to the evaporator

and the space craft electronics. The diode function is accomplished automatically by deprime when the condenser stops condensing vapor and the liquid supply to the wick is interrupted. Alternatively, the CPL can be shutdown by raising the reservoir temperature to initiate a pressure prime of the loop. Either method stops circulation, and hence heat transfer, through the CPL.

2.2.2 Typical testing modes

The following system performance tests have been adopted by industry for analyzing CPL systems [Braun, 1990]: (1) system startup test, (2) maximum transport capability, (3) heat load sharing among two or more evaporators, (4) diode function of the condensers, (5) rapid power cycling, (6) sink temperature variation, (7) pressure prime under heat load, and (8) reservoir set-point temperature variation. A more detailed description of these tests is included as Appendix A. Due to limited power and available astronaut time for testing, the VIEW-CPL flight experiment testing was streamlined to focus on investigation of the CPL physics by exercising multiple start-ups and power variations.

System start-up tests are designed to determine the conditions favorable to successful start-ups. A start-up is successful when two conditions are satisfied (1) vapor is present at the outlet of the evaporator and (2) there is forward circulation of fluid from the evaporator to the condenser. For a successful test, some researchers also require that in addition to the two conditions, that there be no vapor bubbles in the core of the evaporator. This requirement was not placed on VIEW-CPL since the system was designed to facilitate observations of

bubbles and their effect on operation. VIEW-CPL start-ups were attempted with powers varying from 10 to 75 W (maximum power available).

After start-up, power variations and heating of the liquid and vapor lines were performed. Since VIEW-CPL was cooled by ambient air, variation between the condenser and sink conductance was achieved by turning off one or more fans. Additional details on the VIEW-CPL testing are discussed in Chapter 4.

2.3 CPL Experiments and Applications

The investigation of CPL technology began at NASA Lewis Research Center in the mid-1960s [Stenger, 1966]. Stenger built two water CPLs, one with a copper evaporator and the other with a nickel evaporator. The CPLs demonstrated transport capability (a product of the evaporator heat load and the distance between the evaporator and condenser) greater than 1.1 kW-m.

Many CPL experiments have been built and tested since 1966. Figure 2.4 contains a summary time line of CPL and LHP development as distilled from the references listed in this study. In the early 1980's NASA Goddard Space Flight Center and aerospace contractors rekindled the CPL development effort with a proof-of-concept breadboard using R-11 as the working fluid [Ku et al., 1986b]. Following the success of the breadboard feasibility experiment, two engineering development units (CPL-1 and CPL-2) were built and tested with ammonia as the working fluid [Ku et al., 1986b]. Transport capabilities up to 70 kW-m were demonstrated.

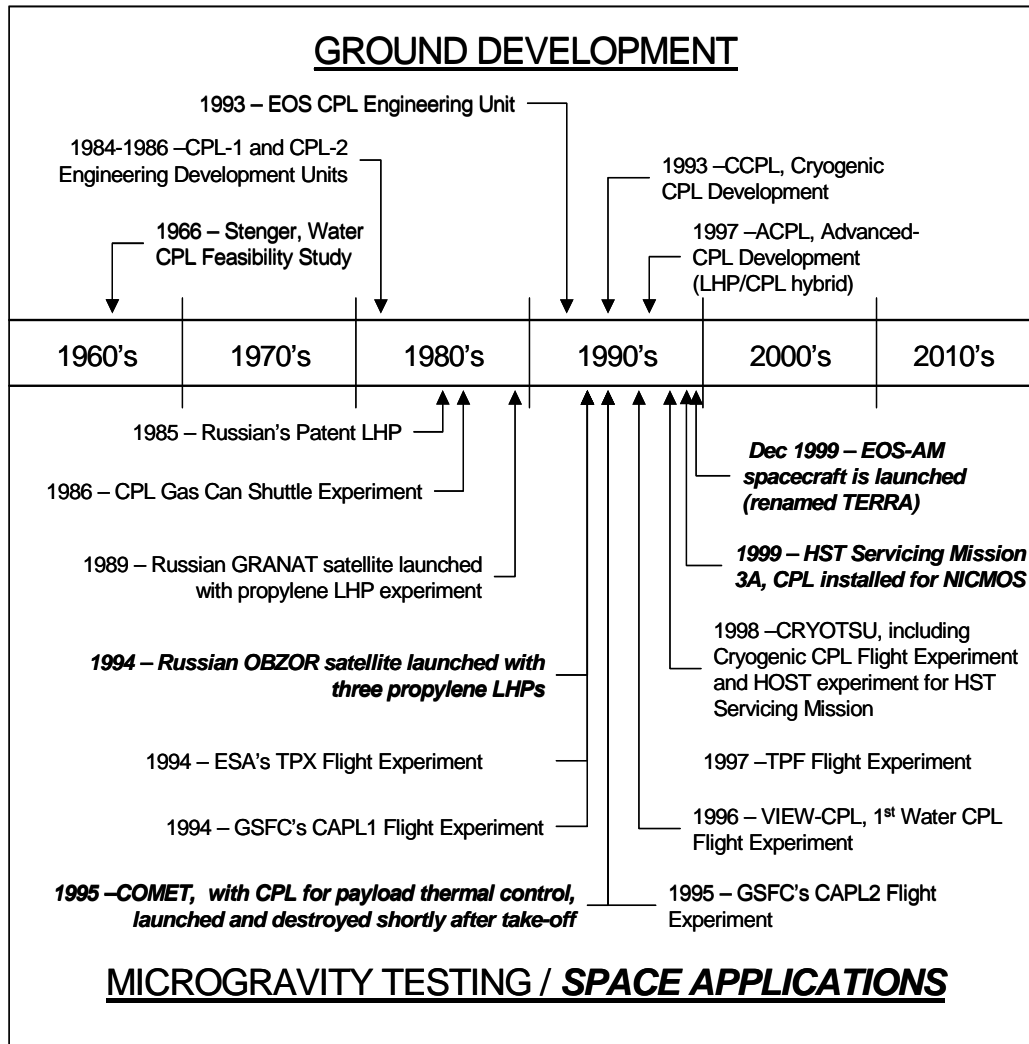


Figure 2.4 Time line of CPL and LHP development, testing, and applications.

CPL systems have been tested over a wide range of transport capacity and temperatures. One of the largest systems was the High Power Spacecraft Thermal Management (HPSTM) System [Ku et al., 1988]. The HPSTM could transport 500 kW-m (50 kW over 10 m transport line length) as a CPL with mechanical pump assistance and 250 kW-m without the pump. While most CPL applications have used ammonia at room temperature, Kroliczek and Cullimore

[1996] demonstrated a prototype cryogenic CPL using nitrogen at 85 K, carrying a heat load of 3 W and starting from a supercritical state.

Several representative Loop Heat Pipe (LHP) references are included on the time line (Figure 2.4) to give the reader a sense of the parallel LHP and CPL development. The LHP was patented in the U.S. in 1985 [Maidanik et al.]. As described in Chapter 1, LHPs have the reservoir directly connected to the evaporator and are filled with the appropriate amount of liquid to keep the evaporator always wetted [Wolf et al., 1994]. By 1989, an LHP experiment was flying on the Russian GRANAT spacecraft [Goncharov et al., 2003].

2.3.1 Flight experiments

Flight experiments have focused on proof-of-concept and testing of advanced CPL features to ready the technology for space applications. In 1986, a Get Away Special Canister, an experimental carrier for the Space Shuttle known as a GAS can, that flew on the STS-61C mission contained a CPL [Ku et al., 1986a]. The CPL consisted of two parallel evaporators, a single multi-pass condenser (attached to the GAS can cover for a heat sink), and a reservoir. The working fluid was ammonia. The CPL was operated for short intervals (maximum five hours) with a cool-down period between intervals. The cool-down period was needed because the input power to the CPL evaporator was larger than the heat transfer rate that could be rejected by the radiator. Low power instabilities were observed in the evaporator inlet during this testing. At 50 W per evaporator, heat transfer within the evaporator, resulting from the low fluid flow rate, caused liquid

in the evaporator inlet to evaporate. The minimum stable power level was 100 W per evaporator.

In 1994, the European Space Agency (ESA) flew a two-phase experiment with an ammonia CPL having two capillary evaporators [Delil et al., 1995] aboard the Space Shuttle on the STS-60 mission. The experiment demonstrated variable evaporator heat load, heat load sharing, and variable set point operations. Both flat and cylindrical evaporators were flown.

The CAPL-1 flight experiment also flew in 1994 on the STS-60 mission and is an important example of why flight testing is so important. In CAPL-1, ground testing masked some basic operating conditions that were uncovered during micro-gravity testing. In particular, CAPL-1 had start-up difficulties [Antoniuk, 1995] (with multiple evaporators) due to capillary action in the evaporator vapor grooves which were not discovered until testing in micro-gravity. In 1-g, start-up was facilitated by gravity-assisted groove drainage. Although not successful in demonstrating multiple evaporator start-ups, the three-port evaporator “starter pump” in CAPL-1 operated as designed. A follow-up flight experiment was developed and CAPL-2 was flown in 1995 on the STS-69 mission [Butler et al., 1996]. In contrast to the CAPL-1 experiment, the CAPL-2 experiment contained only one evaporator of the three-port design.

CAPL-3 flew on the STS-108 mission in December 2001 [Ottenstein et al., 2003]. CAPL-3 demonstrated that multiple evaporators and hardware for deployable radiator assemblies were flight worthy. The start-up issues

encountered with CAPL-1 were corrected with a back-pressure regulator to ensure that vapor exiting the three-port starter pump would displace liquid in all the vapor grooves of the other evaporators prior to attempting their start-up. To reduce the possibility of deprime, the evaporators also contained a mesh structure to prevent any vapor bubbles that may exist in the core from entirely blocking the wick [Kim et al., 1997]. All three CAPL experiments used ammonia as the working fluid.

Other CPL experiments include the Two-Phase Flow (TPF), tested on board the STS-85 mission in August 1997 [Ottenstein and Nienberg, 1998]. In 1998 a cryogenic CPL was tested as part of the CRYOTSU experiment during the STS-95 mission [Bugby et al., 1998]. The HST Orbital System Test (HOST) was also tested during the STS-95 mission as a flight test of the CPL configuration to be used on the Hubble Space Telescope [Buchko et al., 1999].

2.3.2 Visualization experiments

Visualization experiments in CPLs began with Stenger [1966], who used glass condensers for observing the condensate flow. In subsequent experiments, attention turned to the evaporator. Previously mentioned in Section 2.2.1, Ku et al. [1993] used a flow visualization experiment to observe radial liquid (ammonia) motion in and out of the wick that corresponded to differential pressure oscillations. Observations of bubbles in a glass evaporator, performed at Martin Marietta, showed bubbles that would grow, shrink, and oscillate

[Cullimore, 1993]. Decreases in either sink temperature or evaporator load caused bubble growth which resulted in evaporator deprime.

Glass viewports at the inlet and exit of the CAPL-1 starter-pump were used by Douglas et al. [1997] to observe vapor back-flow into the evaporator during start-up. The vapor volume of back-flow was directly related to the superheat observed during the pressure surge at start-up. The purge superheat disappears after the vapor line is cleared of liquid during start-up. This visualization experiment was used to verify the theory that vapor penetrated the wick during CAPL-1 flight testing during the pressure surge. Vapor penetration was observed only for high power start-ups.

Other flow visualization experiments have used water to examine fluid flow phenomena inside CPL components [Kiper, 1991; Kolos et al., 1996]. Water is a good fluid for flow visualization experiments because the design of transparent components is less complicated for low vapor pressure fluids (like water) than it is for high vapor pressure fluids (like ammonia). The use of water at sub-atmospheric conditions also permits the investigation of CPL phenomena such as subcooling requirements and system performance limits that are obscured in high pressure systems. Kiper [1991] operated a water CPL to study transient behavior in the evaporator. Typical CPL evaporators use cylindrical wicks with axial vapor grooves. The atypical evaporators used by Kiper were made with brass screen and felt layers in a cylindrical Pyrex chamber in a vertical orientation. The brass/felt wick was pressed to the bottom heating plate

enclosing the chamber and extended into the liquid line to draw the liquid to the heated plate. The remainder of the loop contained a reservoir to maintain operating pressure, a condenser, and liquid and vapor transport lines. The loop was operated at a saturation temperature of 30°C, corresponding to an operating pressure of 4.25 kPa. Although the CPL operation was successful, results are difficult to interpret due to the details of the subcooler and evaporator designs.

The VIEW-CPL system uses cylindrical evaporators (similar to flight hardware) and operates on water at sub-atmospheric pressure. Prior to design of VIEW-CPL, a flow visualization CPL test facility was constructed at the University of Maryland and tested with water as the working fluid [Kolos et al., 1996]. The system was designed as a proof-of-concept experiment to demonstrate a water CPL system under sub-atmospheric conditions and provided enough information to design the VIEW-CPL experiment. To create the flow visualization facility, transparent components were used to make the evaporator, condenser and reservoir. The evaporator was made from a Pyrex tube encasing a porous polyethylene wick. The condenser was made from a machined aluminum block with a Lexan top, making the condensing tube section visible. To allow for the monitoring of liquid levels, the reservoir was constructed from a Pyrex vessel. The transparent CPL components allowed for the observation of phase interfaces and fluid motion to correlate visual data with temperature and pressure data. Visualization into the evaporator inlet showed that the CPL system was able to continue running with small vapor bubbles on the liquid side

of the evaporator. Under certain conditions, the system was able to tolerate a small vapor bubble in the evaporator core. If the conditions were changed, such as increased flow rate or additional inlet subcooling, the wick appeared to re-wet. Equilibrium vapor bubbles were observed in the core, which apparently represent a dynamic balance between condensation on the surface in contact with the liquid and vapor generation due to either back flow or conduction through the wick.

2.3.3 Space applications

The Russians have been using LHPs for flight applications since 1994 with the first service on the OBZOR spacecraft [Goncharov et al., 1995; Goncharov et al., 2003]. This particular satellite used three propylene LHPs for thermal control of various components.

In the United States, the first instruments to use CPLs for thermal control were on the Earth Observing System EOS-AM (renamed TERRA) spacecraft. Development of the CPLs began with a ground-tested engineering unit [Kaylor et al., 1993] and culminated in the CAPL-2 flight experiment [Butler et al., 1996]. The EOS-AM spacecraft was launched in December 1999.

Commercial Experiment Transporter (COMET) Service Module that was supposed to launch in 1993, was designed with a multi-evaporator CPL to keep payloads at a constant temperature [Roukis et al., 1992]. The CPL working fluid was ammonia and there were eight evaporators plumbed in parallel, a starter pump, and a mechanical pump for ground operations at the launch pad. The launch was delayed until October 1995 at which time all payloads were destroyed

during a rocket failure. Another CPL that did not make it to space was designed and built for the Mars Surveyor Lander [Clayton et al., 1997]. It was designed as a hybrid variable/fixed conductance CPL with a purposely under-sized reservoir to allow the condenser to control saturation temperature under certain operating conditions. The system experienced anomalies (during ground testing) during transitions from constant conductance to variable conductance and was subsequently rejected by the Mars Surveyor Program.

During the Hubble Space Telescope (HST) Servicing Mission 3A, the Near Infrared Camera and Multi Object Spectrometer (NICMOS) was fitted with a mechanical refrigerator to circulate neon gas to assist the existing detector cooling system [McIntosh, 1998]. The operation of the cooler generates 500 W that is transported by a CPL to a newly installed external radiator. The CPL was chosen for this application because of the temperature control requirements and the flexibility for in-orbit assembly onto the existing HST hardware (i.e., there was limited space for integrating new components) by the Space Shuttle crew.

As of the date of this thesis (2004), industry has largely switched to LHPs for their self-priming feature. LHPs are routinely flown on commercial satellites. One example is the Boeing 702 which began flying LHPs in 1998 [Goncharov et al., 2003]. However, LHPs do not fit all applications and CPLs are still used, particularly in cases where the LHP reservoir cannot be accommodated as in the HST application described above.

2.3.4 Enhancements

CPL technology continues to mature, resulting in continuously improving CPL performance. In the evaporator, electrohydrodynamic (EHD) techniques [Ohadi et al., 1997] and vaporization enhancement grooves (VEG) [Pohner and Antoniuk, 1991] have demonstrated increased evaporation heat-transfer coefficients. The EHD-assisted CPL also has the benefit of increasing heat transport capability by increasing the circulation with EHD-pumping that is additive to the capillary pumping. Heat pipes inside the evaporator wick core also help distribute energy within the liquid inside the core [Kim et al., 1997; Ottenstein and Nienberg, 1998]. Wick development is providing wicks with high pumping capability; with titanium or nickel, sintered metal wicks can achieve an effective pore radius of 1 to 3 μm [Ku, 1997]. Bidisperse wicks with both small and large pore radii are being developed for high heat flux applications [Ku, 1997].

In addition to evaporator enhancements, system design changes are resulting in more robust systems with the ability to recover from conditions leading to deprime. The Advanced-CPL (ACPL) [Hoang, 1997] was been designed to allow quick start-up of a CPL system and to assure robust operation with the ability to flush vapor bubbles from the evaporator core on demand. The ACPL uses a secondary evaporator and condenser, located near the reservoir, to circulate liquid through the loop. Future CPL development and advancement will likely result in hybrid loops with LHP or mechanically pumped components assisting with bubble control in the CPL evaporator core.

3.0 VIEW-CPL DESIGN

The Visualization In an Experimental Water Capillary Pumped Loop (VIEW-CPL) payload is a CPL test facility with flow visualization capabilities in the evaporator. The experiment flew in the Middeck of the Space Shuttle Columbia during the STS-80 mission. The payload design process involved balancing the Middeck interface and safety requirements with the CPL functionality requirements.

VIEW-CPL was designed as a shuttle Middeck experiment, instead of a GAS can experiment (located in the shuttle cargo bay), for two main reasons: (1) the Middeck atmosphere and ambient conditions are less extreme than the cargo bay, and (2) crew operation and manual controls made the design less complicated, particularly for video taping of the evaporator test section. A perspective view of the on-orbit configuration is given in Figure 3.1.

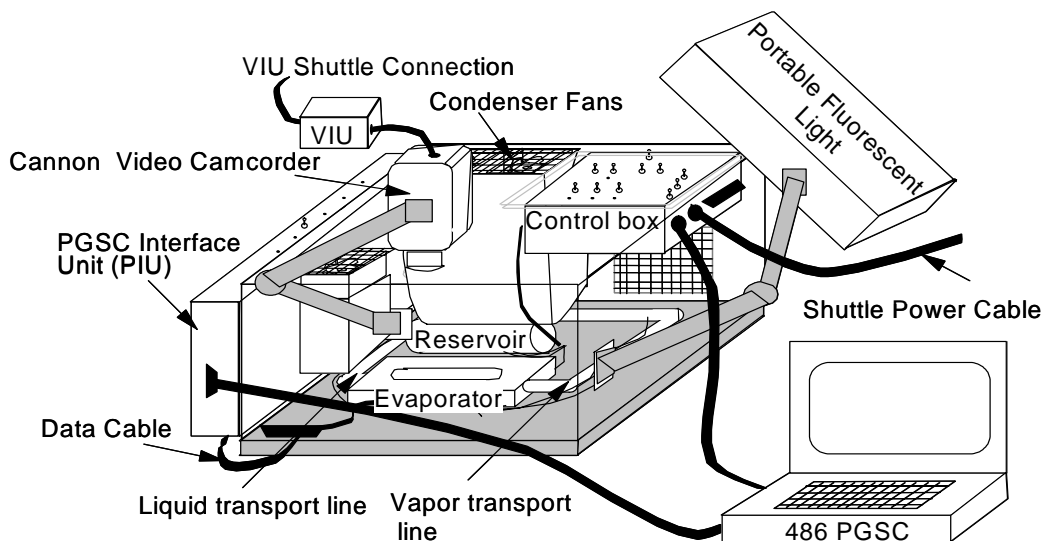


Figure 3.1 VIEW-CPL configuration during operations in the Space Shuttle Middeck.

3.1 Shuttle Interfaces

A summary of the shuttle interfaces and requirements are listed in Table 3.1 with the corresponding VIEW-CPL solution or design parameter. The shuttle interfaces are defined in NSTS-21000-IDD-MDK Rev. B, the version of the Middeck Interface Definition Document current at the time of the VIEW-CPL manifesting. VIEW-CPL was classified as a nonstandard secondary payload [NASA JSC, 1995]. The nonstandard classification was given because: (1) the VIEW-CPL storage requirements exceeded one Middeck locker, and (2) the maximum payload power exceeded the standard power allowance of 130 W [NASA JSC, 1996a]. The “secondary” payload classification refers to the priority placed on achieving the payload objectives (compared to the primary payload(s) that have first priority during the shuttle mission).

Physical Interfaces. The payload was stowed in one large stowage tray and one small stowage tray that were fit into one-and-a-half Middeck lockers. The CPL portion of the experiment weighed 18.1 kg (39.7 lb) and was stored in one locker with cables and spare fuses. The remainder of the components were packed in one half of a separate shared locker. All components were snugly surrounded by fitted isolating foam to protect the payload from transient and random vibration responses at lift-off. Vibration and acoustic susceptibility tests were not required of the VIEW-CPL payload because it was stowed in the lockers for ascent and descent and the loads are dampened by the isolating foam.

Table 3.1. VIEW-CPL and shuttle interfaces.

Section # ^A	Middeck Requirement specified in NSTS-21000-IDD-MDK	Section # ^B	VIEW-CPL Design - NSTS-21343-ICA
3.4.1	Large Stowage Tray (1 per locker): 36.7 cm x 24.2 cm x 47.3 cm (14.5 in x 9.5 in x 18.6 in)	5.0	VIEW-CPL in shroud: 34.5 cm x 19.7 cm x 43.4cm (13.6 in x 7.75 in x 17.1 in) [Incorrectly listed in ref.]
4.1	Ascent and descent vibrations and accelerations	2.b	Stowed in locker during launch and landing.
4.1	Accelerations from RCS and OMS maneuvers	none	Analysis of reactions UMCP-VCPL-ANL-006, Rev. A
4.2	Emergency Landing	none	Repack in locker
4.4	Kick/Push-off loads: 556 N (125 lb) limit load distributed over a 10 cm x 10 cm (4 in x 4 in) area	none	Brackets and supports designed to withstand stated kick/push-off loads
4.6	Fracture control	none	Non-fracture critical
4.7.3	Payload Generated Acoustic Noise	2.0	SSP approved waiver obtained for exceedance
4.8.1	Maximum payload mass (per locker): 24.5 kg (54 lb)	5.0	VIEW-CPL in shroud - 18.1 kg (39.7 lb) [Incorrectly listed in NSTS 21343-ICA]
5.3	Illumination	3.0	SSP supplied portable fluorescent light
6.2	Active Payload waste heat dissipation over 60 W	none	Fans to circulate air across finned heat sinks
7.2.1	Electrical power Interfaces: 24 to 32 VDC from Middeck Utility Panel (MUP) or 10 A Middeck ceiling outlet	3.0	Maximum power of 168 W during high power tests. Continuous power of 15 W to keep CPL primed.
7.3.1	AC power	3.0	230 VA to power fluorescent light for 15.6 hr
8.0	Conducted and Radiated Electromagnetic compatibility and susceptibility	2.0	-SSP approved waiver for generated conducted emissions exceedance
10.0	Payload and General Support Computer (PGSC)	5.0	Shared PGSC and video camcorder for collecting data

^ANSTS-21000-IDD-MDK, Rev B., Middeck Interface Definition Document [NASA JSC, 1996a].

^BNSTS 21343 ICA - Orbiter Crew Compartment Interface Control Annex for VIEW-CPL [NASA JSC, 1996b].

Upon removal of the experiment from the locker for on-orbit testing, the experiment was mounted to the floor using Velcro. Velcro allowed the crew to quickly place the experiment in a variety of locations. The on-orbit configuration (Figure 3.1) was subject to accelerations due to engine firings during Reaction Control System (RCS) and Orbiter Maneuver System (OMS) maneuvers and kick/push-off loads from inadvertent contact with the crew. While able to withstand the on-orbit loads, the Velcro could not hold the experiment in place during an emergency landing. Since VIEW-CPL requires stowage in a locker for emergency landing, a “rapid safing” plan was prepared to hasten the stowage process in emergency situations.

Thermal Interfaces. Due to presence of air in the Middeck, it is possible for payloads to transfer heat to the Middeck ambient via convection. A passive heat transfer coefficient of $1.42 \text{ W/m}^2\text{-K}$ ($0.25 \text{ Btu/hr-}^\circ\text{F-ft}^2$) with an allowable rejection of 60 W for a passively cooled payload is specified in NSTS-21000-IDD-MDK, Rev. B, Section 6.2 [NASA JSC, 1996a]. Since VIEW-CPL required rejection of up to 75 W, forced convection via circulating fans was used to cool the payload. The maximum allowable outlet temperature in the Middeck was 45°C (113°F). Due to the high air flow rate, the VIEW-CPL exit air temperatures were less than 1 K greater than the inlet temperature (described further in Section 3.2.2).

Electrical Interfaces. During operation, the experiment draws nominal 28 VDC power from either the Middeck Utility Panel (MUP) or the 10 amp Middeck

ceiling outlets. Radiated and conducted electromagnetic compatibility (EMC) and susceptibility tests were performed on VIEW-CPL to verify that there would be no adverse effects on VIEW-CPL operations due to shuttle power ripples/transient spikes and other shuttle or payload electronics. Conducted and radiated electromagnetic interference (EMI) tests were also performed to verify that VIEW-CPL electronics operated within allowable limits for shuttle safety.

The on-orbit video recording system for VIEW-CPL required the use of a video camcorder, fluorescent light, and Payload and General Support Computer (PGSC) supplied by NASA Johnson Space Center (JSC). The PGSC was a 486 IBM ThinkPad and was used to monitor the VIEW-CPL temperatures. An AC powered portable fluorescent light was supplied by JSC to illuminate the evaporator section during video taping. A Cannon L-1 camcorder and video interface unit (VIU) allowed video footage to be recorded on Hi-8mm video tapes and to be downlinked from the shuttle to the customer support room (CSR) for real-time viewing. The camcorder, light, and PGSC were considered shared equipment (not dedicated for sole VIEW-CPL use) and, therefore, were not charged against VIEW-CPL allowable space and weight.

Safety. The safety of the crew aboard the shuttle depends upon the detection and prevention of hazards that affect both personnel and the shuttle itself. In order to assure a safe payload, payload safety data packages (PSDP) were prepared to address potentially dangerous conditions. The items addressed in the VIEW-CPL safety data packages were issues of: (1) toxicity, (2)

flammability, (3) material compatibility, (4) structural design, (5) fluid containment, (6) high operating temperatures and pressures, (8) payload generated acoustic noise, and (7) rapid safing. In addition to a PSDP, a ground safety package would normally be prepared for personnel processing the payload at NASA Kennedy Space Center. Since VIEW-CPL was packed in a Middeck locker at Johnson Space Center, a ground safety package was not required.

In order to avoid toxicity and flammability, the materials and processes used in manufacturing the VIEW-CPL payload required approval from the Materials Branch at JSC. In particular, all materials used in the payload had to meet the offgassing and flammability requirements for Middeck payloads [NASA OSMQ, 1991]. Payload off-gas testing was performed at White Sands Test Facility in New Mexico [WSTF, 1996]. A listing of materials and approved configurations are presented in Appendix B.

Payloads that can cause injury or damage to the shuttle due to propagation of pre-existing flaws require fracture control [NASA JSC, 1996a]. A fracture control plan was not required for VIEW-CPL because: (1) there was no hazard from leakage of the deionized water contained in the experiment, and (2) the contents were under subatmospheric conditions, not under pressure.

Surfaces exceeding 60°C are considered high temperature surfaces and must be covered to prevent crew contact. The heaters at the reservoir and evaporator on VIEW-CPL had the potential for exceeding 60°C and were, therefore, covered with cloth insulation (Nomex Aramid brand) and over-wrapped

with aluminum foil tape (3M 425 brand); the insulation is A-rated for flammability in 30% oxygen when layered to the prescribed minimum thickness of 0.15 cm (0.06 in). The insulation is actually a third level of protection. The first level of protection is the safety shroud covering the CPL structure, and the second level of protection is a warning displayed on the data acquisition system with instructions to remove heater power in the event a temperature sensor reads above 60°C. With a heater surface temperature of 60°C, the temperatures on the outside of the insulation will not exceed 45°C based on design calculations and confirmed by measurements.

In addition to protecting the crew from warm surfaces, the VIEW-CPL safety shroud also prevented crew contact with the fans and other parts of the experiment. The experiment was designed with all sharp edges rounded and an absence of pinch points that could potentially injure the crew or damage equipment (e.g., putting holes in pressurized suits used for space walks) located in the Middeck area.

For crew comfort, payload generated acoustic noise is limited [NASA JSC, 1996a]. An acoustic noise measurement was performed on VIEW-CPL with all three fans turned on. The cooling fans above the condenser and subcooler were the only components generating noise in the experiment. The measurements were taken on all sides of the experiment to determine the maximum noise output. Table 3.2 summarizes the results as compared to the Middeck limits for a continuous noise source. A continuous noise source is defined as any source

which exists for a cumulative total of eight hours or more in any twenty-four hour period. VIEW-CPL was considered a continuous noise source because the VIEW-CPL operations were scheduled in 5 to 9 hour blocks of test time. VIEW-CPL acoustic noise emissions exceeded the maximum limits at most frequencies and therefore a waiver was requested and granted for the exceedance [NASA JSC, 1996b]. It is noted that the Middeck acoustic limits are very restrictive.

Table 3.2 VIEW-CPL acoustic measurement data.

Hz	63	125	250	500	1000	2000	4000	8000	O/A	dBA
Middeck Limits (dB)	64	56	55	51	52	53	48	44	66	58
VIEW-CPL (dB)	72 ^b	65 ^b	59 ^b	59 ^b	56 ^b	53 ^b	48 ^a	41 ^a	85 ^b	61 ^b
^a Measured 1 foot above the condenser intake screen ^b Measured 1 foot away from the condenser outlet screen Middeck Limits from NSTS-21000-IDD-MDK Section 4.7 [NASA JSC, 1996a]										

The VIEW-CPL payload required stowing in the locker during launch and landing. This requirement meant that the payload had to be repacked in the locker in the event of an emergency landing. A “rapid safing” procedure was written to minimize the time required to repack the experiment in the locker. This procedure was included in the crew training sessions. The term “rapid safing” refers to the steps that the crew must take to prepare the shuttle for an emergency landing.

Heritage Hardware. In order to streamline the payload design and qualification process, the VIEW-CPL design incorporated designs from previously flown flight hardware. Safety and performance concerns are reduced by

choosing designs similar to previously flown experiments. Table 3.3 lists the components from two flight experiments (HPP and CAPL) that were incorporated in the VIEW-CPL design. Table 3.3 also lists successful designs drawn from ground experiments that also contributed to the development of VIEW-CPL. The design of VIEW-CPL and the utilization of the heritage hardware is described in detail in Section 3.2.

Table 3.3 Hardware or designs previously used in experiments flown in the shuttle and ground-based designs.

FLIGHT EXPERIMENTS	
Source	Heritage Hardware
Heat Pipe Performance (HPP) Experiment flown on STS-66, November 1994	Papst fans, Model 8124G PIU - Board RDAS 1050 Thermik brand temperature switches PICO II, very fast acting fuses, type 251 with axial leads C&K brand locking toggle switches, part no. 7201KZQE Potter & Brumfield brand Hermetically sealed relay, KHS17D12
Capillary Pumped Loop (CAPL) Experiment flown on STS-60 Feb. 3-11, 1994	Ultra-High Molecular Weight Porous Polyethylene (UHMW-PE) from Porex Technology for capillary wick

GROUND EXPERIMENTS	
Source	Heritage Hardware
GSFC	See-through Evaporator Design
Swales Aerospace	Reservoir Design
UMCP	Water-based CPL

3.2 CPL Design

The VIEW-CPL payload was designed for flow visualization during the operation of a capillary pumped loop (CPL) in a micro-gravity environment through the use of an evaporator with a window. Deionized water was chosen

as the working fluid for VIEW-CPL because of its low toxicity and other attributes favorable for studying CPL physics. Water exhibits high surface tension and high latent heat with the added benefit of being non-toxic. However, water systems operate at pressures below atmospheric pressure, and a limit to the system performance is that the system pressure losses are on the same order as the absolute system pressure. A benefit of operating at pressures below atmospheric is that the design of components for flow visualization becomes relatively easy. The use of water at sub-atmospheric conditions also permits the investigation of CPL phenomena such as subcooling requirements and system performance limits that are obscured in high pressure systems.

CPL systems are normally made from aluminum because it is light weight and has a high thermal conductivity. However, aluminum oxidizes in the presence of water and air, making it a poor choice for the VIEW-CPL system. While the CPL system is designed to be leak tight, it was decided that trouble shooting and leak detection in the early manufacturing stages could potentially lead to conditions favorable for the corrosion of the aluminum if air was introduced into the system. In addition, some of the CPL components, such as pressure transducers, had wetted stainless steel parts. A system with water and dissimilar metals ran the risk of accelerated corrosion due to electrochemical effects. Stainless steel was chosen throughout to eliminate corrosion concerns.

A detailed figure of VIEW-CPL is shown in Figure 3.2. VIEW-CPL incorporates a simple CPL design comprised of four major components: a

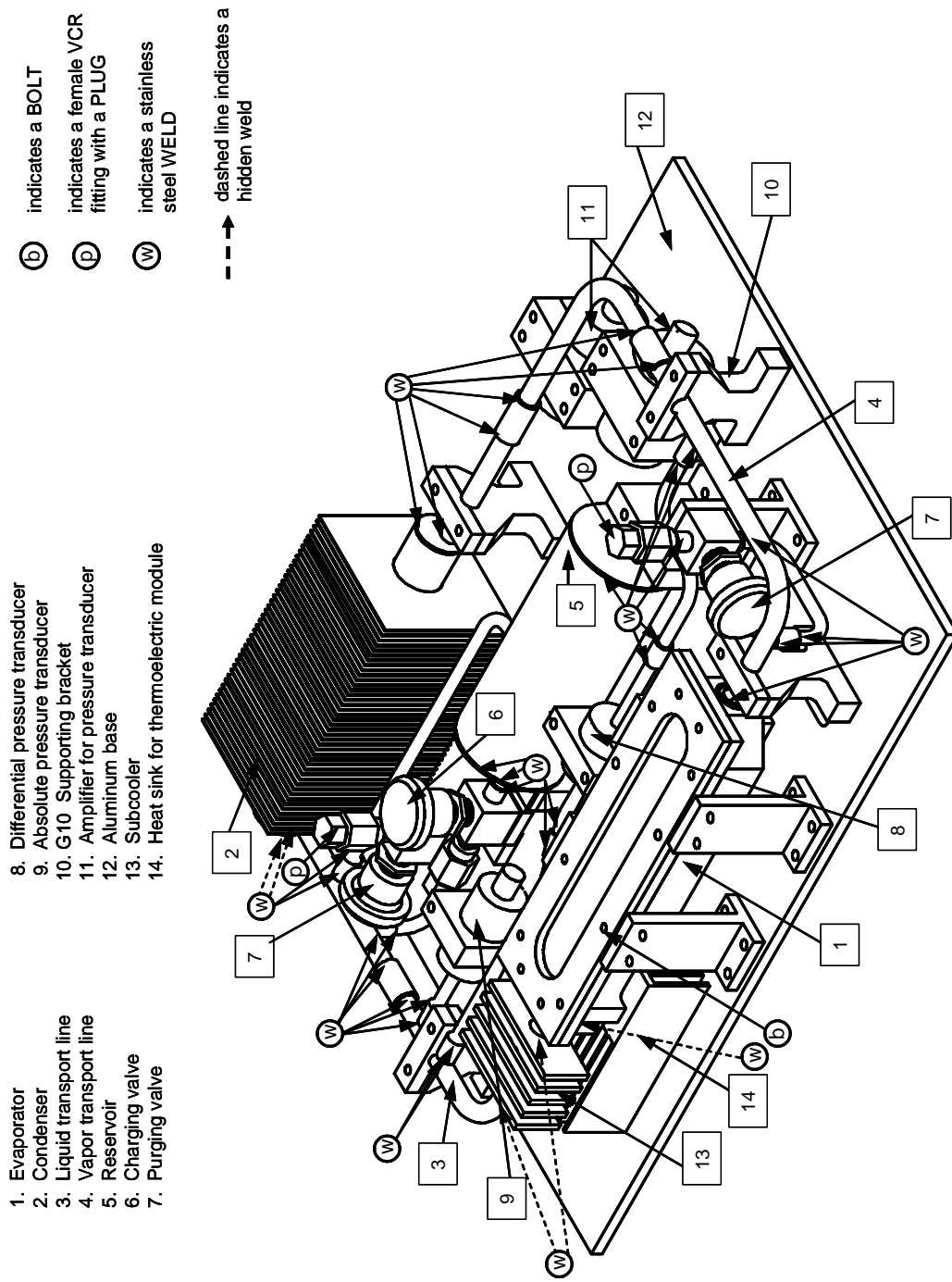


Figure 3.2 VIEW-CPL capillary pumped loop structure, shown without the protective shroud, payload control box and insulation that covers all tubing, the evaporator, and the reservoir.

capillary evaporator, a finned condenser, transport lines, and a reservoir. Not shown in Figure 3.2 are the following items: the insulation covering the transport lines, the protective polycarbonate (GE Lexan brand) shroud, the payload control box (PCB), and the fans over the heat sinks. Figure 3.3 is a rendering of the entire VIEW-CPL system enclosed in the protective Lexan shroud.

Details of the mechanical design of the CPL system are described in Sections 3.2.1 - 3.2.4. Throughout the mechanical design effort, consultation was provided by Swales Aerospace to draw upon their extensive experience in building flight qualified hardware.

VIEW-CPL PROPERTIES

Mass: 18.1 kg (39.7 lbs)

Center of gravity:

21 cm, 18 cm, 7.6 cm
(8.4 in, 7.1 in, 3.0 in)

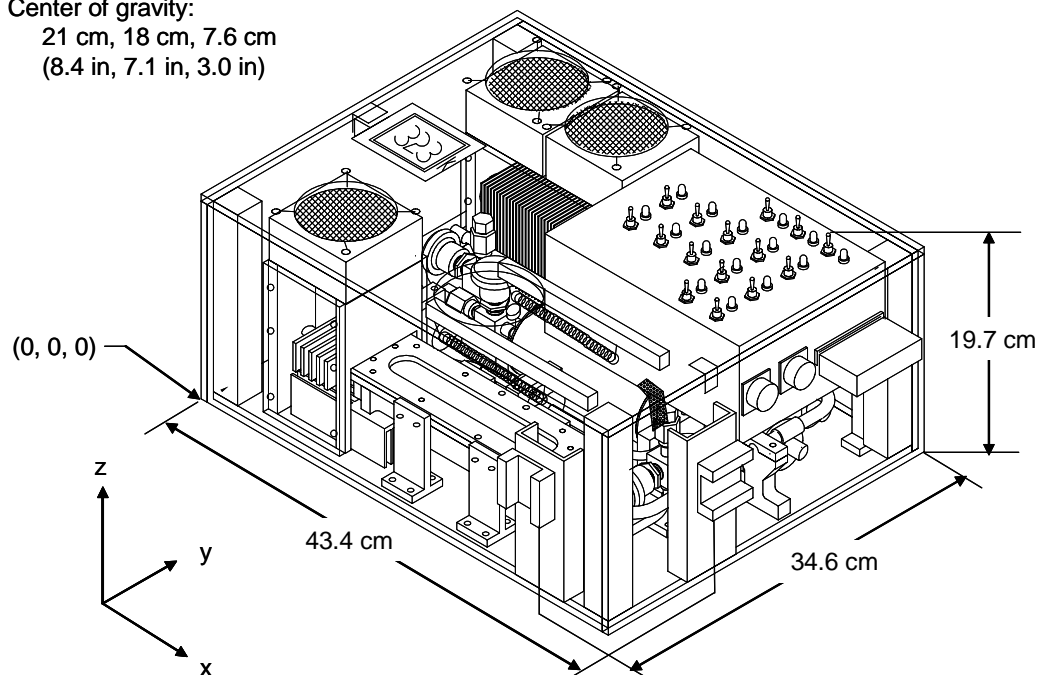


Figure 3.3 Rendering of the VIEW-CPL experiment with protective shroud, support brackets, and electronics box.

3.2.1 Evaporator design

Figure 3.4 shows the details of the VIEW-CPL capillary evaporator assembly. In order to meet the visualization objective of recording the life cycle of vapor bubbles in the liquid core of the wick, an axially halved capillary evaporator was used with a design similar to the evaporator in the work of Ku et al. [1993]. A starter pump (see Section 2.1.1) design was originally considered in order to observe the flushing action and recovery from deprime. However, the axially cut evaporator design reduces the wick core flow area to 66 mm^2 (0.10 in^2), making it difficult to include a 3-mm (1/8-in.) diameter bayonet tube without obstructing the natural flow of bubbles. Thus, a two-port capillary pump, as shown in Figure 3.4, was chosen for the study.

Mechanical Design. The capillary evaporator base is formed from a block of stainless steel with a machined groove for placement of a porous polyethylene wick. A Lexan sheet is clamped and sealed to the stainless steel base as a clear cover allowing for visualization into the capillary evaporator. To provide rigidity, a stainless steel cover plate, with a window cut-out, is used on top of the Lexan. Corners of the base were angled and pockets were cut in places where there was excess material in order to reduce the weight of the evaporator. Details on the evaporator construction are summarized in Table 3.4.

The wick was machined from a tube of porous polyethylene with axial vapor-grooves cut into the outer diameter. The wick pore-size and permeability

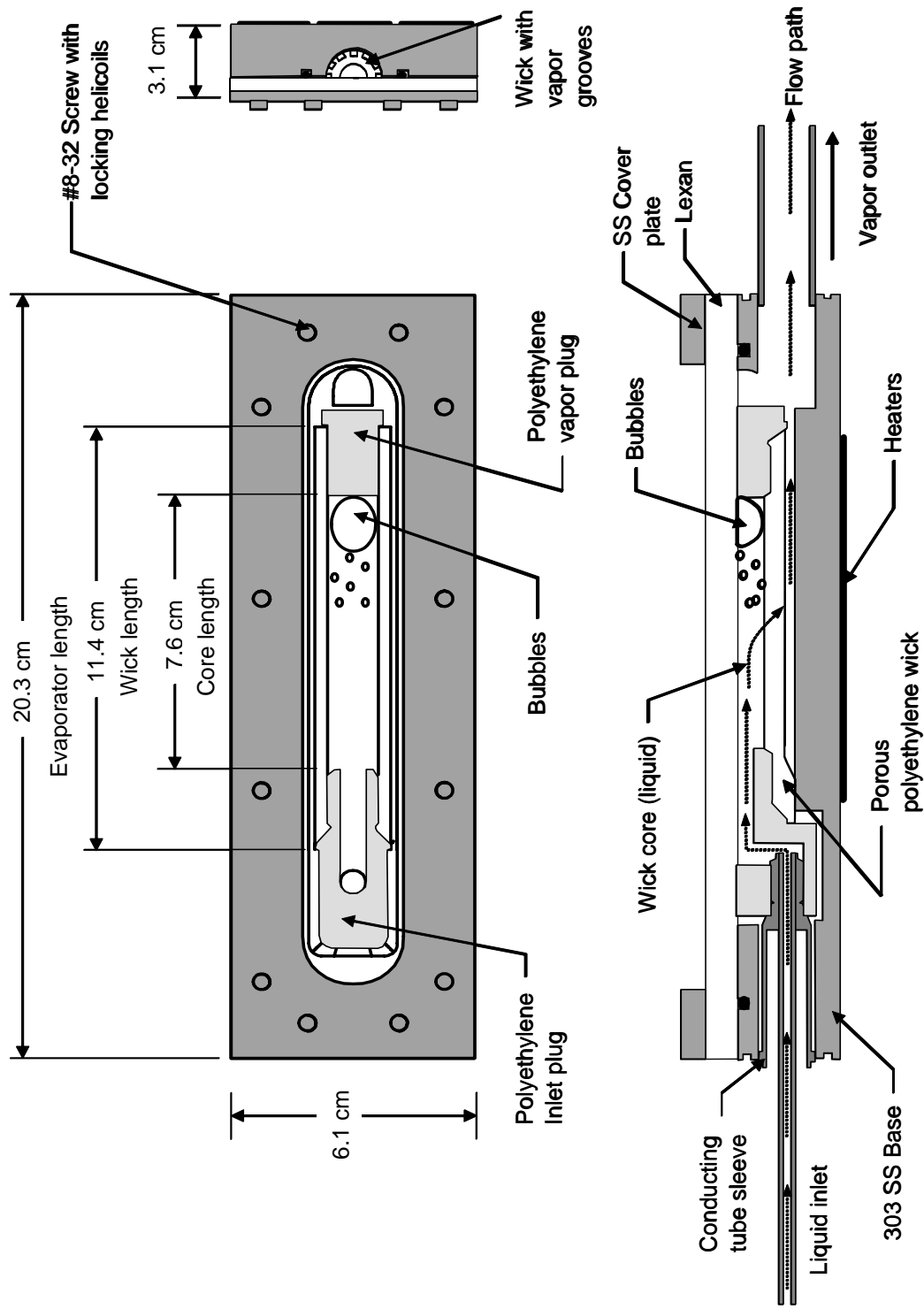


Figure 3.4 VIEW-CPL capillary evaporator with Lexan window for flow visualization capabilities.

Table 3.4 Characteristic dimensions of components in the VIEW-CPL evaporator.

Component	Characteristic Dimensions
Base	Material = 303 Stainless Steel (for machinability of intricate design) Pocketed and angled corners for reduced weight
Wick	Material = Porous Polyethylene pore size, $r_p = 13.7$ microns (measured value) permeability, $k = 6.2 \times 10^{-13} \text{ m}^2$ (measured value) porosity = 50% (measured value) Total Length = 11.4 cm (4.5 in.) Outer diameter = 22.2 mm (0.875 in.) Inner diameter = nominally 13-mm (0.51 in.) tapped to mate with threaded polyethylene plugs Core length = 7.62 cm (3.0 in.) after plugs are installed
Vapor Channels	Machined axially into the wick, starting 12.7 mm (0.5 in.) from the wick edge. 12 rectangular-grooves equally-spaced around the OD <ul style="list-style-type: none"> Only 7 grooves (5 whole + 2 halves) remain after wick is cut in half Equivalent of 6 whole grooves at final assembly Active Length = 101.6 mm (4.0 in.) Groove dimensions = 3.2-mm (0.125 in.) wide x 1.9-mm (0.075 in.) deep Groove wetted perimeter = 1.02 cm (0.40 in.) each Groove area = 0.0605 cm^2 (0.00938 in^2) each Groove hydraulic diameter = 0.238 cm (0.0938 in.) each
Clear Cover	Polycarbonate Plastic (GE brand 9034 Lexan) 20.3-cm long x 6.1-cm wide x 0.56-cm thick (7.96 in. x 2.4 in. x 0.22 in.)
Top Cover	304 Stainless Steel 0.48-cm (0.188 in.) thick Bolted 12 places with #8-32 x 2.22-cm (7/8 in.) long screws
Seals	<ul style="list-style-type: none"> Solid polyethylene plugs heat welded at wick ends Viton o-ring between Lexan and stainless base Silicone between plastic fittings and Lexan Oversized wick compressed against Lexan

are important characteristics and were measured in an alcohol bath using standard techniques [Nguyen, 1996]. The evaporator core (liquid side) is separated from the vapor side by a solid polyethylene plug. A second solid polyethylene fitting (polyethylene inlet plug in Figure 3.2) was machined in the form of a bulk head fitting and threaded into the wick. The inlet plug was sized

to have a minimum clearance of 1.3 mm (0.050 in.) between the plug and the stainless steel base to reduce conduction from the base to the inlet. The wick end fittings were heat sealed (also known as plastic welding), using a pencil size stream of hot air, to ensure that flow paths did not exist between the vapor and liquid side that would be larger than the largest pore size in the wick.

Once the wick and end fittings were assembled, the wick was laid in the groove in the evaporator base and cut in half with a 0.5 mm (0.019 in.) excess height. The excess was to allow compression of the wick assembly in order to form a tight seal with the Lexan cover. Since the polyethylene wick would compress more than the solid polyethylene end fittings, a line of silicone sealant was placed on the end fittings (not on the porous wick), with a hypodermic needle, prior to tightening the Lexan cover.

A viton o-ring is used to seal between the stainless steel base and the Lexan cover. The bolt pattern for attaching the Lexan and stainless steel cover plate is uniform with a spacing slightly under 6.4mm (0.25 in.) around the o-ring groove to achieve uniform compression of the o-ring. Locking devices (Helicoil inserts) were used to ensure the screws did not back out during the vibrations associated with launch.

Thermal Design. A conducting tube sleeve assembly was used to reduce conduction from the stainless base to the subcooled liquid flowing to the evaporator through the liquid line. The broken conduction path was necessary based on observations during tests, conducted at Goddard Space Flight Center

by the University of Maryland, with a see-through evaporator [Ku et al., 1993]. As shown in Figure 3.5, a 9.5-mm (0.375 in.) OD 316L stainless steel tube, with 0.8-mm (0.030 in.) wall, surrounds the 3.2-mm (0.125 in.) OD liquid inlet tube. The outer tube is welded to the evaporator base while the liquid inlet tube passes to the polyethylene inlet plug without contacting the hot evaporator base. Thus, conduction heat leaks from the base to the inlet tube must follow the path of the outer tube through a cross-section of only 21 mm² (0.033 in.²) over a distance of 25 mm (1 in.).

Three heaters are attached to the base of the evaporator block to enable various power input conditions specified for the operation of VIEW-CPL. The heaters are turned on and off manually by activating switches. Four normally closed thermostats are attached to the evaporator to interrupt the heater power if the evaporator temperature exceeds 60°C. Details of the evaporator electronic

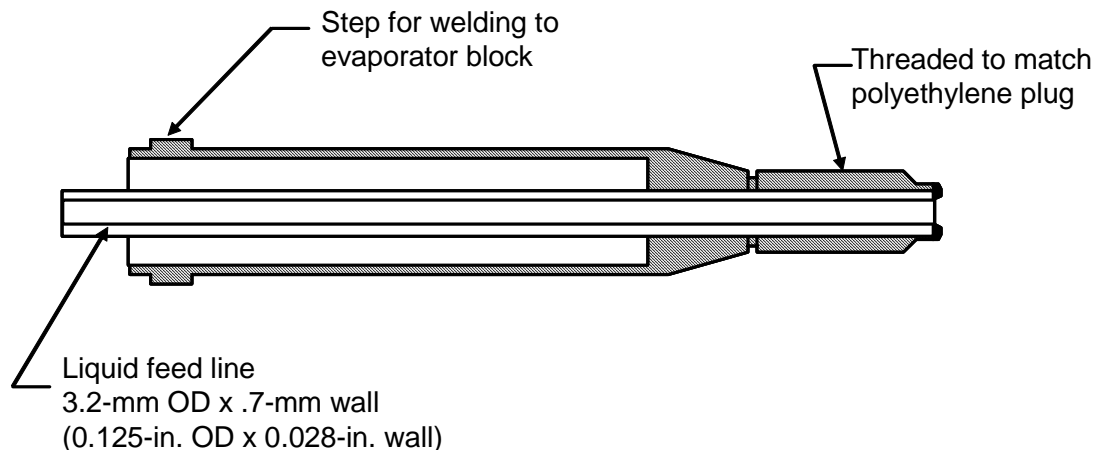


Figure 3.5 Cross-section of conducting tube assembly used to increase the resistance to conduction from the evaporator block to the liquid feed line.

components are provided in Sections 3.3.1 and 3.3.2.

Since the evaporator body has a low thermal conductivity, a significant temperature gradient exists between the heater surface and the evaporating fluid inside the evaporator. The minimum distance between the heaters and the working fluid is 9.8 mm (0.387 in.) which occurs at the bottom of the semicircular cut-out for the wick. Assuming 75 W (maximum heater power) is evenly distributed over the available heater area of 62 cm² (9.6 in.²), the expected temperature difference between the heated surface and the fluid is 8 K according to steady-state conduction calculations. This temperature difference was accounted for in the design of the thermostats to allow nominal operation at 50°C.

The time required to cool-off the evaporator between tests is another concern when using a stainless steel evaporator. A seven-hour cool-down period for the evaporator was predicted using a lumped capacitance assumption

$$\frac{d}{dt}(mcT) = -hA_s(T - T_\infty) \quad (3.1a)$$

where m is the mass of the evaporator, c is the specific heat of the evaporator, h is the convection coefficient inside the cabin, A_s is the surface area of the evaporator T is the final evaporator temperature as a function of time, t, with an uninsulated evaporator transferring heat to the cabin air resulting in

$$t = \frac{mc}{hA_s} \ln \left(\frac{T - T_\infty}{T_o - T_\infty} \right) \quad (3.1b)$$

where T_0 is the initial evaporator temperature and T_∞ is the air temperature. Table 3.5 lists the parameters used to model the cool-down period. Since such a long cool-down period was undesirable, a thermoelectric cooling module was installed on the evaporator base to decrease the time (see Section 3.3 for details on the thermoelectric cooling module).

Subcooling requirements. The capillary pressure rise across the meniscus in the evaporator causes a difference between the saturation temperature of the vapor and the saturation temperature of the liquid core, as described in Section 2.1.1. At 75 W, the viscous pressure drop in the VIEW-CPL system is 0.255 kPa (1.76 psi), resulting in a saturation temperature difference of 0.4 K when the vapor saturation temperature is 50°C. This requires that the fluid in the liquid core be cooled 0.4 K below the vapor saturation temperature. If not, then the possibility of flashing and forcing vapor into the liquid core exists because the liquid will enter at a temperature above the local saturation temperature of the liquid. There was a concern that the low flow rate in the loop will not be able to prevent heat transfer to the liquid inlet via conduction. Peclet numbers for the liquid line ranged from 4.4 to 33 for 10 W and 75 W, respectively. Since Pe is less than 100, axial conduction can be important in transferring heat from the evaporator to the liquid inlet. A fan-cooled subcooler was included in the VIEW-CPL design as a precautionary step to ensure adequate subcooling.

Table 3.5. Parameters used to estimate the cool-down time for the uninsulated VIEW-CPL evaporator transferring heat via convection with ambient Middeck cabin air.

Symbol	Description	Value
T_{∞}	Middeck cabin air temperature ^a	29.4°C (85°F)
T_o	Initial evaporator temperature	60°C (140°F)
T	Final evaporator temperature	40°C (104°F)
h	Heat transfer coefficient for convection ^a	1.42 W/m ² -K (0.25 Btu/hr-ft ² -°F)
c	Specific heat of stainless steel ^b	477 J/kg/K (0.114 Btu/lb-°F)
A_s	Evaporator surface area Bottom: 20.3 cm x 6.1 cm (8 in. x 2.4 in.) 2 Long Sides: 20.3 cm x 2.1 cm (8 in. x 0.825 in.) 2 Short Sides: 6.1 cm x 2.1 cm (2.4 in. x 0.825 in.)	0.023 m ² (36 in. ²)
m	Evaporator mass	1.67 kg (3.67 lb)
k	Thermal conductivity of stainless steel ^b	14.9 W/m-K (8.6 Btu/hr-ft-°F)
L	Evaporator length	20.3 cm (8 in.)
Bi	Biot number, $Bi = h \cdot L / k$	0.02
t	Time required to cool-down	7.2 hours

^a[NASA JSC,1996a]

^b[Fox and McDonald, 1985]

3.2.2 Condenser and subcooler design

Condenser. The VIEW-CPL condenser section is a finned tube with forced air flowing over the outside finned portion of the tube and steam/water flowing inside the tube, as shown schematically in Figure 3.6. Characteristics of the condenser components are summarized in Table 3.6. The outside of the condenser incorporates square copper fins brazed to the outside of a 316L

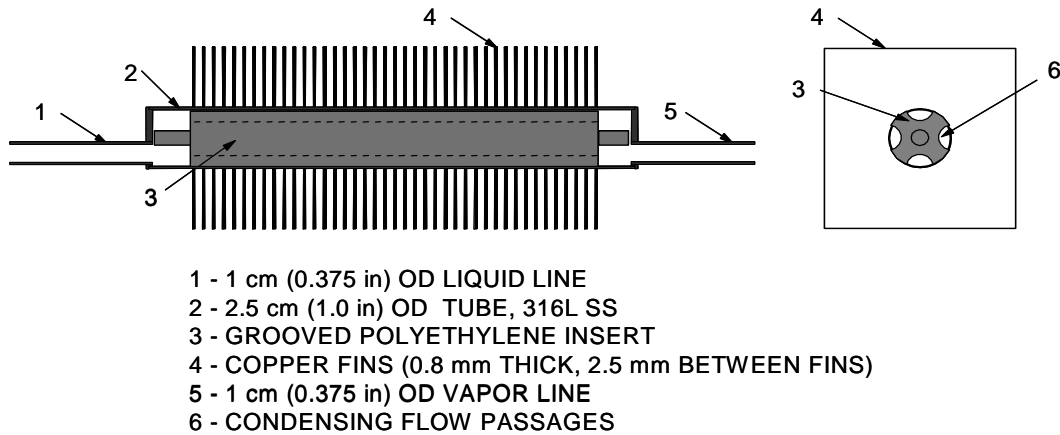


Figure 3.6 VIEW-CPL copper-finned condenser with polyethylene insert.

Table 3.6 Characteristic dimensions of components in the VIEW-CPL condenser.

Component	Characteristic Dimensions
Copper Fins	Quantity = 41 Spacing = 2.5 mm (0.098 in.) between fins 7.2-mm (3.0-in.) square x 0.8-mm (0.032-in.) thick 2.57-cm (1.01-in.) diameter hole, centered Active condenser length = 13.5 cm (5.33 in.)
Stainless Outer Tube	Length = 17.8 cm (7.0 in.) 2.5-cm (1.0-in.) OD with 0.9-mm (0.035-in.) wall
60/40 lead/tin solder	Centered on stainless tube over a length of 13.8 cm (5.45 in.)
Polyethylene Insert	Length = 14.2 cm (5.6 in.) 4 grooves for vapor channels Groove wetted perimeter = 2.4 cm (0.945 in.) each Groove area = 0.368 cm ² (0.057 in. ²) each Groove hydraulic diameter = 0.61 cm (0.24 in.)

stainless steel tube. The central section of the stainless steel tube was plated with 60/40 lead/tin solder to coat the area where 41 copper fins were to be attached. The fins were sheared in strips and cut square to minimize machining time; the fins were then stacked and a hole, slightly greater than the diameter of the plated stainless steel tube, was drilled through. A fixture was made to ensure

that the fins were evenly spaced as they were slipped onto the stainless steel tube and individually soldered in place.

A grooved solid-polyethylene rod is inserted inside the condenser tube to reduce the fluid volume and hence reduce the system charge. Short posts are positioned on the ends of the grooved rod to prevent the rod from moving to the end of the condenser tube and blocking the flow path at either the vapor inlet or liquid exit. The polyethylene rod is also sized slightly smaller than the condenser to prevent it from melting when welding on the endcaps. The condenser inlet and exit tubes are attached to the bottom of the endcaps to prevent liquid puddling in the bottom of the condenser during ground testing.

Air-side pressure drop. For the air-cooled condenser, the operating condition can be determined from the fan curve. The air-flow over the condenser fins is driven by two fans, PAPST Model 8124G [PAPST, 1994]. The fans are mounted on top of the condenser, and the air is directed over the fins using Lexan ducts. The arrangement is shown schematically in Figure 3.7. The pressure drop calculations and fan curves were evaluated to determine the fan operating point as shown in Figure 3.8.

For the VIEW-CPL condenser, the pressure drop for air flowing through the condenser system includes:

- (1) pressure drop in the duct surrounding the condenser,
- (2) pressure drop in accelerating flow at contractions (i.e., duct to fins),
- (3) pressure drop due to expansions (i.e., fins to duct),

- (4) pressure drop between fins,
- (5) pressure drop due to flow around a cylinder at the condenser tube,
- (6) pressure drop due to bends, and
- (7) pressure drop due to screens or filters.

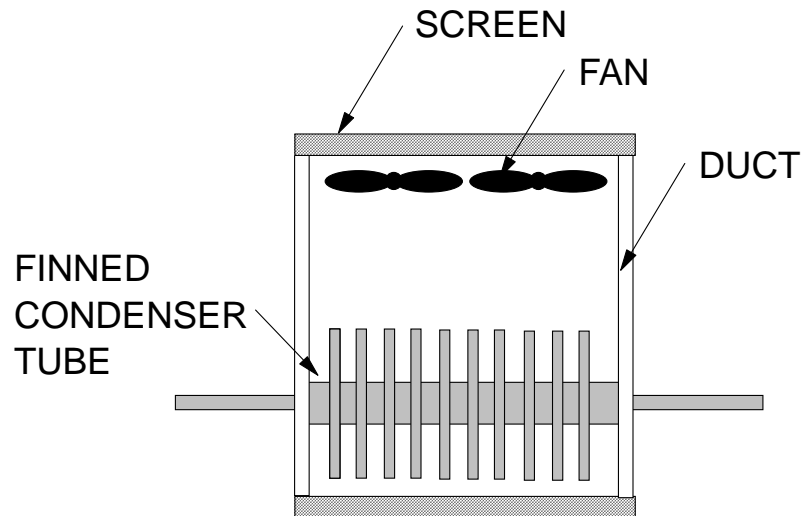


Figure 3.7 Schematic of the VIEW-CPL air-cooled condenser with fans and duct.

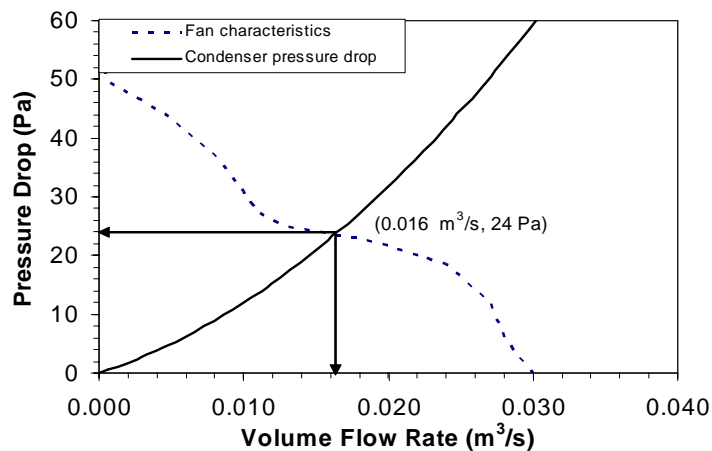


Figure 3.8 Fan performance and system curves for the VIEW-CPL air-cooled condenser. Volume flow rate reflects rate available from two fans.

Determining the appropriate pressure drop for the seven components described above involves determining the appropriate loss coefficients, K , and velocities to characterize the pressure drop using

$$\Delta P = \rho K \frac{\bar{V}^2}{2} \quad (3.2)$$

Table 3.7 gives loss coefficients for the flow conditions described in (1) through (7) along with the values for the VIEW-CPL geometry. The intersection of the pressure drop on the fan characteristic curve, shown in Figure 3.8, determines the flowrate of air flowing through the condenser. The flow rate can then be used to find the pressure drop and heat transfer coefficients for the finned condenser.

Heat transfer coefficients for finned condenser. Two overall heat transfer coefficients, U_1 and U_2 , are determined for the air-cooled condenser. U_1 is the overall heat transfer coefficient for the condensing length of the condenser, and U_2 is the overall heat transfer coefficient for the remaining length. The difference between U_1 and U_2 is the change in the internal heat transfer coefficient, h_i , as the fluid transitions from two-phase flow to single-phase flow after the condensing length. The remainder of the condenser resistance is the same for both the condensing and non-condensing sections, and the overall heat transfer coefficient is calculated from [Incropera and DeWitt, 1990]:

$$\frac{1}{UA} = \frac{1}{(\eta_o h A)_{air}} + \frac{\ln(d_o/d_i)}{2\pi k L} + \frac{1}{(h A)_i} \quad (3.3)$$

Table 3.7 Loss coefficients for determining pressure drop for flow through the VIEW-CPL finned condenser system.

	Loss Coefficient	Parameters	Pressure Drop (Pa)
1	Ducts $K_{laminar} = \frac{64}{Re} \frac{L}{D_h}$ $K_{turbulent} = 0.3164 Re^{-0.25} \frac{L}{D_h}$ Re based on hydraulic diameter, D_h	Lexan duct after the fans $D_h = 3.87$ in, $L = 3$ in $V_{duct} = 1.60$ m/s, $Re_D = 9970$ $K = 0.025$	0.04
2	Contractions <ul style="list-style-type: none"> determined graphically [Fox and McDonald, 1985] velocity based on smaller flow area 	Contraction from duct to fins $V_{fins} = 2.12$ m/s ; $K = 0.12$ Contraction from between fins before tube to fins after tube $V_{tube} = 3.19$; $K = 0.15$	0.31 0.88
3	Expansions <ul style="list-style-type: none"> determined graphically [Fox and McDonald, 1985] velocity based on smaller flow area 	Expansion at exit of condenser Area ratio = .7 $K = .1$ $V = 2.12$ m/s	0.26
4	Fins $K_{fins} = 4 \frac{Po}{Re_{D_h}} \frac{L}{D_h}$ <ul style="list-style-type: none"> $Po = C_f Re_{D_h}$ can be determined graphically for a given aspect ratio [White, 1991] 	Fins before tube: $D_h = 0.189$ in, $L = 1$ in, $V_{fins} = 2.12$ m/s, $Po = 24$, $Re = 642$, $K = 0.79$ Fins at tube $D_h = 0.178$ in, $L = 1$ in, $V_{fins} = 3.19$ m/s, $Po = 24$, $Re = 906$, $K = 0.59$	2.06 3.50
5	Flow around cylinder: $K = C_D$ <ul style="list-style-type: none"> C_D is the drag coefficient determined graphically based on Reynolds number [Fox and McDonald, 1985] 	$V = 2.12$ m/s $K = 1.5$	3.93
6	Bends <ul style="list-style-type: none"> same as ducts using equivalent length, L_e/D Fox and McDonald [1985] provide L_e/D for bends based on deflection angles 	90° bend between fins (after the tube) $L_e/D = 20$ $K = 3.0$ $V_{fins} = 2.29$ m/s	7.83
7	Screens K found from charts based on screen free area ratio and screen to duct area [ASHRAE Fundamentals, 1997]	20 x 20 Square mesh screens wire diameter = 0.49 Duct flow area ratio = 1 $K = 1.76$ $V = 1.60$ m/s	5.23 (for two screens)
	TOTAL PRESSURE DROP		24.04 Pa

The first term in Eq. 3.3 is the air-side resistance and depends upon the geometry of the fins. The second term is the conduction through the condenser tube, and the final term is the internal heat transfer coefficient.

The square-finned condenser shown in Figure 3.6 can be described as a single finned row of the plate fin geometry. The important dimensions for determining the air-side heat transfer coefficient are the tube outer diameter, d , the spacing between the fins, s , the fin thickness, t_{fin} , and the heat exchanger depth, w (same as the fin width for a single row). Webb [1980] summarizes various correlations for the j factor ($j = St Pr^{2/3}$) as a function of the Reynolds number for air flow through the flow passage area, A_c ,

$$Re = \frac{G_c D_h}{\mu} \quad (3.4)$$

$$D_h = \frac{4A_c w}{A} \quad (3.5)$$

The Nusselt number is

$$Nu = j Re Pr^{1/3} \quad (3.6)$$

with the j factor is determined graphically for the given fin pitch. Webb [1980] suggests that the j factor for single row tubes is 30% lower than deep tube bundles; therefore, the j factor determined graphically was reduced by 30% for the VIEW-CPL condenser. The air-side heat transfer coefficient is then determined from the definition of the Nusselt number

$$h = \frac{Nuk}{s - t_{fin}} \quad (3.7)$$

The overall surface efficiency, η_o , is calculated from the finned surface area, A_f , the total surface area, A_t , and the fin efficiency, η_f :

$$\eta_o = 1 - \frac{A_f}{A_t}(1 - \eta_f) \quad (3.8)$$

The fin efficiency for annular fins of rectangular profile are plotted by Incropera and DeWitt [1990] based upon fin parameters of length, thickness, and thermal conductivity; tube outer radius; and heat transfer coefficient. The fin efficiency curves for various values of $(L_c + r_1)/r_1$ are plotted versus the parameter $L_c^{3/2}(h/kL_c t)^{1/2}$ where L_c is the corrected fin length calculated from $L + t/2$. As shown in Figure 3.9, the fin length is not constant in the case of a square fin. The fin length varies according to

$$L(\theta) = \left\{ \begin{array}{ll} \frac{w}{2|\cos\theta|} - r_1 & 0 \leq \theta \leq \frac{\pi}{4}, \frac{3\pi}{4} \leq \theta \leq \frac{5\pi}{4}, \frac{7\pi}{4} \leq \theta \leq 2\pi \\ \frac{w}{2|\sin\theta|} - r_1 & \frac{\pi}{4} \leq \theta \leq \frac{3\pi}{4}, \frac{5\pi}{4} \leq \theta \leq \frac{7\pi}{4} \end{array} \right\} \quad (3.9)$$

The efficiency for the square fin is approximated by averaging the maximum and minimum efficiencies based on the minimum and maximum fin length, respectively. For the VIEW-CPL geometry the minimum fin length is 25.4 mm (1 in.) resulting in a fin efficiency of 86% and the maximum length is 41.1 mm (1.62 in.) for 75% efficiency, which averages to a total efficiency of 81%. Since the

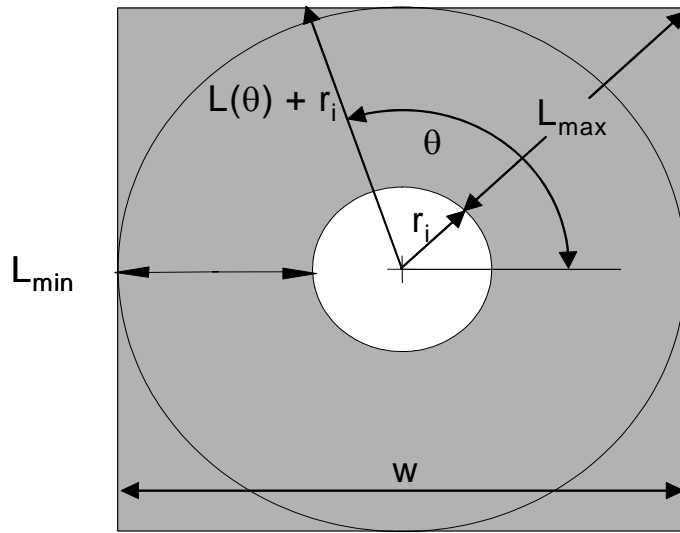


Figure 3.9 Geometrical characteristics of a square fin.

ratio of fin area to the total surface area is nearly unity, the overall surface efficiency η_o is also 81%.

Table 3.8 summarizes the heat transfer through the VIEW-CPL condenser components for the external conductance. The air-side heat transfer coefficient is $49 \text{ W/m}^2\text{-K}$, determined from Eqs. 3.4 through 3.7. The conductance, per unit length on the air side and through the tube wall is 130 W/m-K and 1160 W/m-K , respectively, resulting in a total external conductance of 117 W/m-K .

For a typical air-cooled condenser, the inner heat transfer coefficient for the two-phase flow is much larger than the heat transfer coefficient for the air side. However this is not the case for VIEW-CPL which operates with a low flow rate and under micro-gravity conditions. The condenser is divided into an active length, L_a , and a liquid-covered length, $L-L_a$. Therefore, there are two different internal heat transfer coefficients. Carey [1992] derives a formulation for the heat

Table 3.8 External conductance calculations through VIEW-CPL condenser components on a per unit length basis.

Component	Governing Equation(s)	Values
Air side	$Nu = jRePr^{1/3} \quad (3.6)$ $h = \frac{Nuk}{s-t} \quad (3.7)$	<p>$j = 0.007$ (degraded from 0.010) $Re = 713$, $Pr = 0.71$, $Nu = 6.49$</p> <p>$k = 401$ W/m-K, $s = 0.33$ cm / fin, $t = 0.81$ mm (0.032in) $h = 49$ W/m²-K</p>
Fins	$\eta_o = 1 - \frac{A_f}{A_t}(1 - \eta_f) \quad (3.9)$ $\frac{hA_{air}}{L} = \frac{\eta_o hA}{L} \quad (\text{From 3.3})$	<p>$\eta_f = 0.86$ for $L = 2.82$ cm (1.11 in.) $\eta_f = 0.75$ for $L = 4.11$ cm (1.62 in.) $\eta_{f,avg} = 0.805$</p> <p>$A_f = 0.435$ m², $A_t = 0.443$ m² Active Length = 0.135 m (5.33 in.) $A / L = 3.27$ m²/m $\eta_o = 0.81$, $hA_{air} / L = 130$ W/m-K</p>
Tube	$\frac{UA_{tube}}{L} = \frac{2\pi k}{\ln(d_o/d_i)} \quad (\text{From 3.3})$	<p>$k = 13.4$ W/m-K [Note 1] $d_o = 2.54$ cm (1.0 in.) $d_i = 2.36$ cm (0.93 in.) $UA_{tube} / L = 1160$ W/m-K</p>
Total External Conductance	$\frac{UA_{ext}}{L} = \left(\frac{L}{UA_{tube}} + \frac{L}{UA_{air}} \right)^{-1} \quad (\text{From 3.3})$	<p>$UA_{ext} = 117$ W/m-K</p>

transfer coefficient if it is dominated by conduction through the liquid (of thickness δ) at the heat transfer surface. The derivation is based on the momentum balance of a differential element (dz in the axial direction and y distance from the tube wall) in the liquid that includes the hydrodynamic body force, $\rho_l g$, and the interfacial shear stress, τ_i , and dP/dz for the total axial pressure gradient (gravity, friction, and deceleration)

$$(\delta - y)dz \left[\rho_l g - \frac{dP}{dz} \right] + \tau_i dz = \mu_l \left(\frac{du}{dy} \right) dz \quad (3.10)$$

with inertia and downstream diffusion contributions neglected, for downwards flow in a vertical tube. In this derivation, radial effects from the round tube geometry are neglected and the terms in Equation 3.10 are based on one-dimensional two-phase separated-flow analysis. For VIEW-CPL operations in micro-gravity, the body force term is neglected. The pressure gradient is constant along the tube diameter and can be determined from a sum of the frictional and deceleration pressure gradients for the vapor

$$\frac{dP}{dz} = -\frac{4\tau_i}{(D-2\delta)} - \frac{2xDG^2}{\rho_v(D-2\delta)} \frac{dx}{dz} \quad (3.11)$$

where D is the tube diameter, τ_i is the interfacial shear stress approximated by a single-phase correlation in a round tube for the vapor (because liquid flow is much slower than the vapor flow)

$$\tau_i = f_v \left(\frac{\rho_v u_v^2}{2} \right) = f_v \left(\frac{G^2 x^2}{2\rho_v(1-4\delta/D)} \right) \quad (3.12)$$

and G is the mass flux

$$G = \frac{\dot{m}}{A} \quad (3.13)$$

The deceleration term (last term in Equation 3.11) is approximated from

$$\left(\frac{dP}{dz} \right)_{dec} = -G^2 \frac{d}{dz} \left[\frac{x^2}{\rho_v \alpha} + \frac{(1-x)^2}{\rho_l(1-\alpha)} \right] \quad (3.14)$$

by assuming that the liquid density is much larger than the vapor density, that the film is thin, and that the variation in the void fraction, α , along the tube is small compared to the variation in quality, x . The quality gradient is evaluated from an energy balance with the amount of heat transferred to the wall equal to the amount of vapor condensed

$$h\pi D(T_w - T_{sat}) = \dot{m}\lambda \frac{dx}{dz} = G \left(\frac{\pi D^2}{4} \right) \lambda \frac{dx}{dz} \quad (3.15)$$

and the local condensation heat transfer coefficient is a function of the axial distance, z , and the local film thickness, $\delta(z)$

$$h(z) = \frac{k_l}{\delta(z)} \quad (3.16)$$

for conduction-dominated laminar flow. The local film thickness is found at each location along the length of the condensing section by satisfying

$$\rho_l \lambda \left[\left[\frac{\tau_i}{(D - 2\delta)} + \frac{x G k_l (T_{wall} - T_{sat})}{\rho_v \lambda \delta (D - 2\delta)} \right] \delta^4 + \tau_i \frac{\delta^3}{3} \right] = k_l \mu_l (T_{sat} - T_{wall}) z \quad (3.17)$$

where the interfacial shear stress (τ_i) and the mass flux (G) are determined by Equations 3.12 and 3.13, respectively. The average heat transfer coefficient over the condensing length is determined by

$$\bar{h} = \frac{\int_0^L h(z) dz}{\int_0^L dz} \quad (3.18)$$

and is plotted as a function of net evaporator power in Figure 3.10. The net evaporator power is the electrical heat minus the heat loss. The traces in Figure 3.10 were calculated for the VIEW-CPL condenser geometry and saturation temperature 50°C with air temperature at 25°C. The internal heat transfer coefficient is weakly dependent on the air temperature resulting in an approximate change of 1.3% per degree variance from 25°C over the power range (based on calculations, not shown in Figure 3.10). Curve fits to the heat transfer coefficient and the condensing length are shown and are used in bubble dynamic models developed in Chapter 4.

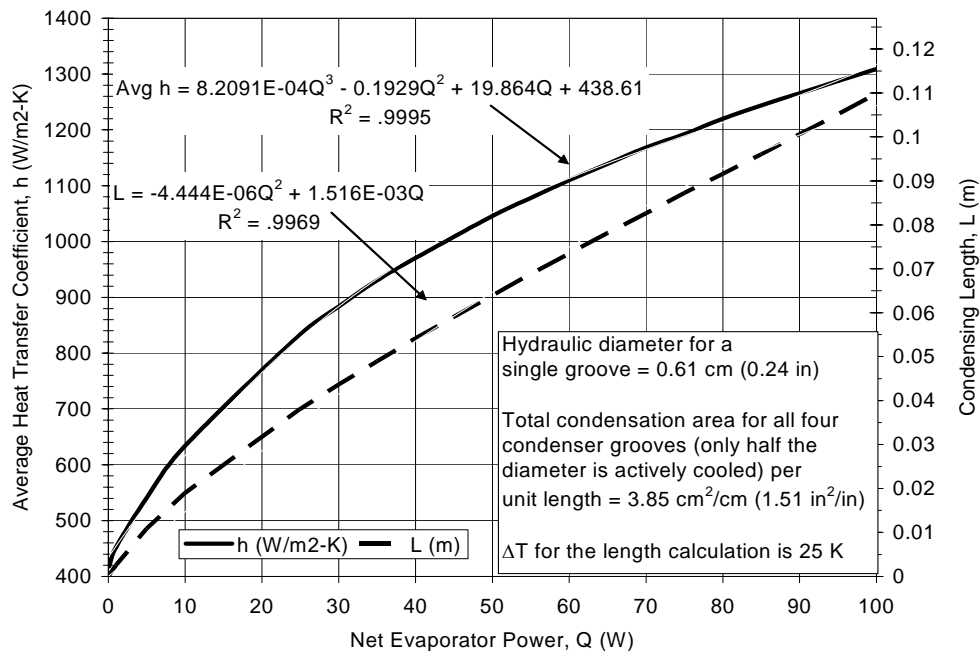


Figure 3.10 Condensation film coefficient and condensing length as a function of net evaporator power (total power minus heat loss to ambient) for VIEW-CPL.

For the non-condensing portion, the inner heat transfer coefficient is determined from $Nu = 4.36$ for a circular tube with uniform heat flux in the laminar flow regime [Incropera and DeWitt, 1990]. The resulting heat transfer coefficient for the single-phase liquid flow is $458 \text{ W/m}^2/\text{K}$. The thermal capacitance of the air is much larger than that of the water because of the high flow rate driven by the fans. The air temperature rise is so small that it is not noticeable for all cases within the design range of 10 to 75 W evaporator heater power. The steady-state temperature profile of the water in the condenser is plotted in Figure 3.11 for 5, 25, and 75 W net evaporator heat-loads. As shown in Figure 3.11, sufficient subcooling will be developed because the liquid exiting the condenser is at the same temperature as the air. The wall temperature (not shown on figure) over

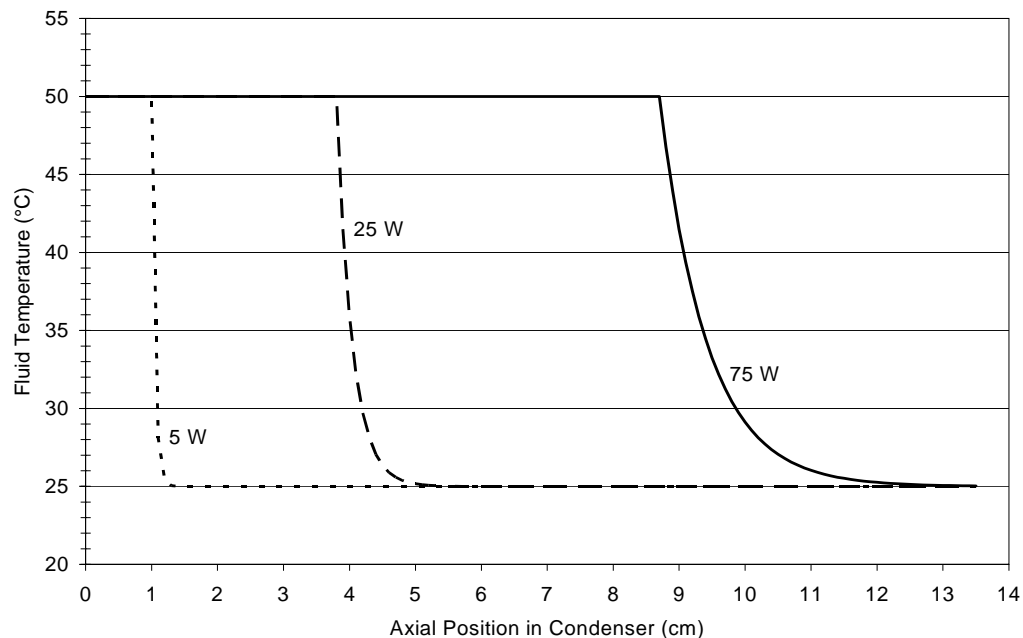


Figure 3.11 Water temperature profile in the condenser for net evaporator power of 5, 25, and 75 W.

the condensing portion is 28.8, 30.4, and 32.0°C for 5, 25, and 75 W, respectively. These values are well below the safety limit of 60°C.

Two-phase pressure drop. A one-dimensional separated-flow model is used to estimate the steady-state two-phase pressure drop [Carey, 1992]. For the one-dimensional assumption, the fluid properties are considered constant over the cross-section of the tube and the velocities of the liquid and vapor phases are uniform over the portion of the channel occupied by each (that does not necessarily mean that the liquid and vapor phase velocities are equal). For steady flow, the interfacial shear forces balance and the resulting momentum balance is a combination of frictional terms and acceleration terms as follows

$$-\left(\frac{dP}{dz}\right)_{dec} = -\left(\frac{dP}{dz}\right)_{fr} + \frac{d}{dz}\left(\frac{G^2 x^2}{\rho_v \alpha} + \frac{G^2 (1-x)^2}{\rho_v (1-\alpha)}\right) \quad (3.19)$$

The body forces are neglected and the tube is assumed to have a constant cross-sectional area. Using a two-phase multiplier

$$\phi_{lo} = \left[\frac{(dP/dz)_{fr}}{(dP/dz)_{lo}} \right]^{1/2} \quad (3.20)$$

that is based on the ratio of the two-phase frictional pressure drop to the pressure drop if only liquid (lo = liquid only) were flowing in the tube at the same total mass flow rate and a pressure gradient determined by single-phase flow, the frictional pressure gradient is

$$\left(\frac{dP}{dz}\right)_{fr} = \phi_{lo}^2 \left(\frac{dP}{dz}\right)_{lo} = \frac{f_{lo}}{2} \frac{G^2}{\rho_l D_h} \phi_{lo}^2 \quad (3.21)$$

where f_{lo} is the Darcy friction factor. The two-phase multiplier for round tubes is

$$\phi^2 = 1 + (C/\chi_{tt}) = (1/\chi_{tt}^2) \quad (3.22)$$

where χ_{tt} is the Martinelli Nelson parameter which is a function of quality, x , and may be approximated by

$$\chi_{tt} = \left[\frac{1-x}{x} \right]^{0.9} \left[\frac{\rho_v}{\rho_l} \right]^{0.5} \left[\frac{\mu_l}{\mu_v} \right]^{0.14} \quad (3.23)$$

and C is 20 for turbulent vapor – turbulent liquid flow, 12 for turbulent vapor - laminar liquid flow, 10 for laminar vapor – turbulent liquid flow and 5 for laminar vapor – laminar liquid flow. The relationship between the liquid two-phase multiplier (in the area occupied by liquid) and the liquid-only two-phase multiplier is

$$\phi_{lo}^2 = \phi_l^2(1-x)^{1.75} \quad (3.24)$$

The acceleration term can be approximated by

$$\frac{d}{dz} \left(\frac{G^2 x^2}{\rho_v \alpha} + \frac{G^2 (1-x)^2}{\rho_v (1-\alpha)} \right) \approx G^2 \left(\frac{1}{\rho_v} - \frac{1}{\rho_l} \right) \quad (3.25)$$

[Fredley and Braun, 1988]. The resulting pressure gradient over the length of the condenser is

$$\Delta P = - \left(\frac{f_{lo}}{2} \frac{G^2}{\rho_l D_h} \int_0^L \phi_{lo}^2 (1-x)^{1.75} dz \right) + G^2 \left(\frac{1}{\rho_v} - \frac{1}{\rho_l} \right) \quad (3.26)$$

Most derivations assume a linear relationship between quality and length. A comparison of various fluids, temperature and powers during VIEW-CPL analysis indicated that this assumption over-predicts the pressure drop by 5 to 15% with

the error decreasing as temperature increases. Since the error is on the same order as the accuracy of the calculation of heat transfer coefficient, the assumption is also used in this study and the pressure drop determined from Equation 3.26.

Subcooler. A subcooler was added to the VIEW-CPL evaporator inlet as extra protection against any unpredicted on-orbit conditions that would allow the liquid line temperature to increase. Because the condenser was sufficiently sized and the evaporator inlet design protected the liquid from heat conduction from the evaporator, the subcooler was not necessary and did not affect the VIEW-CPL operations. The subcooler fan was used to provide adequate air circulation to cool the VIEW-CPL electronics box. The following paragraphs summarize the subcooler design for completeness.

The air-cooled aluminum subcooler, shown in Figure 3.12, is attached to a reducer fitting on the liquid line just before the evaporator. The reducer fitting connects the 9.5-mm (0.375 in.) OD liquid line to the 3.2-mm (0.125 in.) OD evaporator liquid inlet line. Air is pulled over the subcooler with the same style fan, PAPST Model 8124G, that is used on the condenser. However, the intake air is used for multiple cooling purposes before it is used to cool the subcooler. Figure 3.13 is a flow diagram of the path the intake air follows as it flows to the subcooler. The air comes from the far side of the experiment and is drawn across the electronics box, reservoir, and evaporator. As the air passes underneath the evaporator it is drawn through the finned TEC heat sink and into

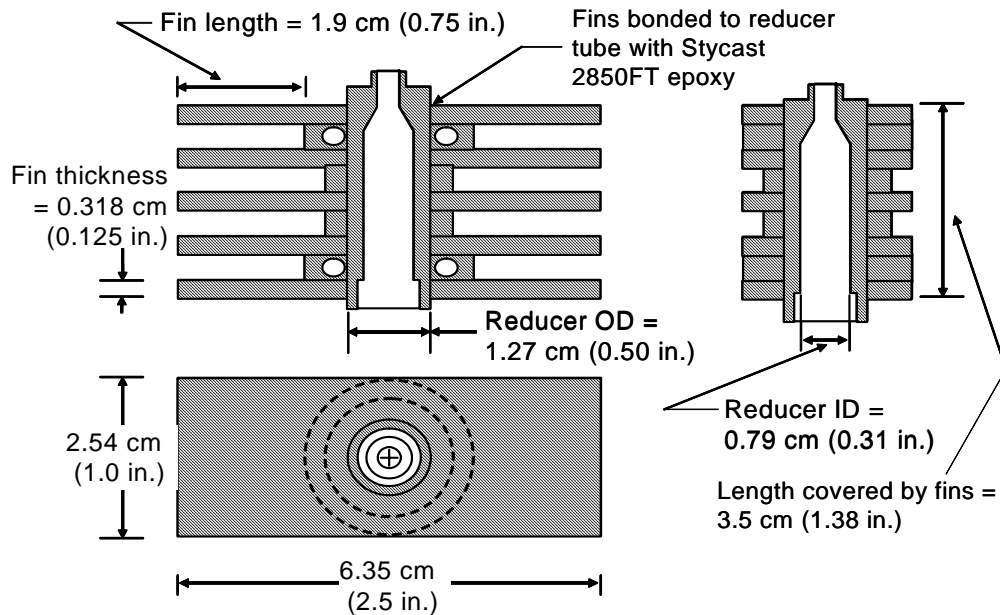


Figure 3.12 Air-cooled subcooler attached to VIEW-CPL liquid line.

the Lexan duct surrounding the TEC heat sink and subcooler. After passing through the subcooler, the fan on top of the duct forces the air into the surrounding atmosphere.

The purpose of this flow path was to save space and weight by having one fan perform the following tasks: (1) subcool liquid flowing into the evaporator, (2) cool the TEC module during evaporator cooldowns, and (3) keep the electronics box from getting hot during operations. Since the air flow path is irregular, determining the fan operating condition is complicated. Based on Table 3.7 and observing that the high pressure drop regions of the condenser air flow were the flow between fins, flow around the cylinder, the 90 ° bend, and flow through the screens, the pressure drop in the subcooler/heat sink circuit is approximated by

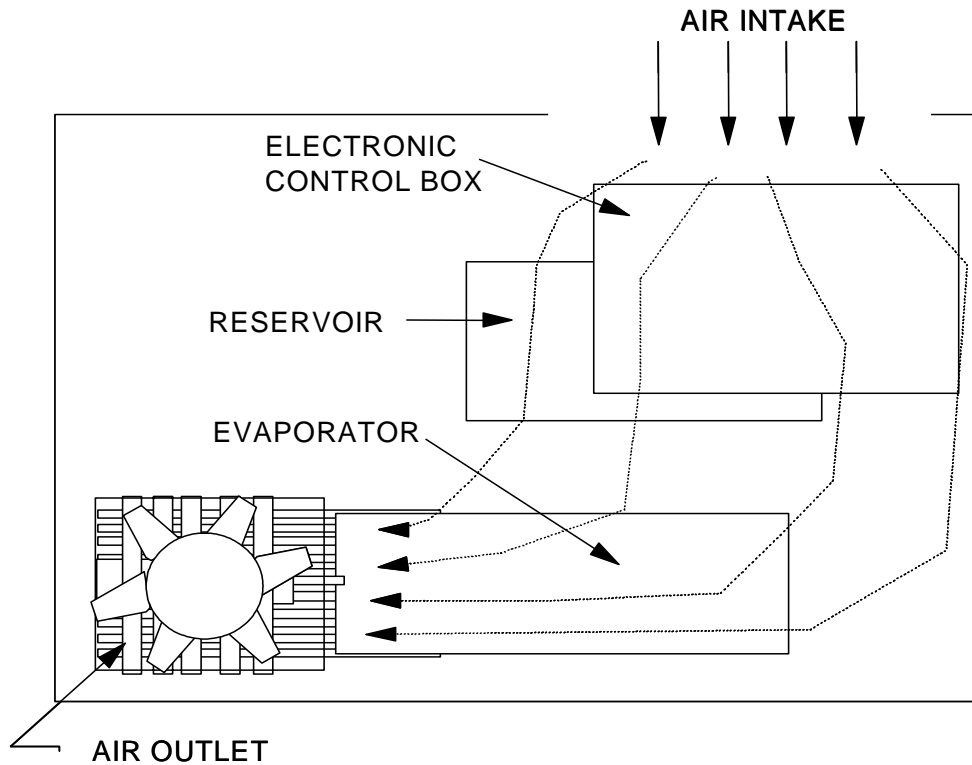


Figure 3.13 Flow path of air used to cool the electronics box, reservoir, thermoelectric cooler heat sink, and the liquid line subcooler.

neglecting the pressure drop as the air flows from the intake to the heat sink. Table 3.9 contains summary information on the subcooler/heat sink fan operating condition.

The air-side heat transfer coefficient for the subcooler is $29.8 \text{ W/m}^2\text{-K}$ using the correlations from Webb [1980]. The overall conductance of the subcooler is 0.21 W/K , including the contribution from the external heat transfer coefficient, the internal heat transfer coefficient, and the wall resistance. Noting that the liquid-side capacitance is much smaller than the vapor-side capacitance

and using the NTU value based on the liquid mass flow rate at 75 W, the subcooler effectiveness is 0.81.

Table 3.9 Subcooler fan operating conditions.

	Geometry	Parameters	Pressure drop (Pa)
1	Flow between fins of subcooler	$V_{\text{fins}}=9.6$ m/s $Pr=18$ $Re=4060$ $K=0.15$	7.87
2	Flow between fins of heat sink	$V_{\text{fins}}=5.1$ m/s $Pr=20$ $Re=1950$ $K=0.40$	5.87
3	20 x 20 Square mesh screens wire diameter =0.49 Duct flow area ratio = 1	$K = 1.57$ $V_{\text{screen1}}=1.20$ m/s $V_{\text{screen2}}=0.60$ m/s	1.46 0.36
4	90° bend between fins of heat sink	$L_e/D = 20$ $K =0.66$ $V_{\text{fins}}=5.1$ m/s	9.90
	TOTAL PRESSURE DROP		25.46 Pa

3.2.3 Micro-gravity reservoir

A stainless steel reservoir with an internal polyethylene wick structure, as shown in Figure 3.14, is used to regulate liquid level within the loop. The design was patterned after one of the reservoirs evaluated for the CAPL-1 flight experiment [Buchko, 1992]. The reservoir is formed from tubing that is hermetically sealed with flat welded endcaps. The flat endcaps save space over hemispherical endcaps and are allowable from a stress consideration since the maximum pressure differential is 1 atm. A valve on the end of the reservoir is for charging the CPL; the valve is plugged during normal testing and while on orbit.

- 1 – Stainless steel shell, 5.72 cm OD x 13.2 cm long x 0.089 cm wall
(2.25 in. OD x 5.2 in. long x 0.035 in. wall)
- 2 – Flat end caps 0.312 cm (.125 in) thick
- 3 – 20 μm wick, 5.54 cm OD x 4.78 cm ID (2.18 in. OD x 1.88 in. ID)
grooved at heater locations for venting vapor
- 4 – 5 W heater (attached to temperature controller)
- 5 – 20 W heater (attached to temperature controller)

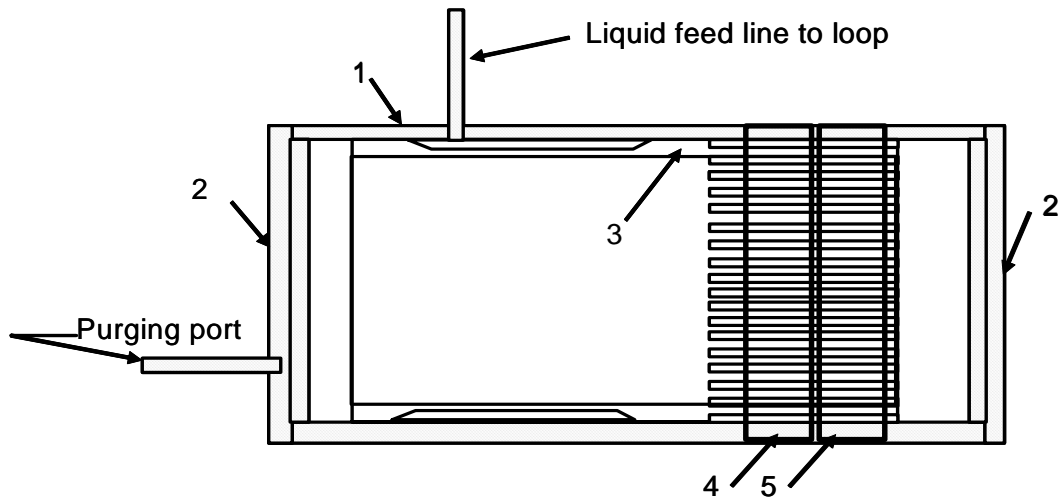


Figure 3.14 Two-phase, temperature controlled reservoir for VIEW-CPL with internal polyethylene wick for restricting vapor flow through the liquid feed line.

A liquid feed line to the loop is positioned over a cut out in the reservoir wick, which is designed to let only liquid pass to and from the reservoir.

As introduced in Section 2.1.3, the reservoir always has a liquid/vapor interface, such that the pressure of the closed loop is controlled by the saturation pressure of the water in the reservoir. The wick material inside the reservoir prevents the release of vapor into the liquid line by creating a barrier around the liquid port and allowing only the passage of liquid through the wick under normal conditions. Figure 3.15 shows the details of the wick design. Vapor grooves are

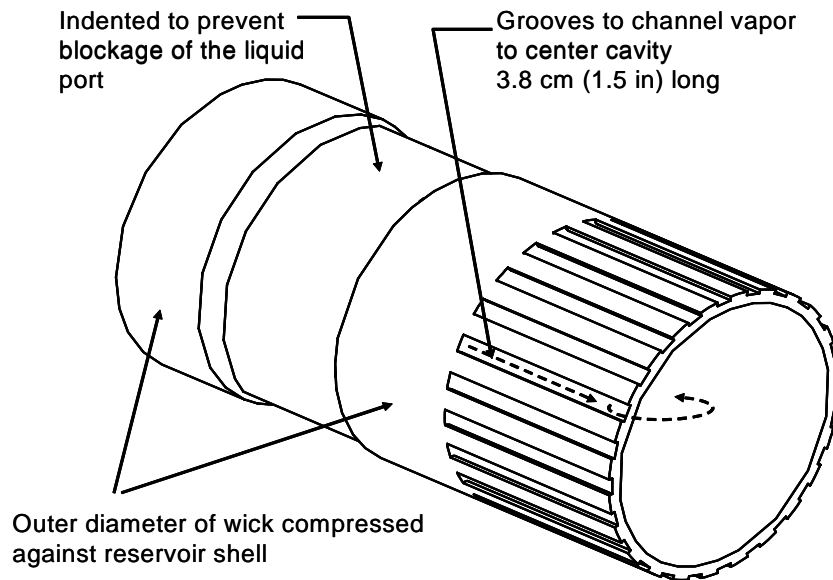


Figure 3.15 Internal wick structure for the VIEW-CPL reservoir made from porous polyethylene with 20 μm pore radii.

machined into the wick at the location of the reservoir heaters. The grooves permit vapor generated by the heaters to vent into the reservoir cavity. As the pressure increases inside the reservoir due to generation of vapor at the heaters, liquid is forced through the wick to the liquid port.

The volume of the reservoir is designed to satisfy the two extreme conditions described in Section 2.1.3; mainly that there be liquid and vapor present in the reservoir when: (1) the CPL evaporator, condenser, and transport lines are fully flooded with liquid, and (2) the CPL condenser is fully open. A third condition, that the reservoir contain liquid and vapor when the rest of the CPL is completely filled with vapor, was imposed by NASA as a safety requirement for

the VIEW-CPL system. The last condition ensures that the internal pressure is always regulated by the reservoir saturation temperature which has a limit of 50°C set by the temperature controllers and dual thermostats (i.e., two-fault tolerant). The VIEW-CPL reservoir volume is 264 cc (16.1 in.³) after the wick and compression fittings are subtracted from the shell volume. The total volume of the CPL components, other than the reservoir, is 115 cc (7.0 in.³). The system was charged with 240 cc (14.6 in.³) of deionized water. These data are summarized in Table 3.10. At the start-up condition, with the CPL system filled with liquid, the reservoir volume is 51% filled with liquid.

The reservoir controls the operating pressure of the system through the saturation temperature which is regulated with the use of heaters attached around the circumference of the reservoir. The heaters are connected to on/off temperature controllers to maintain a constant reservoir temperature of 50°C. To assist with temperature regulation of the reservoir, the air passing through the

Table 3.10 Reservoir fluid inventory calculation.

CPL Component	Volume		Start-up at 25 °C		
	(cc)	(in3)	liquid fraction	temp (C)	mass (gms)
Evaporator (vapor side)	7.26	0.44	1.00	50	7.2
Evaporator (liquid side)	9.70	0.59	1.00	50	9.6
Vapor transport line	21.85	1.33	1.00	25	21.7
Condenser (vapor side)	41.19	2.51	1.00	25	40.9
Condenser (liquid side)	5.57	0.34	1.00	25	5.5
Liquid Transport Line	11.07	0.68	1.00	25	11.0
Reservoir Free Volume	246.13	15.02	0.51	50	123.5
Other volumes	20.69	1.26	1.00	25	20.6
TOTAL	363.46	22.18			240.0

subcooler is directed across the reservoir to provide a small load (cold biased). Thermostats are located on the reservoir to keep the internal temperature of VIEW-CPL below 60°C (140°F) and the corresponding internal pressure below 19.9 kPa (2.88 psia). Details on the reservoir electronic components are described in Section 3.3.1.

The two reservoir heaters (5 and 20 W) were sized to provide: (1) elevation of the reservoir temperature from 25 to 50°C in a 30 minute period for rapid pressure priming, (2) minimal power to maintain 50°C saturation temperature by balancing heat leaks to ambient, and (3) power necessary to heat liquid displaced to the reservoir during start-up. Using a lumped capacitance model, the first heater was sized to raise the temperature of 240 g of water and 1 kg of stainless steel by 25 K in approximately 30 minutes for pressure priming. Thus, a heater with 39 Ω resistance was chosen to provide 20 W at the shuttle supply voltage of 28 VDC. However, the 20 W heater draws too much power to use during normal testing, so a second smaller heater for maintaining the reservoir temperature during tests was added.

The second heater was sized at 5 W to offset heat loss from the reservoir to ambient. The size was determined using a conduction model of a composite cylindrical wall. The main resistance to heat transfer is layers of Nomex insulation, $k = 0.13 \text{ W/m-K}$ [McMaster-Carr Catalog, 1996], that are wrapped around the reservoir for a total thickness of 0.5 in. Assuming a forced convection heat transfer coefficient of $10 \text{ W/m}^2\text{-K}$, resulting from the subcooler fan blowing

across the reservoir, the estimated heat loss from the 50°C reservoir to the 25°C ambient is 4 W. If the subcooler fan is not operating, the expected heat loss from the reservoir to ambient from the $1.42 \text{ W/m}^2\text{-K}$ convection heat transfer coefficient (specified for the shuttle Middeck) is 1 W.

The third condition considered in sizing the second heater was the effect of cold-shocking, or rapidly dropping the saturation temperature inside the reservoir, during start-up. The volume of liquid displaced during a start-up is equal to the vapor line volume plus the portion of the condenser volume occupied by vapor for the given heat rejection rate. Adding the subcooled liquid (displaced from the vapor line to the reservoir at typical saturation temperature for VIEW-CPL tests) will result in a decrease in saturation temperature when the two fluids mix. The effect on the reservoir temperature was roughly calculated assuming instantaneous and ideal mixing. The drop in reservoir temperature is plotted as a function of the condenser vapor volume in Figure 3.16 along with the energy required to restore the reservoir to its initial temperature. The analysis indicated that the 5 W heater would be too small for a quick recovery to saturation temperatures. For instance, if 50% of the condenser was filled with vapor during the start-up, then it would take 4.4 kJ to recover from the 6 K temperature drop. This would take 15 minutes with a 5 W heater. The time lag between start-up and restoring the reservoir temperature is a condition that could lead to deprime, therefore a recovery plan was added to the VIEW-CPL operating procedures after each start-up that would allow the use of the 20 W heater. A more detailed cold-

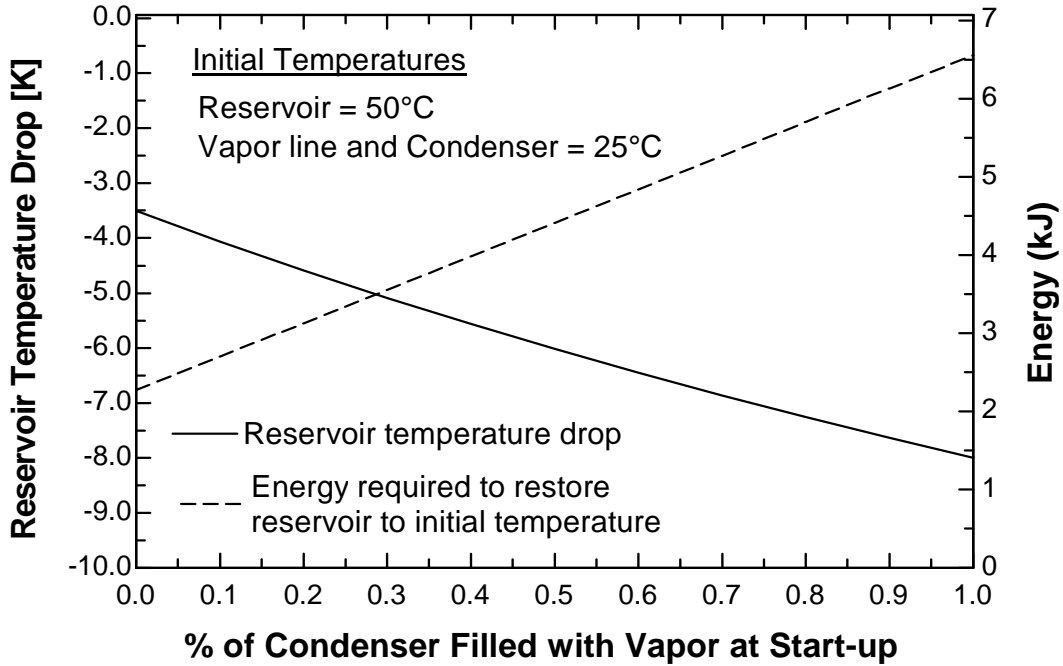


Figure 3.16 Reservoir temperature drop based on the percentage of the condenser that is filled with vapor during the VIEW-CPL start-up along with the energy required to restore the reservoir to its initial temperature (50°C). Perfect mixing is assumed between the reservoir fluid and the incoming liquid from the vapor line and the condenser (at 25°C).

shock analysis is presented in Chapter 4 with consideration given to the transient clearing of liquid from the vapor line during start-up.

3.2.4 Transport lines

The liquid and vapor transport line sizes are typically designed to keep viscous pressure losses below the capillary limit during both start-up and steady-state operations at maximum power. Since the capillary limit of water is large, neither steady-state nor start-up operations were expected to be a factor in the transport line sizes at the low powers for which VIEW-CPL was operated. Since the contact angle for water and the polyethylene wick is unknown, the actual

capillary limit is also unknown (see Section 2.1.1) causing some uncertainty in the design of the transport line diameters.

Table 3.11 summarizes the transport lines used in VIEW-CPL. All lines were 304L stainless steel. Pressure containment was not an issue because the internal CPL pressure was below atmospheric pressure at all times. All joints were welded and valves between the CPL internals and atmosphere were plugged with welded fittings (Cajon VCR brand), consistent with NASA safety requirements. Standard tubing bend radii were used to reduce both the number of welds and the viscous pressure drop. Minor losses from flow through bends

Table 3.11 Transport line dimensions and associated fittings.

	Dimensions	Fittings
Liquid line	<p><u>Evaporator inlet tube:</u> OD = 3.18 mm (0.125 in.) ID = 1.75 mm (0.069 in.) Length = 69 mm (2.7 in.)</p> <p><u>Tubing:</u> OD = 9.53 mm (0.375 in.) ID = 7.75 mm (0.305 in.) Length = mm (in.)</p> <p>Effective Length = 26.9 m (1060 in) for 7.75 mm ID</p>	<ul style="list-style-type: none"> • Area change in condenser A/R = 0.1, K = 0.5, loss is negligible because of low velocity • Sharp 90° bend out of condenser, L/D = 60 • Gradual 90° bend with r/D = 2.5, L/D = 12 • Subcooler fitting with 120° reducing angle • Polyethylene fitting: ID change from inlet tube to poly fitting • 90° bend in poly fitting, and area reduction to evaporator core
Vapor line	<p>OD = 9.53 mm (0.375 in.) ID = 7.75 mm (0.305 in.) Length = 394 mm (15.5 in.)</p> <p>Effective Length = 63 cm (25 in.) for 7.75 mm ID</p>	<ul style="list-style-type: none"> • Evaporator outlet • Condenser tube • Two 90° bends • Area change in condenser, A/R = 0.1, K = 0.8, loss is negligible because of low velocity
Reservoir line <small>see Note</small>	<p>OD = 6.35 mm (0.25 in.) ID = 4.57 mm (0.180 in.) Length = 165 mm (6.5 in.)</p>	<ul style="list-style-type: none"> • Flow through bend in Tee, L/D = 60 • 90° bend, L/D = 12

Note: Reservoir line does not contribute to steady-state pressure drop

and tees were accounted for using effective lengths ($L/D = 12$ for bend with $r/D = 3$, $L/D = 60$ for 90° corner, etc. [Fox and McDonald, 1985]).

The steady-state pressure drop as a function of power is plotted in Figure 3.17. The major component at lower power is the back pressure in the condenser due to the meniscus across the cross-section of the groove. The back pressure is similar to the pressure developed in heat pipes that are overcharged. The dimensions relevant to calculating the pressure drop of the VIEW-CPL components, other than transport lines, are summarized in Table 3.12.

An increase in pressure drop at start-up, known as the pressure surge, occurs during the displacement of liquid from the vapor line and is plotted in Figure 3.18 as a power-dependent pressure drop. The velocity of the liquid is

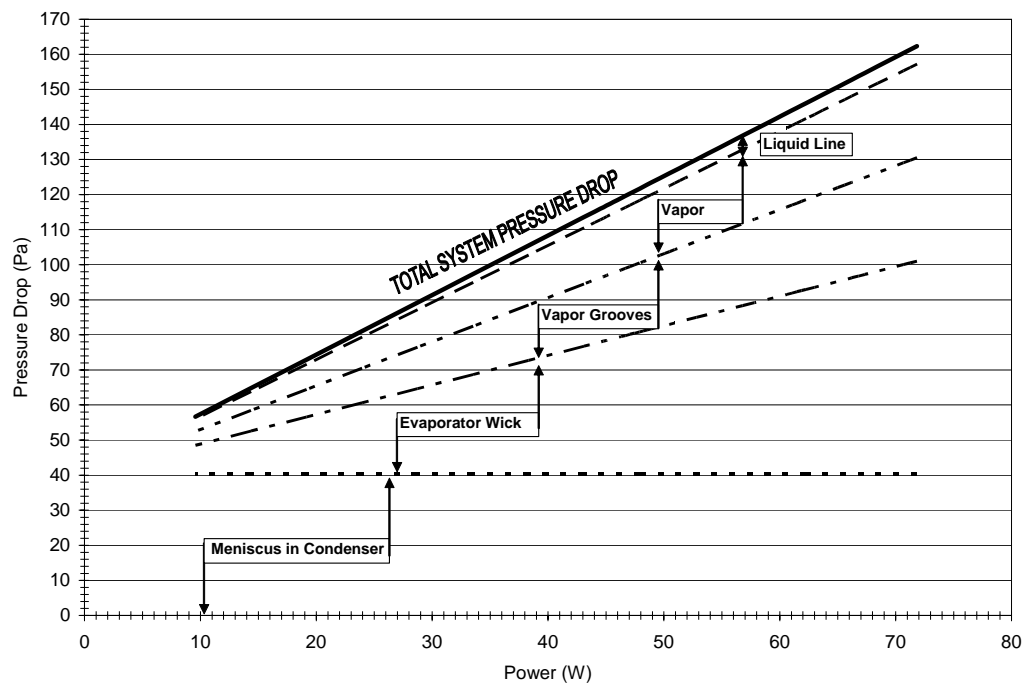


Figure 3.17 Predicted steady-state pressure drop components for VIEW-CPL.

Table 3.12 Summary of dimensions from CPL components.

Component	Dimensions
Condenser Grooves	Number of Grooves = 4 Length = 127 mm (5.0 in.) Area = 32.9 mm ² (0.051 in. ²) WP= 24.0 mm (0.945 in.) Hydraulic Diameter = 6.12 mm (0.241 in.) Radii of Curvature = 2.5 mm & 6.5 mm (0.1 in. & 0.245 in.)
Evaporator wick	Permeability = $6.2 \times 10^{-13} \text{ m}^2$ $r_p = 13.7 \text{ }\mu\text{m}$ OD = 22.2 mm (0.875 in.) ID = 13.0 mm (0.51 in.) Active length = 76.2 mm (3.0 in.)
Vapor Grooves	Number of Grooves = 6 Width = 3.2 mm (0.125 in.) Depth = 1.9 mm (0.075 in.) Hydraulic Diameter = 2.4 mm (0.0938 in.) Length = 101.6 mm (4.0 in)

equal to the velocity of the vapor at the flowrate corresponding to the power used for evaporation (i.e., not including power for sensible evaporator heating). From Figure 3.18 it would appear that the energy for evaporation will be limited to powers below 2 W at the onset of nucleation in order to remain below the capillary limit of the wick. However even this power limit would leave the liquid in the liquid line (typically at 25°C) and the evaporator core superheated because the local pressure (equal to 500 Pa for the example of 50°C saturation temperature and corresponding pressure of 10500 Pa minus the pressure drop of 10000 Pa for pressure surge at 2 W from Figure 3.18) will be below the vapor pressure (3170 Pa at 25°C). In order to prevent nucleation, the evaporation power is limited to 1.6 W. This power corresponds to a pressure drop equal to

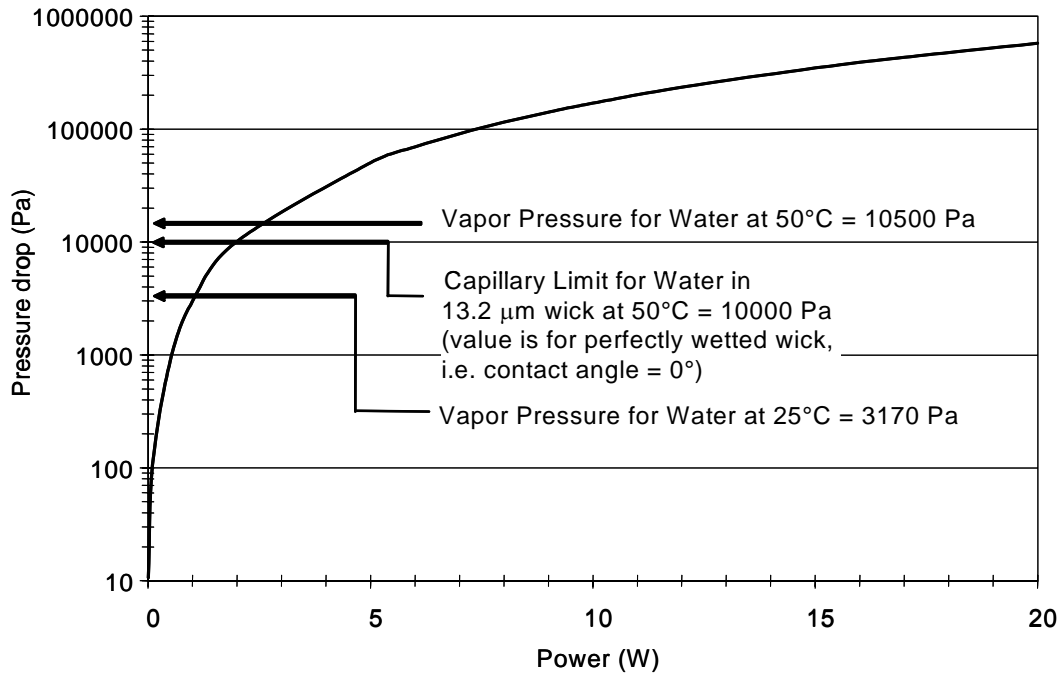


Figure 3.18 VIEW-CPL predicted pressure drop during start-up as a function of power contributing to evaporation. Capillary limit for water is calculated for a 0° contact angle. For contact angles greater than 0° , the capillary limit is calculated using Eq. 2.1.

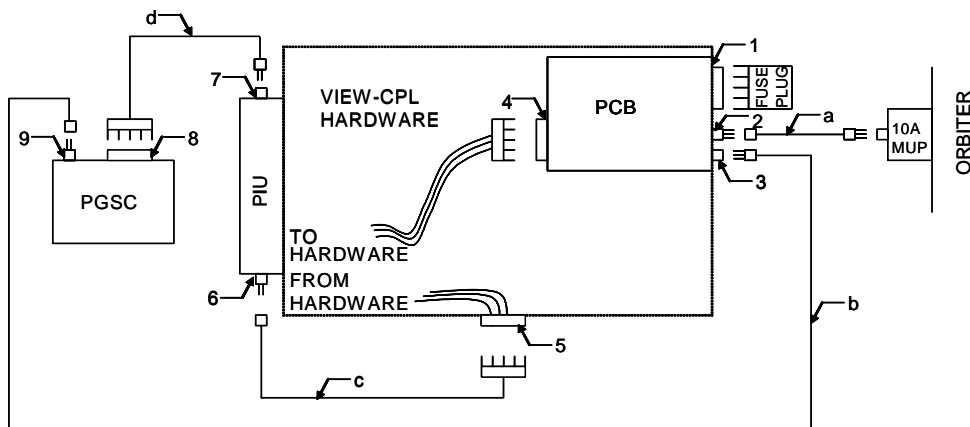
the difference in vapor pressure between the vapor and the liquid sides of the evaporator. A transient model presented in Chapter 4 more fully describes the system dynamics during the pressure surge.

Valves. Flight qualified valves and fittings, similar to the ones flown in the CAPL flight experiment, were selected for charging and purging ports. The valves were Nupro brand, 6.35-mm (1/4 in.) H series bellows sealed valves with a tube extension on one end and a Cajon Brand VCR fitting attached to the other end. VCR fittings with nickel gaskets were used instead of stainless steel because the nickel is softer and the fittings are less likely to be damaged during assembly. The valves were plugged during the shuttle flight to prevent the

inadvertent release of water into the cabin. In-line liquid and vapor line valves were desired for flow control during ground testing, however pressure drops through the vapor side valve were high and space was limited. Since the liquid and vapor line valves were not to be used during flight testing, they were not included in the final design.

3.3 Electrical Components and Data Acquisition

VIEW-CPL requires electric power for the electronics and for the heaters and fans. Throughout the electrical design effort, consultation was provided by the Thermal Engineering Branch at Goddard Space Flight Center to draw upon their extensive experience in managing Space Shuttle experiments. The Payload General Support Computer (PGSC) and PGSC Interface Unit (PIU) for data collection are auxiliary components that are powered through the VIEW-CPL payload control box (PCB). The PIU is the data acquisition system connecting to the PGSC via an RS232C cable and connectors. Together, the PIU and PGSC collect and display temperature, pressure, power, and voltage data. Figure 3.19 is a layout of the electrical connections made between VIEW-CPL and auxiliary hardware. The shuttle supplies DC voltage, in the range of 28 to 32 VDC, to the PCB. The PCB then distributes power to the evaporator heaters, reservoir temperature controllers, fans, and data acquisition system (PIU and PGSC). A wiring diagram of the PCB and a layout of the wiring for electronics on the CPL are presented in Appendix C. A 37-pin connector links the electronics in the PCB to the electronics on the loop as shown in the two wiring diagrams.



PCB – Payload Control Box
 PGSC – Payload General Support Computer
 PIU – PGSC Interface Unit

CABLES

a - Orbiter DC Power cable (P/N 10108-10082-07)
 b - PGSC Power cable (P/N SED33103334-311)
 c - VIEW-CPL PIU/DATA cable
 d - RS232C Data cable (P/N SED33103335-305)

CONNECTORS

1 - 37 Pin, Fuse Plug Receptacle
 2 - Bendix MS3470L-14-12P,
 Orbiter power connection
 3 - Bendix MS3470L-14-12S,
 PGSC power connection
 4 - 37 Pin, PCB to Loop connection
 5 - 25 Pin, PIU/DATA Connection
 6 - 25 Pin, PIU/DATA Connection on PIU
 7 - RS232C, Data Connection on PIU
 8 - RS232C, Data Connection on PGSC
 9 - PGSC power connection

Figure 3.19 VIEW-CPL electrical layout with auxiliary equipment connections.

Figure 3.20 is a schematic showing the location of the heaters, fans, temperature sensors, thermostats, thermoelectric cooling module, and pressure transducers on the CPL hardware.

3.3.1 Electronic control box and power distribution

In the shuttle, VIEW-CPL connects to either the Middeck Utility Panel (MUP) or the Middeck ceiling outlet for 28 to 32 VDC power with a maximum 10 A rating. The cables for carrying the power to the experiment are supplied by the Johnson Space Center (JSC). For ground testing, a 6 Amp-28VDC power supply was used.

The controls of the CPL are contained in the payload control box (PCB). The PCB is a 20.3 cm x 15.2 cm x 8.9 cm deep (8 in. x 6 in. x 3.5 in.) aluminum chassis. The box was anodized to make it non-conductive and to protect both the experiment operator and the electronics inside. Figure 3.21 shows the layout of the switches on the PCB. From the PCB, the reservoir temperature controllers are activated; switches controlling the power to the evaporator heaters and switches for turning on the fans are accessible. Details on the electrical design for distributing power to the experiment are described in the following paragraphs.

Switches. All commands to VIEW-CPL are issued through manual switches. Locking toggle switches are used to turn on the temperature controllers, heater, and cooling fans. The locking feature of the toggle switches prevents inadvertent switching while in orbit due to the increased possibility of bumping into the experiment in the microgravity environment.

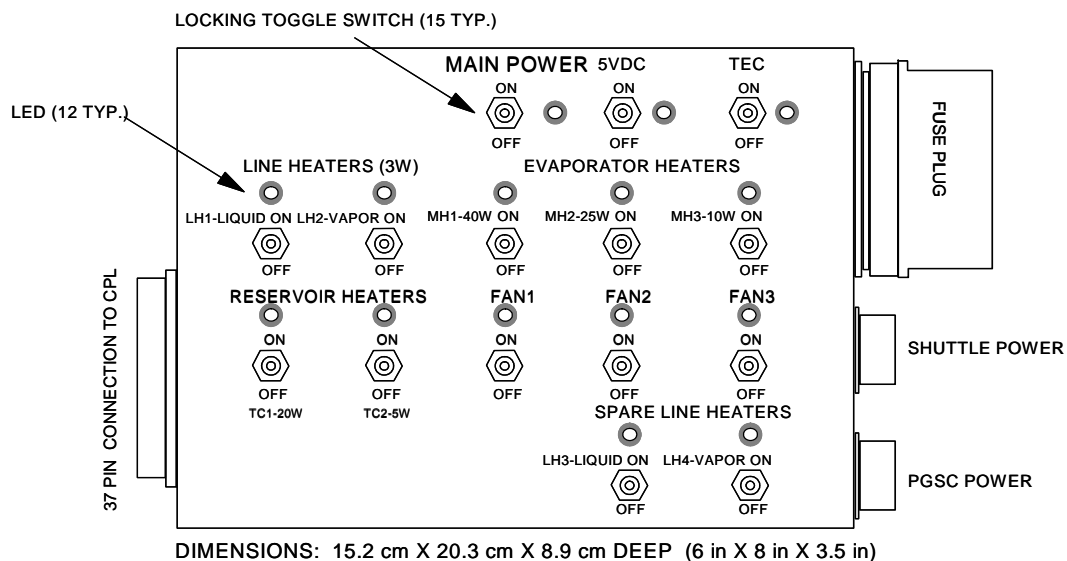


Figure 3.21 VIEW-CPL payload control box (PCB) switch layout.

LEDs. Each switch has an associated light-emitting diode (LED) to indicate when power is applied to the electronic components. There are a total of 15 LEDs and each uses 0.4 W when on.

Heaters. Electrical resistance heaters are located on both the reservoir and evaporator. The heaters are thermfoil heaters with Kapton Insulation and are glued to the evaporator and reservoir surfaces with epoxy (STYCAST 2850FT). To avoid heater burnout, the design watt density is less than 2.3 W/cm² (15 W/in²). A nominal supply voltage of 28 V (from the shuttle) was used to size the heaters. Details on the heater selections are included in Appendix C.

The area available on the evaporator for attaching the heaters is 10.2-cm long by 6.1-cm wide (4 in. x 2.4 in.) on which the three main heaters are installed. The main heaters (MH1, MH2, MH3) are used to supply heat (nominally 40, 25, and 10 W, respectively) to the evaporator. The three-heater arrangement is used to provide a wide range of power (10, 25, 35, 40, 50, 65, and 75 W) under the control of on/off switches.

The reservoir heaters are connected to temperature controllers to maintain the temperature of the reservoir at the desired set point. The heaters are attached to the outside of the cylindrical surface of the reservoir housing and are located directly adjacent to the portion of the internal wick with vapor venting grooves.

In addition to the evaporator and reservoir heaters, two (prime and backup) 3 W heaters are attached to both the liquid and vapor return lines. The

two liquid-line heaters are mounted on the evaporator inlet line, and the two vapor-line heaters are attached to the evaporator exit line using epoxy and heat-shrink plastic. The vapor-line heaters were added to mitigate start-up difficulties in micro-gravity; they are used to help displace liquid from the evaporator vapor plenum and the vapor line if the evaporator heater power is not sufficient to start the loop. The liquid-line heaters were also added as a precautionary action to ensure the VIEW-CPL could be deprimed. The liquid-line heaters are available to intentionally nucleate on the liquid side of the wick by reducing the subcooling.

Temperature controllers. On/off temperature controllers are used to control the reservoir heaters [Minco Products, 1994]. The controllers were chosen because they operate with a DC supply voltage in the range of 8 VDC to 32 VDC, which matches the voltage supplied by the shuttle. The controller uses special heaters to sense the heater temperature by measuring the heater resistance; thus, it incorporates the sensing function and the heater in one component. The controller properties are detailed in Appendix C.

The controller set points were calibrated using a digital thermocouple thermometer and a type T thermocouple attached to the reservoir. The reservoir temperature controllers were set to maintain the temperature of the reservoir at 50°C by cycling the heater power on as temperature decreased below 50°C and cycling power off when temperatures above 50°C were sensed. The set-point was adjusted for both controllers by adjusting the set-point screw until the heaters

were cycling on and off when the reservoir was at 50°C. The set-point was not varied during the on-orbit testing.

Fans. Fans are used to cool the condenser and liquid line. In accordance with shuttle requirements for Middeck experiments, the fans have brushless motors. The Lexan shroud, wire fan guards, and screens are used to make the fans inaccessible during operation for safety. Fan curves are presented in Section 3.2.2.

Thermoelectric module. A thermoelectric cooler (TEC) module is included to reduce the cool-down time of the evaporator. The TEC module is a semiconductor chip that has good thermoelectric properties and a low thermal conductivity. In operation, one side of the chip gets hot and the other gets cold. By placing the chip in the right location, it is possible to pump energy out of the evaporator body, when needed, by turning on the TEC module. The TEC operates at 5 VDC and draws approximately 15 W while cooling at 5 W. Thus, the heat rejection is 20 W and the efficiency is 33%. These values are nominal values; the actual performance depends on the temperature of the module.

The TEC module was assembled between the evaporator and a finned heat sink. An insulating spacer was placed between the heat sink and evaporator to prevent the TEC from being crushed during installation. Thus, the only contact between the heat sink and the evaporator is the bolts and TEC.

Relay. A hermetically sealed relay is used to make sure that neither the high power reservoir (RH1) heater nor the thermoelectric cooler (TEC) can be

activated when the 40 W (MH1) evaporator heater is on. The relay is normally closed in the RH1 and TEC circuits, but opens when the MH1 switch is toggled on. The purpose of the relay was to ensure that maximum power consumption of VIEW-CPL was limited to 190 W.

Power supplies. Two DC/DC converters were necessary to supply regulated power to certain electronic components. The converters take 28 to 32 VDC and output ± 15 VDC and/or 5 VDC.

Summary of power requirements. During the design phase, the VIEW-CPL power requirements were estimated for a supply voltage of 28 V. In reality, the shuttle power supply during operations ranged from 24 to 32 V with a mean value of 29 V. However, this information was not available until after the mission. Based on previous experimenters recommendations, the power consumption was measured for 30 V and is summarized in Table 3.13. The measured power values in Table 3.13 were taken on ground using a digital multimeter with sensitivity of 1 μ V, 1 nA, and 1 m Ω for a 0.011 % basic accuracy. The multimeter was used to check the current draw of the VIEW-CPL components. The power consumed by each component was calculated by multiplying the voltage read from the VIEW-CPL data acquisition system (30 VDC) and the current measured from the multimeter.

During non-testing segments (stand-by periods), a minimal amount of power is required (11 W) to maintain the reservoir temperature above ambient conditions using the 5 W heater. In order to monitor the reservoir temperature,

Table 3.13 Power distribution for VIEW-CPL with 30 VDC power supply.

Switch	Components Powered	30 VDC Design Value (W)	Measured Power (W)
MAIN PWR	LED (2 k Ω , 30V)	0.5	0.4
5VDC	Power Supply 1 (PS1) 80% efficient: <ul style="list-style-type: none"> • LED • Panel meter (3mA, 5V) • AD590 (Qty 11, 15V, 13kΩ) • Absolute Pressure Trans. • Differential Pressure Trans. • Pull-up Resistor (600Ω, 5V) 	4.2	4.0
PIU	PIU	5	4.7
TEC	Power Supply 2 (PS 2) 80% efficient: <ul style="list-style-type: none"> • LED • TEC (3A, 5V) 	19.3	24.6
FAN1, FAN2, FAN3	3 LEDs, 3 FANs	12.6	12.8
MH1	LED, MH1 (19.4 Ω , 30V)	46.8	47.0
MH2	LED, MH2 (30.5 Ω , 30V)	30.0	29.2
MH3	LED, MH3 (83.5 Ω , 30V)	11.2	11.0
TC1	LED, RH1 (39 Ω , 30V), TC1	23.6	22.7
TC2	LED, RH2 (156 Ω , 30V), TC2	6.3	5.5
LH1, LH2, LH3, LH4	4 LED, 4 LH	15.2	14.8
-	PGSC (NASA JSC supplied equipment)	40	NA
-	Video Camcorder (NASA JSC equipment)	15	NA
	Total Power of VIEW-CPL component	174.7	176.7
	Total Power including SSP equipment	229.7	231.7
	Maximum Power during testing (using relay to remove power from TC1 and TEC circuits) including JSC equipment	186.8	184.4
	Stand-by power (MAIN PWR, 5VDC, TC2)	11.0	9.9

the temperature panel meter is also powered during the stand-by periods, therefore requiring that power supply PS1 be powered on. Power is not required during launch and landing.

3.3.2 Circuit protection

The electronics were mounted inside the PCB chassis, either directly on the chassis or on a circuit board that was secured to the chassis with screws. A card edge connector was used to make connections from the circuit board to the appropriate circuits. The electronics were assembled by technicians at Goddard Space Flight Center. In addition to good workmanship, other modes of ensuring safe circuits included proper material selection, overload protection, EMI filters, and grounding.

Conformal coating. To eliminate offgassing from the electronics, components were sealed with a coat of urethane (Uralane brand) that conforms to the shape of the components. The coating also protects the circuitry from damage if contacted with water or other fluids that may be floating in the shuttle Middeck.

Fuses. To protect the shuttle, all circuits are wired with very fast-acting fuses. The fuses were packaged in a connector, potted with urethane, and covered with copper tape to reduce EMI/EMC issues. Spare fuse assemblies were flown with the experiment but were not used.

Fuses used in micro-gravity are derated, meaning that the fuse will blow at a current lower than the rated amperage, due to the lack of natural convection.

While circulating fans inside the Middeck provide some convection, electronics enclosed in boxes experience minimal convection. Derating guidelines [NASA GSFC, 1995] were followed when choosing proper fuse sizes for VIEW-CPL.

Thermal switches. Temperature activated switches (Thermik -05 series) designed to open at $60\pm5^{\circ}\text{C}$ and reset automatically at 45°C were used. The switches open circuits to remove power from heaters if the temperature of the CPL surfaces exceeds 60°C . Two thermal switches are used in series with all heaters on the evaporator, reservoir, and return lines for redundancy in the event that one switch fails.

In order to verify that the switches function properly, each switch was tested by immersion in a water bath to determine the actual open and re-close set points. A continuity meter was connected in series with the thermal switches to observe when the switch opened or closed. All of the thermostats chosen for use in VIEW-CPL opened within the range of 59°C to 62°C and reset at temperatures above 38°C . Details on the thermostat selection and other verification procedures are included in Appendix C.

EMI filters and capacitors. Filters and capacitors were used in the VIEW-CPL electronics to reduce electromagnetic interference and susceptibility. In-line EMI filters (RF Interonics model 13619/RF5005-2) were attached to the +28 VDC power and return lines, and then grounded to the chassis. EMI filters (Interpoint model FM-461) were placed in both power supply circuits along with $0.1\ \mu\text{F}$ capacitors attaching the 5 VDC and return lines to the chassis. In order to reduce

both EMI and RF interference, resin sealed EMI/RFI suppression filters (Spectrum Control Inc. P/N 51-717-001) were attached across the +28V DC supply and return lines (for both the shuttle input power and the PGSC power) and grounded to the chassis. These capacitors were placed on the lines immediately as they entered the control box and were essential to eliminating the common mode noise resulting from the RF susceptibility observed during initial EMI testing of VIEW-CPL.

Grounding. The EMI filters located inside the VIEW-CPL control box require a high frequency chassis ground in order to eliminate common mode noise. Since the experiment is mounted to the shuttle with Velcro, a ground strap is used to ground VIEW-CPL to the shuttle. A solid copper chassis ground also exists inside the VIEW-CPL control box that ties directly to the ground wire in the shuttle DC power cable. However, a braided ground strap was found to be required because the internal chassis ground is inductive and does not provide an adequate ground at high frequencies. The ground strap has a copper alligator clip attached to each end of a tinned copper braided strap. One clip attaches to a toggle switch or fuse plug screw while the other end attaches to any metal portion of the shuttle.

A 3.6 V Zener diode (Motorola part number 1N4739) was placed between the power return and the signal return to tie the signal return to the same level as the ground return.

3.3.3 Data acquisition system

Pressure and temperature transducers are used to monitor the CPL operation and to collect data useful for explaining CPL physics. Voltage and power information are recorded to identify the CPL operating conditions. The data were collected from the CPL using a data acquisition system connected to a Payload and General Support Computer (PGSC). The PGSC stores data received from the experiment through the PGSC Interface Unit (PIU) in a process shown schematically in Figure 3.22. In addition to the numeric data collected with the PIU, a shuttle video camcorder was focused on the evaporator during operation to record all visual data through the Lexan plate of the evaporator.

AD590 (Analog Devices) solid state temperature transducers read the temperature at various locations around the loop; the temperatures are constantly displayed on the computer screen while the data acquisition system is operating. The absolute system pressure and the differential pressure across the evaporator are recorded using pressure transducers (Sensotec brand). Figure 3.20 shows the location of the AD590 sensors and pressure transducers on the CPL.

μMAC-1050 / PIU. The PIU is an analog-to-digital converter that takes the

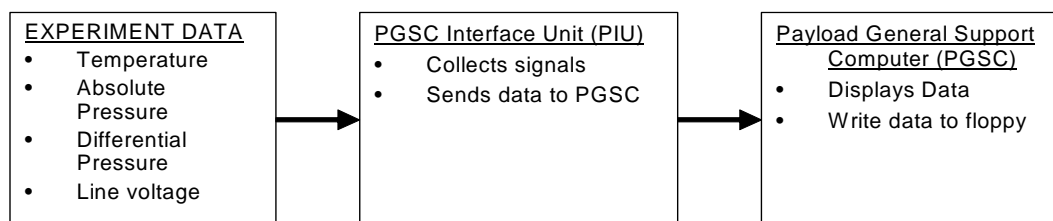


Figure 3.22 PGSC and PIU functional process.

analog signals from the VIEW-CPL and converts them into digital signals before sending them to the PGSC. The data acquisition system uses a μ MAC-1050 board (Cyber Research). The board was a flight-qualified spare for the HPP-2 experiment flown on STS-66 in November 1994, and was borrowed for VIEW-CPL. The system is connected to the PGSC via a RS232C serial link. Table 3.14 lists the PIU channel numbers and instrumentation.

The analog-to-digital converter is 15 bit (Azonix Corp., 1995) with an input signal range of ± 10 V for a resolution of $20 \text{ V} / 2^{15} \text{ bit}$, or 0.0006104 V/bit. An uncertainty analysis and analysis of propagation of error from the transducers

Table 3.14 μ MAC-1050 channel assignment.

Channel number	Sensor
8 and 9	Bus Voltage Monitor
10 and 11	Heater Power
12	Absolute Pressure
13	Differential Pressure
14	AD590 Temperature Transducer, T1 - Reservoir line
15	AD590 Temperature Transducer, T2 - Condenser exit
16	AD590 Temperature Transducer, T3 - Condenser inlet
17	AD590 Temperature Transducer, T4 - Evaporator inlet
18	AD590 Temperature Transducer, T5 - Evaporator exit
19	AD590 Temperature Transducer, T6 - Evaporator block
20	AD590 Temperature Transducer, T7 - Subcooler exit
21	AD590 Temperature Transducer, T8 - Reservoir
22	AD590 Temperature Transducer, T9 - Condenser air
23	AD590 Temperature Transducer, T10 - Subcooler inlet
60	Board Temperature Sensor

through the data acquisition board is discussed in Appendix E.

PGSC. The PGSC used during the shuttle flight was an IBM ThinkPad 755C laptop computer that was supplied by NASA Johnson Space Center. For ground testing, a compatible laptop was used. The PGSC runs the VIEW-CPL software.

Software. The data are collected using a program written in QuickBasic that stored the data every 5 s to a binary file on a floppy disk. The program is compiled with the μ MAC-1050 library QB1050.QLB [Azonix Corp, 1995] into a stand-alone executable that runs directly from the floppy disk under MS-DOS. The software reads the PIU channels for voltage output from the experiment transducers, converts the voltages to physical quantities, and prints the data to the screen and/or a binary data file. Options available include listing the data, plotting a time series of the data, or displaying the data on a CPL schematic in appropriate locations. Appendix H contains a listing of pseudo-code, the QuickBasic code and a software user's manual. Post-testing data manipulation programs were written in QuickBasic to read the binary file and write to ASCII data files for transfer into spreadsheets.

Video camcorder. The video camcorder (Canon L1 Hi-8mm) was supplied by NASA Johnson Space Center (JSC). In addition to the camcorder, a Video Interface Unit (VIU) and a VIU cable were required so that the camcorder could operate using the Middeck 28 VDC power supply and an AC powered fluorescent light was provided to illuminate the VIEW-CPL evaporator during video recording.

During operation, the camcorder and light were mounted to the VIEW-CPL shroud using a JSC supplied multi-use bracket (mounting arm). Fifteen Hi-8mm video tapes were also supplied by JSC; each tape could hold up to 2 hours of video.

For post-test analysis, the bubble measurements are taken from single images obtained from the video tapes (Appendix F). The zoom and camcorder distance from the evaporator cause the size of the picture to vary, so a method of scaling was developed to ensure the measurements between different photographs are comparable. For each image, the length between the extreme edge of the evaporator inlet hole and the vapor plug was compared to the actual length of $10.80 \pm .05$ cm. The ratio of the measured length to the actual length is the scaling factor for the subsequent measurements necessary to find the volume of the bubble.

AD590 temperature sensors. The temperature measurements in key locations on the CPL are made with solid-state AD590K temperature transducers (Analog Devices). Appendix G details the operation and calibration of the transducers. The transducers are in series with a 13 k Ω resistor powered with 15 V for a power draw of 0.017 W each. In addition to the 10 temperature data collected with the PIU, a temperature panel meter mounted on the top of the protective shroud constantly displays the temperature of the reservoir using a single AD590 circuit with a 1 k Ω resistor and a 2000 mV digital voltmeter (Acculux model DP-652). This meter permits monitoring of the system temperature,

without the PGSC, while 5 W is applied to the reservoir to maintain a primed condition during stand-by periods.

Pressure transducers. The pressure transducers (Sensotec) are light weight stainless steel transducers. Both transducers were powered with matched inline-amplifiers to regulate the supply voltage. Table 3.15 lists the range and accuracy of the transducers. An offset of -0.65 kPa was determined from measured values using the differential pressure transducer.

Table 3.15 Manufacturer's accuracy data for the pressure transducers.

Model	Transducer Type	Range	Error	
MA	Absolute Pressure	0 to 172 kPa 0 to 25 psia	Accuracy $\pm 0.3\%$ FS Nonlinearity $\pm 0.2\%$ FS Hysteresis $\pm 0.1\%$ FS Non-repeatability: $\pm 0.1\%$ FS	± 0.5 kPa (± 0.08 psi) ± 0.3 kPa (± 0.05 psi) ± 0.2 kPa (± 0.03 psi) ± 0.2 kPa (± 0.03 psi)
P-30-P	Differential Pressure	-35 kPa to +35 kPa -5 to +5 psi	Accuracy $\pm 0.3\%$ FS Nonlinearity $\pm 0.2\%$ FS Hysteresis $\pm 0.1\%$ FS Non-repeatability: $\pm 0.1\%$ FS	± 0.2 kPa (± 0.03 psi) ± 0.1 kPa (± 0.02 psi) ± 0.1 kPa (± 0.01 psi) ± 0.1 kPa (± 0.01 psi)

Voltage and power measurements. A voltage divider circuit, shown in Figure 3.23 and built with precision resistors, was used to measure the voltage input to the experiment. The supply voltage measured by the PIU was verified using a multimeter (Fluke 77) and found to be accurate within 0.05 V.

The power displayed by the PGSC is a measurement of the power applied to the evaporator and connecting lines through the film heaters and resistor

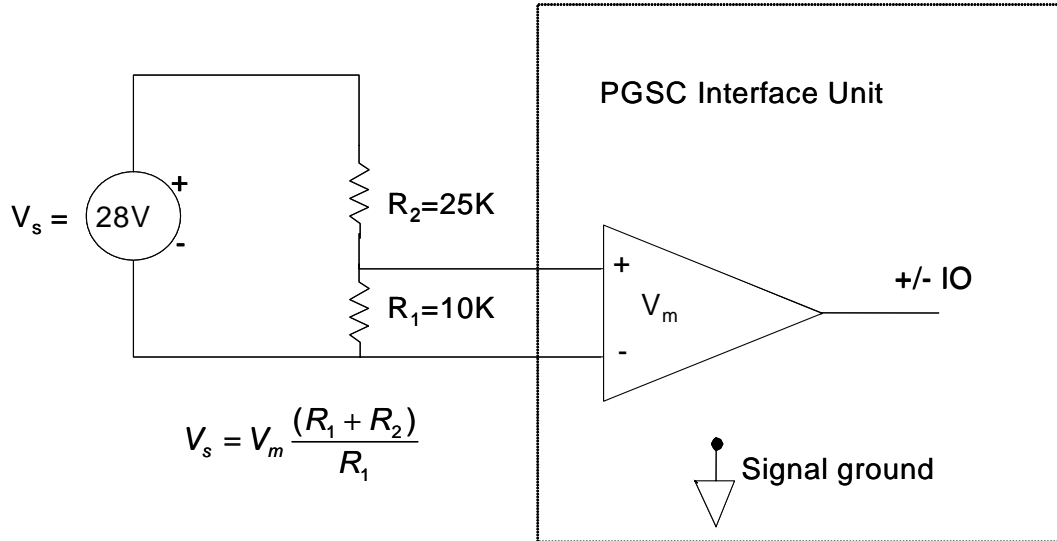


Figure 3.23 Voltage divider circuit for monitoring 28 V bus.

heaters, respectively. A current shunt was used to measure the power drawn by the heaters by measuring the voltage drop across a 0.1 Ω resistor. The voltage measurement, V_m , was converted to a current measurement and then multiplied by the measured supply voltage, V_{ms} , to determine the power draw across the heaters. The power measurement was compared to the design power (V_{ms}^2/R) according to the measured heater resistance value with the results presented in Table 3.16.

Table 3.16 Heater power measurements using the PIU compared to expected values.

Heater	Heater resistance (Ohms)	Measured Power ^a (W)	Design Power (V_{ms}^2/R) (W)	% Difference
MH1	19.4	40.1	40.3	0.468%
MH2	30.5	25.5	25.7	0.660%
MH3	83.5	9.59	9.37	-2.40%

^aMeasured at 27.97 supply voltage using $V_{ms} (V_m/R)$

Voltage differences were observed in the recorded data each time switches were changed in the experiment as it was operated in the shuttle. The voltage changes proved useful for determining the sequence and timing of switching events. When switches were toggled on or off, the voltage supply from the shuttle would drop and rise, respectively, in a magnitude proportional to the power consumed by the component being controlled. Appendix I provides details on the voltage differences and the implication on the VIEW-CPL results.

3.4 Johnson Space Center (JSC) Supplied Equipment

Some equipment required to operate VIEW-CPL was supplied by JSC. A detailed list of the equipment, dimensions, and weight is found in the “Orbiter Crew Compartment Interface Control Annex”, NSTS 21343 ICA [NASA JSC, 1996b] and is summarized in Table 3.17. Dedicated equipment indicates that the equipment is flown specifically for use with VIEW-CPL, while shared equipment is flown for more than one purpose and is not only used for VIEW-CPL.

3.5 System Preparation Procedures

The flowchart for VIEW-CPL processing is presented in Figure 3.24. The mechanical (1) and electrical (2) fabrication and assembly efforts were started in parallel. Final integration (4) of the electronics occurred after the loop was completely processed and charged (3). Verification testing (5) included initial start-up tests, EMI/EMC testing, acoustic noise measurement, off-gas testing, and external temperature measurements. Two astronaut training sessions (6)

Table 3.17 Equipment supplied by NASA Johnson Space Center for VIEW-CPL use on STS-80.

Part number	Description - use	Quantity
<u>Dedicated Equipment</u>		
10108-10082-07	DC power cable - 7.3 m (24 ft) long	1
SED33103334-311	PGSC DC power cable - 7.3 m (24 ft) long	1
SED33103335-305	PGSC RS232C data cable	1
SED33104076-302	Multiuse bracket assy - for mounting camcorder and light	2
SED33103757-303	Hi-8mm cassette assy - video cassettes for recording observations	15
<u>Shared Equipment</u>		
SED33104331-xxx	Cannon L-1 camcorder	1
SED33104774	Camcorder lens, 3X	1
SED39122893-301	Camcorder power/video cable	1
SED39122650-303	VIU-CM - Video Interface Unit for down linking video to customer support room at JSC during flight	1
SED39122650-301	VIU to shuttle cable	1
SED39126968-305	PGSC 755C computer assy	1
SED39123751-302	LCD monitor - for watching video without having to use the camcorder eyepiece	1
SED39122260-315	LCD monitor cable	1
SED33103311-301	Fluorescent light - for illuminating the VIEW-CPL evaporator during video recording	1

were held at JSC. The experiment was sent to JSC for a Bench Review (7), which is a final lookover of the experiment by astronauts and JSC safety personnel, before JSC sent the experiment to KSC for loading into the shuttle.

Helium leak check and proof pressure test. A helium leak test was performed on the VIEW-CPL prior to proof pressure testing. A helium detector

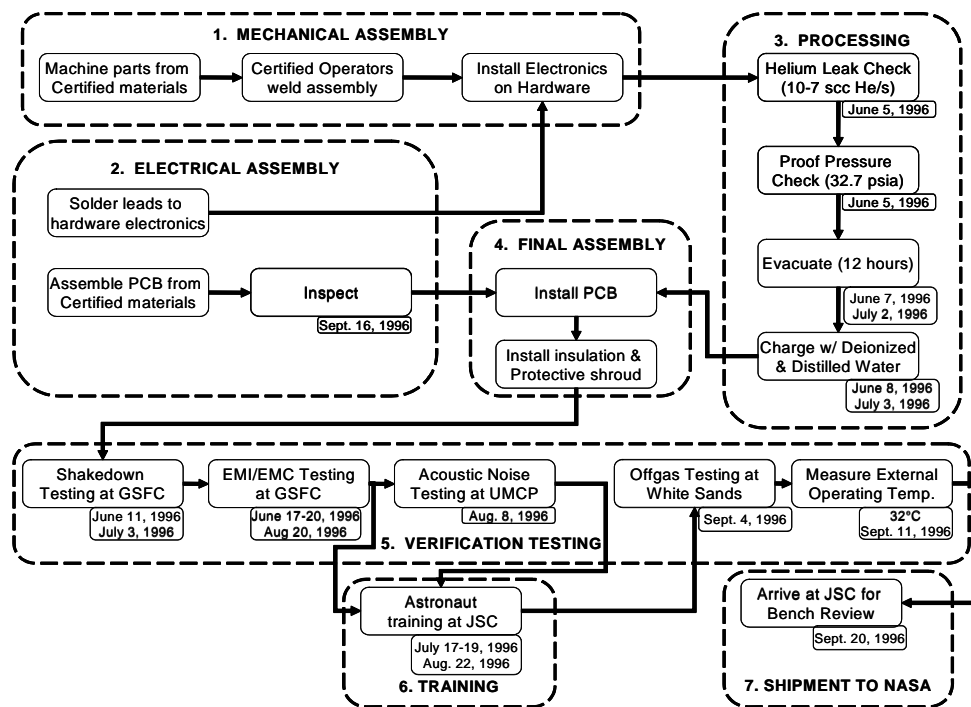


Figure 3.24 VIEW-CPL manufacturing and verification processing flow diagram.

(VEECO brand, model MS-170) was connected to the loop and used to evacuate it. The detector sensitivity was set to detect helium leak rates above 8×10^{-8} cc/s concentrations. Helium was blown over all joints in the loop. No leaks were detected.

A proof pressure test was performed by filling the loop with helium to 34 psia (note for future proof testing: dry nitrogen should be used because helium is difficult to evacuate). Pressure was maintained for 10 minutes without a change in the pressure gauge measurement. The helium leak check was repeated after pressure testing to confirm that there was no propagation of leak

paths. Afterwards, the loop was evacuated for a minimum of 12 hours and charged with deionized water.

Charging. VIEW-CPL was weighed before and after charging in order to ensure that the correct amount of water was charged into the loop. A turbo vacuum-pump was connected to the loop (through the liquid line, vapor line, and reservoir valves) and the lines connecting to the charge station. The system was evacuated for a minimum of 12 hours prior to charging. Figure 3.25 is a schematic of the charge station set-up.

Deionized water (16 M Ω resistivity) was refluxed (boiled and condensed)

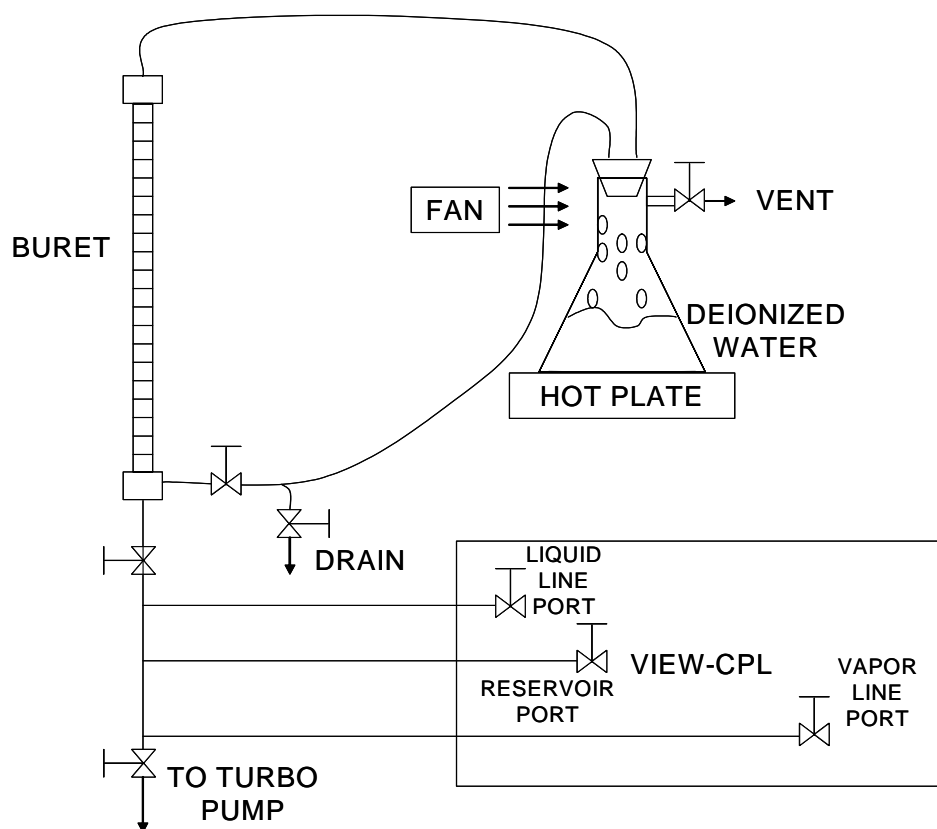


Figure 3.25 Schematic of water charging station for VIEW-CPL.

in a flask to remove air. The refluxed water was evaporated and condensed in the charge station lines and burette. The loop valves were opened to allow water to flow into the loop. Volumetric control was maintained at the burette by keeping a meniscus in the graduated portion. A total of 240 g of water was charged to VIEW-CPL.

Shake down testing. The initial pressure prime of VIEW-CPL was performed at GSFC. At this time, the reservoir temperature controller set-points were adjusted to 50°C. As expected, liquid filled the evaporator. The evaporator heaters were then turned on and vapor filled the vapor grooves, confirming that the water CPL would operate. A series of pre-flight tests were performed at the University of Maryland. Results of these tests are further discussed in Chapter 5.

4.0 VIEW-CPL TEST PLAN AND ANALYSIS

The VIEW-CPL testing occurred in three different phases: (1) pre-launch ground testing, (2) flight testing, and (3) post-flight ground testing. The ground testing was performed at the University of Maryland, with the exception of crew training at Johnson Space Flight Center. Flight testing of VIEW-CPL was performed by two astronauts, Dr. Tamara Jernigan and Commander Kent Rominger, in the Space Shuttle Orbiter Middeck during the STS-80 mission (November 19 through December 7, 1996). In order to achieve consistency between different test operators, detailed test plans were written with appropriate follow-up actions depending on the operator's interpretation of the real-time test results and the objectives of the test.

Since shuttle planning begins years before launches actually occur, the planning for VIEW-CPL operations was required (August 1995) before any hardware fabrication began (April 1996). In order to assist in scheduling astronaut time for flight testing, estimates of time required for VIEW-CPL testing were analyzed for several operating conditions. These analyses were described in Chapter 3 and used to design VIEW-CPL. They included:

- Determination of the pressure prime duration
- Time requirements for sensible heating of the evaporator prior to nucleation
- Pressure drop experienced during start-up (known as pressure surge)

- Time to recovery from reservoir temperature drop (known as cold-shock) after start-up
- Cool-down requirements.

Refinement of these analyses and an additional analysis on bubble life cycles were performed after the ground and flight test data were reviewed. In order to enhance understanding, individual segments of the testing process were modeled separately due to the complex characteristics observed in testing.

4.1 Payload Commands (Astronaut Instructions)

Astronaut involvement in VIEW-CPL activities included the following tasks: (1) remove the experiment from the locker and set it up in the Middeck area, (2) perform testing sequence and record data, and (3) stow experiment in the locker after testing is complete. Instructions for performing all of VIEW-CPL activities were listed in the Payload Operations Checklist [JSC, 1996c] for STS-80. The documentation included instructions for test preparation, operation, and conclusion. Tables 4.1 and 4.2 summarize the procedures to prepare for and conclude testing. Table 4.3 summarizes the tests, listing test objectives and commands to be exercised by the astronauts. The same tests were repeated during ground testing.

4.2 Test Plan Objectives and Expected Observations During Testing

Ground testing [Cullimore, 1993; Ku et al., 1993; Kolos et al., 1996] has indicated that a CPL system can operate, at least temporarily, with vapor bubbles on the liquid side of the wick. Due to gravity, these bubbles tend to consolidate

Table 4.1 Procedures for preparing VIEW-CPL testing.

Title	Objective	Command Summary
ASSEMBLY	Set-up payload in Middeck Area for Testing	Remove CPL and data acquisition system from locker and attach to Middeck area with Velcro. Attach fuse plug, power cables, and data cables. Attach video camcorder.
TEST PREPARATION	Begin collecting data (video and instruments) from payload	Attach PGSC, insert floppy disk and activate data acquisition system. Begin recording video of evaporator area.
PRESSURE PRIME	Fill the evaporator, condenser and transport lines with liquid by elevating the reservoir temperature	Turn on temperature controllers with a total of 25 W heater power. Wait 45 minutes.

Table 4.2 Procedures for concluding VIEW-CPL testing.

Title	Objective	Command Summary
PARTIAL PWRDN or TEMPORARY PWRDN	Stop collecting data after testing is finished or if power is interrupted	Deactivate data acquisition system and camcorder. Turn off all power to experiment.
STANDBY MODE	Prepare experiment for non-test periods by minimizing power while maintaining reservoir temperature above the rest of the loop (pressure priming)	Turn off power to the experiment. Turn off PGSC power and remove if needed elsewhere. Turn on the 5 W reservoir temperature controller and the reservoir temperature meter.
COOL-DOWN	Cool the evaporator and pressure prime (30 minutes) to prepare for the next test	Turn on fans, thermoelectric cooler, and 20 W + 5 W reservoir temperature controller. Wait 30 minutes.
STOWAGE	Repack the experiment in the locker for landing.	Stop collecting data and disconnect the PGSC and data acquisition system. Remove the camcorder. Disconnect power cables and fuse plug. Stow the experiment in the locker.

Table 4.3 VIEW-CPL test objectives and procedures (continued on next page).

TESTING	Objective	Command Summary
TEST IS40 and TEST S10 (S25, S35, S40, S50, S65, S75)	To start the CPL with the specified amount of power and observe the CPL operations with a vapor bubble in the core	Complete TEST PREPARATION. Pressure prime with 20 W temperature controller for 5 minutes. Turn on heater power according to Test Plan Matrix. Note observations and chose next step (Wait 10 minutes, go to HANDLING VAPOR IN EVAP CORE, or go to NO VAPOR IN EVAPORATOR) according to observations. Power off and go to COOL-DOWN or PARTIAL PWRDN.
TEST PV-LOW	To observe the effect of decreasing evaporator power.	Complete TEST PREPARATION. Pressure prime with 20 W temperature controller for 5 minutes. Turn on 35 W evaporator heater power. Note observations and chose next step according to observations. Decrease power to 25 W and note observations. Decrease power to 10 W and note observations. Power off and go to PARTIAL PWRDN.
TEST PV-GRAD	To observe the effect of gradual power variations on the evaporator	Complete TEST PREPARATION. Pressure prime with 20 W temperature controller for 5 minutes. Turn on 35 W evaporator heater power. Note observations and chose next step according to observations. Decrease power to 25 W. Increase power to 40 W. Increase power to 50 W. Increase power to 65 W. Power off and go to PARTIAL PWRDN.
TEST PV-JUMP	To observe the effect of drastic power variations on the evaporator	Complete TEST PREPARATION. Pressure prime with 20 W temperature controller for 5 minutes. Turn on 50 W evaporator heater power. Note observations and chose next step according to observations. Decrease power to 25 W wait 10 minutes. Power off and go to PARTIAL PWRDN.
TEST SS-25	To maintain evaporator power at 25 W until steady-state is reached.	Complete TEST PREPARATION. Pressure prime with 20 W temperature controller for 5 minutes. Turn on 25 W evaporator heater power. Note observations and chose next step according to observations. Maintain power for 120 minutes or until evaporator temperature reaches 60°C. Power off and go to PARTIAL PWRDN.
TEST SC	To observe the effect of reduced subcooling	Complete TEST PREPARATION. Pressure prime with 20 W temperature controller for 5 minutes. Turn on 65 W evaporator heater power. Decrease power to 25 W. Note observations and chose next step according to observations. Increase power to 35 W. Turn off subcooler fan. Power off and go to PARTIAL PWRDN.

Table 4.3 VIEW-CPL test objectives and procedures (continued from previous page).

TESTING	Objective	Command Summary
TEST CV	To observe the effect of decreased heat transfer coefficient at the condenser	Complete TEST PREPARATION. Pressure prime with 20 W temperature controller for 5 minutes. Turn on 25 W evaporator heater power. Turn off one condenser fan. Wait 10 minutes and turn off the other condenser fan. Wait 10 minutes or until there is no liquid in the evaporator core. Power off and go to PARTIAL PWRDN.
HANDLING VAPOR IN EVAP CORE	To modify test procedure to handle a vapor bubble in the core	Turn off evaporator heaters and turn on 20 W reservoir temperature controller to pressure prime the system. Turn on 25 W evaporator heater when liquid fills one-third of the evaporator core. Log observations and adjust evaporator heater power as instructed. (This procedure is performed only if a vapor bubble in the core is larger than 1 inch and one of the following tests are in progress IS40, S10, S25, S35, S40, S50, S65, or S75)
NO VAPOR IN EVAPORATOR	To modify test procedure if the evaporator will not start pumping and liquid will not boil in the vapor plenum	Turn on vapor line heater to assist with clearing the vapor line and vapor grooves. Turn on all evaporator heaters if vapor line heater does not clear grooves of liquid.

and localize. A key objective of VIEW-CPL was to determine if the bubbles cause more extensive operational problems in micro-gravity as compared to ground testing experience. Specifically, it is of significance to determine if the presence of small bubbles cause rapid wick failure or if the wick tends to be bubble tolerant as found in ground testing.

Typical CPL functionality tests were performed with VIEW-CPL. The test sequence included: (1) several start-up procedures, (2) high and low power limit investigation, (3) incremental and sudden power variations, (4) extended steady-state testing, and (5) subcooling variation. The start-up testing was designed to

determine successful procedures for starting the CPL in a micro-gravity environment. The power variation tests are used to simulate varying cooling requirements of the loop. The high and low power limits investigate the limiting factors in CPL operation. Extended steady-state testing is to investigate the reliability of a CPL system to supply cooling for extended periods of time. Subcooling variation is intended to investigate the restrictions placed on the loop due to the small slope of the vapor pressure curve of water. Test procedures, including instructions for intentionally creating conditions favorable for bubble growth on the liquid side of the wick (in the evaporator core), were included in the test sequence to visually record the effect of bubbles on the system performance.

The typical sequence of VIEW-CPL operation was as follows: (1) pressure priming, (2) start-up, (3) steady-state operation, (4) deprime and (5) re-prime. The objectives are to provide a comprehensive analysis of all five modes.

Pressure priming. As previously described in Section 2.2.1, the purpose of a pressure prime is to fill the CPL with liquid and to collapse vapor bubbles. Reservoir heaters are used to raise the reservoir pressure, forcing liquid to flow from the reservoir to the CPL. After the pressure begins to rise, vapor bubbles in the CPL begin to shrink in size as condensation occurs on surfaces adjacent to the bubble. The process occurs slowly due to the large latent heat and the small temperature difference available to drive the heat. A thermoelectric cooler on the evaporator assists in rejecting heat from the loop, as do the subcooler and condenser fans. When the pressure prime is complete, the loop is filled with

liquid. A detailed analysis of the pressure prime process is presented in Section 4.3.

One of the two different pressure prime procedures listed in Table 4.4 were used to prepare the CPL for testing, depending upon the state of the CPL. The times in Table 4.4 were estimated, from experience, as the time to complete the pressure prime. The analysis described in Section 4.3 predicts that the pressure prime could be completed within four minutes in the absence of NCG, which would indicate that pressure prime periods of thirty and forty-five minutes are conservative. The main difference between the two types of pressure prime is the time duration. Selection of the time duration used depended upon the reservoir temperature and the test plan. A regular pressure prime (45 minutes) was performed if the reservoir temperature dropped below 30°C. The cool-down pressure prime (30 minutes) was only used if another test was to be performed immediately following the preceding test and time limitations did not allow the astronaut to follow the regular pressure prime procedure.

Table 4.4 Description of pressure prime procedures used on the VIEW-CPL experiment.

Type	Purpose	Description
Regular Pressure Prime	To fill the loop with liquid. Performed after an extended unpowered period (i.e. no standby heater used to maintain reservoir above 30°C)	25 W reservoir heaters and evaporator thermoelectric cooler powered for 45 minutes. Both condenser and subcooler fans active.
Cool-down Pressure Prime	Fills loop with liquid while cooling the evaporator. Performed at the end of a test in preparation for the next test.	25 W reservoir heaters and evaporator thermoelectric cooler powered for 30 minutes. Both condenser and subcooler fans active.

Start-up. Start-up procedures were performed after a pressure prime. The first part of the start-up involved a warm-up period to increase the reservoir temperature to 40°C (required for proper testing conditions). Increasing the reservoir temperature to 40°C provided a consistent starting point for tests. Additionally, the fluid properties of water below 40°C are not as suitable for VIEW-CPL testing since the shape of the vapor pressure curve increases subcooling requirements at low temperature (see Section 2.1.1). During the reservoir warm-up period, 25 W is applied to the reservoir heaters for 5 minutes while the condenser and subcooler fans are active.

The start-up period is defined as the time from when the evaporator heater power is first turned on to the time when the vapor line is cleared of liquid and the vapor front is established in the condenser. The length and characteristics of the start-up period are dependent upon the start-up power and can be described in terms of the three segments listed in Table 4.5.

Steady-state operation. Steady-state CPL operation is characterized by the ability of the evaporator to maintain the load temperature at the reservoir set point. The existence of a vapor bubble during steady-state operations depends on the local energy balance within the evaporator. If the bubble size is constant, steady-state operations can still occur with a bubble in the evaporator core, although changes to the energy input to the evaporator are more likely to cause deprime when a bubble is present.

Table 4.5 Segments of the start-up period in VIEW-CPL testing.

	Description	Observations
1	<u>Sensible heating</u> : the time required to bring the evaporator up to saturation temperature. (Details in Section 4.4.1)	<ul style="list-style-type: none">• Increasing evaporator temperature• No change in visual observations, or small increases in the size of pre-existing gas bubbles
2	<u>Evaporation and bubble growth</u> : energy used for evaporation and critical bubble radii are established to support boiling	<ul style="list-style-type: none">• Boiling begins in the vapor grooves• Pre-existing vapor bubbles in the evaporator core expand rapidly through surface evaporation
3	<u>Stabilization</u> : the period for displacing liquid from the loop to the reservoir as vapor fills the vapor plenum and vapor line. Stabilize evaporator temperature. Heater power causes bubble growth (Details in Section 4.4.2)	<ul style="list-style-type: none">• Decrease in the rate of temperature increase for evaporator body.• Sharp increase in the vapor line temperature.• Visually, the liquid inside the vapor plenum boils away.• Pre-existing vapor bubbles in the evaporator core continue to expand and/or new bubbles in the core are formed• Decreasing reservoir temperature

Depprime and bubble life cycle. Under steady-state operations, a bubble is not expected to exist in the core of a CPL evaporator. Liquid return line heaters were included in VIEW-CPL to enable bubble generation inside the evaporator core so that the effect of a bubble on stable CPL operation could be observed. If bubble growth leads to blockage of liquid flow into the evaporator, a sudden increase in the rate of evaporator temperature rise (indicating a deprime) will be observed due to sensible heating of the evaporator body. During the testing of VIEW-CPL, intentional deprimes were caused.

Re-priming the evaporator normally requires removal of the evaporator load to allow the evaporator to re-wet. However, an oscillatory condition was observed in the VIEW-CPL testing that demonstrated a partial recovery of the

evaporator while still under load. Section 4.6.3 is devoted to explaining a theory for the observed phenomena.

4.3 Analysis of Pressure Prime

A pressure prime model was developed to investigate the energy transfer mechanisms in a CPL pressure prime and to predict the time required to collapse all the vapor in the CPL. A thermal analysis of the fluid within the CPL was performed including heat input to the fluid inside the reservoir and heat rejection from the loop as the vapor bubble condenses. Figure 4.1 shows the control volumes used for the analysis.

The reservoir control volume (denoted CV1) contains both liquid and vapor phases at all times. CV1 has constant volume but variable mass. The fluid phase leaving the reservoir is always liquid since the reservoir wick acts as a vapor barrier. The enthalpy, $h_{1,L}$, of the liquid exiting the reservoir is taken as the saturated liquid value associated with the reservoir pressure. This assumes that the fluid in the reservoir is perfectly mixed. In reality, there may be temperature gradients in the liquid and the assumption of perfect mixing is a simplifying approximation.

The second control volume (CV2) is the liquid space inside the loop. The volume of CV2 expands to accommodate the liquid flowing from the reservoir, while the vapor space (CV3) contracts. The control volume CV2 is variable in mass and volume, but the vapor quality is equal to zero. The control volume CV3 is variable in volume and quality, but the mass is constant and equal to the

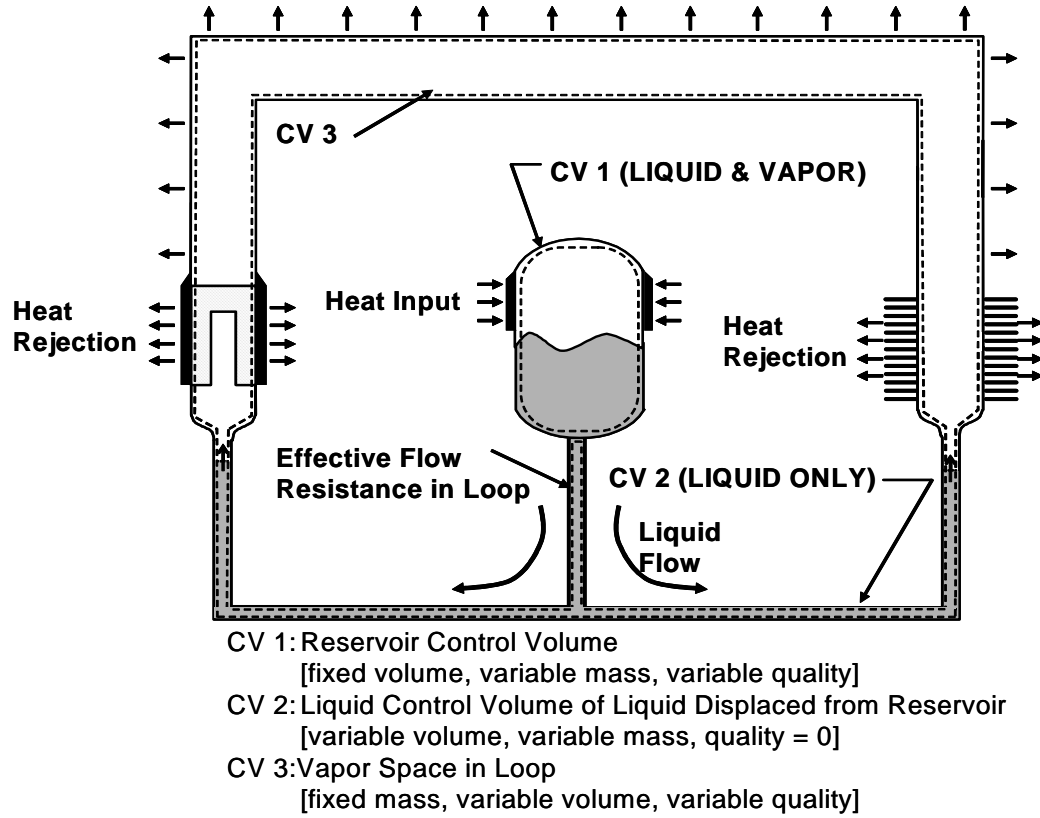


Figure 4.1 Control volumes for the pressure prime model (see Figure 1.1 for details on loop components).

mass of the vapor occupying the initial volume of CV3. This control volume choice led to simplifications in defining the momentum balance of fluid flow in CV2 and the resulting work that the fluid exerts on CV3.

Unsteady energy balances were written on the control volumes in the form

$$\frac{dU_{CV}}{dt} = \dot{Q}_{CV} - \dot{W}_{CV} + \sum \dot{m}_i h_i - \sum \dot{m}_e h_e \quad (4.1)$$

where contributions from kinetic and potential energy have been neglected. To relate the flow rate of liquid from the reservoir to the pressure difference between

the reservoir and loop, the momentum equation

$$\frac{dmv_x}{dt} = F_{x,v} + F_{x,p} \quad (4.2)$$

is used, where $F_{x,v}$ represents the viscous force for fully-developed, laminar flow in a pipe, $F_{x,v} = \tau_x \pi DL = \rho f \frac{L}{D} \frac{\pi}{4} D^2 \bar{v}^2 / 2$, with the friction factor for laminar flow, $f = 64/Re$, and $F_{x,p}$ represents the pressure forces, $F_{x,p} = \Delta P \cdot A$, acting on the control volume. During a pressure prime of VIEW-CPL, the flow regime in the transport lines is laminar and the inertial term in the momentum balance is small compared to the pressure and viscous forces. Therefore Eq. 4.2 reduces to

$$\frac{P_3 - P_1}{\rho} = \sum_{i=1}^n \frac{128 \mu L_i}{\rho^2 \pi D_i^4} \frac{dm_2}{dt} \quad (4.3)$$

The flow resistance, $c = \sum_{i=1}^n \frac{128 \mu L_i}{\rho^2 \pi D_i^4}$, is determined from the sum of the resistances in the transport lines of the path that the fluid takes as it leaves the reservoir. Table 4.6 summarizes the effective flow resistance for the two parallel paths, one through the vapor line and the other through the liquid line. The wick flow resistance is not added to the overall resistance because this is expected to be the point of no flow since it has the largest resistance, meaning that the liquid will flow through the vapor and liquid lines and bound a vapor space that has the wick enclosed within it.

During the pressure prime, the flow starts from rest so there is a period of time over which the core of the flow inside the lines and grooves must be accelerated while the flow near the wall is restrained by friction [White, 1991].

Table 4.6 Effective flow resistance in VIEW-CPL components.

VIEW-CPL Component	Length (cm)	Hydraulic Diameter (cm)	L/D including minor losses	For Laminar Flow Only. Fluid Properties at 25°C. $c = \frac{128\mu L}{\rho^2 \pi D^4 n}$ <m ² /kg-s>
<u>Common Path</u>				
Reservoir line	16.51	0.457	48.1	18.47
Tee (branch)	0	0.775	60	4.73
Common Reservoir Path				c_{COMMON} = 23.20
<u>Path 1</u>				
Liquid line	20.97	0.775	39.0	3.08
Evaporator inlet tube	6.86	0.175	39.1	266.68
Evaporator inlet fitting (poly)	2.54	0.635	4.0	0.57
Path 1 Total				c_{PATH1} = 270.33
<u>Path 2</u>				
Liquid line	3.81	0.775	64.9	5.12
Condenser tube	5.00	2.36	2.14	0.01
Condenser (4 flow channels)	12.70	0.613	20.72	0.83
Vapor Line	39.37	0.775	74.82	5.90
Evaporator (6 vapor grooves)	10.16	0.238	42.67	19.32
Path 2 Total				c_{PATH2} = 31.18
Effective Flow Resistance = c_{COMMON} + 1/(1/c_{PATH1} + 1/c_{PATH2})				51.16
Evaporator (wick)				2546*

*Flow resistance in the evaporator is calculated using Darcy's law (Eq. 2.7) for half the wick

White [1991] presents Szymanski's [1932] solution for the velocity profile of fluid flow in a long pipe with a sudden, uniform and constant pressure gradient applied at time zero. From Szymanski's velocity profile, a transient friction factor was determined from

$$f(t) = \frac{64/Re}{1 - 32 \left[\sum_{n=1}^{\infty} \left(\exp \left(-4 \lambda_n^2 \nu_l \frac{t}{d^2} \right) \frac{1}{\lambda_n^4} \right) \right]} \quad (4.4)$$

where λ_n are the roots of Bessel function J_0 and ν_l is the liquid viscosity. The solution indicated that the velocity profile approached Poiseuille flow for $t^* \approx 0.75$, where

$$t^* = \frac{\nu_l t}{r^2} \quad (4.5)$$

For liquid water at 20°C, the velocity profiles across the flow area of the vapor grooves, reservoir line, condenser grooves, and vapor line would approach the Poiseuille paraboloid after 1.1, 3.9, 7.0, and 11.2 s, respectively. These times are relatively short compared to the duration of the pressure prime. During the transient, the frictional terms are larger than those listed in Table 4.6 which were predicted for fully developed flow.

To check the assumptions of fully developed flow and no flow through the wick, a sensitivity analysis was performed for the flow resistance term, c in Eq. 4.3. The sensitivity of the pressure prime duration to flow resistance was very small (within the resolution of the 5-s time step) for a 20% change in the flow resistance term ($c=51.2 \pm 10.2 \text{ m}^2/\text{kg}\cdot\text{s}$). The resistance term was increased 10 and 100 times with an increase in the pressure prime duration of less than 1% and 8%, respectively. The insensitivity to the resistance term supports the use of the fully developed assumptions.

The equations describing the pressure prime are summarized in Table 4.7 with a list of assumptions for all three control volumes. Using property relations

for the liquid and vapor, these equations can be solved to obtain the time dependent operating conditions of the reservoir and loop.

The pressure prime model predicts the transient response of temperature and pressure of the loop to the reservoir heat input and loop heat rejection. The inputs to the model for the VIEW-CPL system are listed in Table 4.8. The starting point for the model is assumed to be an equilibrium two-phase state at ambient temperature.

The output of the model is a time series of control volume properties that are presented in Figure 4.2. The integration stops when the quality and volume of CV3 approach zero. The time step size governs how close to zero the model can integrate. A time step of 5 s was chosen for the analysis shown here; the accuracy of the time integration was verified by repeating calculations with a 2.5 s time step resulting in a change in temperature and time to complete the pressure prime of less than 0.05%.

The model results predict that the time required to collapse the vapor inside the loop is 225 s given the flow conditions and the heat transfer characteristics described by the flow resistance, c , and the heat transfer coefficient on a unit length basis, UA_{pL_3} in Table 4.8. However, the predicted time to complete the pressure prime is less than that observed in both VIEW-CPL and previous water CPL experiments tested at the University of Maryland [Kolos et al., 1996] which was on the order of 20 minutes. The input value for the heat transfer coefficient UA_{pL_3} of 0.097 W/m-K represents heat transfer on a unit

Table 4.7 Governing equations for the pressure prime control volumes.

CV1	<p>Mass Balance $\frac{dm_1}{dt} = -\dot{m}_e \quad (4.6)$</p> <p>Energy Balance $(u_1 - h_{1,L}) \frac{dm_1}{dt} + m_1 \frac{du_1}{dt} = \dot{Q}_1 \quad (4.7)$</p> <p>Heat Transfer Rate $\dot{Q}_1 = \dot{Q}_{heater} - m_{ss} c_p \frac{dT}{dt} - UA_R (T_1 - T_\infty) \quad (4.8)$</p> <ul style="list-style-type: none"> • Energy is added to the control volume from the reservoir heaters • The reservoir volume is fixed volume, therefore only flow work is performed on the control volume • Only liquid can exit the reservoir; $h_{1,L}$ is saturated liquid enthalpy at reservoir temperature • $m_{ss} c_p$ is the thermal capacitance of the stainless steel reservoir housing
CV2	<p>Mass Balance $\frac{dm_2}{dt} = -\frac{dm_1}{dt} \quad (4.9)$</p> <p>Energy Balance $(u_2 - h_{1,L}) \frac{dm_2}{dt} + m_2 \frac{du_2}{dt} = \dot{Q}_2 - P_3 \frac{dV_2}{dt} \quad (4.10)$</p> <p>Force Balance $\frac{P_3 - P_1}{\rho} = \frac{64}{Re} \frac{L}{D} \frac{\bar{V}^2}{2} = c \frac{dm_2}{dt} \quad (4.11)$ where $c = \frac{128\mu L}{\rho^2 \pi D^4}$</p> <ul style="list-style-type: none"> • Energy, \dot{Q}_2, could be added to the control volume from interaction with CV3 but was neglected for this analysis • The volume is variable and increases according to the liquid displaced from the reservoir; work is performed on CV3 as CV2 increases in volume • Only liquid can enter from the reservoir
CV3	<p>Mass Balance $\frac{dV_3}{dt} = \frac{1}{\rho} \frac{dm_1}{dt} \quad (4.12)$</p> <p>Heat Transfer Rate $\dot{Q}_3 = -UA_3 (T_3 - T_\infty) \quad (4.13)$</p> <p>Energy Balance $m_3 \frac{du_3}{dt} = \dot{Q}_3 + P_3 \frac{dV_2}{dt} \quad (4.14)$</p> <ul style="list-style-type: none"> • No mass change in control volume, only quality and volume change • Energy is transferred from the control volume from interaction with ambient • The overall heat transfer coefficient, UA_3, is a combination of condensation film coefficient and insulation resistance and is dependent on the surface area of the vapor space

Table 4.8 Inputs to the pressure prime model representing VIEW-CPL.

Variable	Value	Description
dt	5 s	Time step for integration
$T_{1,o}, T_{amb}$	25°C	Initial reservoir and ambient temperature
V_1	264.1 cc	Reservoir volume, calculated from VIEW-CPL dimensions
charge	0.240 kg	Charge of fluid into loop, measured from VIEW-CPL
f_{liq}	0.9087	Volume liquid fraction in reservoir, calculated from charge and reservoir volume assuming all liquid is contained in the reservoir
Q_1	25 W	Reservoir heater power
$m_{ss}c_p$	0.25 kJ/K	Thermal mass of reservoir housing
c	27.7 m ² /kg-s	The sum of the liquid flow resistance from fluid flowing through the VIEW-CPL tubing (see Table 4.6)
UA_{pL_3}	.0973 W/m-K (without NCG)	Conductance from the vapor space to ambient. Includes appropriate values for condensation film coefficient, insulation, and free convection to ambient on a per unit length basis.
UA_{pL_3} degraded for effect of NCG	.0059 W/m-K	Condensation conductance is degraded with the presence of noncondensable gas
$V_{3,o}$	94.9e-6 m ³	Vapor space volume, calculated from the VIEW-CPL loop volume
m_3	2.19e-6 kg	Mass of vapor in CV3, calculated from vapor volume and density at initial temperature
UAR	0.29 W/K	Heat loss from the reservoir (see Section 5.1.3)

length basis for a vapor space without any noncondensable gas, which may not be correct for a water system operating at subatmospheric pressure. It is well known [Wang and Tu, 1988; Minkowycz and Sparrow, 1966] that even small amounts of noncondensable gas can significantly decrease the heat transfer rate during a condensation process. Since the results of the pressure prime are

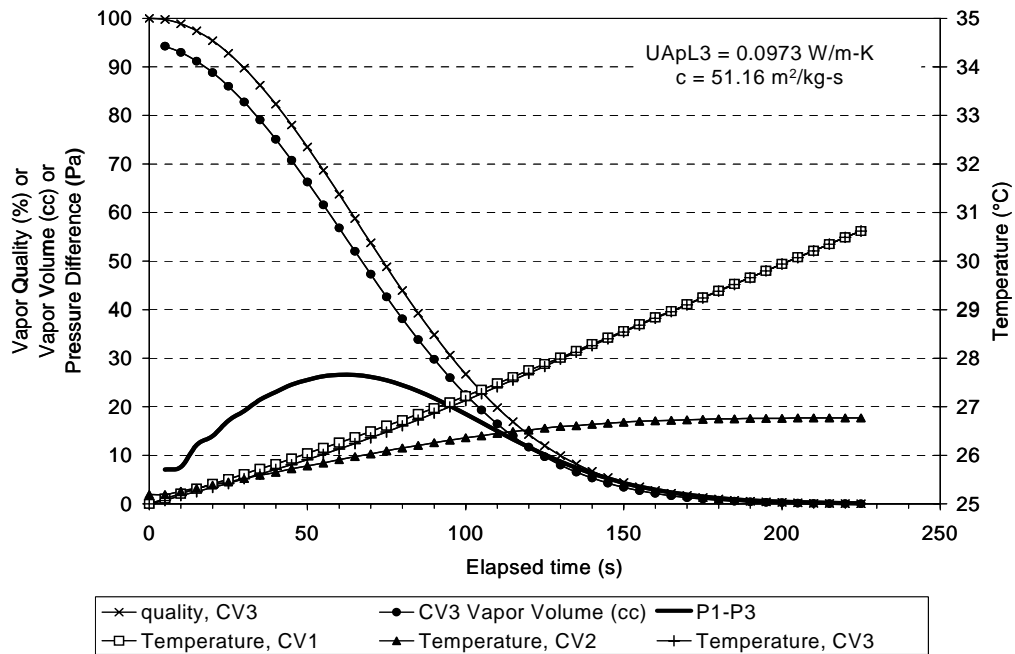


Figure 4.2 Results of pressure prime model using VIEW-CPL inputs from Table 4.8 (assuming no noncondensable gas).

sensitive to the heat transfer coefficient, a parametric study was performed to evaluate the effect on the length of time required to complete the pressure prime. The results are presented in Figure 4.3, which shows a sharp increase in pressure prime duration for overall conductance below 0.01 W/m-K. For the extreme case of a perfectly insulated loop, without the ability to reject the latent heat, the vapor space does not collapse. For larger conductance values only a small temperature difference between the loop and ambient is required to reject the energy and the pressure prime occurs quickly (less than 100 s for values greater than 1 W/m-K).

Figure 4.4 contains the results of the pressure prime model for an overall conductance of 0.00585 W/m-K (6% of the expected conductance without NCG),

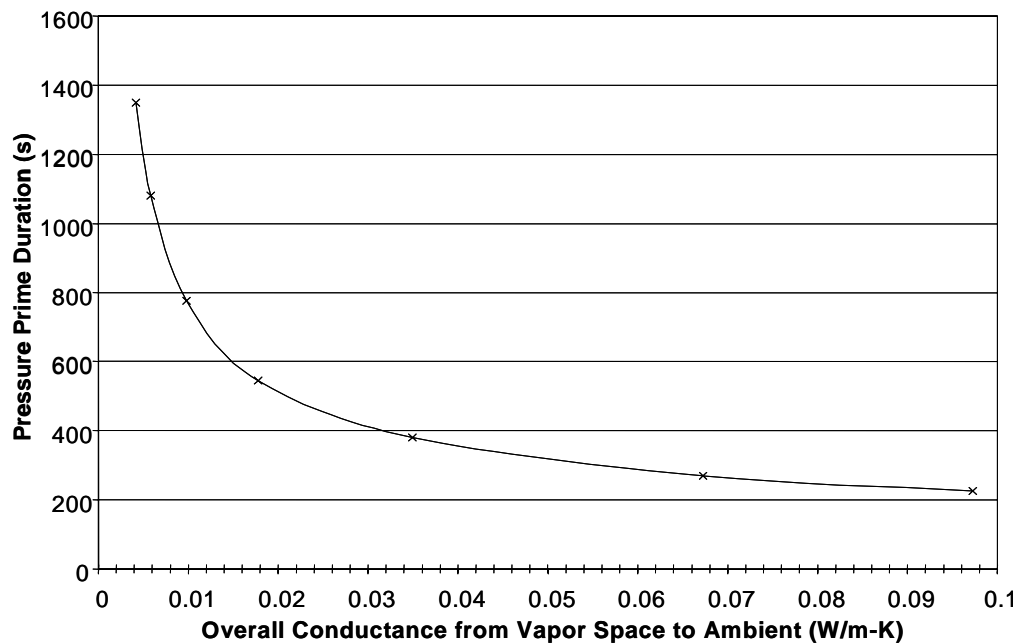


Figure 4.3 Predicted effect of overall conductance on the duration of the pressure prime.

which based on previous experience are more representative of actual pressure primes. The predicted pressure prime was complete at 1080 s when the vapor quality of CV3 was less than 2×10^{-4} and the vapor volume less than 0.005 cc. The temperature difference between the reservoir and loop at the end of the collapse is 18.3 K. A comparison of test data to the pressure prime model prediction is presented in Section 5.1.2.

4.4 Start-up Analyses

The start-up analyses cover the period from initial heat application to the evaporator to the establishment of a vapor interface within the condenser. The first analysis is a transient conduction analysis to determine the time required to heat the evaporator to a temperature necessary to initiate boiling. The second

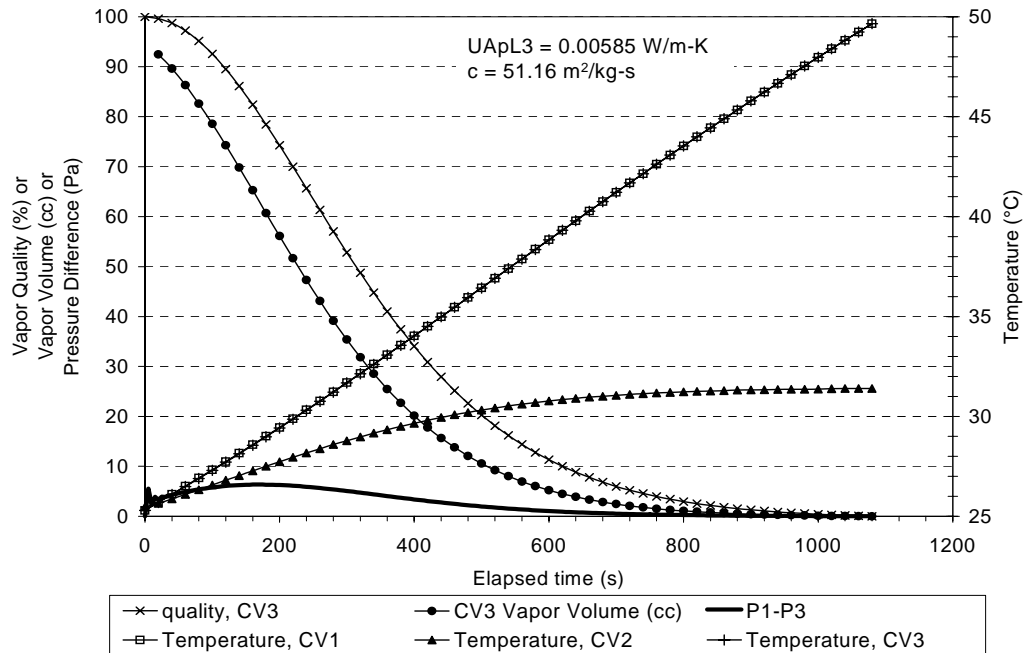


Figure 4.4 Prediction from pressure prime model with heat transfer coefficient modified for effect of noncondensable gas.

analysis is the pressure surge calculation to determine if the capillary limit of the wick was exceeded as vapor displaces liquid from the vapor grooves and vapor line to the reservoir. A cold shock analysis is also performed to explain the observation of bubbles inside the evaporator core during the VIEW-CPL operation.

4.4.1 Sensible heating of the evaporator

In the VIEW-CPL testing, the start-up begins by applying power to the evaporator heaters. Prior to nucleate boiling and evaporation, the temperature of the stainless steel evaporator block, saturated wick material, and liquid must rise up to the saturation temperature. The analysis of this process is based on thermal conduction within the evaporator. The results of the analysis provide a

prediction of the time for boiling to initiate for a given evaporator heater power and saturation temperature.

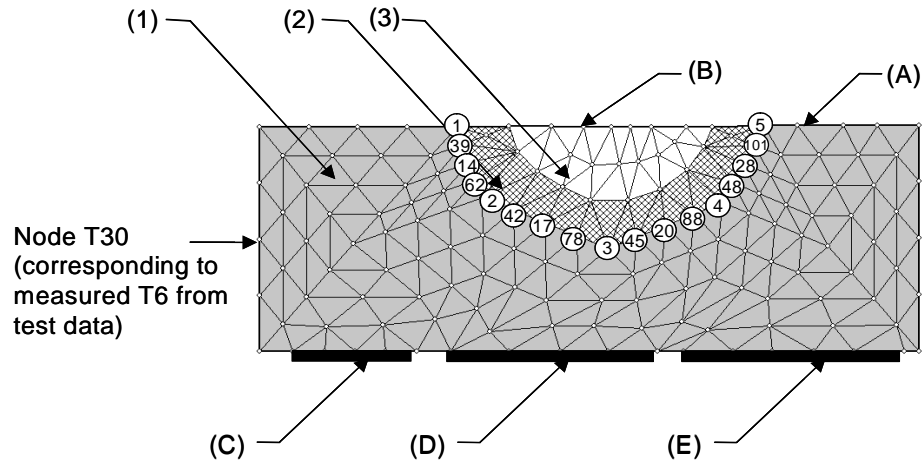
The conduction analysis was performed with a finite element model. The stainless steel evaporator block was analyzed in a two-dimensional domain, as shown in Figure 4.5, which contains a saturated wick in close contact with the block and a liquid filled core inside the wick. Insulated boundary conditions are imposed on the outer boundary except at heater locations. Constant material properties were used for all materials in the domain. Node 30 (refer to Figure 4.5) in the domain corresponds to the location of the VIEW-CPL temperature sensor (T6) on the side of the evaporator block (see Figure 3.20).

The transient model was exercised using a Crank-Nicholson solution method with various combinations of heater powers (to simulate the VIEW-CPL heaters) for boundary conditions. The normalized temperature, \bar{T} , is defined by

$$\bar{T} = T - T_o \quad (4.15)$$

where T_o is the initial temperature of the evaporator block. Normalizing temperature in this manner allows comparison with experimental data having different initial conditions.

The grid in Figure 4.5 contains 268 elements with 156 nodes and was solved with a maximum time step of 10 s. Adequate spatial resolution was verified by refining the grid to 1072 elements with 579 nodes and running at 10 s. Temporal resolution was verified by solving the original grid with a maximum



BOUNDARY CONDITIONS

(A) Insulated from Ambient: $\text{Flux} = 0$

(B) Liquid to Ambient: $dT/dy = 0$

(C) $11 \text{ W} / 11.24 \text{ cm}^2$

(D) $28 \text{ W} / 24.13 \text{ cm}^2$

(E) $43 \text{ W} / 25.13 \text{ cm}^2$

MATERIAL PROPERTIES

(1) 304 Stainless Steel (6.1 cm x 2.2 cm):

$k = 14.9 \text{ W/m-K}$, $c_p = 477 \text{ J/kg-K}$, $\rho = 7900 \text{ kg/m}^3$

(2) Saturated polyethylene wick (50% porosity):

$k = 0.49 \text{ W/m-K}$, $c_p = 3140 \text{ J/kg-K}$, $\rho = 970 \text{ kg/m}^3$

(3) Liquid water:

$k = 0.60 \text{ W/m-K}$, $c_p = 4179 \text{ J/kg-K}$, $\rho = 997 \text{ kg/m}^3$

All material properties are from Incropera & DeWitt [1990] except for polyethylene properties which are from Callister [1991].

Figure 4.5 Two-dimensional finite element grid for the VIEW-CPL transient conduction analysis.

time step of 1 s. Both checks on resolution gave results identical to two significant digits as compared to the coarser grid and time step.

The end of the conduction phase is determined when any location along the outside of the wick reaches saturation temperature. This assumes that no superheat is required to initiate boiling. Such an assumption may be valid for the VIEW-CPL experiment since it is a low-vapor pressure system and other tests of

similar two-phase systems have indicated that noncondensable gas reduces the amount of superheat required to begin nucleate boiling [Wrenn et al., 2000]. Figure 4.6 is a plot of the predicted normalized wick temperature at the warmest node, \bar{T} , as a function of time. The traces on Figure 4.6 correspond to the power available from the VIEW-CPL heaters. Since the heaters are installed asymmetrically, the location of the warmest wick node (identified parenthetically next to the heater power on Figure 4.6) varies according to the heaters selected. When the 43 W heater is used, the warmest wick nodes are located on the right side of the grid where the 43 W heater is located. The 11 W and 28 W heaters and the combination of the two results in the warmest wick node located on the

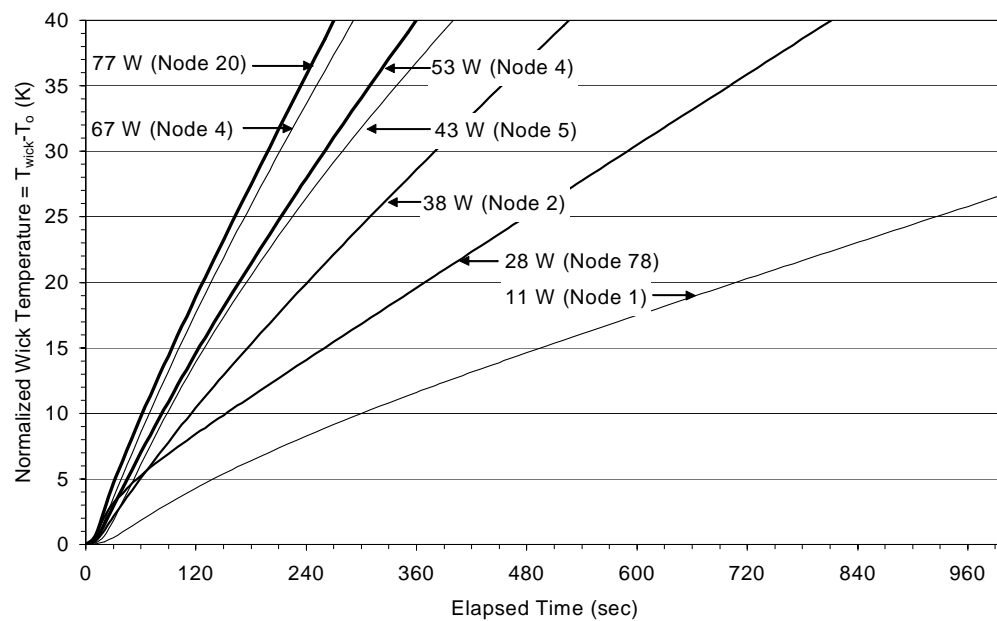


Figure 4.6 Normalized wick temperatures predicted for the VIEW-CPL heater combinations. Temperature traces were selected from the warmest node at the wick/stainless steel interface (refer to Figure 4.5) for each given heater combination.

left side of the grid. The VIEW-CPL evaporator typically starts from room temperature (25°C) and must reach the reservoir set-point (saturation temperature) of 40°C for boiling to occur. This corresponds to a normalized wick temperature, \bar{T}_{wick} , equal to 15 K. The resulting warm-up period ranges from 100 s for the 77 W heater combination (all three heaters with reduced voltage due to extra load on the power supply) to 500 s for the 11 W heater.

Figure 4.7 is a plot of the predicted normalized-evaporator temperature at node 30 corresponding to the VIEW-CPL temperature sensor location T6. This plot is important for comparing model predictions to the measured temperature values. The symbols on the plot indicate the time at which any node on the wick

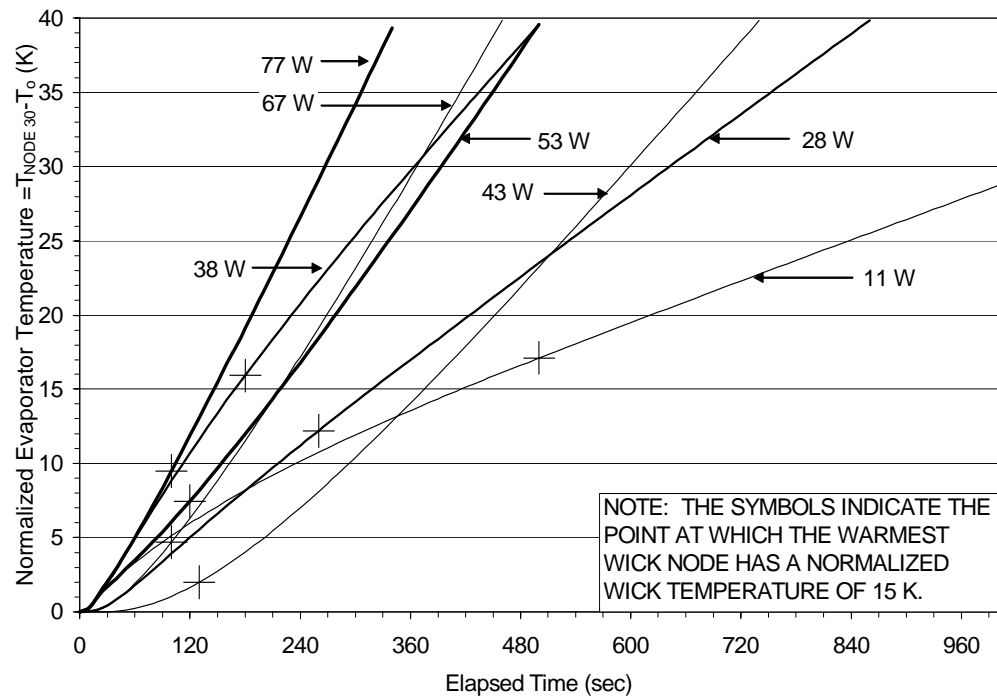


Figure 4.7 Normalized evaporator temperatures predicted at node 30 (refer to Figure 4.5) for VIEW-CPL heater combinations.

reaches a normalized temperature of 15 K (corresponding to a saturation temperature of 40°C and an initial temperature of 25°C, typical of VIEW-CPL tests). Depending upon the heater combination, the temperature sensor can read as low as 13 K below the wick temperature for the worst case of 43 W, or as high as 2 K above wick temperature for the case of 11 W. The difference between the evaporator body temperature and the wick temperature is due to the thick stainless-steel evaporator housing, and the uneven heating on the evaporator due to the discrete heater locations.

4.4.2 Vapor line clearing

The larger than normal pressure drop, known at the pressure surge, that is typically experienced during CPL start-up as liquid is displaced from the evaporator vapor grooves and vapor line to the reservoir is described in Section 2.2.1. A design estimation of the pressure surge for VIEW-CPL that was presented in Figure 3.18 predicted that the capillary limit of the evaporator (10 kPa for water at 50°C for the 13.7 μm pore radius in the wick, assuming a 0° contact angle) would be exceeded during start-up if the net power for evaporation was greater than 2 W, thus allowing vapor into the evaporator core. Additionally, the core could become superheated if the pressure drop causes the local vapor pressure to decrease below the saturation temperature (for the example presented in Section 3.2.4 with a typical saturation temperature of 50°C and local core temperature of 25°C, a pressure drop greater than 7330 kPa would pass the local saturation pressure).

In order to more accurately predict the amount of energy used for evaporation, the magnitude of the pressure surge and the duration over which the high pressure drop is experienced, a model of the pressure surge was adapted from the work of Hoang and Ku [1996] and used to analyze the VIEW-CPL start-up. The mass, momentum, and energy balances for the control volumes in Figure 4.8 were solved to find the pressure difference between the evaporator and reservoir that is required for liquid to flow into the reservoir. Note that the control volume labels (CV1, CV2, and CV3) for the pressure surge model

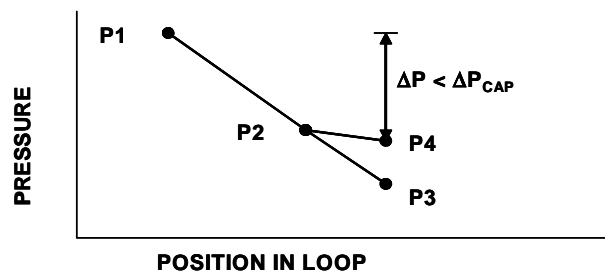
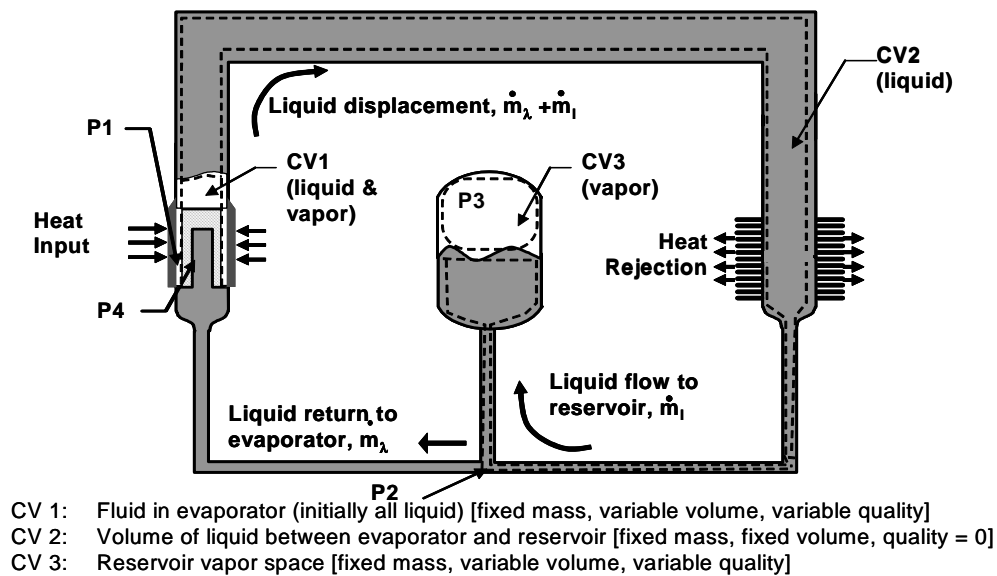


Figure 4.8 Control volumes for the pressure surge model (see Figure 1.1 for details on loop components).

correspond to different CPL components than the control volumes with the same labels in the pressure prime model (in Section 4.3). The control volume change results from the different location of energy input to the loop between the two models. Energy input to the loop is at CV1, which in the pressure prime model is at the reservoir and in the pressure surge model it is at the evaporator. Vapor compression occurs in CV3, which in the pressure prime model is around the loop and in the pressure surge model is around the vapor in the reservoir. CV2 is the same for both models.

At the onset of nucleation in the vapor grooves, liquid can flow to the reservoir through two paths: (1) through the vapor grooves and into the vapor line, or (2) back-flow through the evaporator wick and into the liquid line. The flow resistance through the wick and liquid line (back-flow) is an order of magnitude greater than the flow resistance through the vapor line and therefore the preferential flow direction is through the vapor line. Once a meniscus is established in the evaporator wick, the fluid cannot locally flow back into the wick unless the maximum capillary pressure is exceeded. Therefore the back-flow area through the wick decreases as the vapor grooves clear which further increases the resistance to back-flow into the core of the wick. Finally when the vapor grooves are filled with vapor, there is no path for back-flow into the core. Since the back-flow is small compared to the forward flow through the vapor line, it is neglected in this analysis.

Following the same methodology used for the pressure prime model, governing equations for the control volumes are summarized in Table 4.9. The energy balances on the control volumes are derived from Eq. 4.1. The momentum balance (from Eq. 4.2) is rewritten in terms of the CV2 mass, dm/dt , as

$$\Delta P = \left(\sum_i \frac{f_i}{\rho} \beta_i \right) \left(\frac{dm}{dt} \right) \left| \frac{dm}{dt} \right| + \alpha \frac{d^2 m}{dt^2} \quad (4.16)$$

$$\text{with } \beta_i = \frac{L_i}{D_i} \frac{1}{2A_i^2} \frac{1}{n^2} \text{ and } \alpha = \sum_i \frac{V_i}{A_i^2 n}$$

In Eq. 4.16, the inertial coefficient, α , and the frictional coefficient, β , are functions solely of the VIEW-CPL flow channel geometry (number of parallel flow paths n , length L , diameter D , area A , and volume V) and are summarized in Table 4.10. Equivalent L/D (refer to Table 3.12) were used for flow through bends and fittings.

The liquid flow through the loop remains in the laminar flow regime provided that the flow rate does not exceed 7 g/s. The maximum flow rate predicted during the start-up is 3.5 g/s when using the 75 W heater. Therefore, laminar flow is assumed for all of the start-ups. By nature of the laminar friction factor for smooth wall tubes, the frictional term of Eq. 4.3 is directly proportional to the mass flow rate. The proportionality constants, $\frac{f}{\rho} \beta \left(\frac{dm}{dt} \right)$, given in column 3 of Table 4.10, show that the reservoir line dominates in the flow resistance term by accounting for 74% of the total flow resistance. The frictional terms in Eq. 4.16

Table 4.9 Conservation equations of energy, momentum, and mass for the pressure surge control volumes (continued on next page).

CV1 (Liquid Volume in Evaporator and Volume of vapor in evaporator and vapor line)	$m \frac{du_1}{dt} = \dot{Q}_{evap} - F \dot{Q}_{wall} - P \frac{dV_1}{dt} \quad (4.17)$ $m_{ss} c_{pss} \frac{dT_{ss}}{dt} = \dot{Q}_{in} - UA(T_{ss} - T_{amb}) - \dot{Q}_{evap} \quad (4.18)$ <ul style="list-style-type: none"> Evaporation film coefficient from a correlation for boiling in free convection [Stephan, 1992] applied to the groove surface area bound by the evaporator block. $\dot{Q}_{evap} = h_{evap} w L (T_1 - T_{ss})$ Since there is no mass flow exiting the control volume, and the mass flow rate in is small, the mass balance gives $\frac{dm_1}{dt} = \dot{m}_{in} \approx 0 \quad (4.19)$ Assuming that all of the input power is used to evaporator liquid at 40°C, then by neglecting the energy carried into the control volume the maximum error introduced is 3.5% of the input power Since the change in fluid specific volume is small, the rate of vapor expansion is determined from the amount of vapor generated $\frac{dV_1}{dt} = m x \frac{dv_v}{dt} + m v_v \frac{dx}{dt} + m(1-x) \frac{dv_l}{dt} + m v_l \frac{d(1-x)}{dt} \quad (4.20)$ $\frac{dV_1}{dt} \approx m(v_v - v_l) \frac{dx}{dt}$ Pressure drop due to vapor flow is neglected in CV1 Heat loss UA was determined from experimental data (see section 5.1.2) The wall of the vapor line is heated as the vapor front advances. F is a flag to indicate when the vapor enters the vapor line: $F=0 \text{ if } V \leq 15.9 \times 10^{-6} \text{ m}^3$ $F=1 \text{ if } V > 15.9 \times 10^{-6} \text{ m}^3$ <p>The energy stored in the vapor line wall is a function of the amount of wall exposed. A condensation film coefficient of 500 W/m²-K (approximated for low flow rate from Figure 3.10) is applied around the inner diameter of the tube. The volume of wall exposed during a time step is related to the rate of volume change of the control volume using the geometry of the vapor line.</p> $m c_{ss} \frac{dT_{wall}}{dt} = \dot{Q}_{wall} - UA(T_1 - T_{amb}) + \frac{dm}{dt} c_{ss} (T_{amb} - T_{wall}) \quad (4.21)$ $\dot{Q}_{wall} \approx h \pi D L (T_1 - T_{wall})$
--	--

Table 4.9 Conservation equations of energy, momentum, and mass for the pressure surge control volumes (continued from previous page).

CV2 (Liquid volume between vapor spaces in the vapor line and reservoir)	<ul style="list-style-type: none"> No mass flow into or out of the control volume and no heat transfer in energy balance (neglect frictional heat transfer), therefore the energy balance is trivial. Control volume moves due to vapor expansion; relative to the vapor line wall, the liquid mass flow rate is determined from Eq. 4.20 Momentum balance for the accelerating control volume is determined from Eq. 4.16 where $\Delta P = P_1 - P_3$, β and α values are from Table 4.10.
CV3 (Reservoir gas and vapor volume)	<ul style="list-style-type: none"> No liquid/vapor mixing inside of the reservoir Heat transfer from the gas to the reservoir wall is limited to conduction through the polyethylene wick between the vapor and the wall, $Q_{vap} = UA(T_{res} - T_3)$ $m_3 \frac{du_3}{dt} = \dot{Q}_{vap} - P_3 \frac{\partial V_3}{\partial t} \quad (4.22)$ No change in mass (i.e., vapor compression results in temperature rise, and quality change) Volume inside the CPL is fixed and CV2 is incompressible, therefore any volume change in CV1 is balanced in CV3 $\frac{dV_3}{dt} = - \frac{dV_1}{dt} \quad (4.23)$ Reservoir wall temperature is a function of heater power (5 W) and heat loss to ambient, where UA_{res} is determined from test data. $m_{ss} c_{ss} \frac{dT_{res}}{dt} = UA_{amb} (T_{res} - T_{amb}) - Q_{vap} + Q_{heater} \quad (4.24)$

Table 4.10 Frictional (β) and inertial coefficients (α) from Eq. 4.16 for liquid flow in VIEW-CPL geometry.

VIEW-CPL Component	β <10 ⁹ 1/m ⁴ >	For Laminar Flow Only. Liquid Properties at 20°C. $\frac{f}{\rho} \beta \left(\frac{dm}{dt} \right) = 64 \frac{\mu A}{\rho D} \beta n$ <10 ³ 1/m-s>	α <10 ³ 1/m>
Vapor grooves (n=6)	7.73	7.58	2.67
Vapor line (n=1)	16.84	6.59	9.97
Condenser Inlet	0.00	0.00	0.06
Condenser Grooves (n=4)	0.48	0.74	0.86
Condenser Exit	0.16	0.19	0.06
Liquid Line (to tee at reservoir line)	1.11	0.43	0.81
Reservoir Line	200.56	46.31	11.99
Path 1 Total		61.84	26.42
Wick*	-	1426.10	-
Inlet plug	34.30	11.00	1.76
Conduction tube line	3361.81	297.58	28.43
Liquid line (0.775 cm ID)	12.74	4.98	4.85
Reservoir line	200.56	46.31	11.99
Path 2 Total**		1785.97	47.03

*The frictional coefficient for the wick is calculated using Darcy's law.

**Path 2 is not included in the pressure surge model because the resistance is 28 times larger than path 1 and there will only be a small amount of back-flow

are applicable for fully-developed Poiseuille flow. During the pressure surge, the flow starts from rest so there is a period of time over which the core of the flow inside the grooves and lines must be accelerated while the flow near the wall is restrained by friction [White, 1991]. As in the pressure prime analysis, the transient friction factor is determined by Eq. 4.4 and the solution indicated that the

velocity profile approaches the Poiseuille paraboloid after 1.1, 3.9, 7.0, and 11.2 s for the vapor grooves, reservoir line, condenser grooves, and vapor line, respectively. This indicates that the frictional terms are larger than those predicted in Table 4.10 for the above times. However, the transient friction factor for the reservoir (since this was the dominant pressure drop) caused no change (within two significant digits) in predicted transient values for the vapor volume and temperature solutions compared to the solution using the Poiseuille flow frictional term, even when using a time step 20 times smaller than the time required for the flow to fully develop. The solution using the transient friction factor is the same as the solution using the fully developed friction factor because the pressure surge process is dominated by heat transfer, not viscous pressure drop.

For comparison with test data, the pressure surge is divided into two time segments. The first time segment is the clearing of the vapor grooves and vapor plenum, the time for which can be obtained from VIEW-CPL video data. The second segment is the clearing of the vapor line; these data are inferred from temperature measurements at the entrance to the condenser (T3 in Figure 3.20). Table 4.11 contains a summary of initial conditions and volumes for the pressure surge calculation and the VIEW-CPL geometry. The total pressure surge is over when the vapor line is filled with vapor.

The results from exercising the model with 35 W applied to the evaporator are shown in Figure 4.9. The plot contains time traces of the evaporator wall

Table 4.11 Initial conditions and volumetric summary for VIEW-CPL pressure surge calculation.

	Initial conditions	Conditions during calculations
CV1	<p>Initial fluid mass = 8.59 g</p> <p><u>Initial volume (time = t_0):</u> CV1(t_0) = 8.68 cc [Volume of core, 4.73 cc + Volume in wick, 3.95 cc] Vapor volume = 0 cc Initial quality = 0</p>	<p>Constant fluid mass = 8.59 g</p> <p><u>For comparing to video (time = t_1):</u> CV1(t_1) = 13.63 cc [CV1(t_0), 8.68 cc + volume of vapor grooves, 3.51 cc + volume of vapor plenum, 1.44 cc] Vapor volume = CV1 - Initial vol = 4.95 cc</p> <p><u>For allowing condensation in vapor line (time=t_2):</u> CV1(t_2) = 15.94 cc [Volume CV1(t_1), 13.63 cc + volume of evaporator exit, 2.31 cc] Vapor Volume = CV1 - Initial vol = 7.26 cc</p> <p><u>At completion of pressure surge (time=t_3):</u> CV1(t_3) = 37.79 cc [Volume CV1(t_2), 15.94 cc + volume of vapor line, 21.85 cc] Vapor volume = CV1 - Initial vol = 29.11 cc</p>
CV3	<p>Initial fluid mass = 0.008 g Initial quality = 0</p> <p><u>Initial volume (time = t_0):</u> CV3(t_0) = 121.3 cc [Free volume in reservoir, 246.1 cc - Volume of liquid in reservoir, 124.8 cc]</p>	<p>Constant fluid mass = 0.008 g</p> <p><u>At completion of pressure surge (time=t_3):</u> CV3(t_3) = 92.2 cc [Volume CV3(t_0), 121.3 cc - (CV1(t_3)-CV1(t_0)), 29.1 cc]</p>

temperature, evaporator vapor temperature, vapor line wall temperature, vapor volume, pressure difference between reservoir and evaporator, and the evaporation rate. As evaporation occurs in the evaporator, the vapor space (CV1) expands and pushes liquid (CV2) into the reservoir and compresses the vapor in the reservoir (CV3). There is initially a pressure spike (140 Pa) between

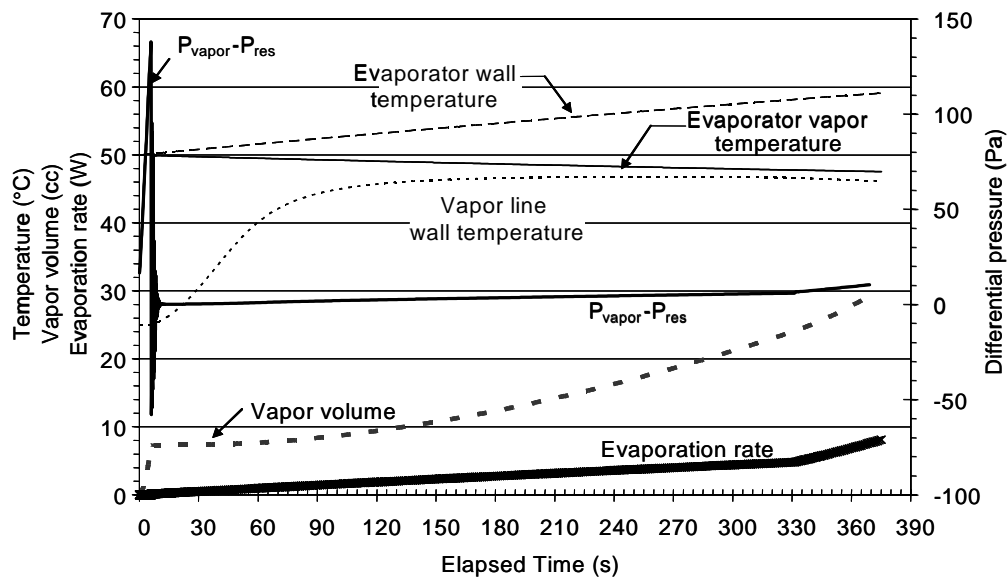


Figure 4.9 Pressure surge prediction for 35 W on VIEW-CPL evaporator.

the reservoir and the vapor space because the vapor volume is limited. The evaporator wall temperature increases steadily during the pressure surge. This occurs because the amount of fluid that is evaporated is limited by the pressure difference between the reservoir and evaporator, resulting in sensible heating of the evaporator. The temperature difference that results from the pressure difference is present in all CPL systems, but is more apparent with a fluid having low vapor pressure.

The pressure spike ends as the vapor from CV1 expands into the vapor line. Prior to the vapor entering the vapor line, there is no heat sink for the vapor space and the vapor temperature is nearly the same as the evaporator wall temperature. Once the vapor enters the vapor line, condensation occurs on the vapor line wall and the temperature of the vapor space is decreased as energy

is removed from the control volume. Figures 4.10 and 4.11 are exploded views of the initial 10 s of the vapor groove and vapor line clearing. Figure 4.10 is a plot of the evaporator, vapor, and reservoir temperatures and Figure 4.11 is a plot of the pressure drop and liquid flow rate. At 5.9 s, the vapor temperature begins to oscillate as the vapor space expands into the vapor line and then contracts due to condensation on the vapor line wall. The oscillations decrease as more fluid is evaporated until the rate of evaporation equals the rate of condensation on the wall. This is shown in Figure 4.9 between 5.9 and 50 s where the vapor volume remains nearly constant. As the vapor line wall temperature approaches the vapor temperature, the condensation rate decreases

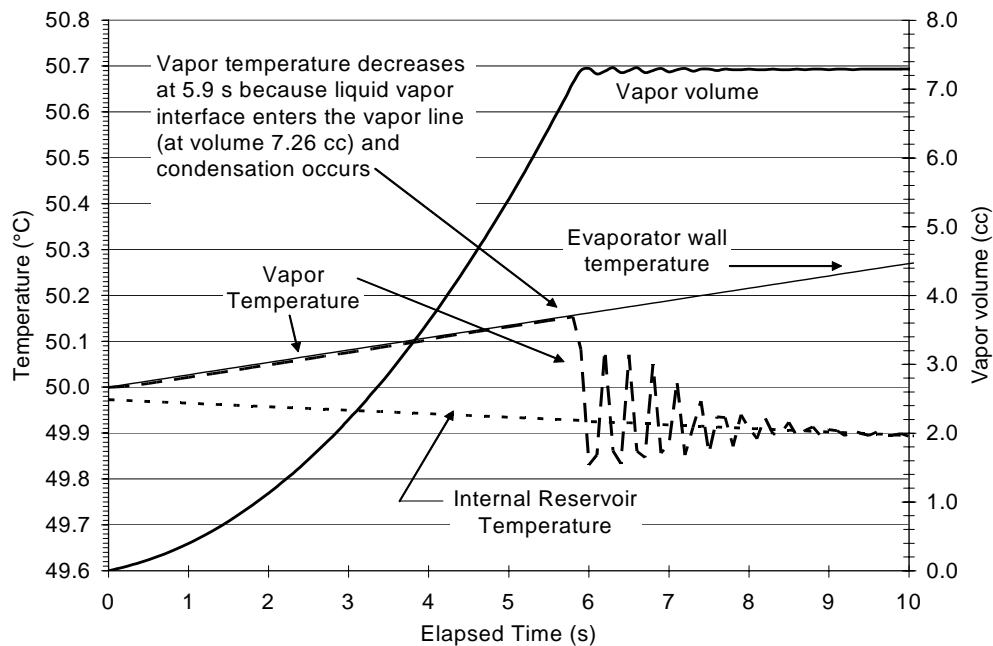


Figure 4.10 Temperature prediction during pressure surge as the vapor / liquid interface moves from the VIEW-CPL evaporator to the vapor line. The vapor temperature decreases to within 0.1 K of the internal reservoir temperature after the oscillations are damped.

and the vapor volume expands. The increase in evaporation rate (Figure 4.9), results from the increased temperature difference between the evaporator wall and the fluid in CV1. The oscillations in the temperature would not register on the data acquisition because the frequency (2.5 Hz) is an order of magnitude larger than the scan rate (0.25 Hz).

As indicated in Figure 4.9, the model predicts that the reservoir temperature continuously decreases during the pressure surge. Although one might expect that the pressure in the reservoir would increase as CV3 is compressed, condensation occurs and the heat of condensation is rejected to ambient. A 5-W heater on the reservoir was supposed to maintain the temperature, but the heat transfer from the reservoir wall at 50°C to ambient temperature of 25°C is 7 W. Therefore the reservoir temperature and corresponding pressure decrease during the pressure surge and would continue to decrease until the temperature is 43°C at which point the heat transfer rates would be balanced.

During the period that the vapor temperature (CV1) is oscillating, the pressure difference between the reservoir and evaporator is also oscillating because the vapor space contains both liquid and vapor phases and the pressure and temperature are not independent along the saturation curve. The pressure difference and the liquid mass flow rate (flowing through the vapor line) are plotted in Figure 4.11. The flow rate in Figure 4.11 is the rate of the liquid flowing through the vapor line. The maximum liquid flow rate is 0.22 g/s, which indicates

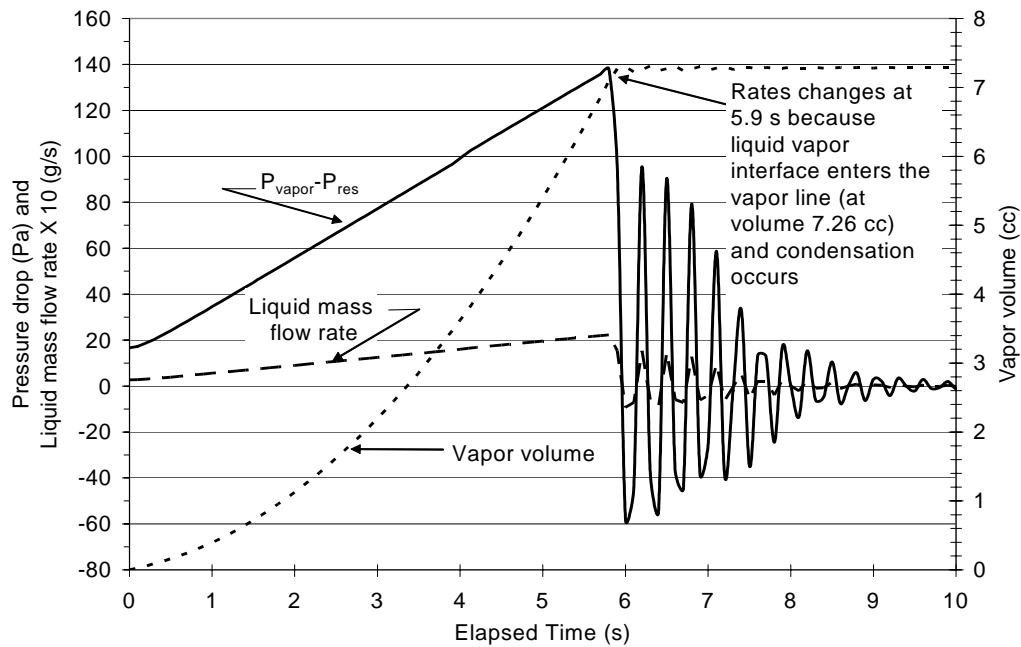


Figure 4.11 Pressure surge prediction during the movement of the vapor / liquid interface from the VIEW-CPL evaporator grooves into the vapor line for 35 W heater power. Pressure decreases with the corresponding decrease in temperature of the vapor space as the vapor transfers heat to the wall of the vapor line.

that the flow is laminar for the duration of the pressure surge. The flow rises rapidly to a maximum at 5.9 s and then decreases as the pressure surge proceeds. The liquid mass flow rate decreases with time because of the heat transfer with the vapor line wall.

Since the fluid velocities are equal for the liquid and vapor phases, the vapor mass flow rate is equal to the liquid mass flow rate multiplied by the ratio of vapor to liquid density. The vapor mass flow rate (not shown in Figures 4.9-4.11) is significantly lower than the steady-state mass flow rate for the same heater power because of the sensible heating of the evaporator. Given an

approximate heat loss of 11 W from the evaporator to ambient, the steady-state vapor mass flow rate is 1×10^{-5} kg/s for a 35 W applied heat load (net heat load of 24 W). The vapor mass flow rate during the pressure surge is almost 700 times less. The thermal mass of the evaporator keeps the flow rate low by reducing the amount of heat available for evaporation. The thermal mass of the vapor line also contributes through condensation in the vapor line which limits the pressure rise as well.

The pressure surge code was exercised for the seven different possible combinations of heaters for the VIEW-CPL experiment. Figure 4.12 is a plot of the time required to displace liquid from both the evaporator grooves and the vapor line, and the maximum pressure gradient across the wick as a function of evaporator power. For all cases, the initial reservoir temperature was 50°C, the evaporator was assumed to be the same temperature as the reservoir (i.e., no gradient due to heater location), and ambient temperature was 25°C. The 10 W case is not plotted because the model predicted that there would not be any vapor generation due to heat loss for the conditions specified.

The conclusion from the pressure surge analysis is that start-up of VIEW-CPL should not result in a deprime. Based on the results presented in Figure 4.12, the maximum pressure drop during the pressure surge is 215 Pa which is well below the capillary limit of 10 kPa (for 0° contact angle) and the vapor pressure limit of 7 kPa. Even if the water and wick were not perfectly wetting, the contact angle would have to be at least 89.994° for the capillary limit to be

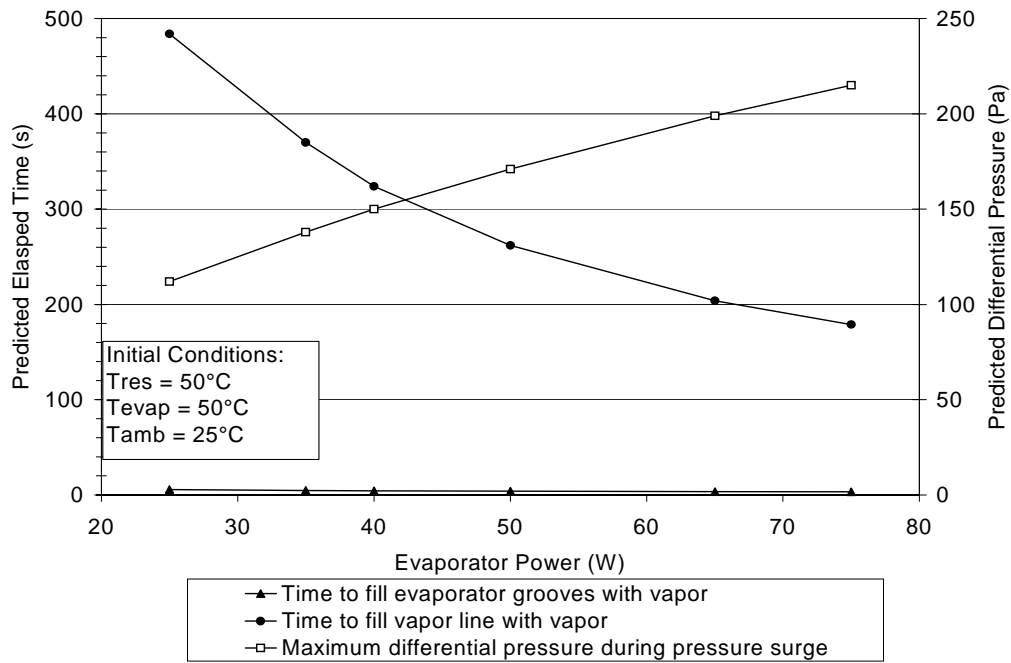


Figure 4.12 Predicted pressure surge results for VIEW-CPL geometry and available evaporator power combinations.

degraded to 215 Pa, which is unlikely based on previous test experience. Therefore vapor back-flow through the wick is not possible since the pressure difference never exceeds the capillary limit. Nucleation in the evaporator core is not possible because the vapor pressure in the core is not less than the local saturation pressure (assuming the core is at the subcooled temperature of 25°C). The pressure surge prediction presented here is less than the pressure drop predicted using a mass-less system (Figure 3.18) because sensible heating of the CPL components, such as the evaporator and transport line, limits the rate at which the vapor / liquid interface moves from the evaporator to the condenser. Section 5.2.3 includes a comparison of the pressure surge predictions to the data obtained from the VIEW-CPL experiment.

4.4.3 Cold-shock analysis

The reservoir discussions presented earlier in Sections 2.1.3 and 3.2.3 indicate that a sudden decrease in reservoir temperature, known as reservoir cold-shock, could occur during start-up if all of the liquid in the evaporator and vapor line is assumed to be instantaneously mixed with the fluid in the reservoir. However, the pressure surge analysis shows that the liquid is not instantaneously mixed. The results (Figure 4.12) predict that it is displaced over a period of time ranging from 180 to 480 s with power ranging from 75 to 25 W, respectively. The 5 W heater on the reservoir was designed to offset heat loss from the reservoir to ambient and to maintain the reservoir temperature as cold liquid is displaced. However based on experience and the pressure surge model, it was found that the heater was slightly undersized and did not balance the heat loss to ambient (as predicted by the decrease in reservoir temperature during the pressure surge). Therefore the reservoir will not maintain temperature control as cold liquid is mixed in during start-up.

Since the 5 W heater is undersized, the effect on the reservoir temperature is dependent upon the temperature of the incoming liquid. During the initial stage of the pressure surge, liquid entering the reservoir passes through the reservoir wick (refer to Figure 3.15) where it displaces warm liquid into the reservoir vapor space. Considering only the annular region around the reservoir wick (in Figure 3.15) and the volume of liquid in the segment of wick with area in contact with the incoming liquid, there is 5.3 cc of saturated liquid that will be displaced before

cold liquid enters the reservoir vapor space. The amount of liquid that is displaced inside the evaporator vapor grooves, plenum, and evaporator exit before vapor enters the vapor line is 7.26 cc. Therefore the rapid displacement of the liquid from the evaporator vapor grooves during start-up will displace mostly saturated liquid into the reservoir vapor space and only 2 cc of cold liquid. Based on this model, the saturation temperature would drop 0.5 K with this amount of fluid displacement.

If there is mixing in the reservoir during the remainder of the vapor line clearing (contrary to the assumption used in the pressure surge model), then the reservoir temperature drop (or cold-shock) can be as large as 3.6 K over the duration of the vapor line clearing when coupled with the heat loss. This temperature was determined from a transient energy balance on the reservoir

$$m_{ss}c_{ss}\frac{dT}{dt} + \frac{dU}{dt} = \dot{m}h_i - UA_{res}(T - T_{amb}) + \dot{Q}_{heater} \quad (4.25)$$

with 75 W evaporator power (worst case), an initial reservoir temperature of 49.5°C (0.5 K less than 50°C to account for the initial temperature drop due to displacement of fluid from the evaporator), an ambient temperature of 25°C, a liquid inlet temperature of 25°C, and an average mass flow rate of 0.12 g/s. The average flow rate was determined by dividing the mass of fluid in the vapor line (22 g) by the time to clear the vapor line (180 s from Figure 4.12).

A 3.6 K decrease in saturation temperature amounts to a 2.0 kPa change in saturation pressure. The pressure that can be supported by the evaporator

wick is 10 kPa and therefore the decrease in saturation temperature will not allow vapor to back-flow through a fully-wetted wick. A contact angle of 79° or greater would reduce the capillary limit to 2.0 kPa and allow vapor back-flow. In order for liquid to flash inside the evaporator core, the temperature of the liquid would need to be higher than the reservoir temperature. This is unlikely since the evaporator heat would have to conduct through the polyethylene wick to heat the core. The conclusion from this analysis is that VIEW-CPL will not deprime due to cold shock during start-up unless the contact angle between the water and wick is greater than 79° .

4.5 Steady-State operation

The expected steady-state pressure drop was documented previously in Figure 3.17 in Section 3.2.4. The maximum pressure drop at 75 W is 162 Pa, which is significantly less than the capillary limit of 10 kPa at 50°C . Also, a capillary pressure increase of 162 Pa across the liquid/vapor interface in the wick results in a saturated vapor temperature difference of less than 0.5 K. Since the condenser is only 65% active at 75 W (refer to Figure 3.9), the evaporator liquid inlet temperature is within 1 K of the sink temperature which provides adequate subcooling to prevent nucleation in the evaporator core. Therefore, VIEW-CPL steady-state conditions are not expected to result in a CPL deprime when using typical CPL analysis techniques. However, the hydrophobic nature of polyethylene requires special consideration that might lead to deprime even under nominal operating conditions. Hysteresis in the pressure required to fill a

wick with a non-wetting fluid is greater than the pressure required to drain the wick [Connor et al., 1984]. If the results of Connor's study are extrapolated to VIEW-CPL, then it may be possible to have portions of the wick that are not fully wetted during pressure priming, and that those dry areas would not grow once power was applied because the capillary pressure is large enough to prevent the pores from draining along the wetted portion of the wick. Additionally, observations of a gravity-induced filling of the core were made in which the liquid column switched from a convex liquid/vapor interface to a concave liquid/vapor interface and back. These observations indicate that some portions of the wick are more readily wetted than others. The following section describes the operating conditions if a portion of the wick is not wetted.

4.5.1 Operating with a partially dry wick

Stable operations with a bubble in the core can exist if the energy required to heat the subcooled liquid returning to the evaporator core balances the energy supplied for bubble growth. In order for this to occur, the wick must continue pumping liquid through partially-wetted areas while vapor back-flows through the dried-out portions of the wick. The vapor flow through a dry portion of the wick can be described by Darcy's law (Eq. 2.5), where the flow of vapor is driven by the capillary pressure developed across wetted portions of the wick. As long as there is enough subcooling to balance the vapor flow, the CPL should continue to operate with a bubble in the core. The equations for determining the steady-

state operating condition are listed in Table 4.12 and the control volumes are sketched in Figure 4.13 with an exploded view of CV1 in Figure 4.14.

The vapor leak through the wick does not change the mass flowrate of liquid circulating through the loop (\dot{m}_l) since the overall evaporator energy balance is still satisfied for the steady-state condition. Fluid temperature boundary conditions are known, because the saturation temperature is set by the reservoir temperature at 50°C and the condenser is oversized to ensure that the exiting liquid is within a degree of the 25°C ambient air.

Determining the condensation heat transfer coefficient between the liquid and the bubble is beyond the scope of this work, especially since the effect of noncondensable gas will create additional uncertainty. The effect of the heat transfer coefficient was studied parametrically with values of 500 and 3,000 W/m²-K to check the sensitivity of the results to the heat transfer coefficient. The condensation occurs over the cross-sectional area of the core (0.66 cm²), assuming that the bubble plugs the core with a flat interface.

A plot of the predicted steady-state bubble length that can exist, when the vapor leak through the wick is perfectly balanced by the inlet subcooling, is given as a function of length of dry wick with evaporator power as a parameter in Figure 4.15. Note that the bubble length does not have to be equal to the length of the dry wick. The major difference between the prediction for the two heat transfer coefficients is that the bubble length can be longer (for any amount of dry wick) when the heat transfer coefficient is 500 W/m²-K. This is because there is a

Table 4.12 Conservation equations of energy, momentum, and mass for the vapor leak through the wick (continued on next page).

<p>CV1 (Portion of the evaporator core that supplies liquid to the wick)</p>	<ul style="list-style-type: none"> Assume that only liquid exits the control volume through the saturated portion of the wick at a constant flow rate $\dot{m}_v = \dot{m}_1 + \dot{m}_2 = \int_0^{L_{core}-L_{bubble}} \frac{\dot{m}_v}{L_{core}-L_{bubble}} dx \quad (4.26)$ $Q_v = \int_0^{L_{core}-L_{bubble}} \frac{\dot{m}_v}{L_{core}-L_{bubble}} h(x) dx = \dot{m}_v h_{avg} \quad (4.27)$ Pressure drop due to liquid flow is neglected in CV1 Assume subcooled liquid entering CV1 completely condenses the vapor leaking through the wick; then the average temperature of the liquid exiting CV1 can be solved from the energy balance $\dot{m}_1 h_{l_1} + \dot{m}_2 h_v - \dot{m}_v h_{avg} = 0$ $T_{l2_{avg}} = T_{l_1} \frac{\dot{m}_1}{\dot{m}_v} + \left(T_{sat P3} + \frac{\lambda}{c_p} \right) \frac{\dot{m}_2}{\dot{m}_v} \quad (4.28)$ There is a temperature drop from the condensation heat transfer coefficient, h (on the order to 500 W/m²-K based on condensation analysis for low flow rate in Section 3.2.2) $dT = \frac{\dot{m}_2 \lambda}{hA} \quad (4.29)$ Also assume that the latent heat from condensation is conducted through the liquid $\dot{m}_2 \lambda = -kA \frac{dT}{dx} = -kA \frac{T_{l_1} - (T_{sat P3} - dT_{sat})}{L_{HT}} \quad (4.30)$ <p>where L_{HT} is the length of the heat transfer zone over which conduction dominates.</p> One-dimensional temperature profile (neglecting radial effects) inside the wick is assumed to be linear as shown in Figure 4.14 $\text{for } 0 < x < L_{HT} \quad T_{l_2}(x) = (T_{sat P3} - dT_{sat}) + (T_{l_1} - (T_{sat P3} - dT_{sat})) \frac{x}{L_{HT}} \quad (4.31)$ $\text{for } L_{HT} < x < L_{wick} - L_{dry} \quad T_{l_2}(x) = T_{l_1}$ <p>(note the x axis is zero at the right end of CV1 and that the T_{l_1} temperature is the liquid temperature outside of the heat transfer zone)</p>
--	--

Table 4.12 Conservation equations of energy, momentum, and mass for the vapor leak through the wick (continued from previous page).

<p>CV2 (Saturated part of the wick)</p>	<ul style="list-style-type: none"> Mass rate from evaporation at the wick surface is equal to the liquid flow into the wick Pressure drop through the wick is determined by Darcy's law and the capillary pressure at the vapor interface is the sum of all system pressure drops $\Delta P_{wick} = P_1 - P_2 = \frac{\mu_l}{\rho_l} \frac{\dot{m}_v}{2\pi(L_{wick} - L_{dry})k_p} \ln\left(\frac{D_o}{D_i}\right) \quad (4.32)$ $\Delta P_{cap} = P_3 - P_2 = \sum \Delta P_{sys}$ <ul style="list-style-type: none"> Neglect heat loss, by assuming that all heat applied to the evaporator is consumed in sensible heating and evaporating the fluid over the saturated portion of the wick $\begin{aligned} \dot{Q}_{evap} + \dot{m}_v h_{l_2} - \dot{m}_v h_v &= 0 \\ \dot{Q}_{evap} + \dot{m}_v c_p (T_{l_2} - T_{sat}) - \dot{m}_v \lambda &= 0 \end{aligned} \quad (4.33)$
<p>CV3 (Vapor Groove)</p>	<ul style="list-style-type: none"> Mass balance is the same as CV1 There are two components to the viscous pressure drop $\begin{aligned} P_3 - P_3' &= \rho_v f_{Re} \frac{1/2(L_{wick} - L_{dry})}{2D_h} \left(\frac{\dot{m}_v}{\rho_v A} \right)^2 \\ P_3' - P_4 &= \rho_v f_{Re} \frac{1/2 L_{dry}}{2D_h} \left(\frac{2\dot{m}_v - \dot{m}_2}{\rho_v A} \right)^2 \end{aligned} \quad (4.36)$ <ul style="list-style-type: none"> Assume adiabatic vapor groove $\dot{m}_v h_v - \dot{m}_1 h_v - \dot{m}_2 h_v = 0 \quad (4.37)$
<p>CV4 (Dry part of the wick)</p>	<ul style="list-style-type: none"> Assume saturated vapor enters the wick and superheated vapor exits the wick, therefore a simple mass balance and a simple energy balance Mass flow rate is determined from the equation for pressure drop across the wick. The pressure from the vapor groove is assumed as the average pressure over the dry portion of the wick $\Delta P_{wick_{dry}} = \left(\frac{P_3' + P_4}{2} \right) - P_1 = \frac{\mu_v}{\rho_v} \frac{\dot{m}_2}{2\pi L_{dry} k_p} \ln\left(\frac{D_o}{D_i}\right) \quad (4.38)$

larger dT_{sat} (refer to Figure 4.14) between the saturation temperature of the core and the temperature of the vapor back-flow for $500 \text{ W/m}^2\text{-K}$, which reduces the average temperature of the liquid portion of the core (CV1). Therefore the length of liquid needed to balance the vapor back-flow is less (bubble is longer) than that

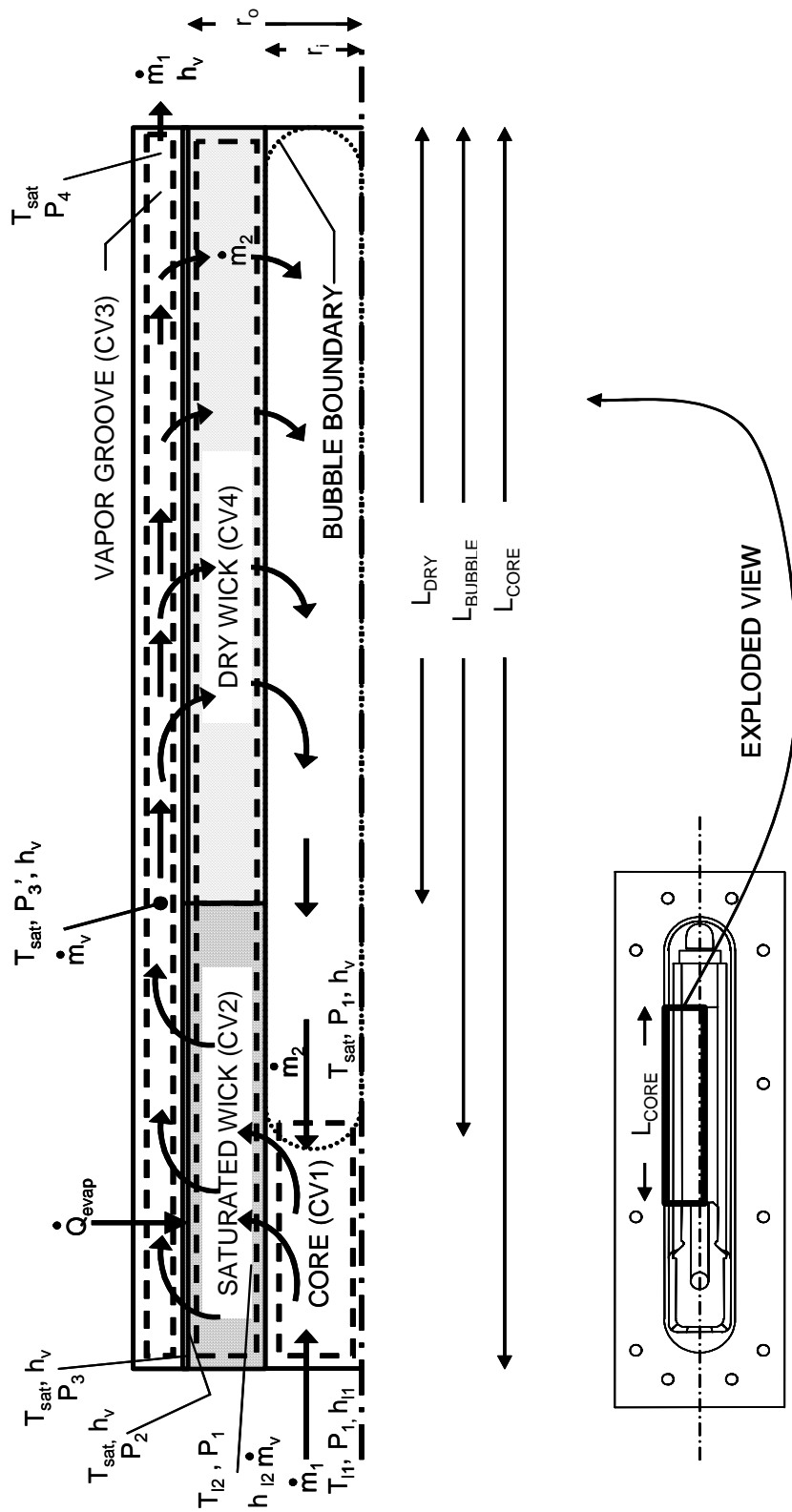


Figure 4.13 Control Volume for vapor flow through a dry portion of the VIEW-CPL wick.

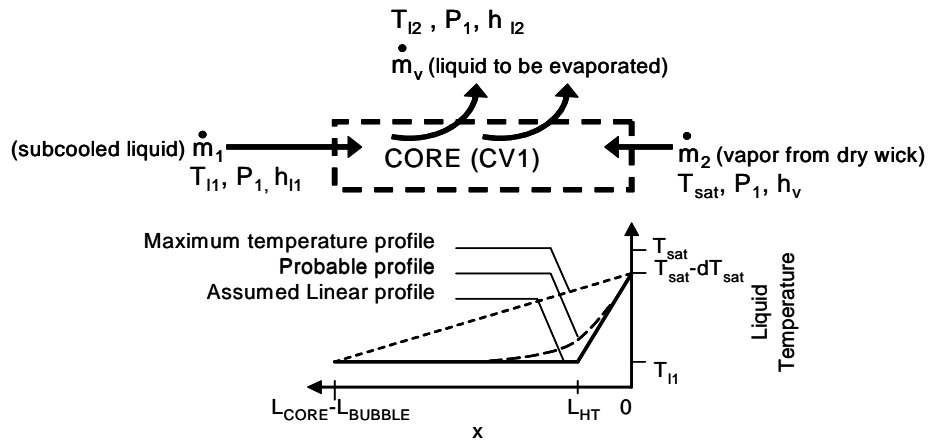


Figure 4.14 Temperature profile in the liquid control volume inside the wick core (refer to Figure 4.13).

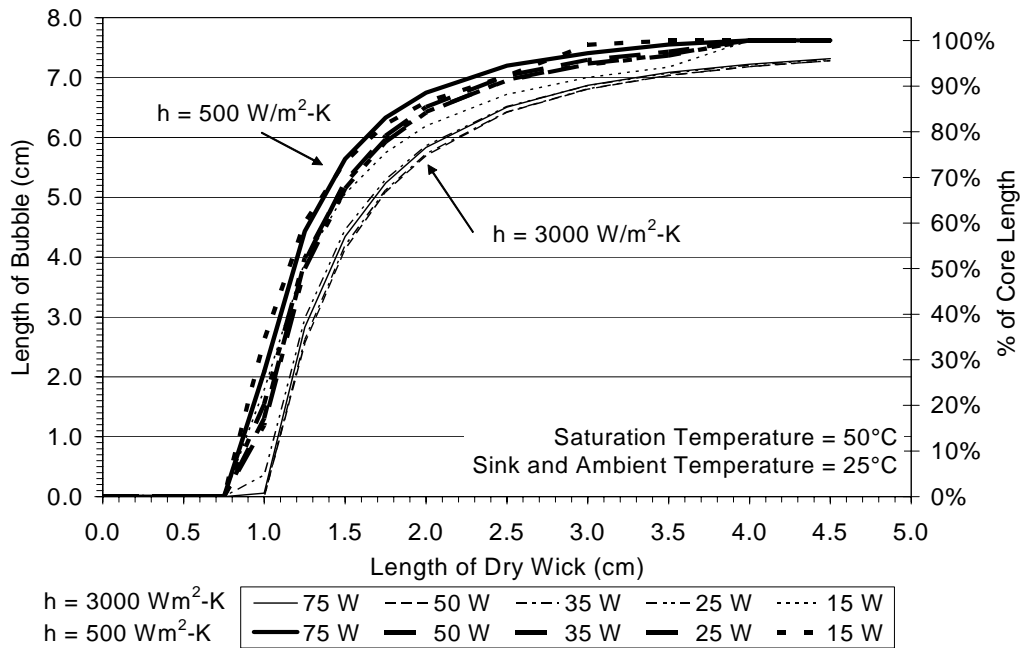


Figure 4.15 Length of bubble resulting from a dry portion of the wick at powers ranging from 15 to 75 W and for condensation heat transfer coefficients of 500 and 3000 W/m²-K.

required for a higher temperature liquid portion that occurs with higher heat transfer coefficients. The results for heat transfer coefficients ten times greater than $3,000 \text{ W/m}^2\text{-K}$ (data not shown) are within 10% of the values plotted in Figure 4.15, indicating that the analysis is not sensitive to large heat transfer coefficients.

Focusing on the $500 \text{ W/m}^2\text{-K}$ predictions, one observation made from Figure 4.15 is that no steady-state bubble will exist for dry wick lengths less than 0.75 cm. The amount of subcooling entering the core will collapse bubbles because there isn't enough vapor to keep a bubble filled. Another observation is that a bubble will fill the core for dry lengths greater than 3.8 cm. This means that the evaporator will be liquid starved if the dry length of wick is greater than 50% of the wick. The conclusion from the analysis is that the wick will continue to provide the capillary pressure difference for steady-state forward flow, even with large portions of the wick dry.

The predicted bubble lengths are closely grouped for different evaporator powers. Recall that the vapor leak is dependent upon the loop pressure drop. At low powers where there is very little subcooling, the pressure drop is dominated by the back pressure in the condenser (shown in Figure 3.17). At higher powers, the percentage of the pressure drop attributed to the back pressure is less, but the increase in mass flow rate increases subcooling to balance the increased vapor leak from the pressure drop. Therefore the predicted bubble length is independent of the amount of subcooling.

The sensitivity of the approximated linear temperature profile (refer to Figure 4.14) was also evaluated. The probable (parabolic) temperature profile was calculated for a given heat leak through the wick by integrating the energy equation, including convective terms for flow of liquid, over the liquid filled length of the core. The temperature profiles shown in Figure 4.16 validate that the linear approximation is a reasonable estimate. The profiles are for 15 W heater power and are an example of one of the larger differences between the temperatures. The error in the core energy balance due to the different temperature profiles is less than 1.5% for all of the VIEW-CPL cases that were predicted using the model.

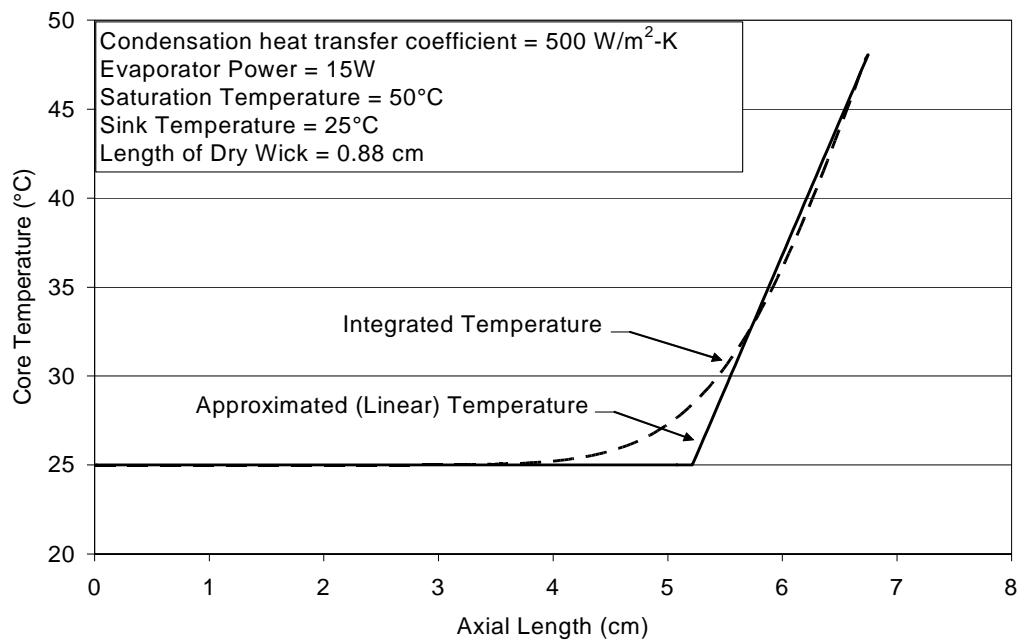


Figure 4.16 Comparison of approximated core temperature profile with the profile determined from integrating the energy balance over the length of the core.

The above analysis includes two key assumptions. The first is that the heat applied to the evaporator is consumed only over the saturated portion of the wick. Actually, the evaporator heaters provide constant flux over the entire area covered by the heaters. Therefore, if there is a dry portion of wick, the evaporator temperature will have an axial temperature gradient. The temperature of the evaporator housing will stabilize at a point where the temperature gradient is large enough to conduct heat through the stainless steel housing to the saturated portion of the wick. The gradient can become very large even for small portions of dry wick. For example, the axial temperature gradient is 15 K when a continuous length measuring 20% of the total wick length is dry and the 25 W heater is on. For the same power, the gradient is 35 K when 30% of the wick is dry. Since the temperature sensors are set to open the power circuit at 60°C, it is unlikely that the evaporator power will remain on with a continuous segment of more than 20% of the wick dry even for the 10 W heater. Of course, this does not indicate that multiple wick segments summing to 20% of the wick will have similar gradients and temperature limitations.

The second approximation is that there is no heat loss from the evaporator. Heat loss will reduce the mass flow rate through the liquid return line since less heat is used for evaporation. Figure 4.15 can still be used to check that operating with a dry portion of wick is feasible, provided that an effective evaporator power is the dependent variable instead of the applied power.

4.5.2 Fluid pumping axially in the wick

The fluid flow in the cylindrical evaporator wick is normally in the radial direction. However the wick can pump fluid in any direction, provided that the pressure drop in the wick does not exceed the capillary pressure that can be developed (see Eq. 2.1). Therefore a dry portion in the wick can exist only if the pressure drop axially along the length of the saturated wick over the core bubble (refer to Figure 4.13) exceeds the capillary pressure. Figure 4.17 is a plot of the axial transport capability (power X distance) that the polyethylene wick is capable of pumping as a function of contact angle. The transport capability is calculated from Darcy's law in the form

$$Q \cdot L = \frac{\Delta P k_p A \rho \lambda}{\mu} \quad (4.39)$$

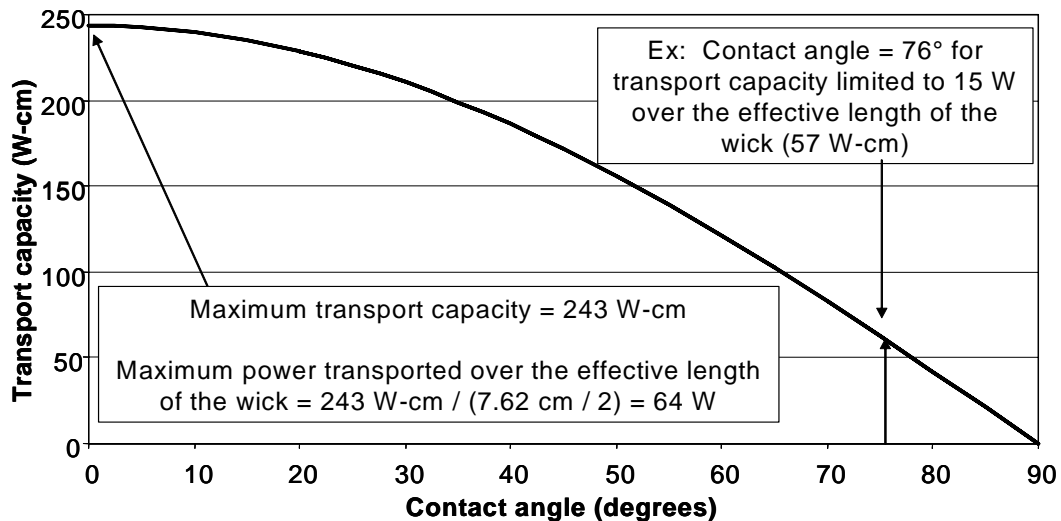


Figure 4.17 Axial transport of liquid water at 50°C in the VIEW-CPL wick as a function of contact angle.

From Figure 4.17, the maximum amount of heat that can be transported axially along the effective length of the wick ($L_{\text{eff}} = 7.62 \text{ cm} / 2$) is 64 W if the wick is perfectly wetted with water ($\theta=0^\circ$). This axial transport indicates that there would be no dry sections along the wick for net evaporator powers up to 64 W even if liquid is supplied to only one end of the wick (i.e. not fed radially through the wick). Difficulty in wetting the polyethylene wick with water may result in lower pumping capability. The actual value of the contact angle would have to be determined experimentally and was beyond the scope of this work. However a minimum value can be inferred from test observations by noting that there were portions of dry wick for evaporator powers of 30 W (discussed further in Chapter 5) resulting in approximately 15 W net power for evaporation. If this power were transported along the length of the wick, the transport capacity would be 57 W-cm which from Figure 4.17 corresponds to a contact angle of 76° . This implies that the contact angle between the water and wick is at least 76° .

Connor et al. [1984] described a hysteresis in which the amount of pressure required to fill a wick with a non-wetting fluid is greater than the pressure required to drain the wick. If the same phenomena were experienced by VIEW-CPL then it would be possible that the contact angle at some portion of the wick is 90° (resulting in a dry portion) and that there is no axial transport. Also that there may be no further axial drying because the wetted portion of the wick is experiencing a different contact angle ($<76^\circ$) that develops a large enough

capillary pressure to prevent draining. Observations were made in which a liquid column inside the core switched from a convex liquid/vapor interface to a concave liquid/vapor interface and back, supporting the theory that some portions of the wick are more readily wetted than others.

4.6 Deprime and Bubble Life Cycle

As described in Chapters 1 and 2, a deprime is a CPL circulation failure mode where a gas or vapor bubble exists on the suction side of the evaporator wick preventing normal capillary pumping operation. A deprime is normally indicated by a rapid temperature rise in the evaporator due to a transition from evaporation of the working fluid to sensible heating of the evaporator housing. A deprime is also recognized by the condenser and vapor line filling with liquid due to the loss of capillary pumping in the evaporator. Although the pressure surge, cold shock, and steady-state analyses indicate that the VIEW-CPL should not experience a deprime under the nominal operating conditions with a contact angle of 0° , deprimes were observed.

If the contact angle between the water and the polyethylene wick is large then the wick has limited pumping capability. For instance, if the contact angle in the wick is 89.5° then, based on Eq. 2.1 and surface tension of water at 50°C , the pressure rise across the meniscus is limited to 93 Pa. No pressure rise will occur for contact angles greater than 90° . Given the hydrophobic nature of polyethylene, it is possible that VIEW-CPL experienced deprimes because the pumping capability was significantly reduced below the 10 kPa that can be

achieved with a fully-wetted wick. Additionally, previous experience with water CPLs has indicated that a deprime is likely to be triggered by adverse effects of NCG and bubbles within the core of the evaporator.

The most likely theory for deprimes observed in VIEW-CPL were a result of bubble growth from vapor flow through dry portions of the wick. Using the results from Figure 4.15 for the case with a $500 \text{ W/m}^2\text{-K}$ condensation film coefficient, a steady-state bubble will occupy 90% of the core if a 2-cm (0.8-in.) segment of wick is dry. If a larger portion of the wick is dry, then the bubble can fill the entire core. When this happens, a series of events (that can lead to deprime) occurs as follows:

1. The bubble blocks the flow of liquid into the evaporator.
2. The fluid remaining in the wick begins to evaporate (see Section 4.6.1).
3. Evaporator temperature increases as more of the heater power goes into sensible heating of the evaporator. This is a result of the conductance change between the evaporator wall and the fluid due to the liquid receding into the wick (see Section 4.6.1).
4. Mass flow rate of fluid circulating in the CPL decreases due to the sensible heating of the evaporator (see Section 4.6.1).
5. Liquid exits the reservoir to fill the condenser, because the rate of vapor flow to the condenser is decreased (see Section 4.6.2).
6. Pressure drop in the loop decreases due to decreased circulation, and therefore the vapor back-flow through the dry wick decreases (see Section 4.6.2).
7. Finally, one of two events occur
 - a. If all of the liquid in the wick is evaporated, then the evaporator temperature increases sharply as all of the heater power goes into sensible heating of the evaporator. The wick no longer supports a

capillary pressure because there is no meniscus in the wick. The evaporator is deprime.

- b. The bubble shrinks and allows liquid to flow into the core and re-wet the wick, pumping resumes and the bubble life cycle (bubble growth and collapse) repeats itself.

Details on these events are analyzed in the following sections culminating with a dynamic model of the bubble life cycle in Section 4.6.3.

4.6.1 Radial dry-out of the wick during deprime

A time lag is expected between the bubble blockage and the temperature excursion on the evaporator as the fluid inside the wick is evaporated. Assuming that there is no liquid feeding the wick, then the time required to dry-out the wick is dependent only on the heat load and the amount of liquid absorbed in the wick. The time, t , to evaporate all of the liquid with an applied heat load, Q , is described with a lumped capacitance model by

$$t = \frac{V\rho\lambda}{Q - mc_p \frac{dT}{dt}} \quad (4.40)$$

where the volume, V , of liquid in the wick is 3.0 cm^3 . Operating at 50°C with the highest VIEW-CPL power of 75 W , it is predicted to take up to one-and-a-half minutes before a measurable increase in the evaporator temperature is registered on the data acquisition system. Therefore the VIEW-CPL video is instrumental in understanding the events during this lag leading to CPL deprime.

As the wick is starved of liquid and begins to dry-out in the radial direction, the conductance inside the evaporator changes. Instead of evaporating fluid on the outside of the wick, heat is required to conduct through the porous

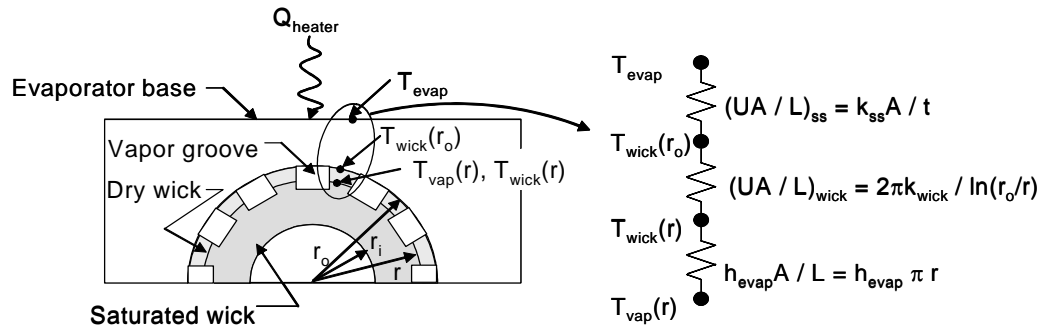


Figure 4.18 Schematic of heat transfer within the capillary evaporator.

polyethylene wick to reach the fluid. Figure 4.18 contains a schematic of the conductance path from the evaporator surface to the evaporating fluid. In normal operation the fluid evaporates at the edge of the wick in contact with the evaporator body, and therefore there is no conduction through the wick if it is wetted to the outer diameter. The evaporation conductance is approximated using an evaporation film coefficient of 19000 W/m²-K [Wolf, 2004]. This value was translated from ammonia test data (125000 W/m²-K) from an LHP to the VIEW-CPL water system with a larger wick diameter using the ratio of liquid thermal conductivity and the wick outer diameters. The evaporation conductance is 663 W/m-K. As the meniscus recedes, the wick conductance controls the heat transfer rate since its conductance (2.3 W/m-K through the thickness of the wick) is much lower than the conductance through the stainless steel and the evaporation conductance.

The effective wick thermal conductivity, $k_{wick} = 0.20$ W/m-K, was determined from Eq. 2.7 with the vapor conductivity ($k_{vap} = 0.02$ W/m-K) in parallel with the polyethylene ($k_{poly} = 0.38$ W/m-K). Making the approximation that the

evaporator temperature is uniform such that $T_{\text{evap}} = T_{\text{wick}}(r_o)$ the change in vapor mass flow rate exiting the evaporator is determined from the heat transfer equation,

$$Q_{\text{vap}} = UA_{\text{wick}}(T_{\text{evap}} - T_{\text{sat}}) \quad (4.41)$$

an energy balance with the capacitance of the evaporator as,

$$\frac{dE}{dt} = (mc_p)_{\text{evap}} \frac{dT_{\text{evap}}}{dt} = Q - Q_{\text{vap}} \quad (4.42)$$

and a mass balance as

$$\dot{m} = \frac{Q_{\text{vap}}}{\lambda} = \rho \frac{dV}{dt} = \rho \pi r \epsilon L_{\text{wet}} \frac{dr}{dt} \quad (4.43)$$

The mass flow rate is a function of the heater power, Q , and wetted wick length, L_{wet} . It is important to know the mass flow rate as the wick dries out in order to determine the evaporator temperature, the position of the vapor front in the condenser, and the pressure drop. This information is used later in Section 4.6.3.

4.6.2 Pressure drop change due to slowed circulation

Since VIEW-CPL operates in the laminar flow regime, the pressure drop is a linear function of the mass flow rate. Referring to Figure 3.17, the overall pressure drop for VIEW-CPL with a slope of $A_1 = 1.695 \text{ Pa/W}$ and a condenser capillary pressure drop is

$$\Delta P_{\text{sys}} = A_1 \frac{\dot{m}}{\lambda} + \Delta P_{\text{cond-cap}} \quad (4.44)$$

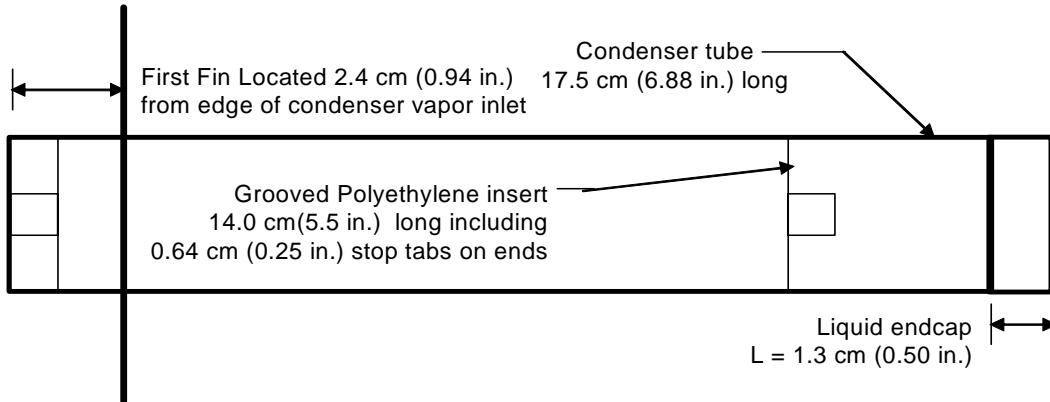
where $\Delta P_{\text{cond-cap}}$ is 40.5 Pa for a meniscus at 50°C in the condenser groove having an effective radius of 3.6 mm (0.14 in.).

The condenser capillary pressure drop is only included in the system pressure drop if the vapor front is positioned in the condenser groove. There is approximately 1 W of heat lost to ambient from the vapor line. Therefore the vapor front will recede out of the condenser and into the vapor line any time the heat load is less than 1 W. Due to the uncertainty of the position of the grooved-polyethylene insert in the condenser, there is a range of heat loads over which the vapor front may not be in the condenser groove. Figure 4.19 contains a schematic that shows the two extreme cases for the insert location. One is with the insert against the vapor endcap on the condenser and the other is with the insert against the liquid endcap. If the insert is against the vapor endcap, the condenser capillary pressure will always exist. If however, the insert is against the liquid endcap, there can be a 3-cm (1.2 in.) active condenser length (corresponding to 17 W heat rejection, see Figure 3.11) where the vapor front is not inside a groove and there is no condenser capillary pressure. Therefore any power below 17 W runs the risk of having the meniscus recede out of the grooves resulting in a sudden decrease in pressure drop of 40 Pa which in turn decreases the driving pressure for back-flow through the wick.

4.6.3 Bubble life cycle

Bubbles in the VIEW-CPL evaporator core that oscillated in size without any observed changes in operating conditions were observed during both ground

Case 1: Grooved polyethylene insert shifted against vapor inlet of the condenser.
Axial location of vapor front will be in the grooved portion of the insert



Case 2: Grooved polyethylene insert shifted against liquid exit of the condenser.
Axial location of vapor front will not be in the grooved portion of the insert, unless the net heat is 19W or greater.

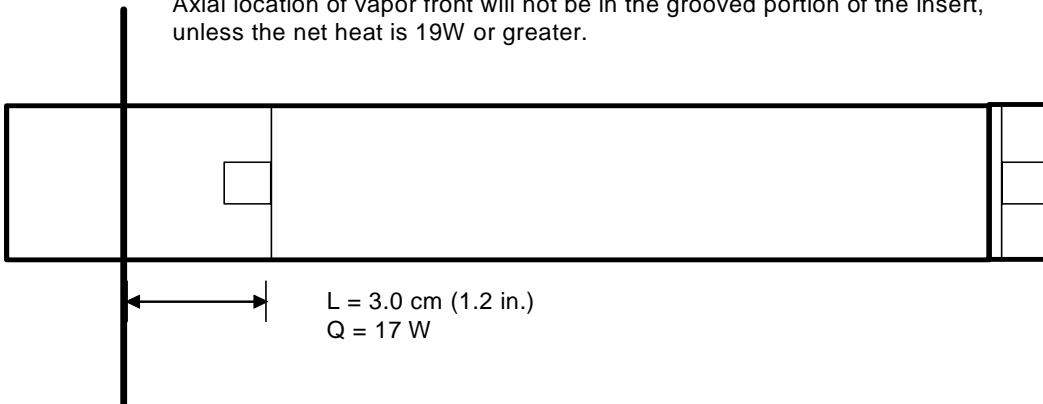


Figure 4.19 Two options for the positioning of the grooved polyethylene insert inside the condenser.

and flight tests. This section describes a theory explaining the changes inside the VIEW-CPL evaporator that allow bubbles in the core to expand and shrink.

The pressure distribution in the VIEW-CPL during typical operation is schematically shown in Figure 4.20 (pressure differences are exaggerated for clarity). The pressure distribution shown in Figure 4.21 is an example of the pressure distribution that would allow liquid to flow from the reservoir into the evaporator. In the explanation proposed here, the pressure change is due to a

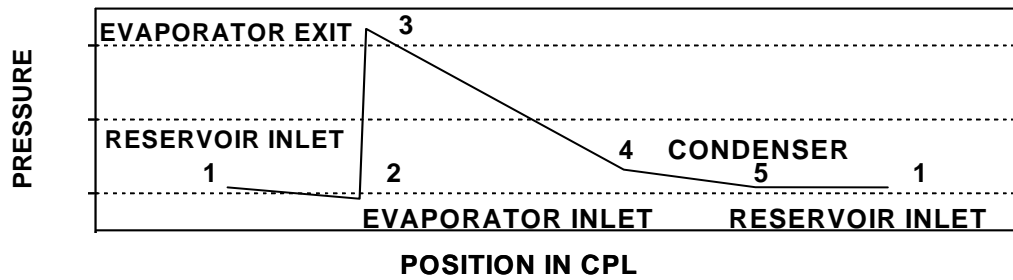


Figure 4.20 Schematic of a pressure profile for VIEW-CPL normal operations.

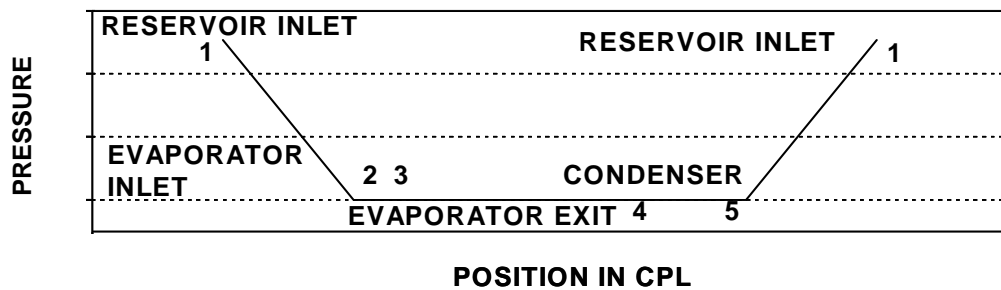


Figure 4.21 Proposed pressure profile due to the loss of meniscus in the capillary evaporator.

decrease in the condenser pressure from a reduction in vapor supply caused by dry-out of the evaporator wick. As a result, the pressure is also reduced in the evaporator core because the core is connected to the vapor line through the dry portion of the wick. It is this reduction in core pressure that allows liquid to flow from the reservoir into the evaporator core.

In understanding the bubble life cycle, condensation at the boundary of the bubble is an important parameter. As shown in Section 4.5.1, bubble size remains constant when there is a sufficient interface area between the bubble and the liquid to conduct away the energy released during condensation. The

calculations performed in Section 4.5.1 were for steady-state conditions with the condensation at the bubble surface perfectly balanced with the energy carried with the vapor leaking through the wick into the bubble. In cases where the vapor leakage is greater than the condensation rate, the bubble will grow and eventually fill the core. During transient (oscillatory) bubble cycles, the heat transfer from the bubble to the liquid in the core varies with time due to changes in area and changes in temperature of the liquid adjacent to the bubble. Figure 4.22 is a sketch of a bubble cycle with a description of the changing boundary conditions which are expanded upon in the following paragraphs.

Initial bubble growth. As the bubble initially grows, the heat of condensation is transferred to the liquid surface layer at the growing bubble boundary following Eqs. 4.29 and 4.30. As in the steady-state analysis of Section 4.5.1, the bubble boundary is assumed to be the cross-sectional area of the core (i.e. bubble fills the cross-section of the core and liquid contact is only on the expanding side) and the condensation film coefficient is $500 \text{ W/m}^2\text{-K}$. Since the bubble is growing, the convection assumption previously used in Section 4.5.1, for determining the temperature of the fluid, may not be valid. Instead, the liquid is treated as a semi-infinite medium with convective heat transfer at the edge adjacent to the bubble. Ozisik [1980] provides a solution for the temperature of the fluid as

$$T(x,t) = (T_{\infty} - T_0) \left(\operatorname{erfc} \left(\frac{x}{\sqrt{4\alpha t}} \right) - \exp(Hx + H^2\alpha t) \left(\operatorname{erfc} \left(H\sqrt{\alpha t} + \frac{x}{\sqrt{4\alpha t}} \right) \right) \right) + T_0 \quad (4.45)$$

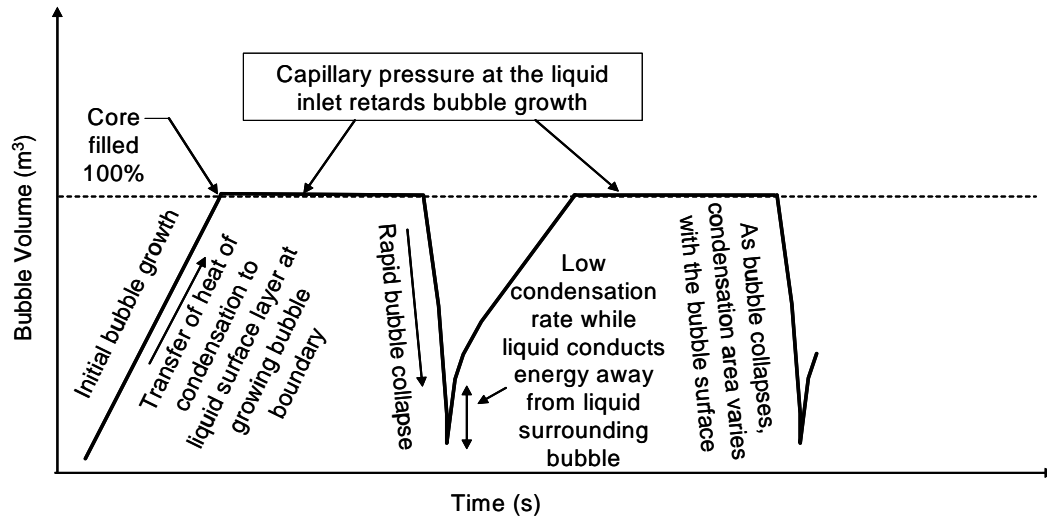


Figure 4.22 Description of bubble life cycle and changing boundary conditions between the bubble and the adjacent liquid.

where H is the ratio of the convective heat transfer coefficient (in this case the condensation film coefficient = $500 \text{ W/m}^2\text{-K}$) and the thermal conductivity of the medium ($k=0.64 \text{ W/m-K}$ for liquid water). The temperature of the liquid adjacent to the bubble is of interest since the rate of condensation is governed by the condensation film coefficient and the temperature difference between the bubble saturation temperature and the adjacent liquid. In order to show the effect of time on the liquid temperature, the temperature at the liquid boundary, $T(0,t)$ is plotted in Figure 4.23 along with the expected heat transfer rate between the liquid and the bubble in the core. If the bubble expansion occurs, because the liquid temperature is elevated, there is a minimal amount of heat transfer that can occur at the bubble boundary and the bubble can expand to fill the entire core.

Bubble growth in the evaporator inlet tube (core filled 100%). The liquid flow into the evaporator is blocked once the bubble expands into the inlet. The

area of the liquid/vapor interface is reduced to 25% that of the core interface area. Further bubble expansion is retarded by the capillary pressure (64 Pa for water at 50°C and perfect wetting conditions) exerted by the meniscus at the edge of the inlet fitting. Since the fluid in the liquid line becomes stagnant and the interface area is reduced, the heat transfer between the bubble and the adjacent fluid is neglected in the bubble life cycle analysis. Therefore there is no potential for shrinking the bubble via condensation. With the liquid blocked at the evaporator inlet, there is no flow to the wick and the evaporator power causes sensible heating of the evaporator body and evaporation of the remaining liquid inside the wick. The evaporation rate is governed by the equations presented in

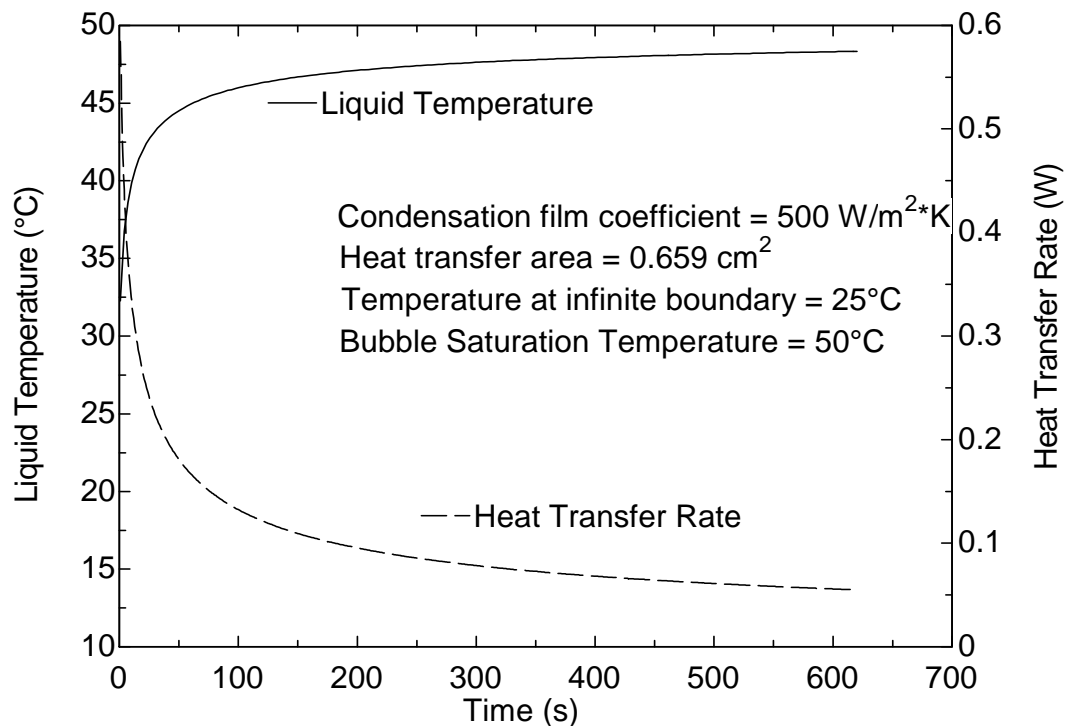


Figure 4.23 Plot of liquid temperature and heat transfer rate at bubble interface inside the core of the evaporator.

Section 4.6.1. This rate along with the condensation rate at the condenser, determines the rate of change of internal energy and the resulting pressure in the vapor line. The bubble and the vapor in the vapor line are connected by the dry portion of the wick and the pressure of each is equal because there is no flow between them. Therefore, when the pressure of the vapor line decreases, the pressure of the vapor bubble will also decrease.

Bubble Collapse. After the bubble in the evaporator core blocks the flow of liquid to the core, the liquid in the wick will continue to evaporate until (1) the pores in the wick dry-out or (2) the capillary limit of the wick is exceeded. The second condition may occur because the viscous pressure drop of the vapor exiting radially through the wick can be up to 200 times greater (by the ratio of vapor to liquid kinematic viscosities) than the viscous losses of liquid flowing through the wick. Even so, exceeding the capillary limit will only happen if the contact angle between the water and wick is very high ($\sim 89^\circ$). If this occurs then a local pressure rise occurs in the wick (because the vapor cannot be vented) which in turn increases the local fluid temperature and reduces the rate of evaporation.

In either case, wick dry-out or pressure drop limit, the pressure will decrease in the vapor line due to the suction from the condenser which continues to operate and condense the vapor in the vapor line. The lower pressure created in the vapor line will cause liquid to flow from the reservoir which has essentially constant pressure. Since there are two flow paths from the reservoir (high

pressure) to the evaporator (low pressure), liquid exiting the reservoir will flow in both directions. The flow rate between the three components, the reservoir, condenser, and evaporator, can be determined from pressure drop and laminar flow calculations. When the liquid flows back into the evaporator and re-wets the wick, the meniscus is recovered and the pumping will begin again (until the next dry-out).

A similar type of oscillatory behavior was described by Borodkin et al. [1995] with a system that they called an “autooscillation two-phase loop”. In their loop, pressure activated valves regulate the flow of liquid in the loop. Dry-out of the evaporator is ensured by blocking incoming flow with a valve until all fluid is evaporated and the pressure drops below the reservoir temperature, at which point the valve is opened and liquid flows from the reservoir. In VIEW-CPL the valve is simulated by the bubble in the core. As the bubble expands it blocks liquid flow to the evaporator causing the pressure to decrease. When the pressure decreases the bubble collapses and liquid is free to flow back into the evaporator where the cycle can begin again.

Using the proposed theory, the VIEW-CPL evaporator temperature and bubble volume for a period of the bubble life cycle was predicted and plotted in Figure 4.24. For the case presented, the loop was operating in 25°C ambient air with heater power of 30 W and a reservoir saturation temperature of 54°C. The dry length of the wick was set at 4.7 cm (1.85 in) in order to assure that the bubble would expand due to lack of subcooling (refer to Figure 4.14). The initial

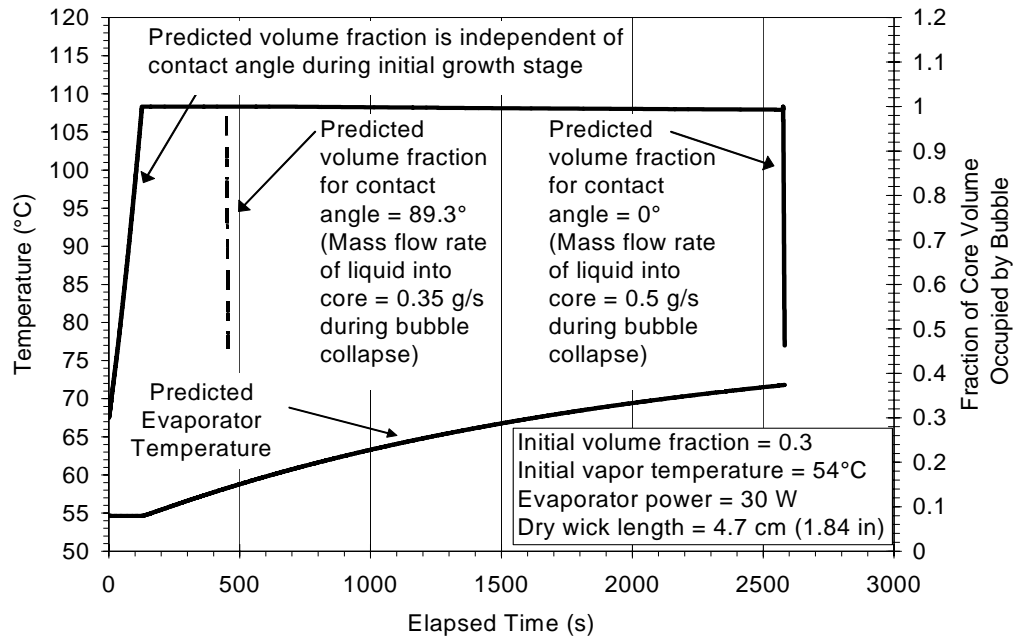


Figure 4.24 Prediction of evaporator temperature and bubble volume for VIEW-CPL operating at 30 W with a dry portion of wick. A bubble volume prediction is provided for a water and polyethylene contact angle of 0° and 89.3°.

volume of the bubble was assumed to be 30% of the volume of the core. A time of 1050 s was used in Eq. 4.45 to set the boundary condition of the liquid temperature adjacent to the bubble at 52.4°C. This was the lowest temperature that would allow the bubble to expand using the proposed bubble life cycle model.

As shown in Figure 4.24 the bubble expands for 126 s at flow rate of 0.1 to 0.2 mg/min. Once the bubble fills the core and liquid flow into the evaporator is blocked, the liquid from the wick is evaporated. For the condition of 0° contact angle, the evaporation continues for 2577 s until the wick is dry. If the contact angle is 89.3° (chosen as the angle that will match test data presented in Section

5.4) then the capillary limit of the wick will be exceeded at 450 s and the rate of evaporation is reduced until the liquid interface in the wick moves closer to the outer diameter (to reduce viscous losses). For this analysis, the rate is assumed to be that which can be supported by 10% of the capillary pressure.

The mass flow rate from the reservoir to the evaporator during the collapse is 0.5 and 0.35 g/s for contact angle 0° and 89.3° , respectively. The resistance to mass flow in the other direction (reservoir through condenser) is less and the flow rate is 100 times higher. With this model, the collapse continues until all of the vapor in the vapor line is condensed. Which occurs when the bubble volume reduces to 46% of the core volume.

The increase in evaporator temperature is a result of sensible heating the evaporator body which is necessary in order to conduct heat through the wick to the liquid interface. The high temperature limit set on VIEW-CPL was 60°C . The temperature for the case of 0° reaches 72°C before the bubble collapses. Given that bubble collapses were observed for the conditions presented in Figure 4.24 implies that the contact angle between water and the wick is closer to 89.3° than 0° .

5.0 VIEW-CPL TEST RESULTS AND DISCUSSION

The VIEW-CPL Test matrix in Appendix J lists the tests performed during the Space Shuttle flight which are also representative of the ground tests. A discussion of the trends observed during the testing is presented in Sections 5.1 through 5.5, including implications for the understanding of CPL physics. Comparisons of the test results to engineering models are also discussed in Sections 5.1 through 5.4.

VIEW-CPL operation included the following key modes: (1) pressure priming, (2) initial start-up, (3) bubble growth and deprime, (4) re-priming, and (5) bubble oscillations. Quasi-stable operations and evaporator overheating were also observed. The objective of this chapter is to document these modes with typical flight and ground test data. Comparison to the CPL operational modes (described in Chapter 2) is made through the analysis of the numerical and visual data obtained from the various tests.

5.1 Pressure Prime Test Results

The process of pressure priming from an unpowered state typically begins with the CPL containing both liquid and vapor at an isothermal, vapor-liquid equilibrium state. Figure 5.1 is a plot of a typical pressure prime (described as regular pressure prime in Table 4.4) during flight testing, while Figures 5.2 and 5.3 are plots of pressure primes performed during ground testing. A note on the x-axis of data plots that are presented in this chapter: The secondary scale at the top of the data plots is the Elapsed Time scale. Time of day was chosen for

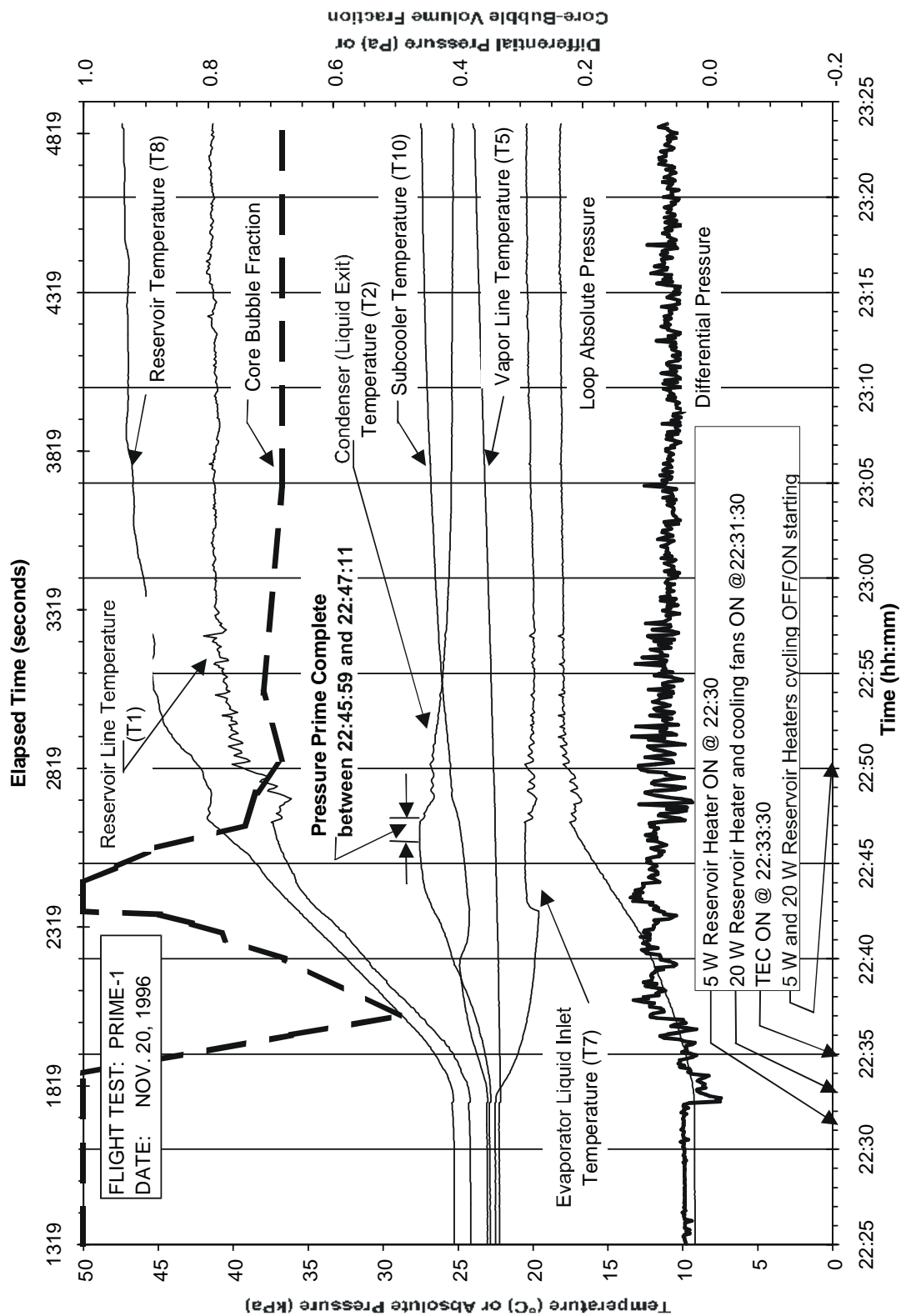


Figure 5.1 Example of pressure prime during flight testing of VIEW-CPL.

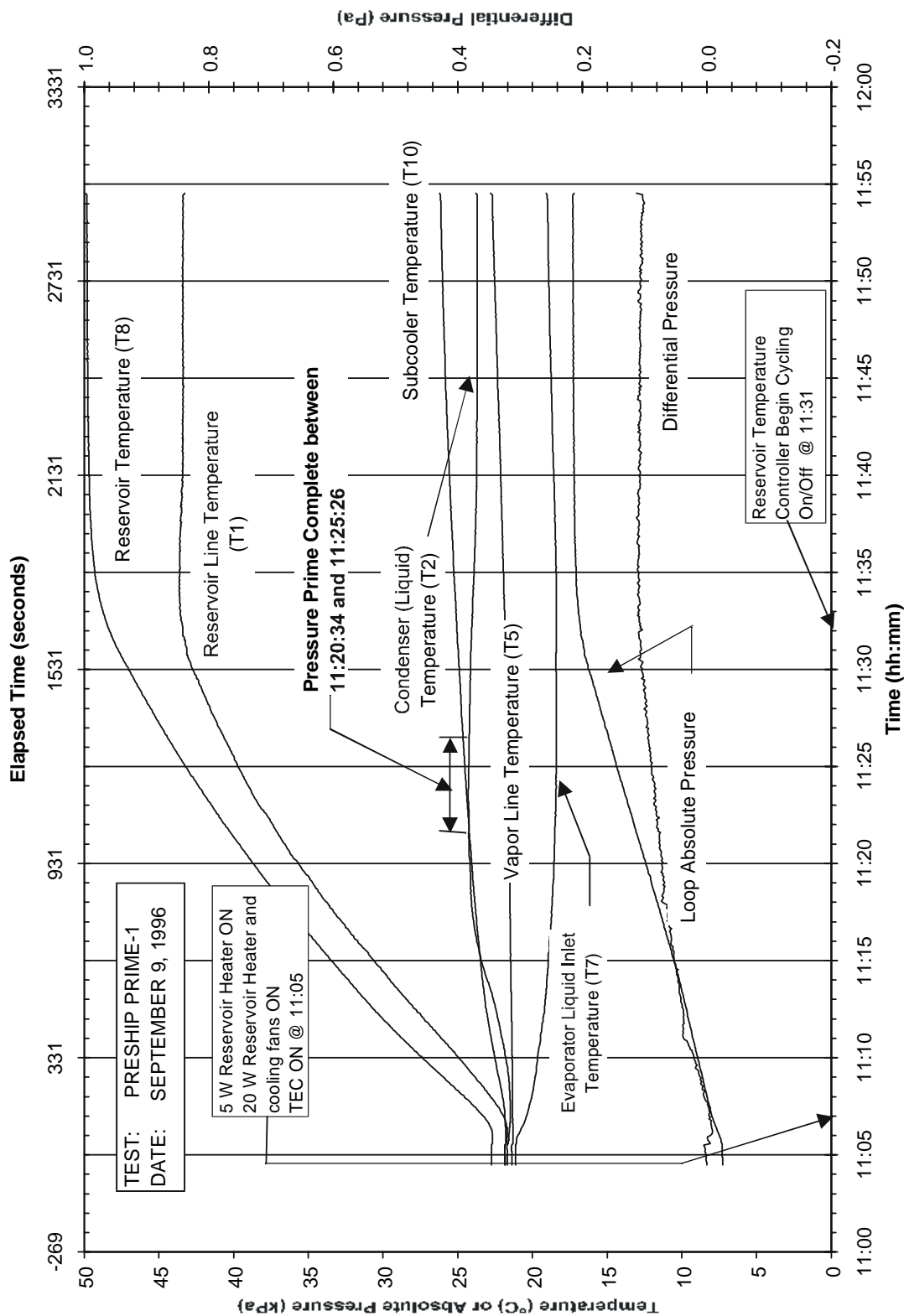


Figure 5.2 Example of pressure prime of VIEW-CPL during ground testing before flight.

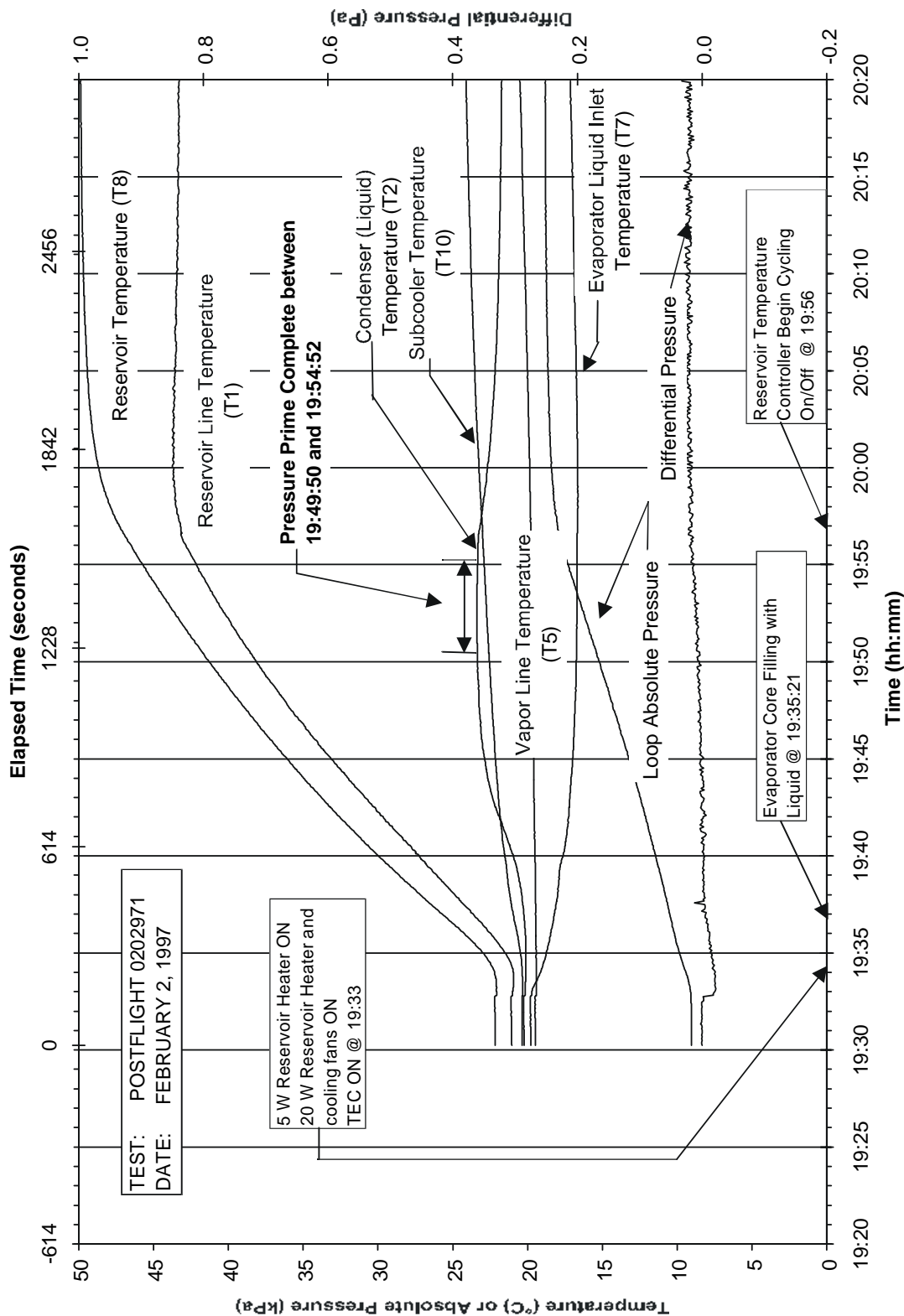


Figure 5.3 Example of pressure prime of VIEW-CPL during ground testing after flight.

the primary scale in this chapter in order that the visual data and testing commands (that were recorded in terms of Time of Day) could be included on the plot. The secondary x-axis scale does not start at zero in order that the primary scale (Time of Day) may have round starting and stopping times. In the flight pressure prime (Figure 5.1), the reservoir heaters were turned on by the astronaut at time 22:30. The temperature sensors on the reservoir indicate a temperature increase approximately 2 minutes after the heaters and temperature controllers are turned on. The lag in temperature response is due to axial conduction along the stainless steel reservoir and the lack of fluid circulation inside the reservoir.

The increase in loop absolute pressure can be seen to follow the shape of the reservoir line temperature very closely. This demonstrates that the reservoir temperature effectively controls loop pressure. The pressure prime is complete when the reservoir temperature is above the loop temperature and there is no indication of flow (either through temperature changes or variations in differential pressure). For the test in Figure 5.1, the pressure prime took 16 minutes to complete.

As the reservoir is heated, the pressure inside the reservoir increases and liquid flows out into the loop. Fluid flow from the reservoir is inferred from the temperature increase on the reservoir line and on the liquid line at the condenser and subcooler. The increase in loop absolute pressure is another indicator of flow. The evaporator liquid line temperature decreases because the fans and the

thermoelectric cooling module (TEC) are in operation. The hot air drawn across the TEC heat sink at the evaporator inlet causes the increase in the subcooler liquid line temperature.

The liquid flowing out of the reservoir and into the loop compresses the vapor space, thereby raising the temperature of the vapor space. There is a slight temperature increase of 1.7 K measured on the vapor line from the beginning to the end of the test. The latent heat must be rejected from the vapor to allow condensation to occur. The energy is transferred as heat to the liquid and the solid walls surrounding the bubble. As described in Section 5.3 covering the pressure prime model, the heat transfer rate determines the speed of the pressure prime process. There must either be a large driving temperature difference, a good conductance from the loop to ambient, or a long time period to allow the energy to leave the system as heat.

In the pressure prime shown in Figure 5.1, the evaporator core was initially filled with vapor. It was observed from the video data that the vapor began to condense on the wick surface at time 22:38, thus decreasing the vapor volume until the evaporator core was approximately 50% liquid (volume basis) at 22:42. At that point, a large slug of gas flowed into the evaporator core from the liquid line and pushed the liquid already in the core through the wick such that the core was completely filled with gas again. Eventually, the liquid flowed back into the core at 22:43, but a few bubbles were still visible. The remaining bubbles are believed to be noncondensable gas.

The same bubbles inside the core were observed to oscillate after the absolute pressure leveled off at 22:47 (16 minutes after start). From Figure 5.1, the oscillations are seen to correspond to oscillations in the reservoir line temperature, evaporator inlet temperature, and absolute pressure measurements at an average frequency of 0.035 Hz. The amplitude of the oscillations in measured data and the visual observations reduced suddenly at the same time (22:57). It is likely that the oscillations are caused by nucleate boiling in the reservoir. The oscillations appear after the loop is largely filled with liquid and may represent volumetric oscillations of the noncondensable gas bubbles. Oscillations of a similar frequency (0.053 Hz) were also measured in a second pressure prime during flight operations.

The ground test pressure primes (in Figures 5.2 and 5.3) showed temperature trends similar to the flight test pressure prime (in Figure 5.1). One difference is the lack of oscillations in the ground test data. In the ground tests, the vapor grooves in the reservoir wick (refer to Figure 3.15) will drain. In micro-gravity, the reservoir wick keeps liquid in contact with the reservoir wall, therefore it may be possible to have oscillations as vapor bubble vent from the grooves in the wick.

Another explanation for such a significant difference between ground tests and flight tests is also based on the location of the liquid inside the reservoir. In ground tests, the phases in the reservoir are stratified, thereby guaranteeing that the T8 temperature measurement device is measuring the vapor temperature.

In flight tests, the liquid is expected to be distributed throughout the internal wick structure. Thus, the wall temperature may not represent the saturation temperature, but rather a subcooled liquid temperature since the wick inside the reservoir, by design, will tend to pull liquid towards the reservoir walls. From Figure 5.2, the dT/dP slope is 3.1 K/kPa when measured between times 11:08 and 11:23 which closely matches the slope (3.3 K/kPa) from the saturation curve for water at the same temperature [Haar et al., 1984]. Similarly, the dT/dP slope for the post-flight data shown in Figure 5.3 is 3.2 K/kPa over the same temperature range. The same is not true of the flight test (Figure 5.1), where the reservoir temperature is nearly linear and the measured dT/dP is 1.9 K/kPa compared to the saturation curve where it is 3.3 K/kPa. The slope comparison is made, rather than a temperature/pressure equilibrium point, because any partial pressure contribution of noncondensable gas (see section 5.1.1) is removed by the slope calculation.

5.1.1 Indications of noncondensable gas

Another observation made from the three pressure primes (presented in Figures 5.1, 5.2, and 5.3) is the difference between measured pressure and saturation pressure based on measured temperature, thus indicating a certain amount of noncondensable gas (NCG) inside the system. In VIEW-CPL, noncondensable gas is most likely introduced either through very small air leaks around the o-ring seal at the evaporator, through the reaction of stainless steel and water (to form hydrogen gas), or air coming out of solution from the initial

charge. The beginning of the pressure primes, when the loop is nearly isothermal, provide an opportunity to quantify the amount of NCG in the system. The amount of gas, n , is calculated with the ideal gas law

$$n = \frac{PV}{RT} \quad (5.1)$$

where T is the loop temperature, P is the partial pressure of the gas (measured pressure minus saturation pressure of water at temperature T), R is the universal gas constant, and V is the volume occupied by the gas (which is the volume not occupied by liquid water, calculated by subtracting the volume of liquid charge from the total VIEW-CPL volume). The amount of NCG calculated using this method is plotted in Figure 5.4 for the three tests shown in Figures 5.1 through 5.3. The shape of the curve-fit to the data supports the theory of an initial

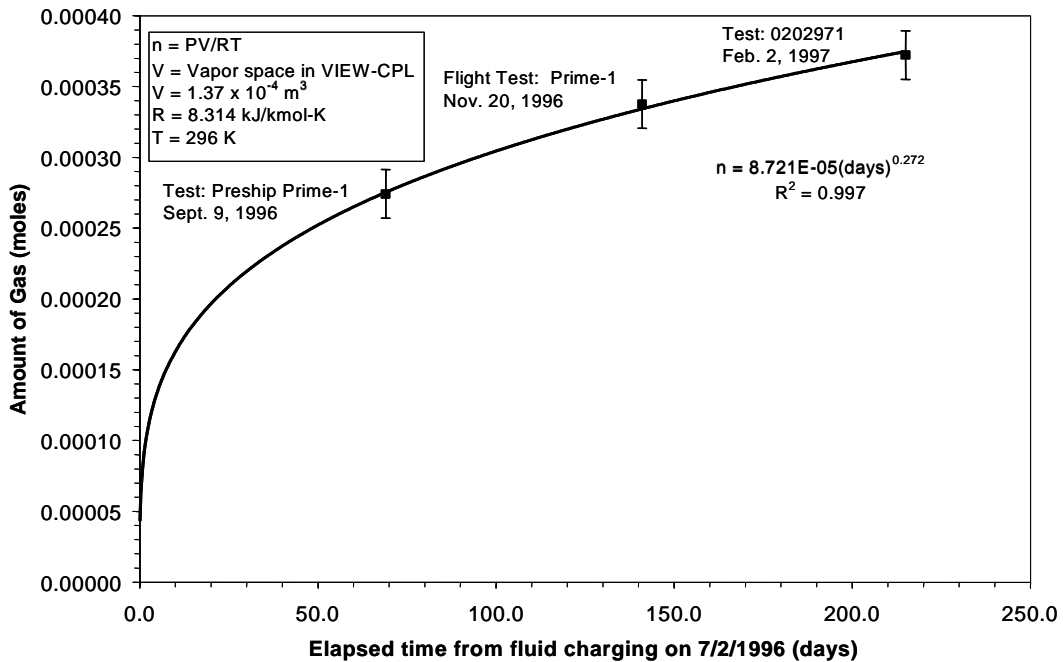


Figure 5.4 Amount of noncondensable gas in VIEW-CPL system calculated from the partial pressure exerted by the gas.

increase in NCG from air coming out of solution in the first couple of days after charging, and then a nearly constant increase in NCG due to a small air leak at 6.7×10^{-7} mole/day equivalent to 0.015 ml/day at standard atmospheric conditions.

In 17 out of 18 flight pressure primes for which video data are available, bubbles suspected to be NCG were observed in the evaporator after the pressure primes were completed. The observations were made after sufficient time had elapsed for all water vapor to condense based on the pressure prime analysis presented in Section 4.3. In general, bubbles were often present in the evaporator core prior to the start of the pressure prime. Only three flight tests were started with bubbles in the core that were longer than 2.5 cm (approximate volume greater than 1.4 cm^3). Only one test, CV-1, was started with all liquid and no bubbles in the evaporator. For that test, it is thought that the NCG was located elsewhere in the loop.

The time required to dissolve the suspected NCG into the liquid would be on the order of hours, rather than the minutes for which the pressure primes were performed. A mass diffusion analysis was performed to determine the time required to dissolve the NCG into a semi-infinite pool of liquid [Ozisik, 1980], assuming that the wick core is filled with nitrogen gas at the same pressure and temperature as the evaporator. A constant molar concentration was assumed at the free surface, which was 25.3 cm^2 based on the area of a 12.7 cm (5 inch) long semi-circular bubble filling the core of the wick. The diffusion area was not

varied during the analysis, therefore the actual time for the gas to diffuse into the liquid is greater than the results that are presented since the area will decrease as the bubble shrinks. The binary diffusion coefficient of nitrogen and water was $D=1.5 \times 10^{-8} \text{ m}^2/\text{s}$ [Incropera & DeWitt, 1990]. Figure 5.5 indicates that the NCG will initially dissolve quickly, but the bubble volume will still be visible even after 24 hours. Thus the length of the pressure primes would not be sufficient to completely dissolve NCG into the liquid.

5.1.2 Data comparison to pressure prime model

The results of the pressure prime model (Section 4.3) showed that the time required to collapse the vapor inside the loop is 1080 sec given the heat transfer characteristic between the vapor space and ambient, $UA_{pL_3} = 0.00585 \text{ W/m-K}$.

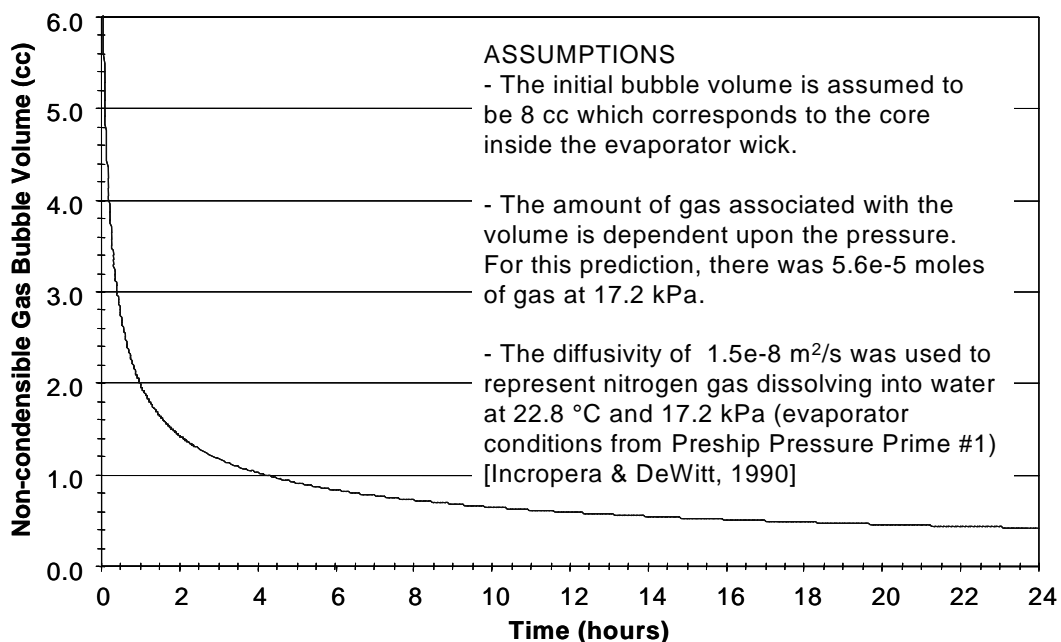


Figure 5.5 Predicted noncondensable gas bubble volume based on mass diffusion into a semi-infinite pool of water.

The first pressure prime during flight testing (Test Name: PRIME-1 in Figure 5.1) is complete at 22:47:11, 937 sec after applying heater power. The pressure prime is determined to be complete based on the video data (a negligible decrease in bubble volume) and the condenser exit temperature (T2) which stops increasing, both indicating that there is no flow from the reservoir. The oscillations in the reservoir line temperature that take place after the pressure prime is complete are likely due to further compression of NCG bubbles during the boiling mode changes in the reservoir which is a detail not included in the pressure prime model. The reservoir inlet temperature sensor is located too close to the reservoir to determine the end of the pressure prime because it is influenced by the reservoir temperature.

Although there were no video recordings of the pressure primes from the ground tests, information on the pressure prime can be observed from the temperature traces. The highest flow resistance is in the evaporator wick, and therefore the flow from the reservoir will follow two paths (described in Table 4.6) that meet at the evaporator wick. The bulk of the flow is through the vapor line and condenser since this is the path of least flow resistance. The first temperature sensor encountered by the liquid as it flows from the reservoir to the evaporator is the sensor (T2) at the (normal) exit of the condenser. The warm liquid exiting the reservoir heats the line as it passes through. Therefore, a good indicator that the pressure prime is complete is when the condenser exit temperature peaks at a maximum value. The temperature of the line decreases

when the flow stops because of heat loss to ambient. In Figures 5.2 and 5.3, the maximum temperature at the condenser exit is found between 11:20:34 and 11:25:26 (909 and 1201 s) for test "PRESHIP PRIME-1" and between 19:49:50 and 19:54:52 (1025 and 1327 s) for test "POSTFLIGHT 0202971". The pressure prime completion is given as a range because the temperature measurements are only accurate to ± 0.1 K.

Table 5.1 lists the predicted and measured durations for all VIEW-CPL pressure primes. The predicted values differ between pressure primes because they start with different initial reservoir temperatures. The predicted and measured values are within the experimental uncertainty and model sensitivity in all instances except for the pressure prime 0226971, where the minimum measured and maximum predicted values differ by only 3%.

Figure 5.6 contains a comparison of the temperature traces predicted by the pressure prime model to the test data for the flight pressure prime that was

Table 5.1 Measured and predicted duration of VIEW-CPL pressure primes.

Test Title	Measured Pressure Prime Duration [sec]	Predicted Duration [sec]	Prediction sensitivity to vapor space heat transfer (UA = $\pm 20\%$) [sec]
Preship-1	1055 \pm 146	995	-110 / +160
Preship-2	743 \pm 171	1005	-110 / +160
Prime-1	936 \pm 67	1080	-120 / +180
Prime-2	957 \pm 57	1055	-120 / +170
0202971	1176 \pm 151	975	-105 / +155
0226971	1150 \pm 48	920	-100 / +145
0410971	1165 \pm 66	960	-105 / +155
0804971	986 \pm 39	1140	-130 / +190
AVERAGE	1021 \pm 93	1016	-113 / +164

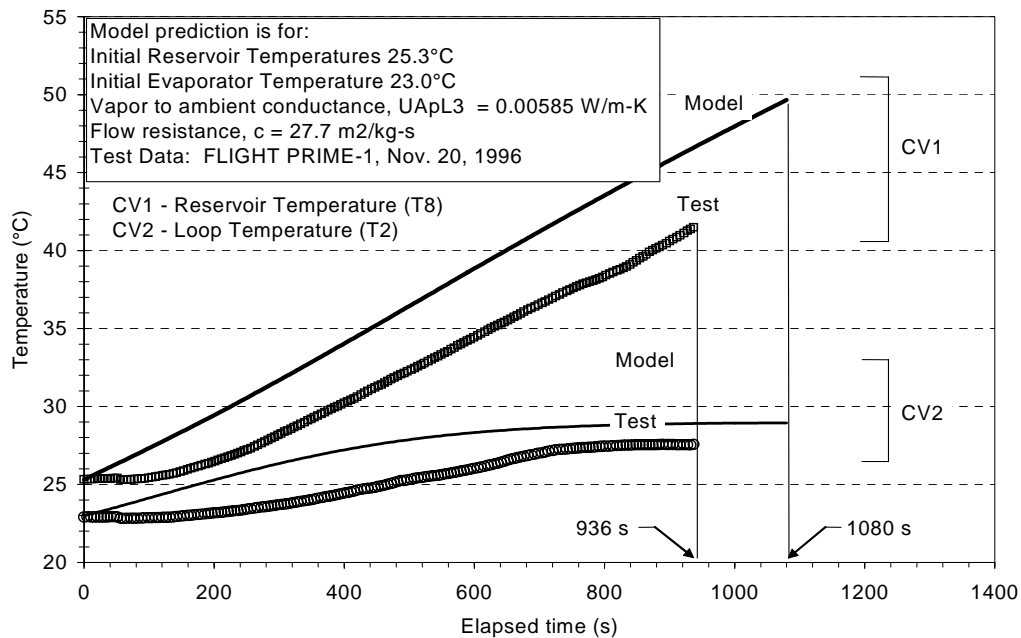


Figure 5.6 Comparison of temperature predictions to test data for VIEW-CPL flight pressure prime PRIME-1.

presented in Figure 5.1. Similar results were obtained for the pre-flight and post-flight data. In Figure 5.6, the measured reservoir temperature has an 80 sec lag before responding to the heater power. This is due to the location of the temperature sensor relative to the heater. The sensor is located 38 and 51 mm (1.5 and 2 in.) from the 5 W and 20 W heaters, respectively. The reservoir is made from thin walled stainless tubing (57 mm OD x 0.9 mm wall) and therefore is not a good conductor from the heat source to the temperature sensor location.

A one-dimensional transient analysis was performed on the reservoir using pure conduction as the heat transfer mode from the heater location to the temperature sensor. Figure 5.7 shows the results of the conduction analysis, indicating that the temperature at a location 38 mm away from the source

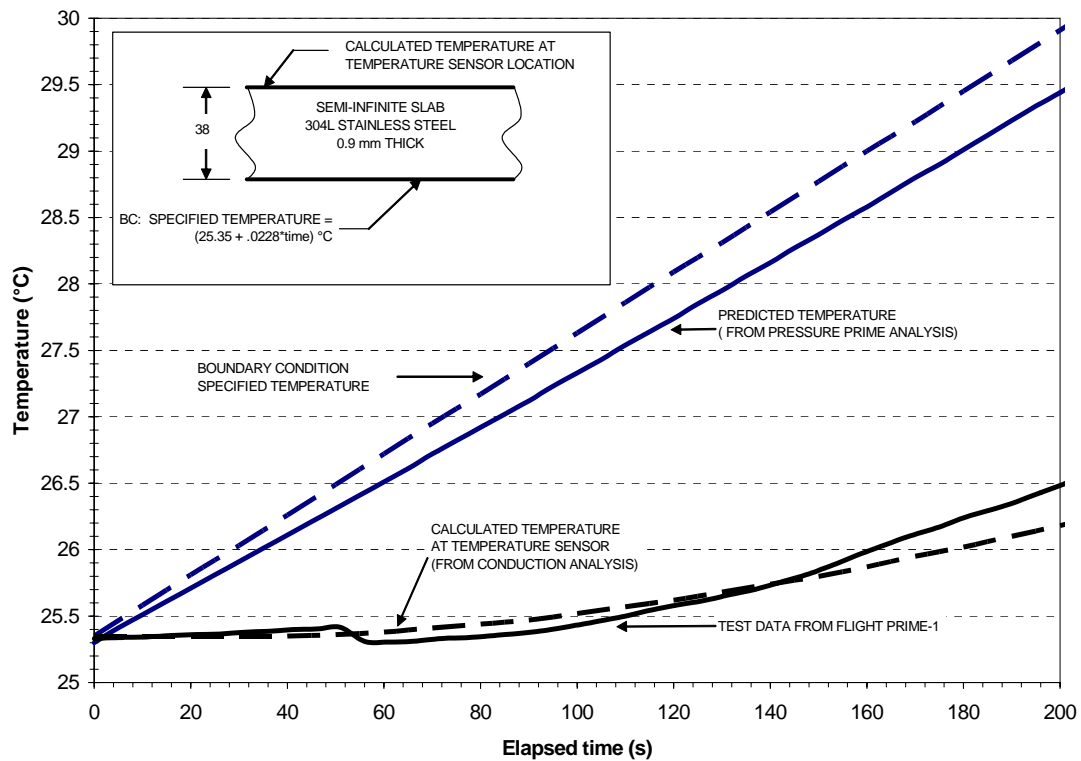


Figure 5.7 Results from a one-dimensional conduction analysis on the temperature lag from the reservoir heater location to temperature sensor.

temperature will lag by the same difference as the pressure prime reservoir temperature and the measured reservoir temperature.

In Figure 5.6, the maximum difference between the predicted loop temperature (CV2) and the measure loop temperature is 3 K. The shape of the loop temperature traces are similar. The end of the pressure prime is indicated by a reduction in the slope of the loop temperature trace. Since the loop temperature increases are due to vapor compression and there is no more vapor compression, the temperature stops changing when the pressure prime is complete and the loop is filled with liquid. The slopes of the predicted

temperature traces in Figure 5.6 are nearly the same as the slopes of the measured temperatures.

5.1.3 Heat loss from the reservoir

The heat loss from the reservoir during the pressure prime is small compared to the power input. The test data can be used to find the heat loss because the 5 W reservoir heater operated at steady-state between tests. For example, the reservoir temperature at the start of three tests where the experiment had remained off for several hours (with the exception of the 5 W reservoir heater) are listed in Table 5.2 along with the calculated conductance to ambient. Based on these results, the average heat loss to ambient from the reservoir is 0.29 W/K. This conductance is used in the reservoir models discussed in Section 4.3 and 4.4.2.

Table 5.2 Heat loss from the reservoir in the shuttle cabin during flight testing.

Test (following 5 W reservoir heating)	Temperatures		UA (W/K)
	Reservoir T8 (°C)	Ambient T9 (°C)	
S-75	44.7	26.8	0.28
S-10	45.6	29.4	0.31
S40R-1	44.9	27.9	0.30
Average:			0.29

5.2 Observations of VIEW-CPL Start-up

After the pressure prime at the start of each test was complete, power was switched on to the evaporator heaters. Section 4.4 described two segments of the start-up of a CPL system as the sensible heating period followed by the vapor

line clearing. These two start-up segments are illustrated in Figures 5.8, 5.9, and 5.10 for typical flight, pre-flight, and post-flight tests with 35 W of evaporator power.

General trends that were observed in the temperature profiles during start-up are:

1. Once the 20 W reservoir heater is turned off (end of pressure prime), there is a decrease in the temperature of the reservoir line. The temperature sensor on the reservoir line (T1) is close to the reservoir and is influenced by heat conducted from the reservoir. The post-flight test does not show a decrease in the reservoir line temperature at the beginning of the start-up because the 20 W reservoir heater remained on through-out the test.
2. After the evaporator heater is turned on, there is an increase in the temperature of the evaporator body (T6), evaporator liquid inlet (T7), and evaporator vapor exit (T5) to the vapor line. The liquid inlet and vapor exit temperatures increase due to conductive heat leak from the evaporator body; the slope of the temperature traces for these locations is significantly smaller than the rate of rise of the evaporator body.
3. The boiling observation (visual) corresponds with a distinct rise in the vapor line temperature (T5) and a distinct drop in the reservoir line temperature (T1) from cold liquid flowing to the reservoir. There is a sharper increase in the vapor line temperature for the post flight test. This may have been a result of a liquid filled core along with the continued 20

W heating on the reservoir (in the other tests, the 20 W heater is turned off when the evaporator power is turned on). There is normally an increase in both fluctuation amplitude and frequency of the differential pressure signal at the time of boiling. The flight and pre-flight data show the change occurring at the time of boiling, while the post-flight data shows the change after vapor reaches the condenser. The reservoir heater that was on during the post flight testing may have influenced the differential pressure measurement since the amplitude of the signal is very small and within the noise range of the transducer. In four of the 18 start-ups observed during flight testing (Tests S50-1, SS25-1, JUMP-1, S40-2), the change in the differential pressure signal occurred before the sudden increase in the vapor line temperature (T5); in the remaining start-ups the change occurred at the same time the temperature increased at the vapor exit. It is possible that the start-up for the four cases was such that the boiling was contained in the vapor grooves and vapor did not exit the grooves for a couple of minutes. In all cases, there was less than a two minute lag between the differential pressure oscillations and increase in temperature of the vapor line.

4. The slope of the temperature trace for the evaporator body (T6) decreases after boiling begins, indicating that some of the evaporator power is used for boiling the water rather than sensible heating of the evaporator. The reservoir temperature (T8) also decreases when the boiling begins

because room-temperature liquid is displaced from the vapor line by vapor. The decrease in reservoir temperature causes only a slight decrease in the absolute pressure due to the shallow slope of the vapor pressure curve of water at 50 °C.

5. In all three plots for the 35 W evaporator power, the vapor reaches the condenser inlet (T3) approximately 5 minutes after boiling starts.

In general, the start-up profiles for the flight, pre-flight, and post flight tests are very similar for the 35 W power level. Other power levels also show similarity between the ground and flight tests. One difference observed between ground and flight tests is the change in reservoir temperature during the vapor line clearing. For the ground tests the slight decrease in reservoir temperature corresponds to a slight decrease in absolute loop pressure. However, in the flight tests the reservoir temperature decreases by 5 K during the vapor line clearing while the absolute loop pressure decreases by the same amount as it did during the ground tests. The reason for the difference in the reservoir temperature sensor response is that during flight testing, the temperature sensor is likely measuring a liquid temperature rather than a vapor temperature, due to effects of micro-gravity.

During CPL startup, the sensible heating period ends when a vapor bubble is formed in the evaporator vapor grooves or vapor plenum. The vapor line clearing period is the time required to replace the liquid in the vapor grooves, vapor plenum, and vapor line with vapor. The following sections compare test

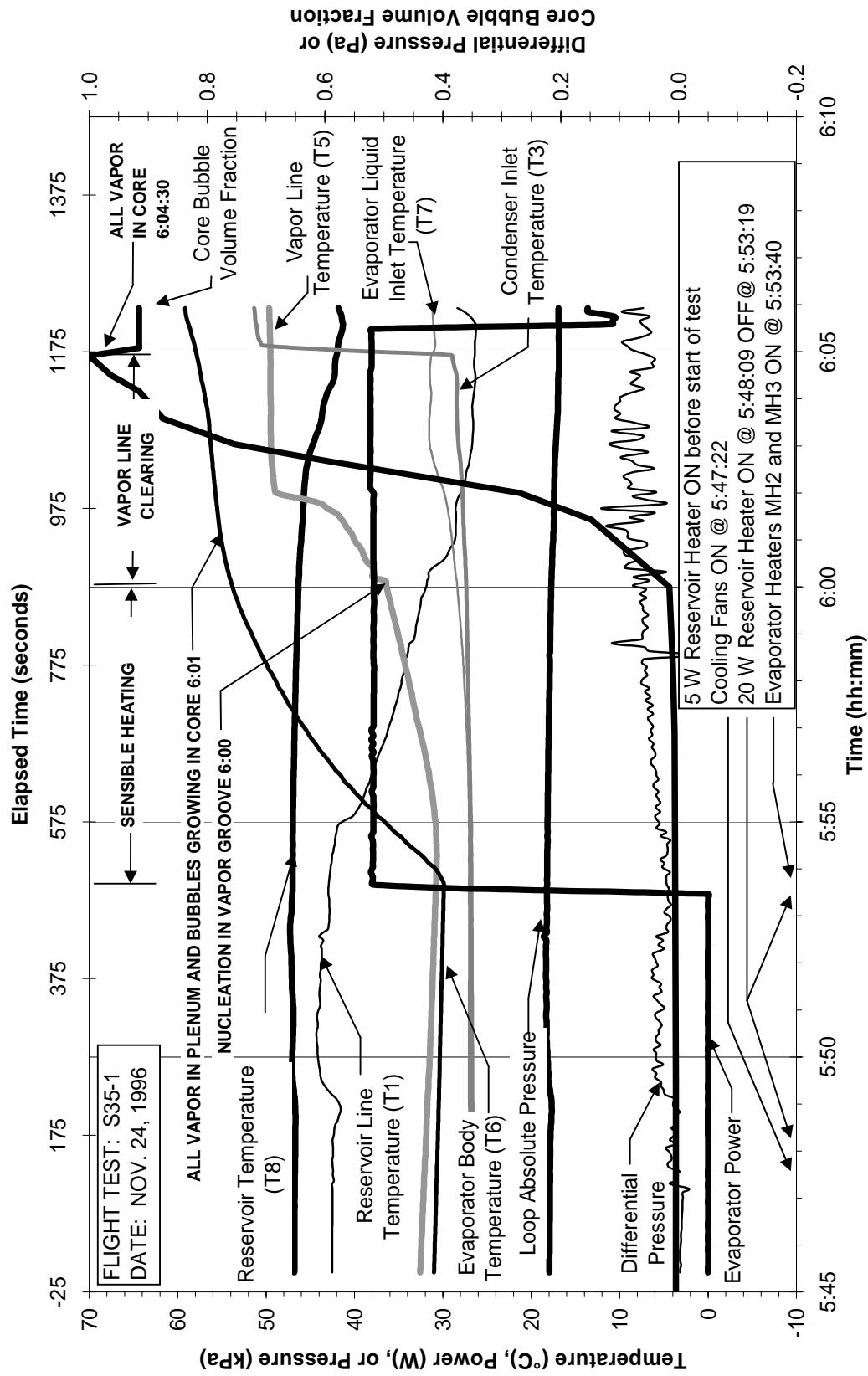


Figure 5.8 Example of start-up during flight testing of VIEW-CPL.

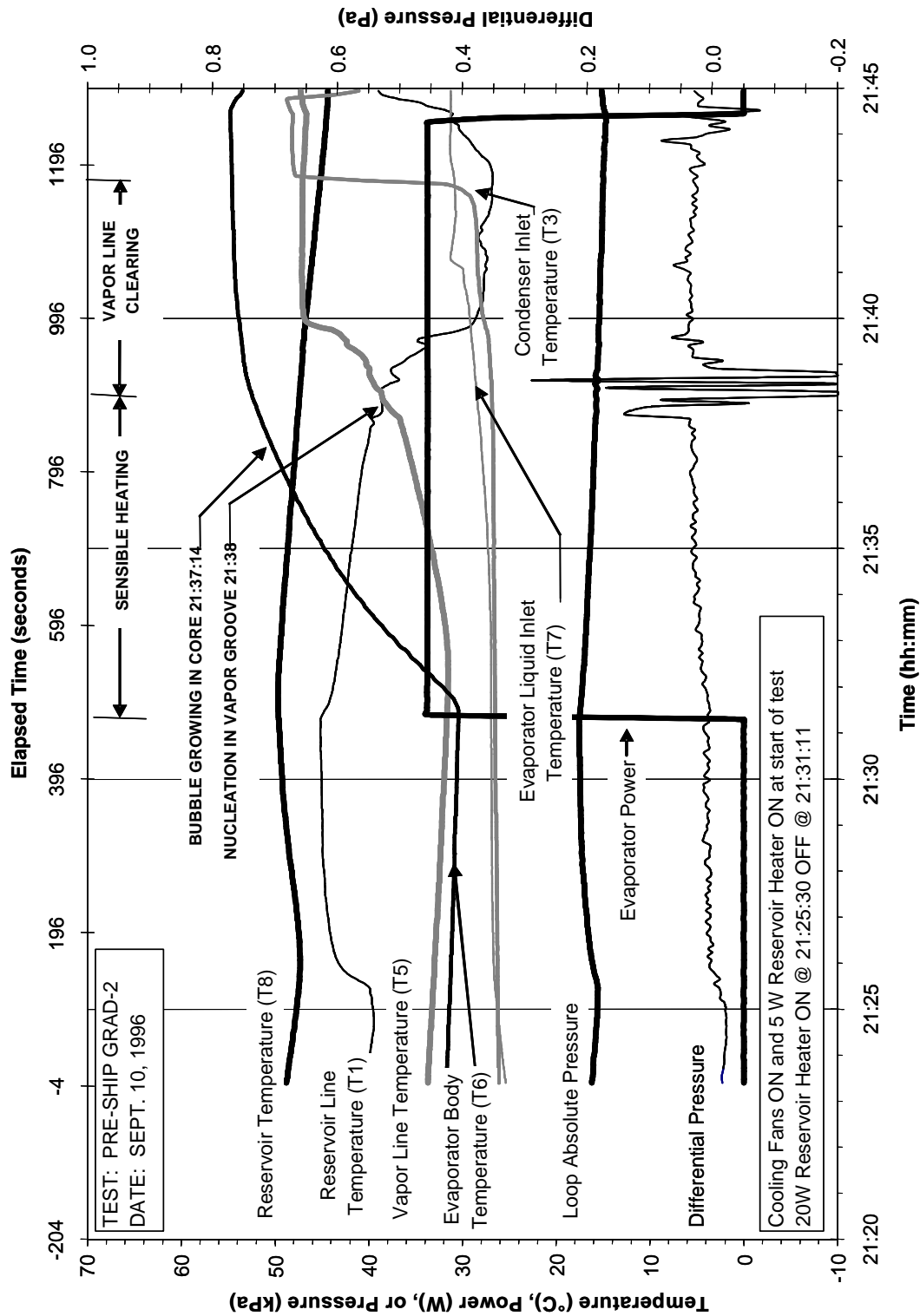


Figure 5.9 Example of start-up during pre-flight testing of VIEW-CPL.

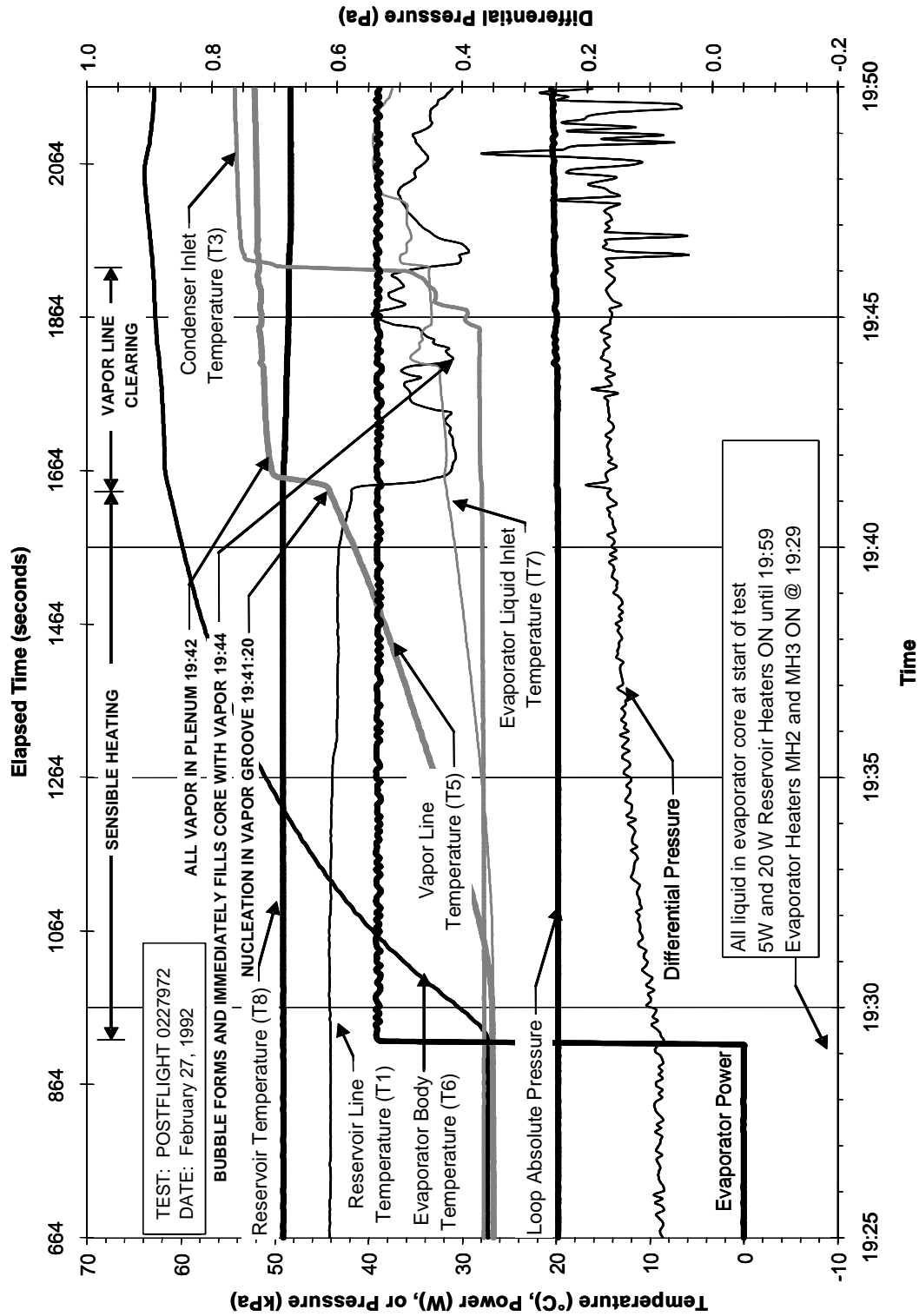


Figure 5.10 Example of start-up during post-flight testing of VIEW-CPL.

data to the system models introduced in Sections 4.4.1 and 4.4.2 that describe the sensible heating and vapor line clearing, respectively.

5.2.1 Sensible heating

Figures 4.6. and 4.7, from the conduction analysis in Section 4.4, provided expected temperature profiles of the evaporator block, at the same location as the temperature sensor T6 (see Figure 4.5), and the temperature profile of the warmest node in the wick structure during the sensible heating period. Figure 5.11 compares the predicted sensible heating time that is required to heat the wick to saturation temperature (as determined by the reservoir temperature) with the actual time that a vapor bubble was observed in the evaporator vapor grooves or vapor plenum. The predicted time was read from the plot in Figure

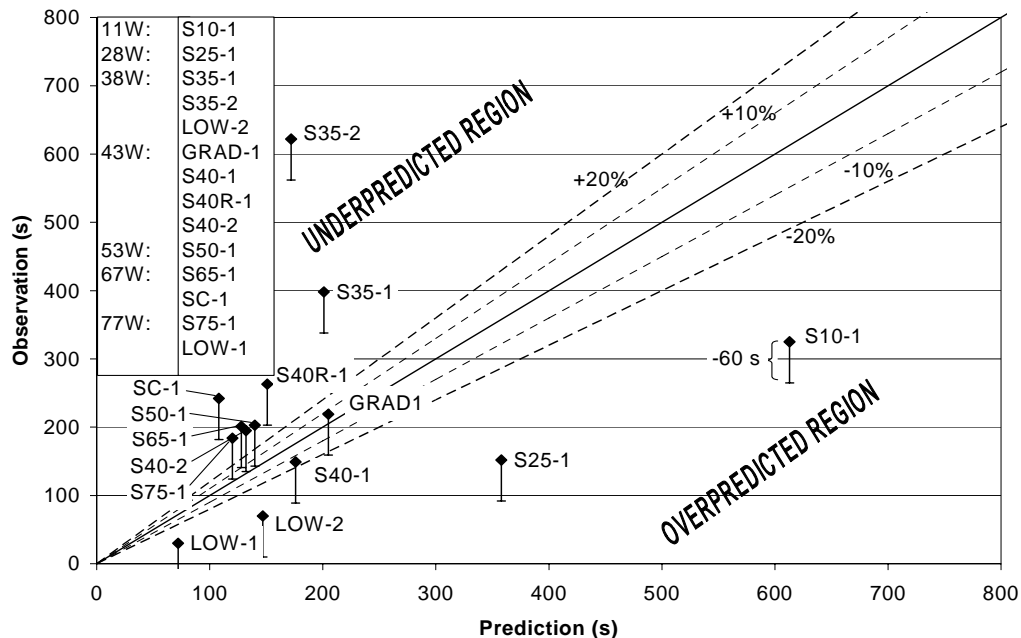


Figure 5.11 Comparison of predicted and observed time for fluid in the VIEW-CPL evaporator to boil after heater power is turned on.

4.6. The values were determined by selecting the curve that matches the heater power and finding the normalized wick temperature ($T_{\text{wick}} - T_o$) location that is equal to the measured reservoir temperature normalized with the initial evaporator temperature ($T_8 - T_6$). The associated time is the prediction for the start of boiling. The error bars in Figure 5.11 on the observed time correspond to ± 60 s since this is the maximum deviation that the camcorder time may deviate from the PGSC. The data scatter in Figure 5.11 indicate that boiling is sensitive to a number of variables. Of the 14 tests that are plotted, the time to boil is over-predicted in 4 cases, under-predicted in 4 cases, and predicted within 20% in 6 cases (if cases with error bar overlap are counted).

The under-predicted outliers, for which the boiling observation exceeded 300 s, may result from the heater position. In particular, the 25 W heater is located in the middle of the evaporator away from the grooves that are visible. The visual observations are limited to the two edge grooves (of seven vapor grooves) and the vapor plenum. Bubbles may form in other grooves that are not visible and provide heat spreading which would delay the observed boiling. Superheat requirements and availability of nucleation sites can cause the observed time to be longer than the predicted time. The over-predicted outliers may also be experiencing unusual transient effects due to noncondensable gas.

The noncondensable gas is not always in the same place in the loop; in fact some tests do not start with gas bubbles in the core. The boiling observations that are made before the predicted time may actually be

noncondensable gas bubbles expanding in the vapor grooves rather than vapor bubbles forming. This is supported by the visual observation that, for the under-predicted tests, the bubble growth is very slow and not characteristic of a boiling mode.

Since the sum of the partial pressures in the evaporator is equal to the reservoir pressure, $P_{\text{gas}} + P_{\text{vap}}(T_{\text{sat, evap}}) = P_{\text{vap}}(T_{\text{sat, res}})$, the saturation temperature in the evaporator is less than the reservoir saturation temperature if noncondensable gas is present in the evaporator. Therefore the working fluid will evaporate at a temperature lower than the saturation temperature corresponding to the system pressure (controlled by the two-phase reservoir). The temperature at which the working fluid inside the evaporator boils is a function of the system saturation pressure and the amount of noncondensable gas present in the evaporator.

If noncondensable gas is present in the evaporator core but not in the vapor grooves, then boiling can occur in the core before the fluid inside the grooves has reached the necessary temperature to nucleate. For fluids with a low vapor pressure (such as water) even a small amount of gas can cause the fluid inside the core to evaporate before the fluid inside the grooves. The ideal gas law can be used to determine partial pressure of the noncondensable gas given a known amount of gas and bubble volume. Subtracting the gas partial pressure from the pressure of the reservoir gives the partial pressure of the vapor inside the evaporator. The saturation temperature inside the evaporator is then

determined from the vapor pressure curve for water. As an example, Figure 5.12 contains a plot of the effect that noncondensable gas has on the temperature at which a bubble inside the core can expand due to evaporation. The plot shows the subcooled temperature (temperature below the reservoir saturation temperature) at which evaporation can occur as a function of the amount of noncondensable gas contained within a bubble. Figure 5.12 contains two curves in order to show the effect at two different reservoir saturation temperatures. For lower reservoir temperature, there is a larger impact of noncondensable gas due to the lower slope of the vapor pressure curve. For example if 2.0×10^{-11} kmol of gas is contained inside a 0.02 cm^3 the bubble, the gas would cause the fluid inside the core to boil at an apparent saturation temperature 5 K below the

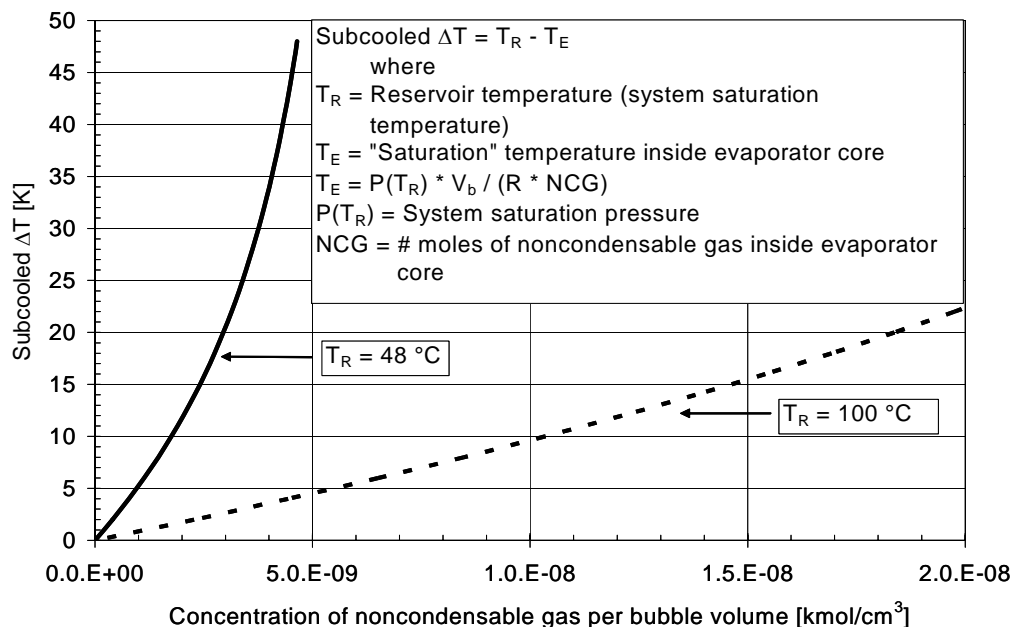


Figure 5.12 Effect of noncondensable gas concentration on evaporator saturation temperature.

saturation temperature for a 48 °C reservoir and only 1 K below saturation temperature for a 100 °C reservoir.

The conduction model presented in Section 4.4.1 was used to predict the evaporator temperatures prior to the onset of boiling. Figure 5.13 is a plot of the predicted normalized core temperature for the different heater powers as a function of time. The time at which boiling is observed in the evaporator for the flight tests and the predicted normalized temperature at the wick outer diameter at those times are also plotted in Figure 5.13. Bars extend from the predicted wick temperature points to the appropriate curve for the core temperature and

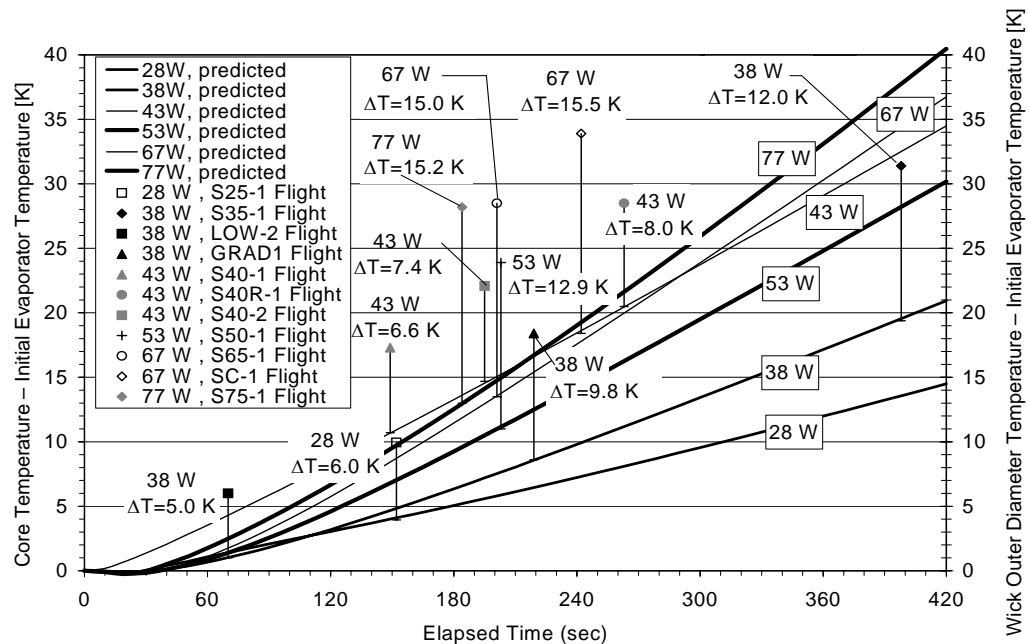


Figure 5.13 Predicted normalized temperatures for the evaporator core and wick outer diameter at the measured time of observed start-up in the VIEW-CPL flight tests. Temperature differences called out on the plot correspond to the gradient between the outer diameter of the wick to the core at the time when either evaporation or boiling is observed in the evaporator core or vapor grooves.

the temperature gradient across the wick is noted on the plot. The significance of the plot is that it helps quantify the gas concentration in the core that will allow the potential for evaporating in the evaporator core before boiling occurs in the vapor grooves. For the VIEW-CPL flight tests, a gas concentration in the core from 1.1 to 2.5×10^{-9} kmol/cm³ (determined from Figure 5.12 for reservoir temperature 48°C and corresponding to a temperature difference between core and wick ranging from 5.0 to 15.5 K) would allow bubbles in the core to expand before nucleation in the vapor grooves. Consequently, predicting the exact start of boiling with the conduction model described in Section 4.4 is limited by knowledge of the NCG concentration in the evaporator.

The conduction model predicts the temperature profile of the evaporator during the pure conduction phase of the start-up (i.e. no evaporation in bubbles or nucleation). Figure 5.14 shows the predicted evaporator temperature with the measured evaporator temperature from the VIEW-CPL flight tests. The predicted temperature is the same plot from Figure 4.7 (without the 11 W trace because there is no data available at 11 W for comparison) with the addition of VIEW-CPL evaporator temperature data from flight testing. The data points correspond to the evaporator wall temperature (T6) at the time of the first observed bubble growth inside the evaporator core or vapor groove. The actual heater power used in the tests is noted in Figure 5.14 and was dependent upon the voltage supply to the experiment at the time of the test.

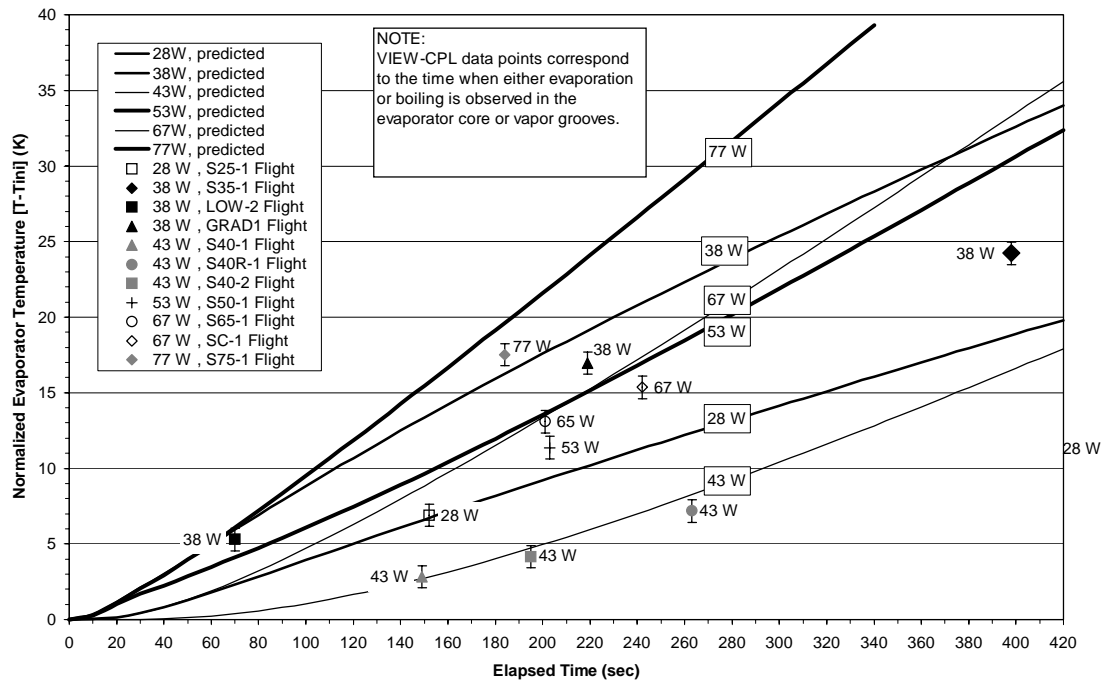


Figure 5.14 Comparison of predicted evaporator temperatures with VIEW-CPL flight data (temperature sensor 6) at the time of start-up.

For those tests where boiling occurred within the first three minutes after heater power was turned on, all data points fall on the predicted temperature curve. For later times, the test data falls below the predicted temperatures. The most likely reason for the deviation is that the model does not account for heat loss to ambient because it assumes that the evaporator is perfectly insulated. However, the insulation on the evaporator is not perfect. In addition, it is possible that some of the heater power is used for evaporation in a section of the evaporator that is not observable. The predicted temperatures are for the case where all of the heat input goes towards sensible heating of the evaporator and

saturated wick. Thus the model would over predict the evaporator temperature for any case where some of the heat is used for evaporation.

A comparison of the conduction model to actual test data is presented in Figure 5.15 for the three 38 W start-up cases presented in Figures 5.8 - 5.10. As shown in Figure 5.15, the data closely match the predicted temperature at the beginning of the conduction phase. As the warm-up continues, the slope of the test data curve is less than the predicted slope, for reasons previously explained.

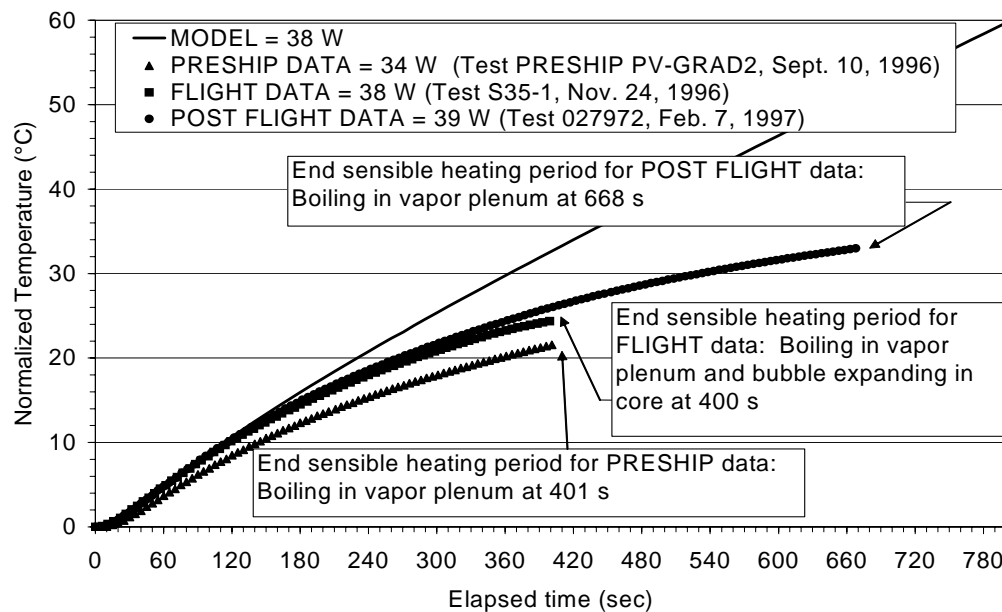


Figure 5.15 Comparison of predicted evaporator temperatures with VIEW-CPL data for pre-flight, flight, and post-flight start-up tests.

5.2.2 Heat loss from the evaporator

Heat loss from the evaporator was determined by fitting curves to the data using a lumped capacitance heat transfer model in the form of

$$mc_p \frac{dT}{dt} = \dot{Q}_e - UA(T - T_{amb}) \quad (5.2)$$

Assuming that the evaporator power, thermal mass (800 J/K for the VIEW-CPL evaporator) and overall heat transfer coefficient (UA) are independent of temperature and time, then equation 5.2 provides a temperature profile

$$T(t) = \frac{\dot{Q}_e}{UA} + \left[T_o - T_{amb} - \frac{\dot{Q}_e}{UA} \right] e^{\left(-\frac{UA}{mc_p} t \right)} \quad (5.3)$$

from which UA can be found by comparing to test data. The validity of the lumped capacitance model was verified by calculating a Biot number ($Bi = hL/k$) of 0.007 for the stainless steel evaporator using a characteristic length calculated from volume divided by surface area for a rectangular box 20 cm long x 6 cm wide x 2 cm thick. The lumped capacitance model is accurate for Biot number less than 0.1 [Incropera and DeWitt, 1990].

The evaporator temperature profiles for the transient deprime periods of flight Tests S25-1, S50-1, SS25-1, and JUMP-1 are plotted in Figure 5.16 along with predicted temperature profiles using a UA heat loss value of 0.54 W/K. The UA value was determined by a least-squares fit to the flight data; the pre-ship data (S40-1) and the 10 W case for PV-LOW-2 were used to confirm the validity of the analysis. The 25 W heater power was chosen in determining the heat loss factor since the 25 W heater was located in the center of the evaporator and provides more uniform evaporator heating than the 10 and 40 W heaters that are located on the evaporator sides (see Figure 3.20). Since the evaporator

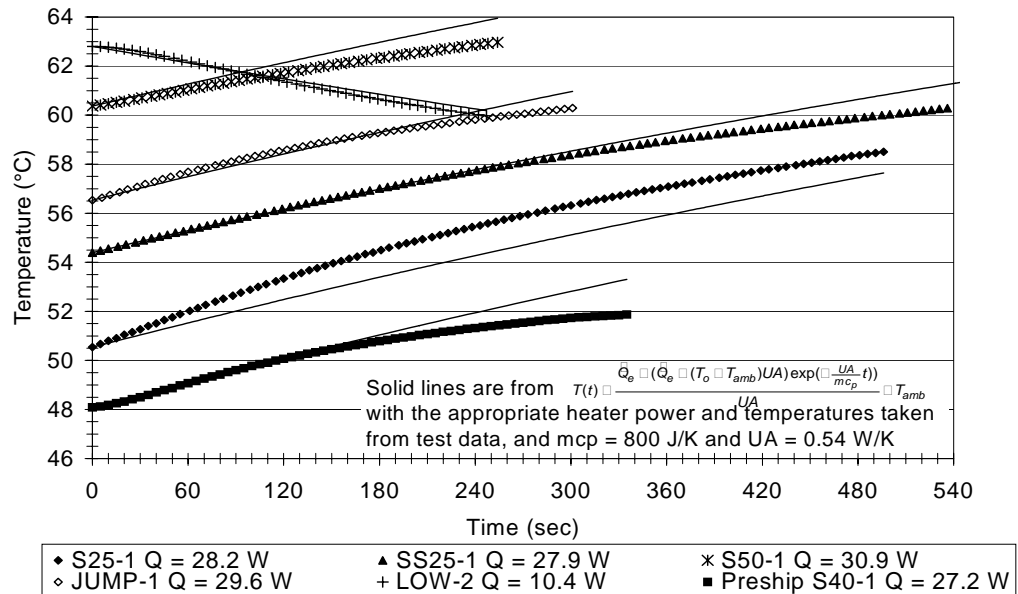


Figure 5.16 Least-squared fit to flight data to determine heat loss ($UA = 0.54$ W/K) from the VIEW-CPL evaporator by the lumped capacitance analysis. DATA from LOW-2 and Preship S40-1 were used to check the correlation. They were not included in the sample for least-squares determination of the UA value.

temperature sensor is located on the side of the evaporator, the data for tests that used the 10 W and 40 W heaters is skewed and more difficult to interpret, especially for the start-up cases. The deprime data were selected because the measured evaporator temperature is more likely to read the average evaporator temperature than during the start-up transient period. Since the deprime occurs after the loop has started, the vapor in the vapor grooves evenly transfers the heat to all parts of the evaporator. The deprime periods were identified by (1) the vapor line filling with liquid as indicated by the condenser inlet temperature at least 10 K less than the saturation temperature ($T_3 \ll T_8$), and (2) the

evaporator temperature increasing above the saturation temperature ($T_6 > T_8$). The conclusion from the analysis is that the average heat loss from the evaporator is characterized by a conductance of $UA = 0.54 \text{ W/K}$.

5.2.3 Vapor line clearing observations

After the sensible heating period, evaporation begins in the evaporator. In the start-up figures (5.8 - 5.10) an increase in the rate of the evaporator exit temperature (vapor line temperature T_5 just after the time where nucleation occurs in the vapor grooves) corresponds to the liquid displacement from the evaporator vapor spaces and vapor line. The liquid interface is visible through the evaporator and tracked by the evaporator and vapor line temperature measurements. The transient pressure surge of liquid displacement is described in Section 4.4.2. The purpose of the pressure surge analysis was to determine if the liquid in the core would flash due to the pressure drop. The model provided evidence that the pressure surge experienced during VIEW-CPL start-ups did not exceed the capillary limit of a fully-wetted evaporator wick (10 kPa) or the vapor pressure of the fluid inside the core of the wick (refer to Figure 3.18). The maximum pressure drop predicted by the model was 215 Pa, which would only exceed the capillary limit of the wick if the contact angle between the polyethylene and water was greater than 89.994° which is considered unlikely. The pressure surge would result in a bubble expansion in the core only if there was portion of wick that was not fully wetted after the pressure prime.

To check the validity of the pressure surge model, a comparison was made with the experimental data. The comparison is based on the length of time required before the vapor front enters the vapor line (indicated by vapor exiting the evaporator vapor plenum) and the elapsed time for the vapor front to pass through the vapor line (indicated by vapor flowing into the inlet of the condenser). Figure 5.17 summarizes the experimental data for these parameters. Heat loss from the evaporator to the surrounding air was estimated from the conductance calculated in Section 5.2.2. A curve fit was made using a hyperbola with time duration (from the displacement of liquid from the evaporator vapor plenum to the arrival of the vapor front at the inlet of the condenser) as a function of net heater power. The hyperbola model is a logical fit to the data since the volume

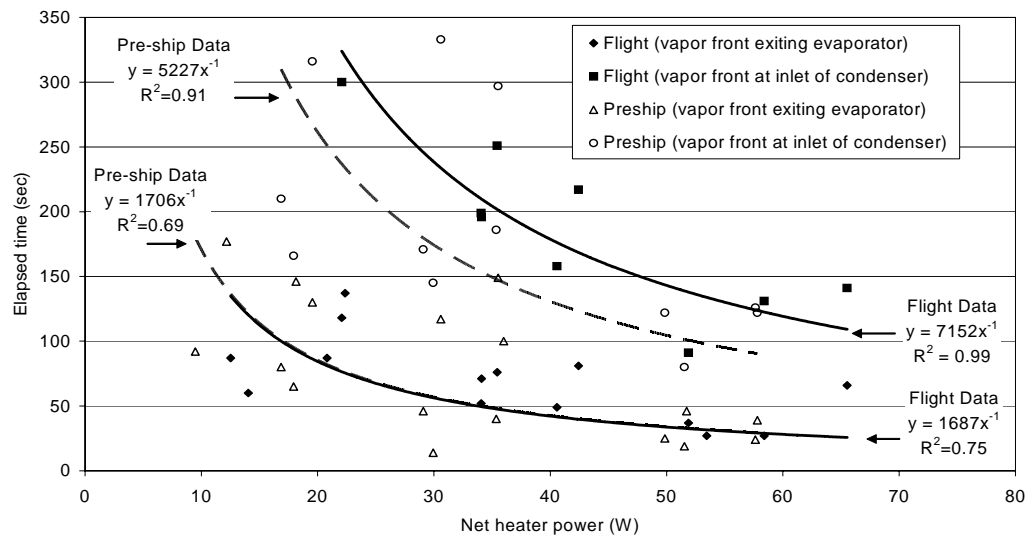


Figure 5.17 Plot of the time required to move the vapor front from the beginning (exiting evaporator) to the end of the vapor line (inlet of condenser) measured during VIEW-CPL flight and ground (pre-ship) tests. Note that the curve fits overlap for the flight and pre-ship data of the vapor front exiting the evaporator.

displacement for laminar flow is inversely proportional to the mass flow rate.

The time required for clearing the evaporator vapor plenum is nearly identical for the flight and the pre-ship data. The time required for clearing the vapor line is 15% shorter for the pre-ship data compared to the time for the flight data at the same power. This may be a gravity effect, where the vapor front in 1-g may not be as sharply defined as in micro-gravity. In 1-g, the vapor/liquid interface inside the vapor line is expected to stratify because the Bond number,

$$Bo = \frac{g(\rho_l - \rho_v)D^2}{\sigma} \quad (5.4)$$

is equal to 8.6 for water at 50 °C inside a tube with a 7.9 mm inner diameter. The Bond number must be less than four for a meniscus to be maintained in the tube to prevent stratification. Since the end of the pressure surge is indicated by a temperature measurement, stratification in 1-g is expected to allow vapor to reach the temperature sensor (located on top of the tube) before all of the fluid is displaced from the vapor line, which leads to shorter times.

The large scatter may be due to several factors including different operating temperatures. Additionally, the pressure surge model indicates that the duration is sensitive to heat loss from the CPL during the pressure surge. This makes the temperature of the evaporator at the start of boiling and the ambient temperature important parameters.

The sensitivity to evaporator temperature and ambient temperature was determined by exercising the model for the 35 W start-up case shown in Figure

5.8 (Flight Test: S35-1, Nov. 24, 1996). By varying the evaporator and ambient temperature, the sensitivity to the duration of the pressure surge was found to be 7 sec/K and 6 sec/K, respectively, which is approximately 4% change in time for a 1 K change in temperature difference. The nominal case shown in Figure 5.18 for an initial evaporator temperature of 54.0 °C and ambient temperature at 24.9 °C (not shown in figure).

In Figure 5.18, it is shown that the pressure surge model over predicts the reservoir and evaporator temperatures. Additionally, the predicted vapor volume initially expands faster than what was observed, resulting in an under prediction of the time to clear the vapor grooves (5 s compared to 118 s measured). The

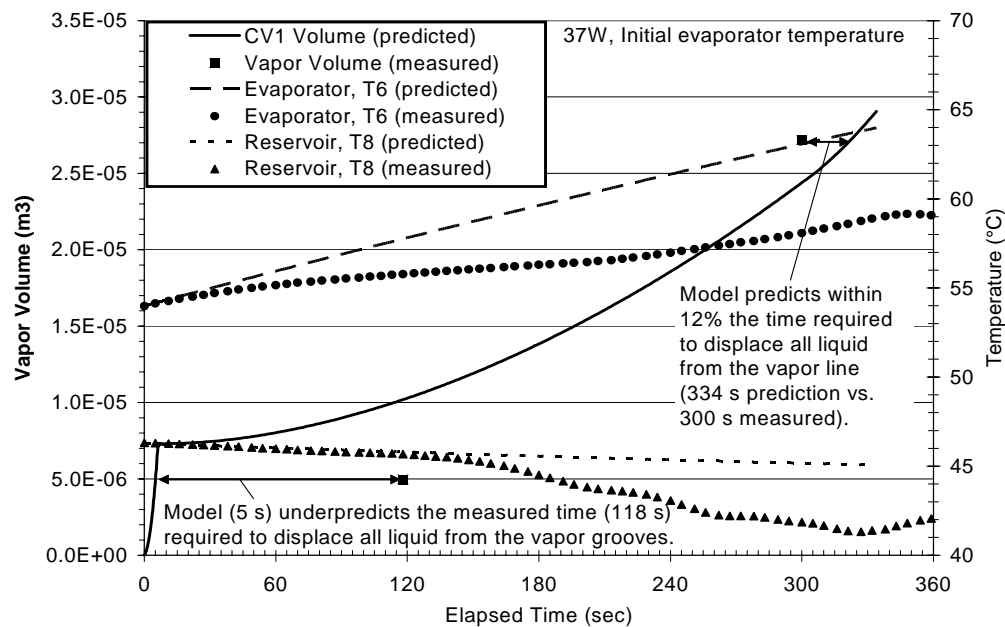


Figure 5.18 Pressure surge analysis for VIEW-CPL compared to start-up data for flight test S35-1. Vapor volume required to displace all liquid from the vapor grooves is 4.95 cc and volume to displace all liquid from the vapor line is 29.11 cc.

time to clear the vapor line is over predicted (334 s compared to 300 s measured). The difference for clearing liquid from the vapor grooves may be attributed additional thermal mass, of the evaporator block at the vapor plenum which is heated only by conduction through the block, that is not accounted for in the model. This time is relatively short compared to the clearing of the vapor grooves which is predicted by the model within 12%. Another difference between the model and actual system is that the vapor and liquid phases inside the reservoir are assumed to be separated in the model (although condensation is permitted inside of the vapor space). This approximation is rationalized because the reservoir contains an internal wick structure intended to control the phases and prevent vapor from exiting the reservoir. However, the decrease in reservoir temperature that is observed in the measured data (T8) may indicate mixing of the reservoir fluid with incoming liquid, which is subcooled at ambient temperature, resulting in a decrease in reservoir temperature. The temperature gradients and absolute pressure measured during the VIEW-CPL pressure surges do not indicate that VIEW-CPL was cold-shocked during startup even though there was a 4 K temperature drop. Although the 4 K reservoir temperature drop that is observed during the flight Test S35-1 (Figure 5.18) corresponds to a pressure drop of 2.25 kPa, the absolute pressure transducer only registered a 0.7 kPa decrease. It is likely that the temperature sensor on the reservoir is measuring a liquid temperature and not a saturation temperature.

Figure 5.19 is a comparison of the pressure surge model results to the flight data for varying heater power. The open symbols were obtained by exercising the model with the measured evaporator power, ambient temperature, reservoir temperature, and evaporator temperature as model input parameters. The prediction results were fit to a hyperbola (the dashed line on Figure 5.19) because the time to displace liquid is inversely proportional to the net heater power. The flight data (solid line) was previously shown in Figure 5.17 and is repeated here for comparison purposes. As shown in the bottom two curves of Figure 5.19, the model significantly under predicts the actual response for the clearing of the evaporator. The curve fit to the predicted data for the time required to move the vapor front to the end of the condenser closely matches the

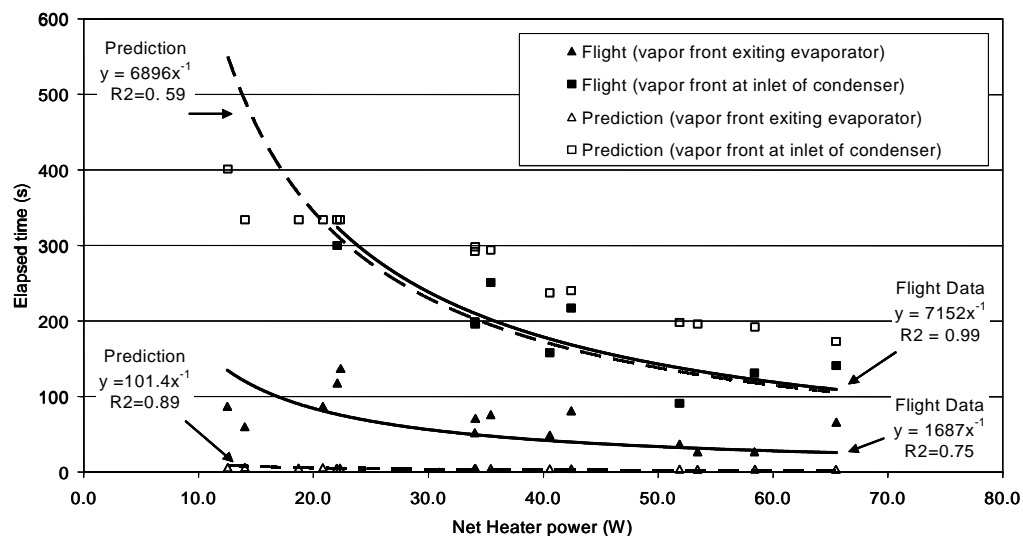


Figure 5.19 Comparison of predicted (open symbols) to measured (solid symbols) time required to move the vapor front from the beginning to the end of the vapor line during the VIEW-CPL flight tests. The curve fit to the predicted times is a dashed line while the curve fit to the actual data is a solid line.

curve fit of the measured data. The accuracy of the measured data is ± 10 s due to the frequency of the data collection (4 to 6 s per scan). While the model does not accurately predict the time to clear the vapor line of liquid, it provides a general description of the pressure surge physics.

The purpose of creating the pressure surge model was to determine if a deprime was inevitable for a water CPL operating at 50 °C. The model indicates that the pressure required to displace the fluid from the vapor line was well below the capillary pressure of 10 kPa for a fully-wetted wick. The differential pressure data obtained from the experiment also indicated that pressure drop was so low that it was within the noise of the sensor. However, vapor was observed in the core of the evaporator by the end of all pressure surges, even for start-ups that began with a liquid filled core. This supports the hypothesis that the evaporator wick is not fully wetted, and had dry portions that allowed vapor to back-flow into the core.

5.3 Steady-State Operations

At the end of start-up, vapor bubbles were observed in the evaporator core for all flight and ground tests. As described in Section 4.5 the CPL can still circulate the working fluid provided that the bubble does not block the flow of liquid to the wick. Backing up this theory are observations of extended periods of steady-state operations made during the VIEW-CPL testing.

Steady operations in this study are defined by two conditions: (1) steady evaporator temperature (less than 0.5 K change in temperature at T6 for a

minimum period of 10 minutes) and (2) a constant temperature difference between evaporator body and evaporator exit (temperature sensors T6 and T5, respectively). The latter condition is included because the heater location can influence evaporator temperature readings and mask an unsteady condition. Maintaining a constant temperature difference between the evaporator body and the exit implies that there is no change in evaporator conductance (i.e. radial dry-out in the wick). Ten minutes was chosen as the time for observing steady-state based on a ground testing experience where VIEW-CPL appeared to be operating steadily with 28 W on the evaporator for 10 minutes, but then deprimed (preship test #S65-2). Note that the two steady-state criteria conditions do not exclude periods where the core bubble oscillates. In fact there was a vapor bubble in the core of the evaporator at some point during all of the tests.

The steady-state conditions were satisfied in six of the 23 pre-ship tests, none of the flight tests, and five of eight post-flight tests. Since steady-state conditions were only observed in ground testing, it suggests that gravity or another condition from testing in the shuttle (i.e. reduced convection, higher ambient temperature, or longer test durations) influenced the tests. The time span between the pre-ship and post-flight tests implies that the noncondensable gas was not a factor in obtaining a steady-state condition. There is a higher percentage of post flight tests with steady-state operations because three of the eight tests were performed with additional subcooling provided at the evaporator

inlet and, during most of the post-flight tests, the 20 W reservoir heater was left on (it was turned off during flight tests because of power limitations in the shuttle).

The plots in Figures 5.20 and 5.21 are examples of the steady-state data collected during preship and post-flight testing. The data from the preship test (Figure 5.20) shows steady-state operations for nearly one hour. Although video footage of the bubble in the evaporator was not recorded, notes on observations that were made during the test indicate that a bubble was flowing in and out of the evaporator inlet during the entire test. The observations are consistent with the oscillating temperatures measured at the evaporator inlet (T7) and the reservoir line (T1). Since the bubble expanded into the evaporator inlet but did not block flow to the wick (deduced from the steady evaporator temperature), it is likely that stratification in the evaporator allowed liquid to pass under the bubble to keep the wick wetted.

Figure 5.21 is a plot of the post-flight test 0228971 during which power changes were made on the evaporator. Note that liquid filled the condenser during the 14 W segment of the test, confirming that the heat loss from the evaporator to ambient is approximately 10 W. This type of test, with several power changes is sometimes used in industry to check for bubbles in evaporators. The test sequence for VIEW-CPL used small variations due to the limited heater power. Based on the evaporator temperature response to the power changes as shown in Figure 5.21 it is not obvious that there is a bubble in the evaporator core. The visual observations in the evaporator indicate that a

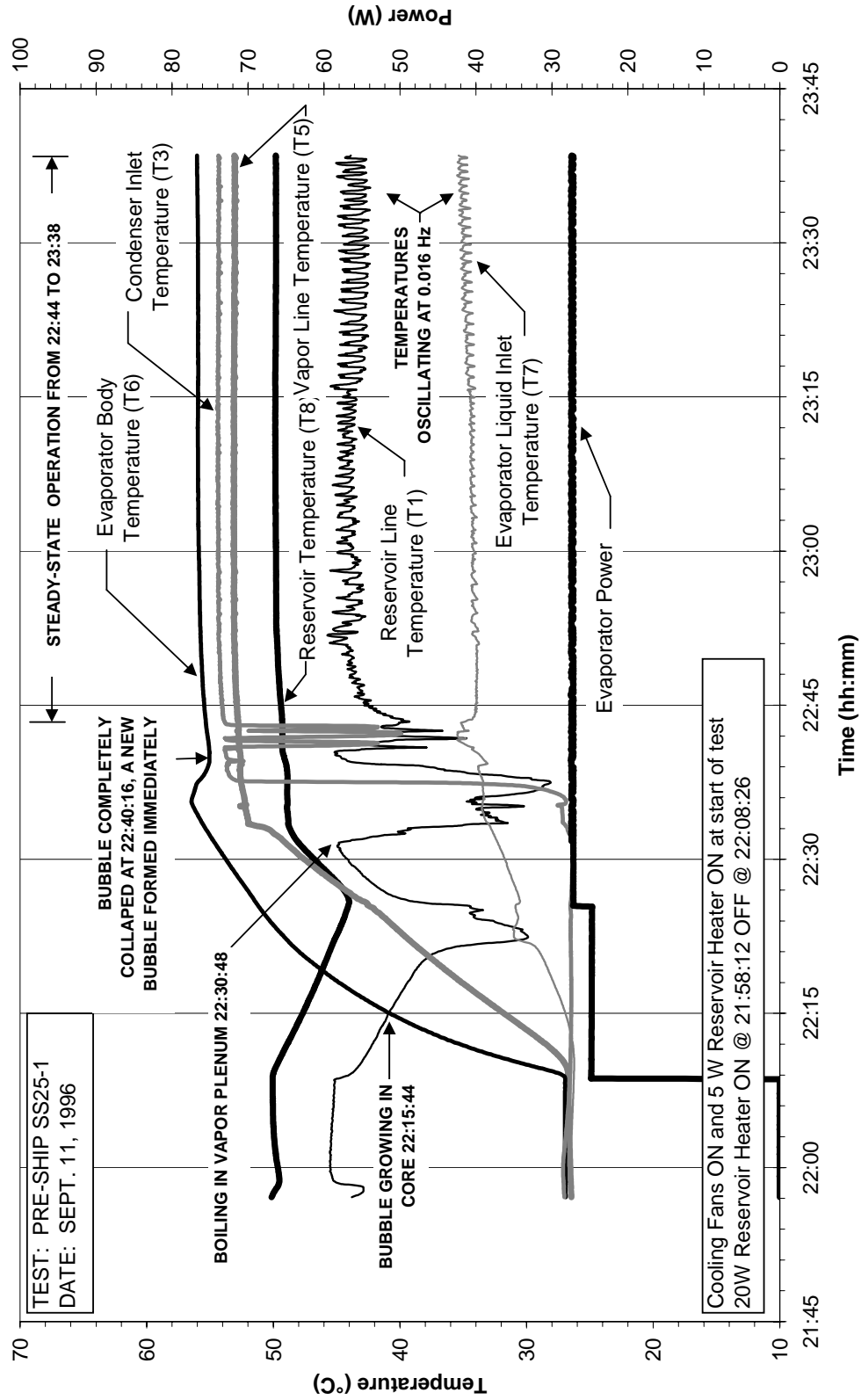


Figure 5.20 Example of VIEW-CPL steady operations during ground testing before flight.

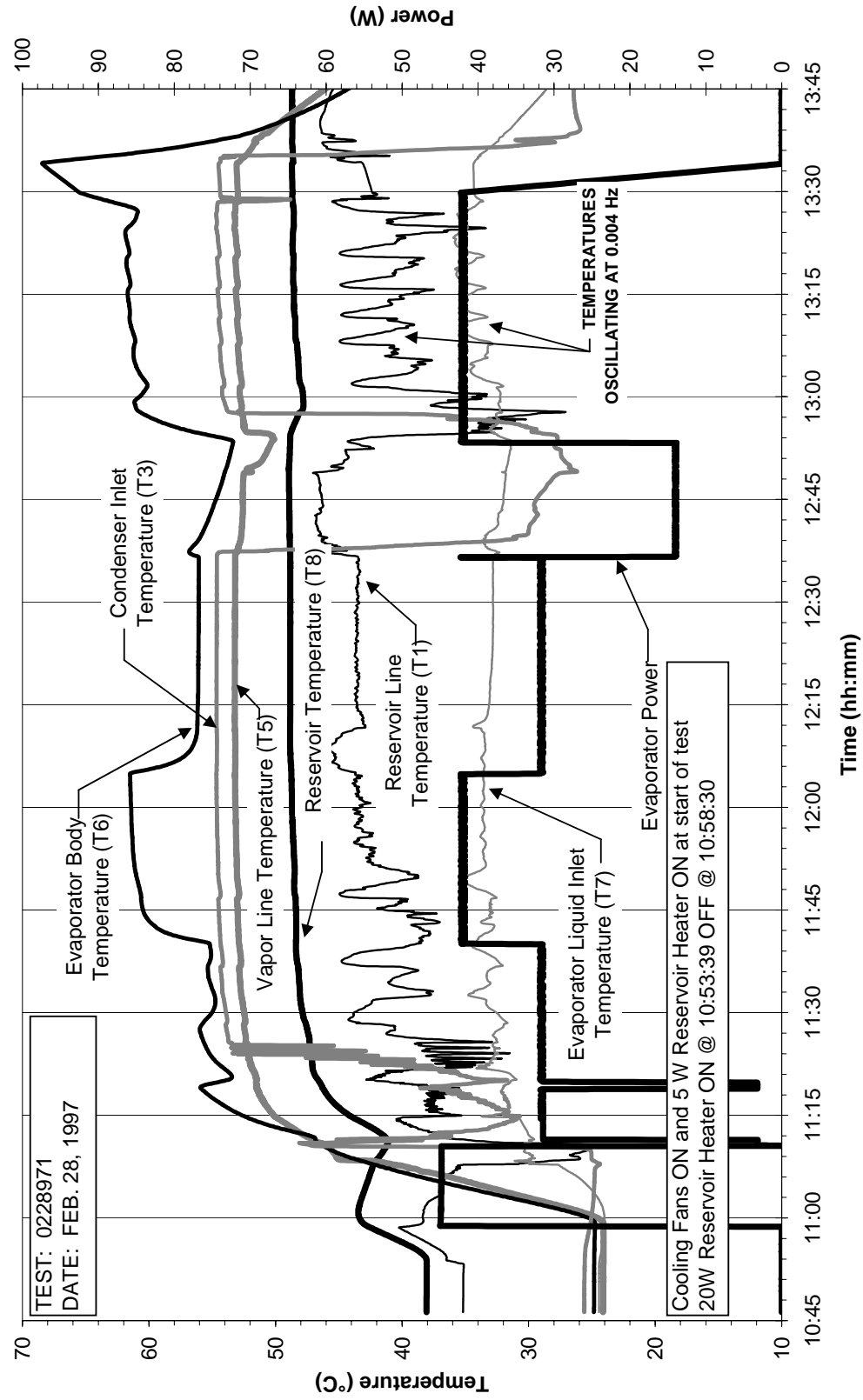


Figure 5.21 Example of VIEW-CPL operations with power changes during ground testing after flight.

bubble is oscillating in the core throughout the entire test, emphasizing the importance of the visualization aspect of the experiment.

Changes in temperature at various locations of the CPL are indicators of oscillatory fluid flow in the system. One example is the indication of flow to and from the reservoir by the change in the temperature at the reservoir inlet (T1). Since the reservoir temperature is greater than that of the liquid exiting the condenser, flow out of the reservoir results in an increase in the reservoir inlet temperature. In Figure 5.20 this occurs at 22:40:16 when the core bubble completely collapses and at 12:32 in Figure 5.21 during the power decrease from 32 W to 14 W. Similarly, the reservoir inlet temperature decreases due to flow of cool liquid from the liquid line into the reservoir. This always occurs at start-up when vapor displaces liquid from the vapor line (e.g., at 22:30:48 in Figure 5.20 and at 11:02 in Figure 5.21).

Similarly, the condenser and evaporator temperatures vary with flow in and out of those components. A relationship is apparent between the flow of liquid from the reservoir and the flow of liquid to or from the condenser where there appears to be a phase shift between the changes in the condenser and reservoir temperatures. This occurs as the vapor front is established in the condenser in Figure 5.20 at time 22:41 through 22:44. It is also observed during the steady operating period between 13:00 and 13:17 in Figure 5.21, although the magnitude of the condenser temperature change is much smaller than that of the reservoir. The flow between the reservoir and evaporator is detectable by the

temperature oscillations at the reservoir line (T1) and the evaporator inlet (T7) that occur at the end of the plots in both figures.

5.4 Observations of Bubble Growth in the Evaporator Core

While there were no flight tests that satisfied the steady-state conditions described in Section 5.3, oscillations were observed where a bubble in the core alternately expanded and collapsed in an apparently stable oscillation. The flight tests revealed 33 instances of liquid flow into the evaporator following apparent dry-outs of the evaporator wick. Other instances of liquid flow into the evaporator were caused by a decrease in the power input to the evaporator, but the power input to the evaporator remained constant during the 33 instances of evaporator refills described above. Figure 5.22 contains a series of three data plots (for the S35-1 test) which show a typical example of a bubble life cycle observed during flight testing. In this test, the bubble in the core collapsed twice (at 2459 and 2793 s) while a constant power of 30 W was applied to the evaporator. The two pauses in heater power (bottom plot at 1200 sec and 1890 sec) were specified in the testing procedures in an attempt to prevent the wick from dry-out by giving the evaporator time to refill after the vapor bubble filled most of the evaporator core.

As with the ground tests (described in Section 5.3), the bubble collapses in Figure 5.22 (top plot) appear to correlate with oscillations in the reservoir inlet, evaporator inlet, and condenser temperature data. The period between the observed bubble cycles (peak #3 to peak #4) is 330 seconds for a frequency of

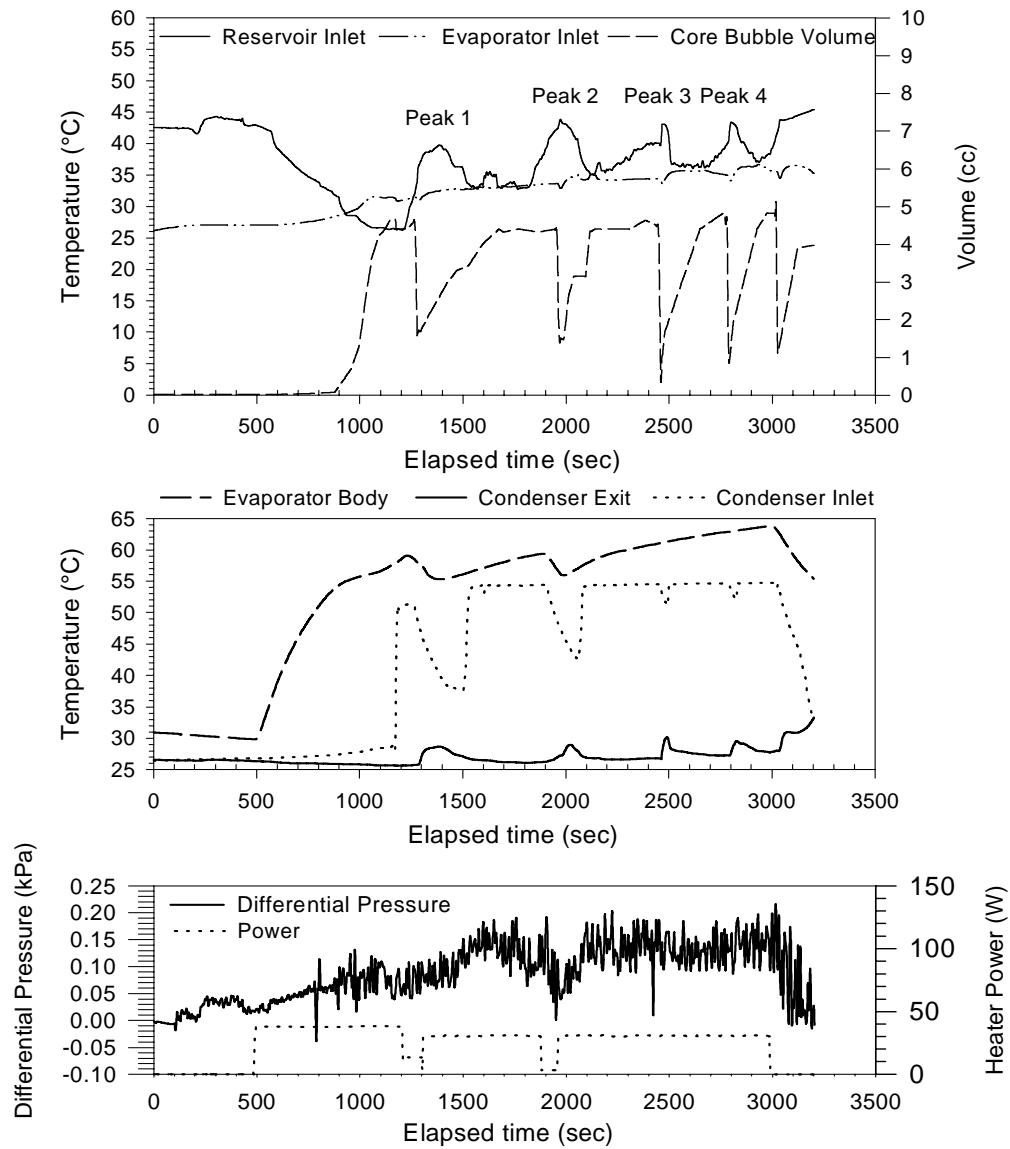


Figure 5.22 Fluctuation in core bubble volume and temperatures during VIEW-CPL flight test S35-1.

0.003 Hz. This corresponds to the frequency range of temperature oscillations ranging from 0.003 to 0.005 Hz that have been observed in other CPL systems [Kiper et al., 1988; Lin et al., 1994; and Ku et al., 1986b].

A theory was presented in Section 4.6.3 that describes a decrease in pressure in the evaporator as the mechanism governing the bubble collapse while the heater power is still applied to the evaporator. A plot comparing the predicted bubble cycle to the actual evaporator temperature and bubble volume data is shown in Figure 5.23. The prediction is not started until 6:20 because the loop had just experienced a power transition from 3 to 30 W at 6:18. As in Section 4.6, an offset of 1050 s was used to set the initial boundary condition on the liquid temperature in the core.

The continual increase in the evaporator body temperature seen in Figure

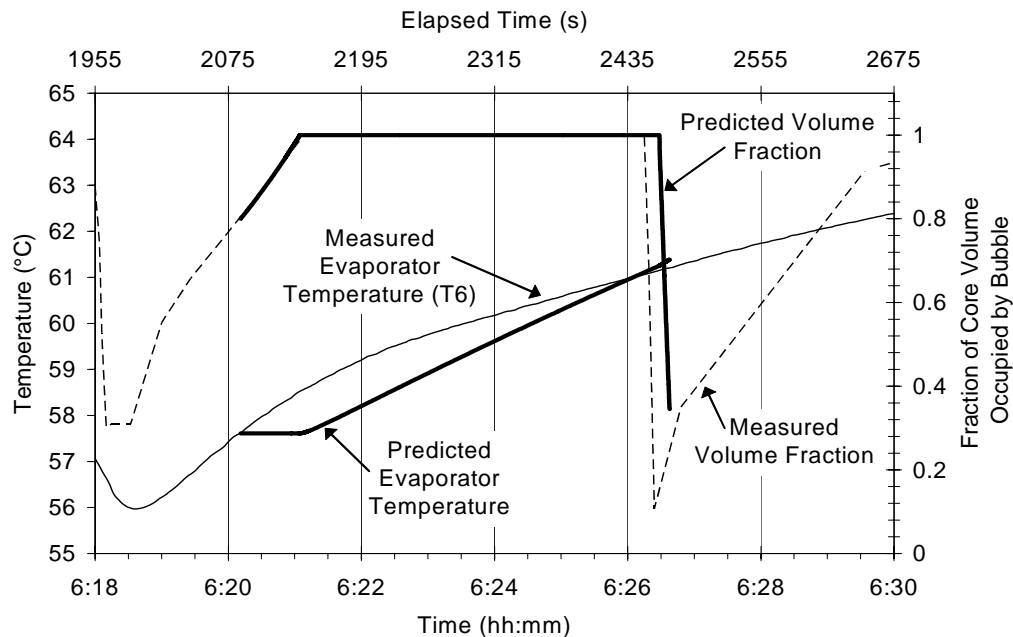


Figure 5.23 Comparison of flight data from test S35-1 to the bubble volume and evaporator temperature predictions made using the theory of vapor back-flow through a dry portion of the evaporator. Matching the model to the test data was achieved by setting the contact angle between water and polyethylene at 89.3° .

5.23 seems to indicate that there are dry portions in the wick (i.e. not all sections of the wick are saturated with liquid even after the evaporator refills with liquid). The second indicator of a non-saturated wick is the time required for the pores to dry-out. For the VIEW-CPL system, the calculated time required to dry out a fully saturated wick with heater power of 30 W is 510 s, which is 3 minutes longer than the period between the evaporator refills. Since the measured evaporator temperature on the evaporator temperature continues to increase during the test it is likely that the evaporator would eventually deprime. The model predicts an increasing evaporator temperature only for the case where there is not enough subcooling to keep the bubble within the evaporator. The evaporator will eventually deprime because of difficulty rewetting the wick under power. A contact angle of 89.3° was used to predict the correct time for bubble collapse (by determining the time that the capillary limit is exceeded). This is a large contact angle for a fluid/wick combination. Ability to operate VIEW-CPL at powers above 47 W would not be possible (see steady-state pressure curve in Figure 3.17) if 89.3° is the true contact angle. However, steady operations were not performed with power greater than 45 W because the large gradient in the stainless steel evaporator caused over-temperature conditions and the tests were prematurely shut down. The over-temperature conditions could have also been caused by evaporator depriming which would support the 89.3° contact angle determination.

Figure 5.24, based on ground test #0227971, is another example of deprime that is preceded by a period of bubble oscillations. The data collected

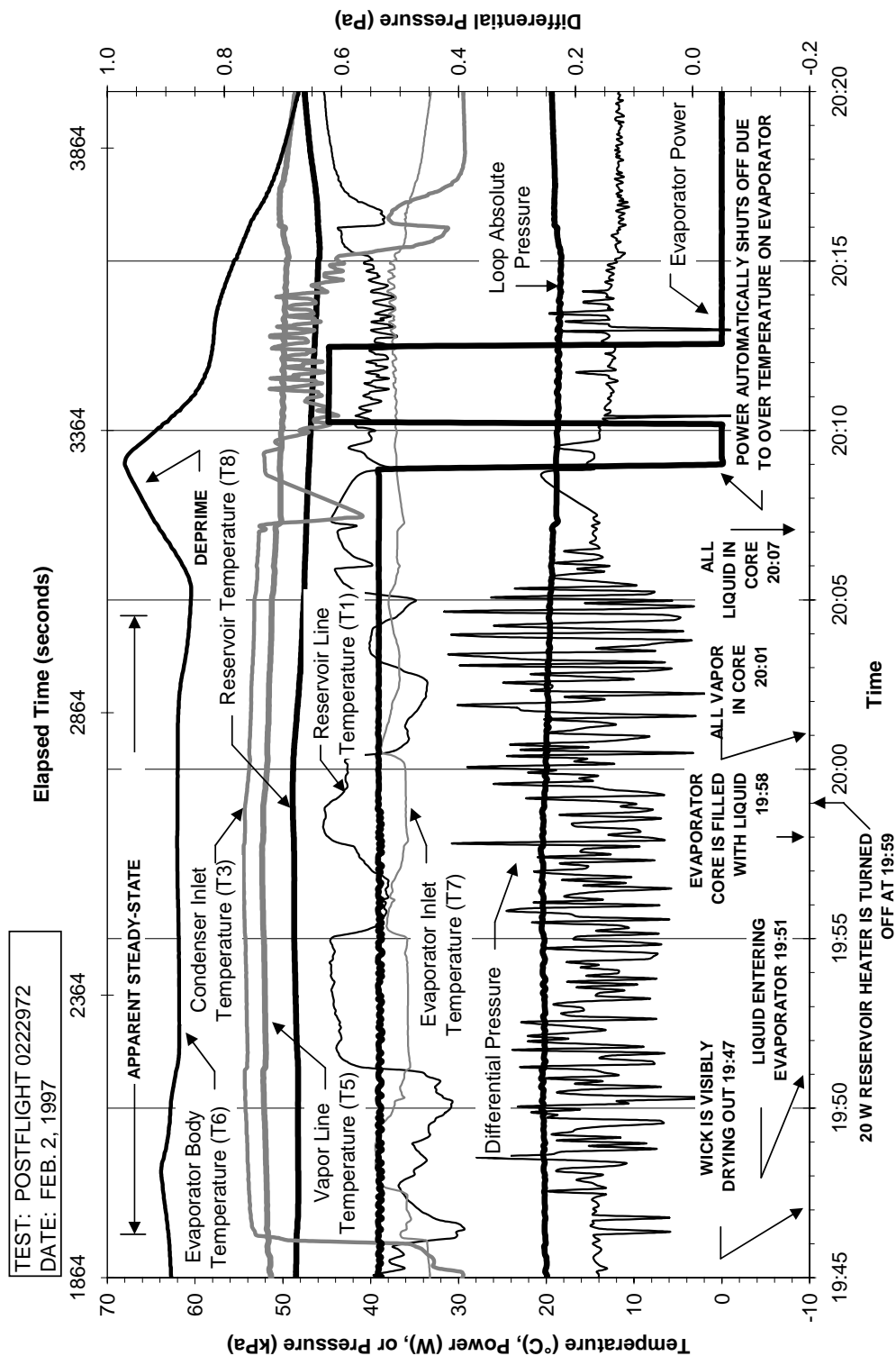


Figure 5.24 Example of a CPL deprime (at 20:06) after apparently steady-state operations for approximately 20 minutes. Test data is from ground testing of VIEW-CPL after flight.

during this test supports the dry wick theory because the wick became visibly dry on the inner diameter appearing “blotchy” in sections at around 19:47. This was followed by a bubble collapse 4 minutes later at 19:51. While the loop appears to be running at steady-state between 19:46 and 20:05, there was a change in operating conditions at 19:59 when the 20 W reservoir heater was turned off. The power was removed from the reservoir to see if the system would deprime as the reservoir temperature drifted down, which in fact it did at 20:06. A possible explanation for this observation is that the decreased reservoir pressure did not provide enough of a pressure difference to fully wet the wick during the last bubble collapse.

In summary the correlation of temperature oscillations with the apparent dry-out of the evaporator wick was visually verified with VIEW-CPL. The frequency (0.01 to 0.003 Hz) of the temperature oscillations measured in the VIEW-CPL system was similar to the low frequency oscillations observed in other CPL systems during low power operations. Refilling of the evaporator core with liquid after the expansion of a vapor bubble was observed repeatedly in both micro-gravity and ground testing. The explanation for the observed oscillatory bubble phenomena due to a dry-out in the evaporator wick has not been reported on for other CPL systems. The occurrence may be attributed to the combination of high thermal mass of the VIEW-CPL evaporator and low heater power that prevented rapid temperature excursions, providing enough time for the wick to dry-out and the pressure to drop in the vapor line.

5.5 Comparison of Micro-gravity and Ground Results

All of the differences observed between micro-gravity and ground tests can be attributed to stratification of the liquid and vapor phases inside the VIEW-CPL. The first observation was during the flight pressure prime where low frequency (0.035 Hz) temperature and bubble oscillations, that were not present in ground testing, were observed. Also, the reservoir temperature sensor measured temperature below saturation. This is evidence that the reservoir wick was working in micro-gravity by pulling liquid to the reservoir walls. Liquid in the reservoir was stratified during ground testing.

Another difference observed between ground and flight testing that was attributed to stratification was the time required for the vapor to reach the condenser during start-up tests. The comparison of times, shown in Figure 5.17, revealed that this occurs faster in ground testing than in flight testing. The large diameter of the vapor line allowed stratification that was not present in micro-gravity, so that the temperature sensor located on the top of the tubing measured a vapor temperature even if liquid was located at the bottom of the tube.

Lastly, steady-state conditions were not satisfied in micro-gravity. Bubble oscillations that were tolerated in ground tests lead to deprime (continuous increase in evaporator temperature) during flight tests. Stratification between the liquid and vapor phases in the core of the evaporator, due to gravity forces, allowed liquid to remain in contact with the wick for longer periods of time during

ground testing. This assisted with wetting the wick and with increasing the heat transfer area between the liquid and the bubble.

One of the objectives for micro-gravity testing was to determine if bubbles in the evaporator core would cause rapid wick failure. This did not occur because oscillatory bubble cycles, similar to those observed during ground testing, prolonged the deprime process by allowing a portion of the heat load to be evaporated. This coupled with the large thermal mass of the evaporator body and the low power (typically 30 W) led to slower evaporator temperature rises than those typical observed during CPL deprime.

6.0 CONCLUSIONS

At the beginning of the VIEW-CPL project, our contacts at NASA and Swales expressed some doubts whether a water CPL would provide insight into the physics of CPL operations. In fact some wondered if it was even possible to operate a water CPL at sub-atmospheric pressure. This work dispels any such doubts although it does point to a series of limitations and difficulties in implementing a CPL using water.

The primary objective of the work described in this thesis was to obtain a more complete understanding of CPL physics through experiments on a flow visualization test facility. The effort involved design, fabrication and testing of the experiment (VIEW-CPL) and subsequent modeling and data analysis. Four modeling tasks were undertaken to explain the VIEW-CPL behavior and the flow visualization capability proved to be crucial in the understanding of operation of a CPL with a bubble on the liquid side of the wick. The results from the work were discussed in Chapter 5 and the conclusions from that discussion are repeated here in summary form.

6.1 General Observations

- One of the objectives for micro-gravity testing was to determine if bubbles in the evaporator core would cause rapid wick failure. Based on results of Section 5.3, this did not occur because oscillatory bubble cycles, similar to those observed during ground testing, prolonged the deprime process by allowing a portion of the heat load to be evaporated. This coupled with the

large thermal mass of the evaporator body (Table 3.5) and the low power (typically 30 W) led to slower evaporator temperature rises than those typically observed during CPL deprime.

- As shown in Figure 5.19, the pressure surge model accurately predicts the time to clear the vapor line, suggesting that the model correctly represents the physics of the pressure surge. Thus, it is concluded that the pressure surge is primarily due to the viscous pressure drop associated with clearing the vapor line of liquid.
- As shown in Figure 3.17, the capillary pressure drop (40 Pa) at the liquid/vapor interface in the condenser was larger than the viscous pressure drops. This unexpected result was mainly because VIEW-CPL operates at low power and viscous pressure drops were low. However, designers of small CPLs with small diameter transport lines and micro-channel condensers need to be aware of the liquid/vapor interfaces in the system and take into account the pressure exerted by them during all stages of operation.

6.2 Micro-gravity Observations

- As discussed in Section 5.1, temperature and bubble oscillations (0.035 Hz frequency), that were not present in ground testing, were observed during flight pressure primes. These oscillations were attributed to vapor venting from the reservoir wick grooves which were filled with liquid in micro-gravity but drained in 1-g.
- Evidence that the reservoir wick was keeping the liquid in contact with the

heated walls in micro-gravity was presented in Section 5.1. This evidence was that the reservoir temperature sensor indicated a temperature below saturation.

- A comparison of times to clear the vapor line during start-up, shown in Figure 5.17, revealed that vapor line clearing occurs faster in ground testing than in flight testing due to stratification that was not present in micro-gravity.
- Based on the criteria in Section 5.3, steady-state conditions were not satisfied in micro-gravity. From the data presented in Sections 5.3 and 5.4, bubble oscillations that were tolerated in ground tests led to deprime (continuous increase in evaporator temperature) during flight tests. For the ground tests, stratification between the liquid and vapor phases in the core of the evaporator assisted with wetting the wick and with increasing the heat transfer area between the liquid and the bubble.

6.3 Noncondensable Gas

While precautionary steps were taken to ensure a leak tight system, through careful design and processing, the test results indicate the VIEW-CPL had a small but non-negligible amount of noncondensable gas.

- As indicated in Section 5.1.1, pressure measurements over a time period of several months indicate a noncondensable gas accumulation rate of 6.7×10^{-7} moles per day. This is assumed to be the system leakage rate.
- Based on the pressure prime model in Section 4.3 and the results in Table 5.1, the pressure prime should have collapsed all vapor bubbles in 17

minutes. The fact that stable bubbles existed in VIEW-CPL even after 30 minutes indicates noncondensable gas was present in the system.

- As discussed in Section 4.3, the reduction in evaporator-to-ambient conductance, from 0.0973 to 0.0059 W/K, that is required to achieve comparable results between predicted and measured pressure prime duration is attributed to noncondensable gas decreasing the rate of condensation.
- Predicted temperature differences between the wick inner and outer diameter (Figure 5.13) range from 5.0 to 15.5 K at the time of start-up. Based on the results of Section 5.2.1, noncondensable gas concentrations as low as 1.1×10^{-9} kmol/cm³ can reduce the saturation temperature in the vicinity of a gas bubble by 5 K and allow boiling to occur inside the evaporator wick. Thus it is possible that noncondensable gas contributed to bubble growth inside the wick. The low slope of the vapor pressure curve for water at the VIEW-CPL operating temperature (50°C) intensify the impact of noncondensable gas by reducing the local saturation temperature (Figure 5.12).

6.4 Heat Transfer Effects

- Based on the results of the two-dimensional conduction heat transfer model of the evaporator cross-section in Section 4.4.1, the temperature sensor location did not provide a representative measurement of the evaporator temperature at the interface between the evaporator and the wick. There were significant temperature differences (from Figure 4.7 and Figure 5.13) between the evaporator body at the temperature sensor location and the

wick, ranging from -13 to +2 K at the time of startup.

- The predictions obtained from exercising the pressure surge model of Section 4.4.2 indicate that the pressure on the vapor side of the evaporator peaks during the clearing of the vapor grooves. The liquid flow rate into the reservoir is reduced from 2 to 0.5 g/s due to condensation on the walls of the vapor line as the vapor front moves out of the evaporator. Thus, the thermal capacitance of the vapor lines contributes very significantly to minimizing the magnitude of the pressure surge.
- As described in Section 4.6, both a reduction in evaporation and an increase in sensible heating of the evaporator body occur as the wick dries out. Radial dry-out in the wick reduces the conductance of the wick from 489 W/m-K for a fully wetted wick to 2.3 W/m-K for a meniscus that has receded to the inner diameter of the wick.

6.5 Bubble Oscillations

- Based on numerous test runs (Section 5.3) it is concluded that the VIEW-CPL evaporator can tolerate bubbles on the inside of the wick, provided that there is sufficient subcooling to balance the vapor leakage through the wick. It is unclear if this mode of operation is unique to VIEW-CPL or common in other CPL systems.
- Based on the detailed analyses of Section 4.5, and a range of observations from VIEW-CPL (Section 5.3 and 5.4), it is concluded that vapor leakage through the wick occurs through dry segments of the wick with dry length

ranging from 0.75 to 3.8 cm (0.13 to 1.5 in).

- When the dry segment of the wick is relatively short (0-3.8 cm), a bubble will collapse in the core because the vapor leakage (backflow through the wick) is less than the condensation on the liquid surface. For dry lengths longer than 3.8 cm (1.5 in.) the condensation rate is not sufficient to keep bubble growth in check. The analysis in Section 4.6, combined with the observations discussed in Section 5.4, describe the events occurring when a bubble blocks the liquid flow into the evaporator. The bubble grows into the evaporator inlet where it is stalled by a capillary pressure of 64 Pa developed by a meniscus in the fitting.
- As determined in Section 4.6, a bubble in the evaporator core will collapse as the pressure in the vapor line drops below the reservoir pressure due to an imbalance between the evaporation rate and condensation rate in the loop.
- Low-frequency (0.003-0.01 Hz) temperature oscillations are attributed to bubble oscillations on the liquid side of the wick (Section 5.3). Based on the data presented in Sections 5.3 and 5.4, flow visualization in the VIEW-CPL evaporator confirmed that temperature oscillations correspond to bubble movement in the liquid core of the capillary evaporator. This had been postulated in the literature to account for low power temperature oscillations in several CPL systems, and VIEW-CPL provides evidence to support those claims.

6.6 Water and Wick Contact Angle

One unknown in the design and analysis of VIEW-CPL is the contact angle between water and the polyethylene wick. Normally a perfectly wetting fluid is selected to achieve the maximum capillary pressure rise across the wick. While it was known that water does not fully wet polyethylene, previous tests results indicated that the CPL could pump with water (therefore contact angle was less than 90°) and the full limitations of the pumping capability were not realized until the analyses of Section 4.5.2 and 4.6 were performed.

- The contact angle is bounded on the lower end by the axial flow analysis in Section 4.5.2. The analysis suggests that the contact angle is at least 76° based on observations that the wick does not fully wet when there is any liquid in the evaporator core.
- Based on the frequency of bubble oscillations (0.01 to 0.003 Hz) a contact angle of approximately 89° between the water and polyethylene is required to create the imbalance by reducing the capillary limit of the wick and forcing a reduction in vapor flow prior to total wick dry-out. Two other unknowns in the analysis, the length of dry wick and the core temperature, contribute to uncertainty in determining the contact angle.
- Based on the pressure surge model presented in Section 4.4.2 the maximum pressure drop experienced during the start-up is 215 Pa. The meniscus in the 13.7 m wick can support this pressure drop even if the contact angle between water and polyethylene is large ($>89.994^\circ$).

7.0 RECOMMENDATIONS FOR FUTURE RESEARCH

7.1 Enhanced Design

The VIEW-CPL experiment could provide even more insight into CPL operations if several modifications were made to the hardware in the areas of (1) instrumentation, (2) CPL enhancement, and (3) operational controls.

7.1.1 Instrumentation

In terms of instrumentation, both the temperature and pressure measurements can be improved. The current AD590 circuits require rewiring with precision resistors in order to reduce the temperature error associated with resistor drift. As with most experiments, additional temperature sensors at key locations in the loop would assist with model verification (it is noted that the data acquisition systems employed had a limit of 14 channels, all of which were used). One example is the addition of sensors to monitor the cooling air inlet and exits to provide information on the heat rejection capability of the subcooler and condenser. A series of temperature sensors along the condenser exit would assist with verification of the pressure analysis by indicating the active length of the condenser.

The differential pressure measurement is more useful if two differential pressure transducers are used. One transducer should be used to measure the capillary pressure rise across the evaporator and a second one to measure the direction of the flow in the liquid line. Also, proper sizing is critical to measure the small pressure differences expected during VIEW-CPL operation.

Temperature sensors should be positioned on both the top and side of tubes to indicate flow stratification in 1-g testing. If telemetry is limited for flight testing, then temperature sensors should be placed on the side.

7.1.2 CPL enhancements

The CPL could be enhanced with the use of a working fluid that readily wets the porous polyethylene wick inside the evaporator. An alcohol would be compatible with the stainless steel CPL structure while still maintaining a low pressure and low toxicity in terms of the shuttle environment. Alcohol has the disadvantage that it has reduced surface tension compared to water. Another option would be to use a metal wick such as those now used in LHPs. Metal wick technology was not available at the time VIEW-CPL was fabricated.

If water is chosen, further attention to degassing the water would help with operations. Noncondensable gas (NCG) in the loop may have helped create conditions conducive for bubble formation, but the presence of NCG is not typical of CPL operations. Heat transfer coefficients were difficult to determine because of the effect of noncondensable gas.

The subcooler at the evaporator inlet could have been more effective. Instead of having the cooling air drawn across the payload control box, the air should not have been preheated. The photo-flood light used for lighting the evaporator section also caused an increase in cabin temperature in the vicinity of VIEW-CPL. This affected the air around the subcooler. The combination of these two factors meant a lack of control of the evaporator inlet temperature that

would have increased operational flexibility considerably.

Another recommended change to the hardware is to switch the carrier for testing VIEW-CPL in space from the middeck to a GAS can. Power constraints in the middeck prevented testing the CPL at high powers while maintaining a constant temperature in the reservoir. This mode of operation caused the CPL to deprime due to the changing set point and masked any oscillatory behavior that may have been observed with a constant reservoir temperature. In addition to increased power availability in the GAS can, the safety requirements are less stringent than operating in the crews inhabited middeck. High temperature limits are increased and a wider variety of working fluids can be explored, including ammonia so that the CPL would be operating with the same working fluid used in currently designed systems. The difficulty with this is the need for a remote control camera system instead of the astronauts as cameramen.

7.1.3 Control

Changing the carrier from the middeck locker to a GAS can would also increase control over the flight testing procedures and allow for real time commanding to facilitate data reduction. The reaction of the CPL to the micro-gravity environment was uncertain with the first flight, so the test procedures included many options for running the CPL in case one procedure did not work. The procedures also relied heavily on visual observations and the astronauts judgements, and therefore the procedures were not always consistent between similar tests (the astronauts did a good job but they had several tasks

to perform and VIEW-CPL was not always the top priority). Test repeatability would be increased if decisions were based on numerical data and occurred at fixed times. The GAS can would allow a more intensive test sequence that could be adjusted from the ground, including repeated tests.

Time synchronization between the camcorder and data acquisition system is also important. Audible time signals on the video tape at the beginning of tests would assist in matching the data between the video tapes and the temperature data from the computer. For automated systems, a beep noting the start of testing could be used to synchronize the data.

Some tests would have provided more valuable information for understanding CPL physics if they were run for a longer period of time. Timing constraints with the astronauts schedules resulted in tests designed for the minimum amount of time. Also, many tests ended early from high temperatures on the evaporator.

7.2 Visualization in Loop Heat Pipes

Loop heat pipes are designed to work with bubbles in the evaporator core because they contain a secondary wick. The theories on the conduction energy transfer from the outside to the inside of metal wicks in loop heat pipes do not currently explain performance degradation that is observed at low powers. Visualization into the loop heat pipe evaporator would provide information on the heat transfer to and inside the core, as well as provide insight on the performance of the secondary wick.

APPENDIX A: TYPICAL TESTING MODES FOR CPLs

Industry has adopted the following system performance tests for analyzing CPL systems [Braun, 1990]:

(1) System Start-up Test

The start-up follows a pressure prime at a set saturation temperature and for a prescribed duration. Power (to simulate payload or a starter heater) is applied to the evaporator. A start-up is successful when two conditions are satisfied (1) vapor is present at the outlet of the evaporator and (2) there is forward circulation of fluid from the evaporator to the condenser.

(2) Maximum Transport Capability

Maximum transport capability defines the maximum amount of heat that can be transported the distance of the vapor line before the system deprimed; it can be limited by pressure drop and/or condenser capacity.

(3) Heat Load Sharing

Heat load sharing tests, performed only on systems with multiple parallel evaporators, demonstrate the ability of moving heat to unheated evaporators to distribute the heat load among multiple evaporators.

(4) Diode Function of the Condensers

Condenser diode tests measure the ability of the system to shut down and prevent evaporator heating when the condenser temperature exceeds the system saturation temperature.

(5) Rapid Power Cycling and (6) Sink Temperature Variation

Rapid power cycling and sink temperature variation determines the robustness of the system during evaporator heat load transients and changes to the condenser conditions; both tests examine the ability of the reservoir to quickly adjust to changes in the loop liquid inventory.

(7) Pressure Prime under Heat Load and (8) Reservoir Set-point Temperature Variation

The reservoir function tests are pressure priming under heat load and set-point variations to verify the reservoir control of the system set-point.

APPENDIX B: VIEW-CPL As-Built Materials

PAYLOAD INORGANIC MATERIALS LIST										PAGE 1 OF 3		
MISSION		STS-80		PAYLOAD		VIEW-CPL						
CONTRACTOR		University of Maryland		ADDRESS		Univ. of MD, Department of Mechanical Engineering, College Park, MD 20742						
PREPARED BY		Kimberly R. Kolos (VIEW-CPL PI)		PHONE		(301) 405-5320		FAX (301) 314-9477		DATE PREPARED		
MATERIALS EVALUATOR				PHONE				DATE RECEIVED		DATE EVALUATED		
ITEM NO.	MATERIAL IDENTIFICATION	CONDITION	APPLICATION	EXPECTED ENVIRONMENT	EVALUATION							
					A	NA	SA					
1	303 Stainless Steel, 1" PLATE	Machined; Welded to 303 and 304 Stainless Steel	Evaporator base and housing for wick; Exposed to water; heater attached	Storage: up to 1 year at RT Space: Shuttle Middeck Filled with distilled water (liquid or vapor)								
2	316 Stainless Steel, 0.188" PLATE	Machined	Evaporator cover plate bolted to ITEM 1 for structural support with LEXAN plate in-between	Storage: up to 1 year at RT Space: Shuttle Middeck Ambient conditions (not exposed to water)								
3	304 Stainless Steel tubing, 0.125" OD, 0.028 wall	Welded to 303 and 304 Stainless Steel	Evaporator inlet tube; carries deionized water	SAME AS ITEM 1								
4	303 Stainless Steel, 0.5" BAR	Machined; Welded to 303 and 304 Stainless Steel	Machined piece to connect the liquid line to the evaporator	SAME AS ITEM 1								
5	316 Stainless Steel, 8-32 Socket head cap screws		Bolt ITEM 2 to ITEM 1	SAME AS ITEM 2								
6	316 Stainless steel tubing, 0.25" OD, 0.035 wall	Welded to 304 Stainless Steel	Differential & absolute pressure connecting line filled with distilled water (liquid and vapor)	SAME AS ITEM 1								
7	304 Stainless steel tubing, 0.375" OD, 0.035 wall	Welded to 303, 304 and 316 Stainless Steel	Vapor and liquid transport lines; carry distilled water (liquid and vapor)	SAME AS ITEM 1								
8	Nupro "H" series bellows sealed valve (see attached for material details)	Welded to 316L and 304 Stainless Steel	Purging and charging ports	SAME AS ITEM 1 Same design flown in CAPL (STS-60)								
9	316 Stainless Steel VCR Metal Gasket Face Seal Fittings and plugs		Valve connections	SAME AS ITEM 1								
10	Nickel VCR Gasket material		Gasket for sealing VCR fitting and plug	SAME AS ITEM 1								
11	316 Stainless Steel tubing, 1" OD, 0.035 wall	Welded to 304 Stainless Steel Brazed to copper fins Lead-tin solder plated on external surface	Condenser tube (water side)	SAME AS ITEM 1								
12	316 Stainless Steel, 1" bar	Machined welded to 316 and 304 ST STL	Condenser endcaps	SAME AS ITEM 1								
13	Copper sheet, 0.032" thick	Cut to size; brazed to 316 Stainless Steel	Air-side condenser fins	SAME AS ITEM 2								

Table B.1 VIEW-CPL Inorganic Materials List (page 1 of 3).

MISSION			STS-80		PAYLOAD INORGANIC MATERIALS LIST				PAGE 2 OF 3	
CONTRACTOR		University of Maryland		PAYLOAD	VIEW-CPL					
PREPARED BY		Kimberly R. Kolos (VIEW-CPL PI)		ADDRESS	Univ. of MD, Department of Mechanical Engineering, College Park, MD. 20742					
				PHONE	(301) 405-5320		FAX	(301) 314-9477		
MATERIALS EVALUATOR				PHONE			DATE RECEIVED			
						DATE EVALUATED				
ITEM NO.	MATERIAL IDENTIFICATION	CONDITION	APPLICATION	EXPECTED ENVIRONMENT	EVALUATION					
14	44" Rosin Core, solder wire 0.031" thick		Brazing material for copper fins	SAME AS ITEM 2	A	NA	SA			
15	321 Stainless Steel tubing, 2.25" OD, 0.035 wall	Welded to 304 and 316 Stainless Steel	Reservoir housing (main body);	SAME AS ITEM 1						
16	316 Stainless Steel bar, 2.25" OD	Machined; Welded to ITEM 6 and ITEM 15	Reservoir housing (endcaps)	SAME AS ITEM 1						
17	304 Stainless Steel bar, 2" OD	Machined	Ferrules for positioning the reservoir wick	SAME AS ITEM 1						
18	316 Stainless Steel Screws		Hold ITEM 17 in place, inside the reservoir	SAME AS ITEM 1						
19	17-4 PH Stainless; part no. MA and P-30-P (see attached descriptions)	Welded to ITEM 6	Absolute and differential pressure transducers	SAME AS ITEM 1						
20	316 Stainless Steel; In-line amplifier housing		In-line amplifier for ITEM 19	SAME AS ITEM 2						
21	6061-T6 Aluminum, 1" bar	Machined brackets	Brackets	SAME AS ITEM 2						
22	6061-T6 Aluminum angle	Machined; bolted to base plate and LEXAN shroud	Various supports	SAME AS ITEM 2						
23	6061-T6 Aluminum plate, 0.25" thick	Machined	Base for supporting experiment	SAME AS ITEM 2						
24	316 Stainless Steel, 10-24 screws		Mounting	SAME AS ITEM 2						
25	6061 Aluminum bar	Machined; bolted to evaporator and epoxied to liquid line	Heat sink for thermo-electric module attached to the evaporator and subcooler	SAME AS ITEM 2						
26	Deionized Water		CPL working fluid, contained in a sealed structure	SAME AS ITEM 1						
27	Copper wire, 18, 20 and 22 AWG		Electronics	SAME AS ITEM 2						

Table B.1 VIEW-CPL Inorganic Materials List (page 2 of 3).

PAYLOAD INORGANIC MATERIALS LIST										PAGE 3 OF 3			
MISSION		STS-80		PAYLOAD		VIEW-CPL							
CONTRACTOR		University of Maryland		ADDRESS		Univ. of MD, Department of Mechanical Engineering, College Park, MD. 20742							
PREPARED BY		Kimberly R. Kolos (VIEW-CPL PI)		PHONE		(301) 405-5320		FAX (301) 314-9477		DATE PREPARED		SEPT 25, 1996 (FINAL)	
MATERIALS EVALUATOR				PHONE		DATE RECEIVED		DATE EVALUATED					
ITEM NO.	MATERIAL IDENTIFICATION	CONDITION	APPLICATION	EXPECTED ENVIRONMENT		EVALUATION							
28	6061 Aluminum plate, 0.0625" thick	Iridited	Electronics chassis	SAME AS ITEM 2		A	NA	SA					
29	ER316L Weld rod	Weld material	Weld for tubing and connections	SAME AS ITEM 2									
30	6337 Solder	Spec. QQ8571	Solder for wiring	SAME AS ITEM 2									
31	60/40 lead tin solder		Coating for condenser tube	SAME AS ITEM 2									
32	Nickel plated steel		Fan guards	SAME AS ITEM 2									
33	Aluminum mesh		Vent screens taped to lexan	SAME AS ITEM 2									
34	Stainless steel mesh		Fan guards bolted to lexan	SAME AS ITEM 2									
35	Tinned copper braided ground strap with copper alligator clips		Ground from VIEW-CPL to Orbiter	SAME AS ITEM 2									
36	Zinc plated (2) springs		Used in lid to cover hole in lexan shroud	SAME AS ITEM 2									

Table B.1 VIEW-CPL Inorganic Materials List (page 3 of 3).

MISSION

(possibly to be manifested on) STS-80

CONTRACTOR

University of Maryland

PREPARED BY

Kimberly R. Koles

MATERIALS EVALUATOR

PAYLOAD

VIEW-CPL

ADDRESS

Univ. of MD, Department of Mechanical Engineering, College Park, MD 20742

PHONE

(301) 405-5320

FAX

(301) 314-9477

DATE RECEIVED

DATE EVALUATED

September 22, 1995

AREA, CM²

Vol, cc

Mass, gm

1. 0-1

A. 0-1

a. 0-1

2. 2-100

B. 2-50

b. 2-50

3. 101-1000

C. 51-500

c. 51-500

4. >1000

D. >500

d. >500

PAGE 1 OF 3

PAYLOAD POLYMERIC MATERIALS LIST

ITEM NO.	MATERIAL IDENTIFICATION	MIX FORMULA	CURE OR OTHER SPECIFICATION	AMOUNT CODE	EXPECTED ENVIRONMENT	REASON FOR SELECTION	EVALUATION		
							A	NA	SA
	CPL EVAPORATOR ITEMS ITEMS 1 - 9				TV: 8°C/35°C Storage: up to 1 year at RT Space: Shuttle Middeck				
1	Ultra-High Molecular Weight Porous Polyethylene (UHMW-PE), Porex Technology			B	All internal to the evaporator, 100% in contact with water. Not exposed to cabin air. Contained in Stainless steel with Lexan cover plate.	Wicking Material typically used in CPL systems; pore size & permeability Similar to material in CAPL evaporators flown on STS-80			
2	RTV 108, General Electric		24 hours	b	All internal to the evaporator, 100% in contact with water. Not exposed to cabin air. Contained in Stainless steel with Lexan cover plate.	Translucent; sealant between wick Lexan cover plate			
3	Fluorocarbon ORING EQUAL ORING part #2-170			b	Sealed within the evaporator Exposed to vacuum and water Contact with LEXAN	Good water compatibility Excellent flame resistance Low weight loss in vacuum			
4	GE LEXAN - 1/4" sheet		9034 grade	B	Evaporator cover plate	Clear and strong Cost and availability			
5	UHMW Polyethylene			B	Protect evaporator inlet tube from thermal heat leaks, and to seal inlet and vapor ends of the wick. All internal to the evaporator, 100% in contact with water. Not exposed to cabin air. Contained in Stainless steel with Lexan cover plate.	Similar to wick material; heat sealed to wick			
6	KAPTON HEATER INSULATION MINCO PRODUCTS, INC. (also attached to the RESERVOIR)		NASA-RP-1081	2	External to the evaporator Attached to stainless steel base with ITEM#7, covered with ITEM #8	Light weight, flexible			
7	STYCAST 2850 / CAT 9 (also attached to the RESERVOIR)		7 days @ 25°C	2	External to the evaporator Used to attach heaters to stainless steel base	Good bond Good heat transfer			
8	NOMEX ARAMID Cloth Insulation		minimum 1/8 inch thick; covered with 3M 425 aluminum tape	3	Used to insulate evaporator; and covers evaporator heaters	Low flammability Thermal insulation			
9	Thermoelectric module (semiconductor) Alumina coating Bismuth Telluride			2	Thermoelectric cooling module for evaporator. Sandwiched between the stainless steel evaporator and an aluminum heat sink.	Peltier cooling module to decrease evaporator cooldown time			

Table B.2 VIEW-CPL Polymeric Materials List (page 1 of 3).

PAYLOAD POLYMERIC MATERIALS LIST									
MISSION		PAYLOAD		VIEW-CPL		PAGE 2 OF 3			
CONTRACTOR		ADDRESS		Univ. of MD, Department of Mechanical Engineering, College Park, MD 20742					
PREPARED BY		PHONE		(301) 405-5320		FAX		(301) 314-9477	
MATERIALS EVALUATOR		PHONE				DATE RECEIVED		DATE EVALUATED	
ITEM NO.	MATERIAL IDENTIFICATION	MIX FORMULA	CURE OR OTHER SPECIFICATION	AMOUNT CODE	EXPECTED ENVIRONMENT	REASON FOR SELECTION	EVALUATION		
							A	NA	SA
10	Uralane (steking)	5753 A / 5753 B	7 days @25°C	B	Staking compound for bolts and wires	Availability; easy application			
	CPL CONDENSER ITEMS 10 and 11				TV: 8°C/35°C Storage: up to 1 year at RT Space: Shuttle Middeck				
11	UHMW Polyethylene rod			b	Provides internal grooves in the condenser	Machinability and good interference fit			
12	PAPST Fan (8124G)			d	Mounted on the experiment to provide air flow over CPL condenser	Same model previously flown on STS-52 and STS-66 in the HPP experiment			
	CPL RESERVOIR ITEMS 13 and 14				TV: 8°C/35°C Storage: up to 1 year at RT Space: Shuttle Middeck				
13	Ultra-High Molecular Weight Porous Polyethylene (UHMW-PE).			B	Sealed within the reservoir	Wicking Material typically used in CPL systems; pore size and permeability;			
14	NOMEX ARAMID Cloth Insulation (SAME AS ITEM 8)		minimum 1/8 inch thick; covered with 3M 425 aluminum tape	3	Used to insulate reservoir; covers reservoir heater	Low flammability Thermal insulation			
	CPL TRANSPORT LINES ITEMS 15 through 18				TV: 8°C/35°C Storage: up to 1 year at RT Space: Shuttle Middeck				
15	NOMEX ARAMID Strip Insulation		minimum 1/8 inch thick; covered with 3M 425 aluminum tape	3	Used to insulate liquid and vapor lines	Low flammability Thermal insulation			
16	3M Type 425 Aluminum Foil Tape			3	Cover ARAMID insulation	Recommended			
17	STYCAST 2850 / CAT 9			B	Bonds thermostats and solid state temperature sensors	Type previously flown on STS-52 in the HPP experiment			
18	G10, fiberglass		L-P-509 Grade, 0.5" thick	c	Bolted to aluminum base; support experiment	Lightweight			
	SAFETY SHROUD & OTHER MATERIALS ITEMS 19 and 20				TV: 8°C/35°C Storage: up to 1 year at RT Space: Shuttle Middeck				
19	GE Lexan		9034 Grade, 0.25" thick	d	Cover for the experiment during operation in the Middeck	Clear and strong Cost and availability			

Table B.2 VIEW-CPL Polymeric Materials List (page 2 of 3).

PAYLOAD POLYMERIC MATERIALS LIST										PAGE 3 OF 3	
MISSION		(possibly to be manifested on) STS-80		PAYLOAD		VIEW-CPL				AMOUNT CODE	
CONTRACTOR		University of Maryland		ADDRESS		Univ. of MD, Department of Mechanical Engineering, College Park, MD 20742				Area, cm ² Vol. cc Mass, gm	
PREPARED BY		Kimberly R. Kolos		PHONE		(301) 405-5320		FAX (301) 314-9477		DATE PREPARED September 22, 1995	
MATERIALS EVALUATOR				PHONE				DATE RECEIVED		DATE EVALUATED	
ITEM NO.	MATERIAL IDENTIFICATION	MIX FORMULA	CURE OR OTHER SPECIFICATION	AMOUNT CODE	EXPECTED ENVIRONMENT	REASON FOR SELECTION	EVALUATION	A	NA	SA	
20	Uralane		5750-A/B (LV)		Conformal coating of circuit board All internal and enclosed in metal electronics box.						
21	Teflon wire insulation			2	Wire insulation metal electronics box.						
22	Kapton tape			2	Harnessing requirements						
23	Dycron lacing cord		MIL-T-43435B, Type 2 finish C	b	Wire ties						
24	G10, fiberglass		L-P-509 Grade, min. 0.063" thick	b	Spacers between brackets and components to reduce heat leaks	Lightweight Thermal break					
25	G10, fiberglass		L-P-509 Grade, min. 0.063" thick	b	Spacers between brackets and	Lightweight					
26	Tyton Ties, fluoropolymer			2	Wire ties						
27	Chotherm, 1/8" thick			2	Increase contact between thermoelectric module and heat sink	Quick release					

Table B.2 VIEW-CPL Polymeric Materials List (page 3 of 3).

APPENDIX C: ELECTRONICS

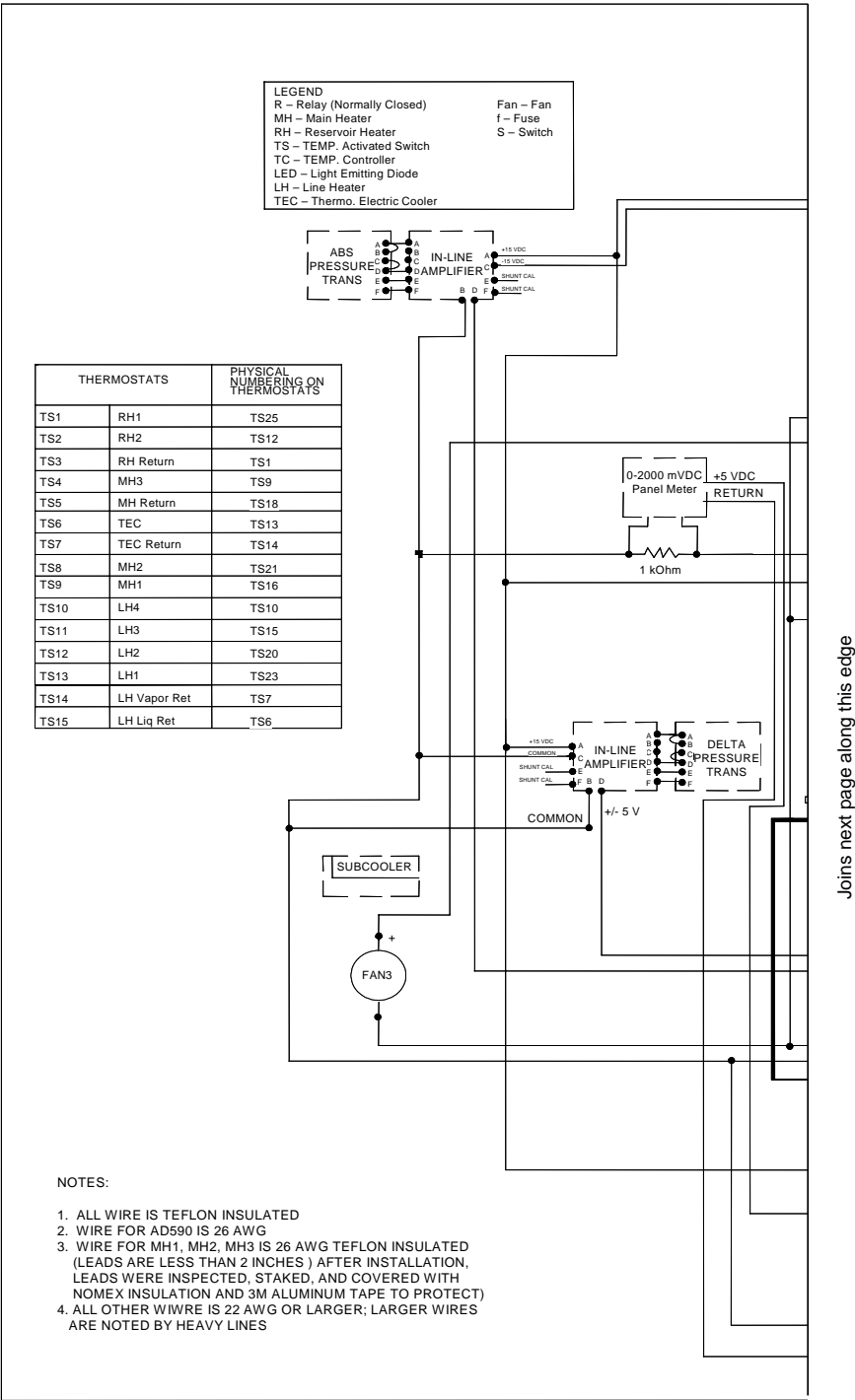


Figure C.1 VIEW-CPL wiring diagram for electronics attached to the CPL (page 1 of 2).

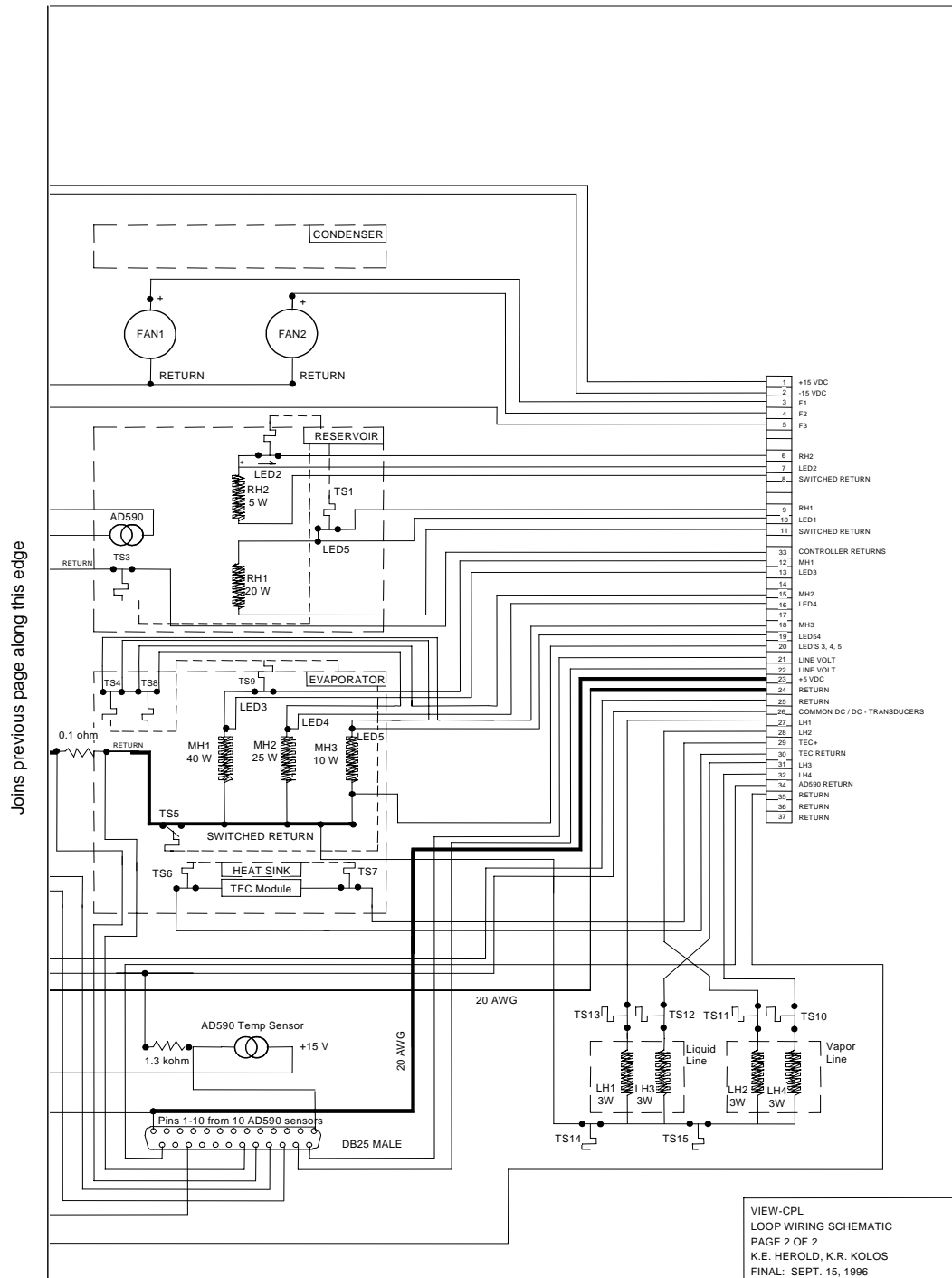


Figure C.1 VIEW-CPL wiring diagram for electronics attached to the CPL (page 2 of 2).

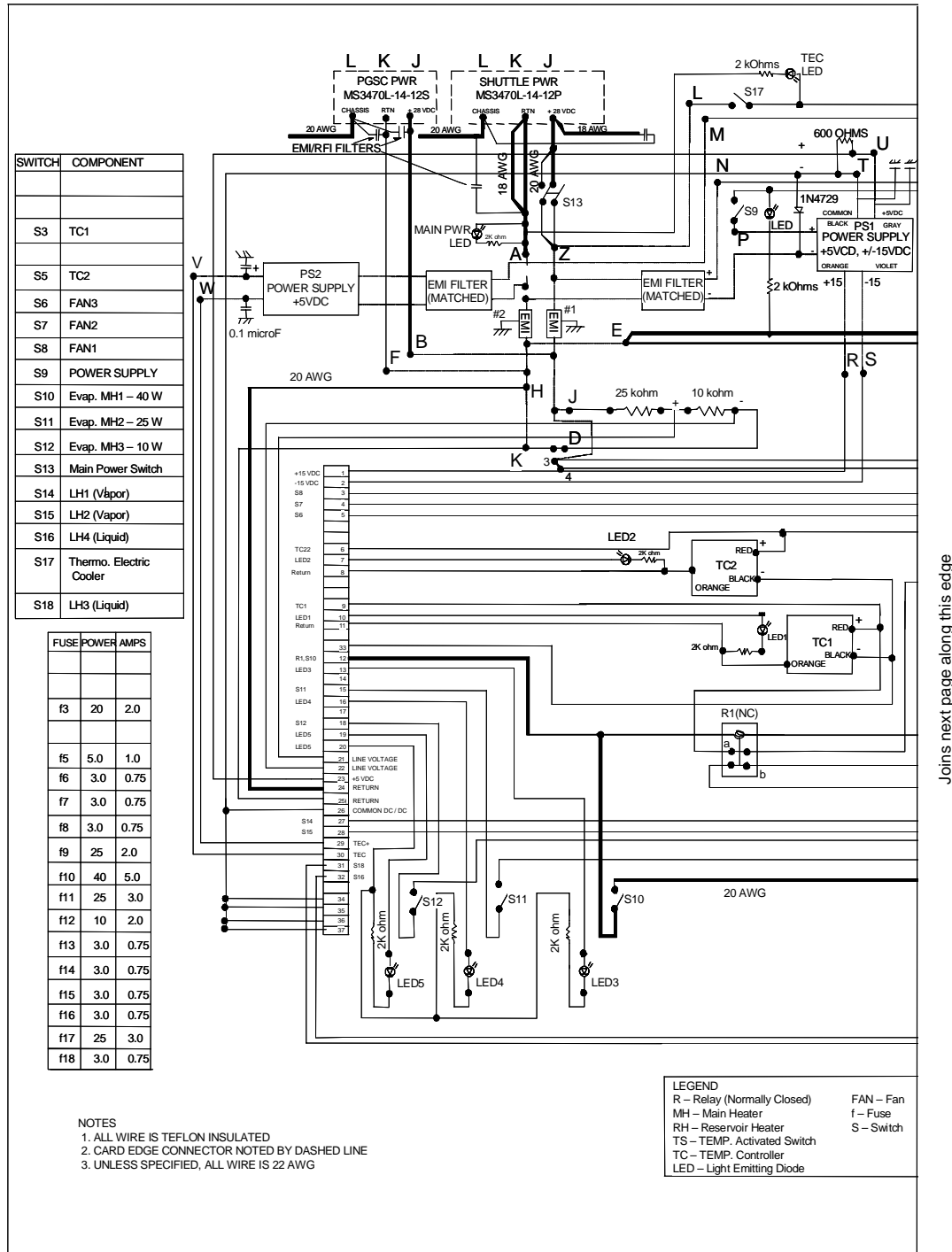


Figure C.2 Payload control box (PCB) diagram for VIEW-CPL (page 1 of 2).

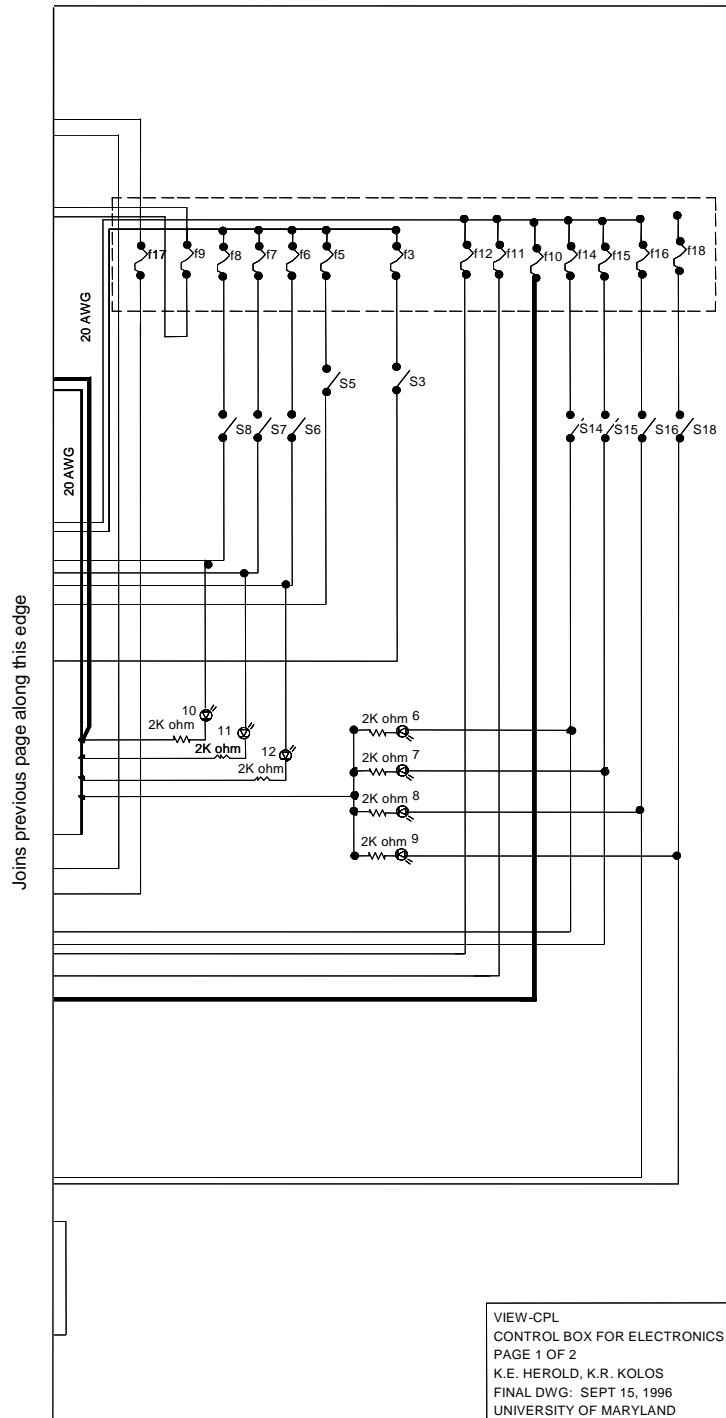


Figure C.2 Payload control box (PCB) diagram for VIEW-CPL (page 2 of 2).

Table C.1 Brand names and sources for electronic components.

Generic Name	Source	Purpose / Notes
<u>Ground support equipment</u>		
6 A - 28 VDC Power supply	Acme Electric Corporation Model SPS/CPS 220	Ground testing power supply
microvolt digital multimeter	Keithley 197 Autoranging	Measuring power consumption
<u>VIEW-CPL experiment equipment</u>		
Aluminum chassis, 8 in. x 6 in. x 3.5 in	BUD P/N CU-3000A	PCB container
Circuit board	Vector	Secured to chassis with screws.
Wire ties	Tyton ties or lacing cord	Tie wires inside the PCB
Conformal coating	Uralane	
Fuses	PICO II, type 251 series with axial leads	Very fast acting
Fuse package 25-pin Male D connector	Amplimite, P/N 206803-2 sealed with Uralane and copper tape	Copper tape for EMI
Locking Toggle Switches, rated for 5 A at 28 V	C&K part number 7201 KZQE	Prevent switching by inadvertent contact
Light emitting diode (LED)	Chicago Miniature Lamp, part number CMD5024	Indicate switch on. Are wired in series with 2 k Ω resistors to achieve the appropriate current draw.
Resistance heaters	Minco Products, Inc.	Electrical heat on reservoir and evaporator
Temperature Controllers	Minco Products, Inc.	
3-W line heaters	Ohmite resistors P/N 23J270, 270 Ω 0.5 cm (0.20 in.) diameter x 1.2 cm (0.47 in.) long	
On/off temperature controllers	Minco brand, model CT198 controllers	Operate with 8 to 32 VDC

Generic Name	Source	Purpose / Notes
Fans are all metal construction with brushless motor	Papst, 8124G model axial fans <ul style="list-style-type: none"> DC powered, drawing 3.0 W of power at 24 VDC and operational range of 18 to 30 VDC Service life of 50,000 hours 7.9 cm x 7.9 cm x 3.8 cm deep (3.1 in. x 3.1 in. x 1.5 in.) Impeller rotation at 3450 rpm 	All metal construction. Brushless motor
Thermoelectric cooling module	Melcor model CP1.0-31-06L	
Hermetically sealed relay	Potter-Brumfield model KHS17D12,	Prevents RH1 and TEC from being on at the same time MH1 is active
In-line EMI filters for +28 VDC	RF Interonics, model 13619/RF5005-2	
EMI filters	Interpoint, model FM-461 were placed in both power supply circuits along with 0.1 μ F capacitors attaching to the 5 VDC and return lines	
EMI/RFI suppression filters	Spectrun Control Inc. Model 51-717-001	
3.6 volt Zener diode	Motorola part number 1N4739	Placed between the power return and the signal return to tie the signal return to the same level as the ground return.
Temperature activated switches	Thermik -05 series Open at 60 \pm 5 °C and reset at 45 °C	

Area for heaters:

- Evaporator heaters is 10.2 cm long x 6.1 cm wide (4 in. X 2.4 in.)
- Reservoir heaters must be over the venting grooves and attached to the circumference of the reservoir which is 17.95 cm (7.07 in.). The venting grooves are 3.81 cm (1.5 in.) long for an available area of 68.4 cm² (10.6 in.²) for attaching the heaters on the reservoir.

Table C.2 VIEW-CPL heater specifications for evaporator and reservoir.

Heater	Minco Part No.	Ω	Power at 28 VDC	Dimensions cmx cm (in. X in.)	Effective Area, cm ² (in. ²)	Watt density W/cm ² (W/in. ²)
MH1	HK5301R19.6L22	19.4 ^m	40.4	2.06 x 12.2 (0.81 X 4.81)	21.5 (3.33)	1.9 (12.1)
MH2	HK5282R30.6L22	30.5 ^m	25.7	1.9 x 12.7 (0.75 X 5.0)	14.5 (2.24)	1.8 (11.5)
MH3	HK5234R76.4L22	83.5 ^m	9.4	1.14 x 9.86 (0.45 X 3.88)	7.5 (1.17)	1.2 (8.0)
RH1	special order	39 \pm 5%	20	2.5 x 17.8 (1.0 X 7.0)	45.2 (7.0)	0.4 (2.9)
RH2	special order	156 \pm 5%	5	1.3 x 17.8 (0.5 X 7.0)	22.6 (3.5)	0.2 (1.4)

^m Measured resistance**Table C.3** Reservoir temperature controller specifications.

VIEW-CPL Part No.	MINCO Part Number	Scan rate	Power	Sensing pulse duration
TC1	CT198-1009R44L1	1 sec	20 W	0.010 sec
TC2	CT198-1016R175L1	1 sec	5 W	0.010 sec

Temperature controllers. The on/off temperature controller uses special heaters to sense the heater temperature by measuring the heater resistance; thus, it incorporates the sensing function and the heater in one component. The heaters are powered for a minimum duration of 0.010 seconds to check the resistance. If the heater resistance indicates that the heater is below the setpoint, the heater remains powered and constantly checks the resistance until the heater element

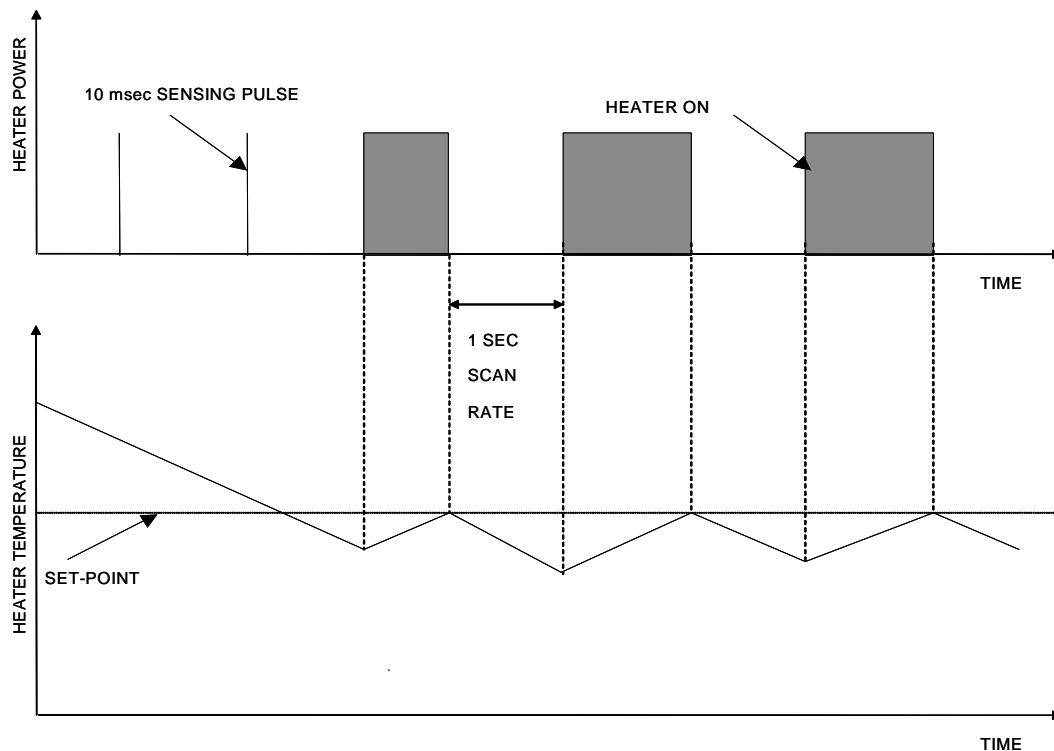


Figure C.3 On/off temperature controller profile.

temperature reaches set point. Figure C.3 shows an example of the heater response for a given heater temperature.

Power supplies. Both power supplies were manufactured by Computer Product Inc. The ES12T12/250XC model supplies 5 or ± 15 VDC and is designated as PS1 in the electrical schematics. In order to achieve the full 5 VDC, a pull up resistor of 600 ohms was connected across the 5 VDC output. The NFC25-24T0515 model supplies 5 VDC and is designated as PS2 in the electrical schematics. Table C.4 summarizes the components attached to each power supply.

Table C.4 Components attached to power supplies and corresponding power consumption.

Supply	Output	Component	Power
PS1	+5 VDC	PIU	4.0 W
	+5 VDC	Panel meter	0.24 W
	± 15 VDC	Absolute pressure transducer	1.35 W
	+15 VDC	Differential Pressure transducer	1.35 W
	+15 VDC	AD590 temperature transducers	0.17 W
Total (80% efficient)			8.5
PS2	+ 5 VDC	Thermoelectric module	20 W
Total (80% efficient)			24 W

Fuse Derating. Fuses used in micro-gravity are derated, meaning that the fuse will blow at a current lower than the rated amperage, due to the lack of natural convection. While circulating fans inside the middeck provide some convection, electronics enclosed in boxes experience minimal convection. Derating guidelines [NASA GSFC, 1995] were followed when choosing proper fuse sizes for the VIEW-CPL experiment. The proper derating for a given fuse depends upon the fuse size. For example, a fuse with a rating of 2 A or more is derated 50% while a 0.5 A fuse is derated 15%. This means that a 2 A fuse will blow at 1 A, while a 0.5 A fuse will blow at 0.08 A in a microgravity environment. Table C.5 lists the fuse sizes for the VIEW-CPL electronics with the corresponding derating requirement and Figure C.4 show the location of the fuses within the fuse plug connector.

Table C.5. Fuse sizing for electronics in VIEW-CPL.

Fuse	Circuit	Power @32VDC	Current (Amps)	Fuse Size (Amps)	Derated Fuse Size* (Amps)
f1, f2	not used	-	-	-	-
f3	Reservoir 20W Heater	30.9	0.97	2	1.00
f4	not used	-	-	-	-
f5	Reservoir 5W Heater	10.0	0.31	1	0.45
f6 - f8	PAPST (Model 8124G) Fan	4.5	0.14	.75	0.23
f9	DC/DC Voltage Converter (70% efficient) 5VDC: AD590, RDAS 1050 ±15 VDC: Pressure transducers and amplifiers	19.4	0.69	2	1.00
f10	40 W Evaporator heater	52.8	1.65	4	2.00
f11	25 W Evaporator heater	33.6	1.05	2.5	1.25
f12	10 W Evaporator heater	12.3	0.38	1.5	0.68
f13	not used	-	-	-	-
f14 - f16	3 W line heater	3.8	0.12	.75	0.23
f17	DC/DC Voltage Converter 5 VDC: TEC (assumed 70% efficiency)	35.7	1.12	3	1.50
f18	3 W line heater	3.8	0.12	.75	0.23

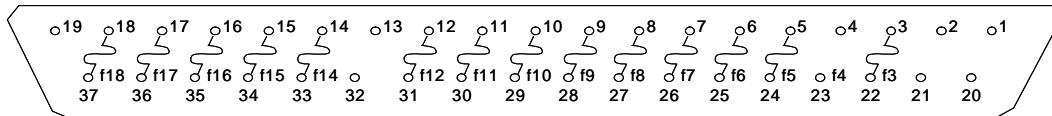


Figure C.4 Location of fuses within the VIEW-CPL fuse plug connector.

Wire. The wire used in the circuits was 22 AWG wire, with the exception of 20 AWG at the evaporator heater return, 20 AWG leading to the Shuttle power connector, and the smaller size leads on the evaporator heaters. The 22 AWG meets the requirements of NASA Memo TA-92-038 [NASA JSC, 1992] for selection of wire such that the wire manufactures' recommended operating temperature limit for the wire insulation will not be exceeded for any possible loading or fault condition of the circuit under worst-case environmental conditions. The evaporator heater lead wires were 26 AWG for the 10 and 40 W heaters and 24 AWG for the 25 W heater; while not complying with the requirements of NASA Memo TA-92-038, they were approved by JSC safety as complying with the intent of the memo because they were (1) staked in place, (2) had lengths less than two inches, and (3) proven to be of good workmanship by ground testing. All wire was covered with teflon insulation rated at 200 °C, as required for flight safety.

PGSC Interface Unit (PIU). Figure C.5 shows the channels corresponding to the DB25 connector on the PIU.

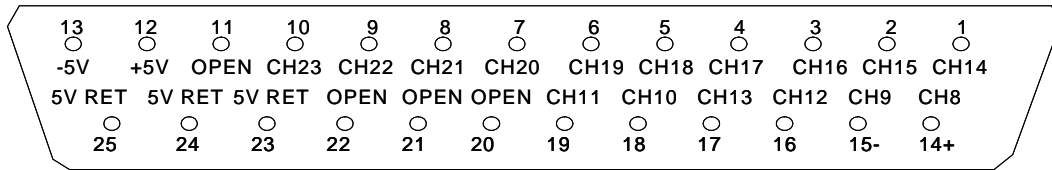


Figure C.5 DB 25 connector and corresponding channels for VIEW-CPL PGSC Interface Unit (PIU).

Pressure transducers. The absolute pressure transducer was a Model MA serial number 520157, with a range from 0 to 173 kPa (0 to 25 psia) . The transducer was powered with +/- 15 VDC from a VAB inline amplifier serial number 498488. The differential pressure transducer was a Sensotec Model P-30-P with range of -5 psi to +5 psi. The transducer was powered with 10 VDC from a VAB inline amplifier. The differential pressure transducer zero has an offset of -0.65 kPa, as determined from the collected data.

APPENDIX D: VERIFICATION DOCUMENTS

UMCP-VER-001-VCPL

VIEW-CPL PROOF PRESSURE TEST AND LEAK CHECK

Performed: June 5, 1996
Swales & Associates, Inc.
Thermal System Group
11313 Frederick Avenue
Beltsville, MD 20705

Contacts: Kimberly Kolos (301) 405-5320
Marc Kaylor (301) 586-1264

Helium Leak Check

Equipment: VEECO MS-170, Helium leak detector
Rejection set point 8×10^{-8} cc/s

Procedure: Sweep detector over all joints in the VIEW-CPL system. Perform proof pressure test and repeat leak check.

Results: No leaks detected prior to proof pressure test. No leaks detected after proof pressure test.

Proof Pressure Test

Equipment: Helium tank with pressure gauges

Procedure: Charge VIEW-CPL with 34 psia of Helium and monitor changes in pressure.

Results: 3:25 PM charged with helium, 3:38 PM released helium. No leaks

Figure D.1 UMCP-VER-001-VCPL: VIEW-CPL proof pressure test and leak check (page 1 of 3)

leak check & pressure test

VIEW-CPL testing of Swales - K. K. Kolo

Helium leak check using Veeco MS-170 leak detector

June 5, 1996

Reject set point 8×10^{-8} accepted

Pressure test - 34 psia.

3:25 PM - Helium into CPL

3:35 PM - Helium vented off 34 psia

3:36 PM - no change in pressure 34 psia

3:38 PM - no change in pressure 34 psia

Retest for with Helium leak test

Reject set point 8×10^{-8} accepted ✓

VIEW-CPL passed both leak testing and pressure testing

Kimberly R. Kolo

©1993 Franklin Quest Co. Printed in USA

CL 11096

15

Figure D.1 UMCP-VER-001-VCPL: VIEW-CPL proof pressure test and leak check (page 2 of 3).

VIEW-CPL INITIAL PRESSURE PRIME

Performed: June 11, 1996
 Goddard Space Flight Center
 Code 724.2 / Thermal Lab

Contact: Kimberly Kolos (301) 405-5320

Equipment: VIEW-CPL hardware, surge protector power strip, HP power supply

Procedure: Turn on the reservoir heaters to fill the CPL with liquid from the reservoir. Check liquid in the evaporator by applying heat to the evaporator.

Data (from lab book pg. 33):

2:45PM	Liquid is in the vapor plenum of the evaporator
2:56	Increased TC1 (20W) set point using the screw adjustment to raise the reservoir set point. An indication of at the heater has reached the set-point value is that the LEDs begin to cycle on and off.
3:00	Increased TC2(5W) set point using the screw adjustment to raise the reservoir set point
3:10	Increased TC1(20W) set point using the screw adjustment to raise the reservoir set point
3:12	Increased TC2(5W) set point using the screw adjustment to raise the reservoir set point
3:30	Decreased TC1(20W) and TC2(5W) set point so the heaters are cycling at 50°C. The evaporator is filled with liquid, indicating that the liquid was forced from the reservoir to the evaporator and there is no blockage between the reservoir and the remainder of the CPL
3:32	Turned on MH2 (25W) on the evaporator
3:35	Turned on MH1 (40W) on the evaporator for a total of 65W.
3:38	Vapor was generated in the grooved and the vapor plenum was cleared of liquid.

Results: There is no blockage between the reservoir and CPL as indicated by the filling of the evaporator with liquid. In this configuration, the reservoir temperature will regulate the pressure in the CPL.

Figure D.2 UMCP-VER-003-VCPL: VIEW-CPL initial pressure prime.

VIEW-CPL Thermal switch and reservoir temperature controller verification

Performed: Thermal switches on May 8, 1996 at UMCP
 Reservoir temperature controller on June 11, 1996 at GSFC
 Test operator: Kimberly R. Kolos
 Department of Mechanical Engineering
 University of Maryland
 College Park, MD 20742
 (301) 405-5320 PHONE
 (301) 314-9477 FAX
 krkolos@glue.umd.edu

1.0 Thermal switch test configuration

The Thermik brand thermal switches were selected from the 05 series to open at $60 \pm 5^\circ\text{C}$ and reset at 45°C . In order to verify that the switches function properly, each switch was immersed in water baths to determine the actual open and re-close set points. A flexible strip heater was taped around a 500ml flask filled with 350ml of tap water. A type T thermocouple was used to monitor the temperature of the water in the flask. A magnetic stirrer was used to maintain a uniform temperature throughout the flask.

The thermal switches were physically labeled with the numbers 1-25 with a black marker and tested individually. The thermocouple was twisted around the thermal switch and immersed in the tap water. A continuity meter was connected in series with the thermal switch to determine when the switch opened and reclosed. Power was applied to the heater to raise the temperature of the water in the flask. When the continuity meter indicated that the thermal switch opened, the temperature was recorded and the heater was turned off. Cool water was slowly added to the flask to bring the temperature down. The flask was air cooled for the final stage of the cooldown to determine the reset temperature of the thermal switch.

2.0 Data

The calibration of a type T thermocouple with a Barnant 115 Thermocouple readout device was checked with a 3" immersion thermometer and determined to provide accurate temperatures within $\pm 0.5^\circ\text{C}$.

Thermocouple ($^\circ\text{C}$)	Thermometer ($^\circ\text{C}$)	Difference	Thermocouple ($^\circ\text{C}$)	Thermometer ($^\circ\text{C}$)	Difference
24.7	25.2	-0.5	32.0	32.0	0.0
26.3	26.3	0.0	34.0	33.7	0.3
27.3	27.4	-0.1	35.3	35.2	0.1
28.8	28.9	-0.1	36.2	36.0	0.2
30.8	30.7	0.1			

Figure D.3 UMCP-VER-005-VCPL: VIEW-CPL thermal switch and reservoir temperature controller verification (page 1 of 5).

Thermal Switch	Open	Close	Open	Close	Avg Open	Avg Close	Accept/ Reject	Location
1	59.7	45.0	59.9	44.5	59.8	44.8	Accept	Reservoir
2	59.0	37.4			59.0	37.4	Reject	
3	62.3	36.1			62.3	36.1	Reject	
4	59.2	35.7			59.2	35.7	Reject	
5	60.8	38.0	61.3	37.4	61.1	37.7	Reject	
6	59.8	38.0	59.7	38.1	59.8	38.1	Accept	Vapor line
7	59.4	39.7	59.6	39.7	59.5	39.7	Accept	Liquid line
8	59.6	36.9	59.6	36.4	59.6	36.7	Reject	
9	61.5	46.5	60.9	45.7	61.2	46.1	Accept	Evaporator
10	59.9	38.1	60.5	38.6	60.2	38.4	Accept	Vapor line
11	59.3	37.0	59.5	36.9	59.4	37.0	Reject	
12	59.0	44.1	59.1	44.2	59.1	44.2	Accept	Reservoir
13	61.1	38.6	61.1	38.6	61.1	38.6	Accept	TEC
14	61.7	38.6	61.5	38.7	61.6	38.7	Accept	TEC
15	61.3	38.2	61.8	38.1	61.6	38.2	Accept	Vapor line
16	60.7	46.3	60.8	46.2	60.8	46.3	Accept	Evaporator
17	61.1	34.0			61.1	34.0	Reject	
18	61.1	39.6	61.1	39.7	61.1	39.7	Accept	Evaporator
19	60.7	37.7	60.5	37.6	60.6	37.7	Reject	
20	59.1	38.6	59.3	38.6	59.2	38.6	Accept	Liquid line
21	59.1	44.1	59.3	43.7	59.2	43.9	Accept	Evaporator
22	62.1	37.3			62.1	37.3	Reject	
23	60.4	38.8	60.3	38.7	60.4	38.8	Accept	Liquid line
24	59.9	34.6	60.5		60.2	34.6	Reject	
25	59.9	45.3	60.1	45.2	60.0	45.3	Accept	Reservoir

Figure D.4 UMCP-VER-005-VCPL: VIEW-CPL thermal switch and reservoir temperature controller verification (page 2 of 5).

The reservoir temperature controllers were calibrated using an Omega digital thermocouple thermometer and a Type T thermocouple. The lab book, pg. 33 documents the temperature controller calibration and initial pressure prime.

2:45PM	Liquid is in the vapor plenum of the evaporator
2:56	Increased TC1 (20W) set point using the screw adjustment to raise the reservoir set point. An indication of at the heater has reached the set-point value is that the LEDs begin to cycle on and off.
3:00	Increased TC2(5W) set point using the screw adjustment to raise the reservoir set point
3:10	Increased TC1(20W) set point using the screw adjustment to raise the reservoir set point
3:12	Increased TC2(5W) set point using the screw adjustment to raise the reservoir set point
3:30	Decreased TC1(20W) and TC2(5W) set point so the heaters are cycling at 50° C. The evaporator is filled with liquid, indicating that the liquid was forced from the reservoir to the evaporator and there is no blockage between the reservoir and the remainder of the CPL
3:32	Turned on MH2 (25W) on the evaporator
3:35	Turned on MH1 (40W) on the evaporator for a total of 65W.
3:38	Vapor was generated in the grooved and the vapor plenum was cleared of liquid.

1. Summary

The criteria for selecting the thermal switches was that the switch open in the range of 59°C to 62°C and reset at a temperature above 38°C. Fifteen switches were selected (TS 1, 6, 7, 9, 10, 12, 13, 14, 15, 16, 18, 20, 21, 23, and 25) to be placed in series with the heaters and thermoelectric cooler on the VIEW-CPL payload. The switches are placed in series with the heaters with one switch on the positive voltage side and a redundant switch on the return line as specified in the VIEW-CPL electrical drawings.

The temperature controllers were shown to regulate the temperature of the reservoir. The controllers were set to switch off power to the heaters at 50°C.

Figure D.3 UMCP-VER-005-VCPL: VIEW-CPL thermal switch and reservoir temperature controller verification (page 3 of 5).

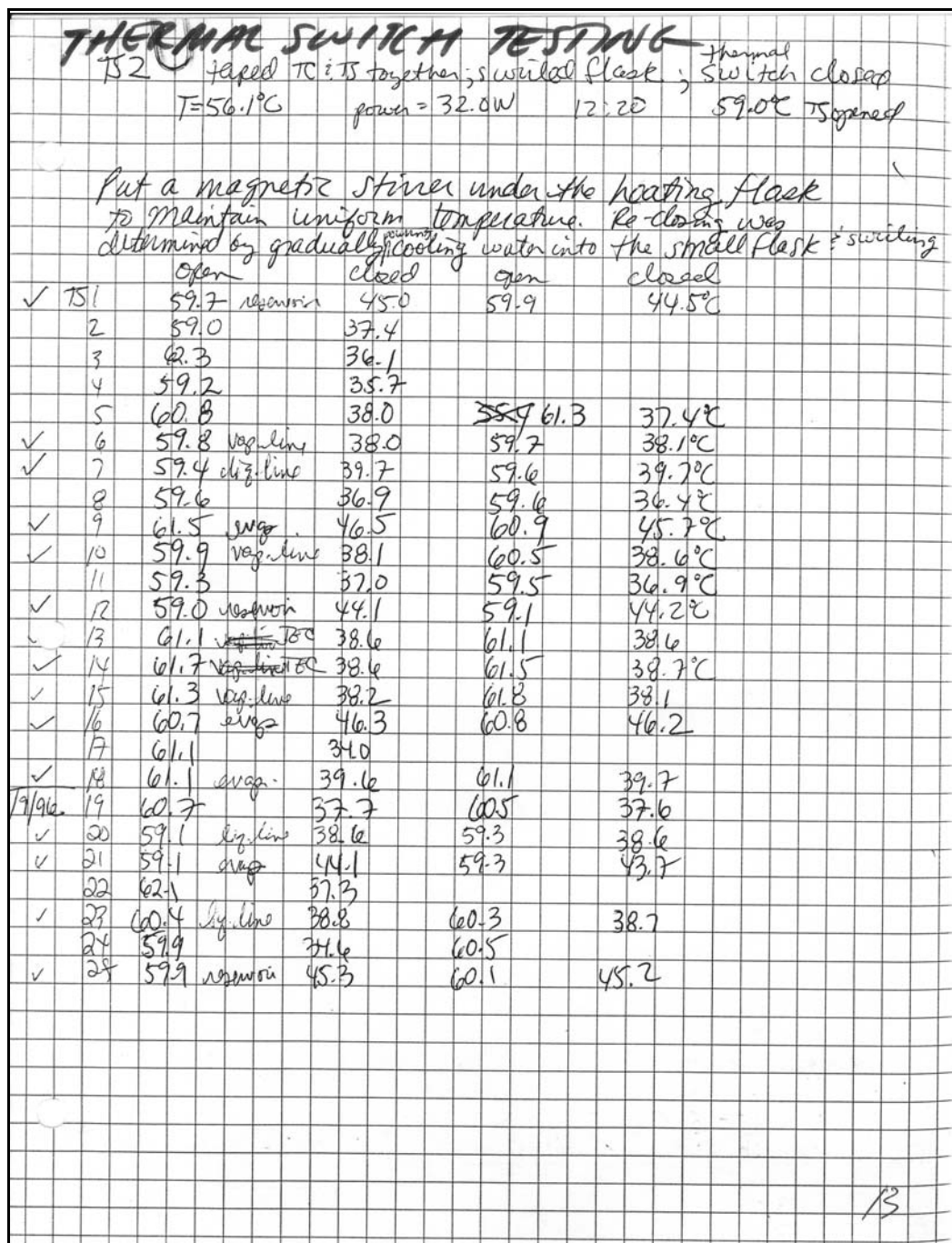


Figure D.3 UMCP-VER-005-VCPL: VIEW-CPL thermal switch and reservoir temperature controller verification (page 4 of 5).

Swala Nicoll 596-1289

June 11, 1996

Reservoir heater shutdown

Pulse is at 15s. intervals. - Likely indicating, that the thermostat thinks it is already hot, even at room temperature

Recalibrating to bring temp. cut off into range.

SW: Moved clockwise 5 turns. Set at room temperature without adding LED back in made the heater stay on because it lowered the resistance.

SW: Moved clockwise 9 turns w/ LED turned plugged in. Added one more turn.

Bob suggests adding single pole double throw switch if heating takes too long.

Initial pressure time 6/11/96 *

2:45 Liquid in vapor plenum

32:56 Increase sensitivity of TC for 50 20W by adding another turn.

3:00 Increased SW by 1 more turn.

3:10 Increased 20W TC by 1 more turn.

3:12 Increased SW by 3 turns

3:30 Decreased SW by 1/2 turn. Evaporator filled w/ liquid. 20W 1/8 turn. Controlling at 50K

3:32 20W heater on evaporator

3:35 25W + 40W on evaporator

3:38 Vapor plenum cleared

3:38:30 Vapor bubbles entered w/ through the in rck

TEMPERATURE CONTROLLERS

Figure D.3 UMCP-VER-005-VCPL: VIEW-CPL thermal switch and reservoir temperature controller verification (page 5 of 5).

VIEW-CPL Surface temperature measurement on Sept. 13, 1996

The insulation surface temperature was measured on the VIEW-CPL payload while operating the evaporator heaters. The measurement was made with a type T thermocouple and found to be 32°C. This temperature is on the aluminum tape enclosing the insulation on the vapor line (hot side) which is only accessible by opening the VIEW-CPL shroud cover. External VIEW-CPL temperatures on the lexan shroud are at room temperature.

Kimberly R. Kolos
University of Maryland
Department of Mechanical Engineering
College Park, MD 20742

(301) 405-5320

Figure D.4 UMCP-VER-006-VCPL: VIEW-CPL surface temperature measurement on Sept. 13, 1996.

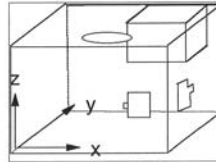
VIEW-CPL Weight, Dimensions, and Center of Gravity

Kimberly R. Kolos (301) 405-5320
Univ. of MD, Dept. of Mech Eng. 20742
Final: August 27, 1996

Weight measured on OHAUS DS20L (calibrated by factory Oct. 1995)
18.05 kg = 39.71 lbs

Dimensions (inches)

width (x) 17.1 including connections
depth (y) 13.6 including bracket
height (z) 7.75 including toggle sw



Center of Gravity - measured by balancing on the edge of a counter

	Measurement 1	Measurement 2	Measurement 3	Average
X	9.0	7.8	8.5	8.4 in
Y	7.3	7.0	7.0	7.1 in
Z	2.8	3.5	2.6	3.0 in

Figure D.5 VIEW-CPL weight, dimensions, and center of gravity.

APPENDIX E: MEASUREMENT UNCERTAINTY ANALYSIS

Uncertainty exists in the measurements and the degree to which the uncertainty affects the conclusion is an important issue. The propagation of measurement uncertainty is determined from the uncertainty of the individual measurements. If a statistical interpretation of uncertainty is adopted, the uncertainty is calculated using a root-sum square formulation and the overall uncertainty (δU_{rss}) takes on a probabilistic meaning. The root-sum square expression can be written as

$$\delta U_{rss} = \sqrt{\sum_{i=1}^N \left(\frac{\partial f}{\partial x_i} \cdot \delta x_i \right)^2} \quad (\text{E.1})$$

where δx_i represents the most probable errors in each of the measured quantities (x) that are variables in a function (f) used to determine a variable. A summary of the measurement uncertainties calculated using Eq. E.1 is presented in Table E.1.

E.1 Resolution from the PGSC Interface Unit (PIU)

The PIU board resolution is required when calculating the uncertainty of the measurements collected with the VIEW-CPL data acquisition system. The PIU contained a 15 bit analog-to-digital converter [Azonix Corp., 1995] with an input signal range of ± 10 V for a resolution of $20 \text{ V} / 2^{15}$ bit, or 0.0006104 V/bit. In the measurement uncertainty calculations, the voltage uncertainty, δV , is the board resolution of $\pm 3.052 \times 10^{-4}$ V.

Table E.1 Measurement uncertainties for data from the VIEW-CPL experiment.

Measurement	Transducer Uncertainty	Total Measurement Uncertainty
PIU resolution, δV	$\pm 3.05 \times 10^{-4}$ V/bit	N/A
Temperature, δT	$\pm 3.05 \times 10^{-4}$ V, ± 0.29 k Ω	± 0.74 K (at 60°C)
Absolute pressure, δP_{abs}	$\pm 3.05 \times 10^{-4}$ V 0.15% Full Scale = ± 0.26 kPa	± 0.30 kPa (at 20.0 kPa)
Differential pressure, δP_{diff}	$\pm 3.05 \times 10^{-4}$ V 0.3% Full Scale = ± 0.21 kPa	± 0.21 kPa (at 0.20 kPa)
Supply Voltage, δV	$\pm 3.05 \times 10^{-4}$ V, ± 10 Ω , ± 25 Ω	± 0.032 V (at 32 V)
Heater Power, δQ	$\pm 3.05 \times 10^{-4}$ V (signal), ± 0.032 V (supply), ± 0.0010 Ω	± 0.10 W (at 10 W) ± 0.14 W (at 75 W)
Bubble Volume, δV	See Appendix F	See Appendix F

E.2 Temperature measurements

The temperature data was collected with AD590 [Omega, 1987] temperature sensors (see Appendix G for details on the sensors) and calculated from

$$T = C \frac{V}{R} \quad (\text{E.2})$$

where $C = 1.0$ K/ μ A represents the transducer characteristic. The factors affecting the temperature calculation are the voltage, V , and the value of the resistance, R , in the AD590 circuit (see Figure G.1 in Appendix G). The uncertainty for the temperature measurement is calculated as

$$\delta T = C \sqrt{\left(\frac{1}{R} \delta V \right)^2 + \left(\frac{V}{R^2} \delta R \right)^2} \quad (\text{E.3})$$

The resistance and tolerance of the resistors used in the experiment were $13.0 \pm 0.65 \text{ k}\Omega$. The resistance uncertainty is assumed equal to the resistance tolerance. A typical voltage at 60°C was $4.331 \text{ V} \pm 3.05 \times 10^{-4} \text{ V}$ resulting in $\delta T = 16.7 \text{ K}$. If the resistance values were certain (i.e. $\delta R = 0$), the temperature uncertainty would only be 0.05 K due solely to the uncertainty of the voltage, δV , resulting from the board resolution. Thus, the temperature measurements are sensitive to the variation of the resistance values in the AD590 circuits. A curve-fit to resistance data is used to reduce the uncertainty on the resistance to $\pm 0.029 \text{ k}\Omega$ (see details in Appendix G), resulting in a typical temperature uncertainty of $\delta T = \pm 0.74 \text{ K}$.

E.3 Pressure measurements

The absolute pressure transducer operates in the range of 0 to 172 kPa (0 to 25.0 psi) with an output of 0 to 5 VDC for a resolution of 34.4 kPa/V; therefore the absolute pressure is determined as

$$P_{abs} = C_r V \quad (\text{E.4})$$

where $C_r = (P_{\max} - P_{\min}) / (V_{\max} - V_{\min}) = \Delta P / \Delta V = 34.4 \text{ kPa} / \text{V}$. Manufacturer data for the transducer gives an uncertainty, δP_{man} , equal to $\pm 0.15\%$ of full scale, which is $\pm 0.258 \text{ kPa}$ ($\pm 0.0375 \text{ psi}$). The propagated measurement uncertainty, δP_m , resulting from the voltage resolution limit of the PIU board is calculated as

$$\delta P_m = \sqrt{2\left(\frac{V}{\Delta V}\delta P_{man}\right)^2 + 2\left(\frac{\Delta P}{\Delta V^2}V\delta V\right)^2 + \left(\frac{\Delta P}{\Delta V}\delta V\right)^2} \quad (E.5)$$

For a typical pressure of 20.0 kPa, corresponding to 0.581 V, the propagated measurement uncertainty is ± 0.0437 kPa. The total measurement uncertainty for the absolute pressure transducer is equal to the sum of the manufacturer's uncertainty and the propagated measurement uncertainty:

$$\delta P_{abs} = \delta P_m + \delta P_{man} \quad (E.6)$$

which is equal to ± 0.302 kPa (0.0437 psi). The manufacturer's uncertainty dominates the uncertainty associated with the absolute pressure measurements.

The uncertainty associated with the differential pressure measurement is determined in a fashion similar to the absolute pressure measurement. The differential pressure transducer operates in the range of -34.5 to +34.5 kPa (-5.00 to +5.00 psi) with an output of -5.02 to 5.00 VDC for a resolution of 6.88 kPa/V (Note: the negative output is different than the positive due to manufacturer's amplifier calibration factors). The accuracy of the transducer, given by the manufacture, is 0.3% of full scale ($\delta P_{man} = \pm 0.207$ kPa). The maximum measurement from the differential pressure transducer was 0.200 kPa, corresponding to a signal of 0.0291 V. Using equation E.5, the propagated measurement uncertainty for the differential pressure transducer is $\delta P_m = \pm 0.00227$ kPa. Thus the total uncertainty for the differential pressure

measurement is $\delta P = \pm 0.209$ kPa, which is the same order as the maximum measurement from the transducer indicating that the pressure transducer was oversized.

E.4 Electrical measurements

The DC power supply voltage to the VIEW-CPL experiment, V_{supply} , was measured using the voltage divider network (see Figure 3.23) containing resistors R_1 and R_2 with values 10 k Ω and 25 k Ω , respectively. The supply voltage was calculated as follows

$$V_{\text{supply}} = V \frac{R_1 + R_2}{R_1} \quad (\text{E.7})$$

The uncertainty of the voltage measurement is calculated based on the resolution of the board, δV , and the uncertainty of the resistors δR_1 and δR_2 as

$$\delta V_{\text{supply}} = \sqrt{\left(\frac{R_1 + R_2}{R_1} \cdot \delta V\right)^2 + \left(\frac{V}{R_1} \cdot \delta R_2\right)^2 + \left(\frac{V \cdot R_2}{R_1^2} \cdot \delta R_1\right)^2} \quad (\text{E.8})$$

The resistors have a tolerance of $\pm 0.1\%$ resulting in an uncertainty of ± 10 Ω for δR_1 and ± 25 Ω for δR_2 . Based on this, calculated uncertainty for the voltage measurement is ± 0.032 V, for a signal of 9.1 V corresponding to a supply voltage of 32 V. Thus the supply voltage measurements have a relative measurement error of $\pm 0.10\%$.

The heater power, Q , is a function of the power supply voltage, V_{supply} (Eq.

E.7) and the current passing through the heater circuits, V_{signal}/R

$$Q = V_{\text{supply}} \frac{V_{\text{signal}}}{R} \quad (\text{E.9})$$

The uncertainty in the power measurements is calculated as

$$\delta Q = \sqrt{\left(\frac{V_{\text{signal}}}{R} \delta V_{\text{supply}} \right)^2 + \left(\frac{V_{\text{supply}}}{R} \delta V_{\text{signal}} \right)^2 + \left(\frac{V_{\text{supply}} V_{\text{signal}}}{R^2} \delta R \right)^2} \quad (\text{E.10})$$

where V_{signal} varies for each heater combination. Table E.2 lists the uncertainty in power measurement based on a typical supply voltage of 32 ± 0.032 V and a resistance, R , of $0.100 \pm 0.001 \Omega$.

Table E.2 Summary of uncertainty in heater power measurements.

Heater (W) Q	Current (A) V_{signal}/R	Measurement Signal (V) V_{signal}	Uncertainty (W) δQ
10	0.313	0.031	0.099
25	0.781	0.078	0.104
35	1.094	0.109	0.109
40	1.250	0.125	0.113
50	1.563	0.156	0.121
65	2.031	0.203	0.134
75	2.344	0.234	0.144

E.5 Vapor volume measurements

The vapor bubbles in the evaporator core are classified as (a) spherical, (b) hemispherical, (c) half-elliptical, and (d) half-cylindrical with spherical ends. The uncertainty functions, δV_b , associated with the bubble volume calculations, V_b , are given in the following four equations and are a result of the uncertainty in

the diameter, length, and width measurements, δd , δl , and δw , respectively.

(a) Spherical:

$$V_b \pm \delta V_b = \frac{\pi}{6} d^3 \pm \frac{\pi}{2} d^2 \delta d \quad (\text{E.11})$$

(b) Hemispherical:

$$V_b \pm \delta V_b = \frac{\pi}{12} r^3 \pm \frac{\pi}{4} r^2 \delta r \quad (\text{E.12})$$

(c) Half-Elliptical:

$$V_b \pm \delta V_b = \frac{2}{3} \pi l d w \pm \frac{2}{3} \pi \sqrt{(l d \delta w)^2 + (l w \delta d)^2 + (d w \delta l)^2} \quad (\text{E.13})$$

(d) Half-Cylindrical with spherical ends:

$$V_b \pm \delta V_b = \left(\frac{\pi}{4} d^2 l + \frac{2}{3} \frac{\pi}{4} d^3 \right) \pm \sqrt{\left(\frac{\pi}{2} d l \delta d \right)^2 + \left(\frac{\pi}{4} d^2 \delta l \right)^2 + \left(\frac{\pi}{2} d^2 \delta d \right)^2} \quad (\text{E.14})$$

An example bubble measurement is given in Appendix F.

E.6 NCG Calculation

The amount on noncondensable gas in the loop is a calculated using the ideal gas law

$$n \pm \delta n = \frac{PV}{RT} \pm \sqrt{\left(\frac{V}{RT} \delta P \right)^2 + \left(\frac{P}{RT} \delta V \right)^2 + \left(\frac{PV}{RT^2} \delta T \right)^2} \quad (\text{E.15})$$

APPENDIX F: OBTAINING DATA FROM VIDEO

The video test footage from VIEW-CPL was recorded in either Hi8 mm, 8-mm or VHS-C format. All shuttle footage was recorded on Hi8 mm tape, which provides 30 frames per second of video information. Information on the size and shape of the bubbles in the evaporator core was extracted from the video data by either downloading the images into a computer and taking measurements from the downloaded images or taking measurements directly from the video monitor during playback.

F.1 Downloading video frames

Photographs from the video tapes were downloaded to the computer via an image “grabbing” device. The Snappy Video Snapshot (SVS), developed by Play Incorporated, plugs into the parallel port. A standard RCA jack port allows the SVS to be connected to a camcorder or video cassette recorder (VCR). Video displayed with a VCR, or through a camcorder, is shown on the computer monitor when the SVS software is executed. When the desired picture is shown on the screen, the image is grabbed, processed, and displayed on the computer monitor. The image can be adjusted and saved in various formats. The physical size of the image to be saved ranges from 64 to 1500 pixels wide, by 48 to 1125 pixels high and the color options range from 16 colors to 16 million colors in the 24-bit true color format.

The SVS scans at 72 ppi (pixels per inch). The maximum image size for the SVS is 1500 pixels wide by 1125 pixels high for a printable size of 20.8 inches

by 15.6 inches. When the picture is reduced to fit on a piece of 8 ½ x 11 inch paper, the number of pixels per inch increases for a higher resolution image (102 ppi). When larger images are saved, more disk storage space is required. To retain picture quality while reducing the storage space, image data was stored as 24-bit true color images with dimensions of 1024 pixels by 768 pixels (14.2 inches by 10.7 inches at 72 ppi) resulting in a file size of approximately 400 kilobytes per image. The SVS allows images to be saved in the many industry standard formats. The JPEG format allows the image to be compressed, resulting in good quality picture at a smaller file size than would be obtained with the other formats.

The SVS can be adjusted for higher quality still pictures. By changing the length of time spent sampling the video source, more frames can be sampled. If more frames are sampled, the color accuracy will be higher and the video noise will be reduced through data interpolation software. With a moving scene, such as images from video tapes, the sampling time is 1/60th of a second and only one sample is obtained. If images are still, a longer sampling time is used to take more than one sample from the video source. For still video a two-field sample is taken and image processing software enhances the picture. A video field is one half the information stored in a video frame or screen of information, i.e. one video frame consists of an odd and an even field. The frames for NTSC, the standard video format for the United States, are displayed at a rate of 30 Hz, which result in a field rate of 60 Hz

To obtain the best quality video images at precise times from the Hi8 mm

video tapes, the desired frame was paused on the VCR and the SVS mode was set at moving scene. This setting allowed only one sample of the video to be scanned and eliminated the use of the software interpolation for adjusting the image. The moving scene setting was necessary because even slight changes in the lighting on the video tape affected the quality of the multi-scanned images.

After scanning, the image was stored in the JPEG format and imported into Adobe Photoshop 4.0 for sizing and measurement.

F.2 Measuring bubbles

The distance from the extreme edge of the evaporator inlet hole to the vapor plug was measured on the hardware and found to be $L_h + \delta L_h = 10.80 \pm .05$ cm. This value was used to find the scaling factor

$$F \pm \delta F = \frac{L_h}{L_p} \pm \sqrt{\left(\frac{\delta L_h}{L_p}\right)^2 + \left(\frac{L_h \delta L_p}{L_p^2}\right)^2} \quad (\text{F.1})$$

for the pictures by scaling the same distance in the image (photograph or monitor), L_p . The physical length, x , is calculated from the length measured on the image, x_p by

$$x \pm \delta x = F x_p \pm \sqrt{(\delta F x_p)^2 + (F \delta x_p)^2} \quad (\text{F.2})$$

When using the SVS, the images were scaled to 5 inches wide (resolution of 205 ppi) and scaling guidelines (horizontal and vertical lines) were added to determine the scale factors required to obtain measurements from the images.

Dimensions of bubbles were obtained by zooming in on details and using the internal ruler bars available in Adobe Photoshop. Measurement made directly from the video monitor were faster, but more measurement uncertainty existed (see Appendix E).

Figure F.1 is an example of the measurements taken from the VIEW-CPL photographic data. Table F.1 summarizes the variables in the measurement.

Table F.1 Example bubble measurements.

	Bubble Diameter d (cm)	Bubble Length l (cm)	Reference Length L (cm)
Measured from image	0.73 ± 0.05	2.09 ± 0.05	$L_p = 8.40 \pm 0.05$
Actual dimension	0.94 ± 0.06	2.69 ± 0.07	$L_h = 10.80 \pm 0.05$

From Figure F.1, the physical size of the bubble is calculated from Eq. E.13 (volume of half cylinder with spherical ends) using the actual diameter and length calculated from Eq. F.14 with a scaling factor of $F = 1.286 \pm 0.006$. The bubble shown in Figure F.1 had a volume of $2.08 \pm .26 \text{ cm}^3$.

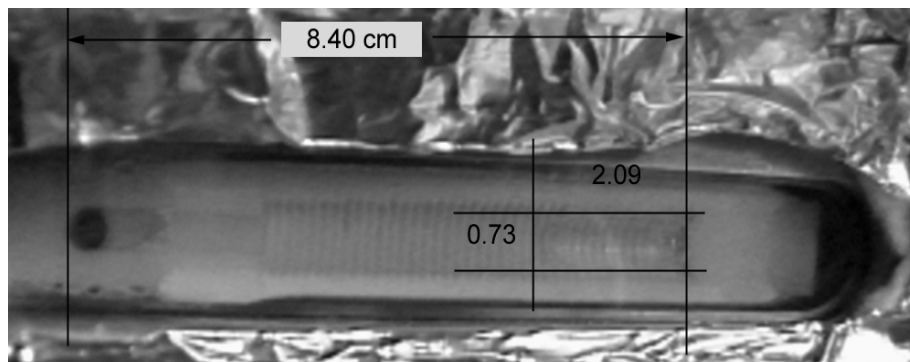


Figure F.1. Example of measuring bubbles from photographs downloaded from the VIEW-CPL experiment.

APPENDIX G: VIEW-CPL TEMPERATURE MEASUREMENTS AND CORRECTIONS

G.1 Temperature sensor circuits

The temperature measurements in the VIEW-CPL experiment are collected using AD590 temperature transducers [OMEGA, 1987]. The transducers are powered with 15 VDC and act as current sources, supplying current output proportional to the absolute temperature of the transducer with a proportionality constant of $C = 1\mu\text{A/K}$.

$$T = \frac{V}{R} C \quad (\text{G.1})$$

By placing a resistor, R , in the AD590 circuit (see Figure G.1), a voltage measurement, V , is used to infer the temperature, T , at the AD590 sensor from Eq. G.1.

G.2 Temperature sensor calibration and sensitivity

Each of the AD590 temperature sensors were calibrated using YSI

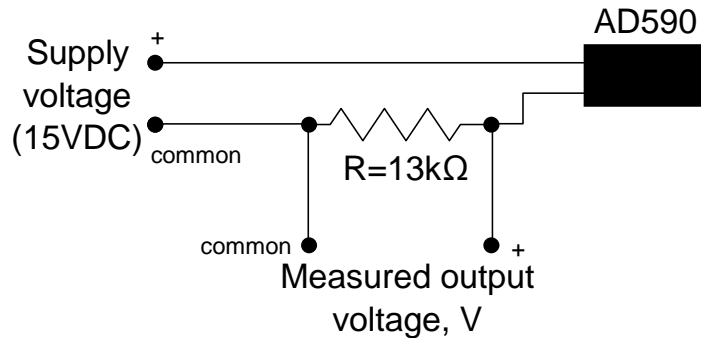


Figure G.1 AD590 temperature transducer circuit as used in the VIEW-CPL experiment.

precision thermistors [YSI, 1995] placed in contact with the AD590 locations on the experiment at the condenser, evaporator, and reservoir. The thermistors were used as independent measurements in calibrating the transducers as prescribed in the AD590 literature [OMEGA, 1987]. The AD590 temperature sensors were calibrated either using measurements taken at ambient air conditions, measurements at 40°C while in an oven, or a weighted average of the two measurements. In calculating the slope calibration factors, weighted averages were assigned to the oven or ambient temperature measurements according to the temperature range that the particular sensor would operate within. For example, since the air temperature measurement (T9) never exceeded 30°C, the calibration depended entirely on the ambient temperature measurement and the oven temperature measurement was not a factor in calibrating T9. The resulting calibration factors were obtained by calculating the slope required to match the AD590 temperature measurements to the thermistor measurements. The slope calibration factors, S , are the inverse of the resistor values inferred from Eq. G.1 by assuming $C=1$. The calibration factors for the VIEW-CPL AD590 circuits, are listed in Table G.1. The accuracy of the temperature measurements depend upon the accuracy of the voltage and the resistance as described in Appendix E.2.

Table G.1 Slope calibration factors for the AD590 temperature sensors used in the VIEW-CPL experiment.

ΔT = Temperature from the AD590 sensor - temperature from the thermistor					
AD590 circuit	Slope calibration factor, S, (K/Volt)	Resistance R, (k Ω)	ΔT at ambient	ΔT in 40°C oven	Location on VIEW-CPL
T1	72.26	13.84	-0.29	0.34	Reservoir inlet
T2	72.66	13.76	-0.04	0.36	Condenser exit
T3	73.43	13.62	-0.28	0.75	Condenser inlet
T4	73.30	13.64	-0.01	-0.47	Evaporator inlet
T5	71.09	14.07	-0.10	-0.74	Evaporator exit
T6	73.80	13.55	-0.31	0.46	Evaporator block
T7	71.89	13.91	-0.32	0.51	Evaporator inlet
T8	72.81	13.73	-0.00	0.90	Reservoir
T9	70.91	14.10	0.00	0.67	Condenser exit air
T10	71.60	13.97	-0.05	0.91	Liquid line

G.3 Resistor drift correction

The temperatures, measured with the AD590 system described in section G.1, are very sensitive to the resistance over which the voltage is measured; therefore any change in the resistor values adversely affects the output. A gradual decrease in the AD590 temperature values, as displayed on the VIEW-CPL PGSC Interface Unit (PIU), was observed when compared to the VIEW-CPL panel meter. The sensed temperatures were also lower than values obtained from thermocouples placed on the experiment after it returned from the shuttle flight. This apparent decrease in the AD590 temperature measurements on VIEW-CPL led to an investigation of the AD590 circuits.

The panel meter temperature is measured with an AD590 sensor on a circuit similar to the main AD590 circuits. While both circuits are powered with the same +15 V supply, the panel meter resistor is a $1\text{ k}\Omega \pm 0.1\%$ precision resistor while the other sensors used standard $13\text{ k}\Omega \pm 5\%$ carbon film resistors. The only other difference between the circuits is that the voltage measured with the panel meter is read across the $1\text{ k}\Omega$ resistor using a 0-2 V digital meter, while the PIU board measures the voltage across the $13\text{ k}\Omega$ resistors. Based on the circuit comparisons, the possible causes of the temperature variation were determined to be either (1) the PIU board calibration had drifted, (2) a bug in the software code, or (3) the resistance values had drifted. The possibility of sensor degradation is unlikely since a degradation in the sensors would have been obvious in all of the circuits, including the circuit with the precision resistor.

A check on the PIU board calibration and software calculations was performed and results matched baseline, confirming that both the board and the software were working properly. The resistors were then measured and found to be approximately 2% lower than the installed values. Since the resistance values were lower than expected, the change resulted in lower than expected output voltages from the AD590 temperature sensors and therefore lower than expected temperature readings. The fact that the AD590 temperatures were consistently lower in all of the circuits containing standard resistors led to the theory that the resistors were the cause of the temperature degradation.

It was discovered, after the experiment had flown, that resistors can change resistance during both storage and during use [Sinclair, 1990 and Wellard, 1960]. The resistors used in the AD590 circuits were standard 13 k Ω , 1/4 watt carbon resistors with 5% tolerance. Humidity effects on carbon composition resistors cause the resistance to increase due to expansion of the resin in the resin-carbon resistance matrix, which then separates the carbon particles. The increase can be partially reversed upon drying, however a total recovery is not expected due to the structural change of the element [Wellard, 1960]. Carbon composition resistors also see changes in resistance during the load life due to polarizing voltages reorienting the resistive particles within the binders and due to expansion and contraction effects within the carbon-resin structure. It is possible for the resistance to decrease with usage, due to both drying effects from the heat generated during use and reorientation of carbon particles, and then to increase during storage from collecting moisture. This increase and decrease in resistance was observed in the VIEW-CPL data.

Recalling that the temperature calculation is sensitive to changes in resistance (the 2% observed change in the resistance values results in a 5.7 K error in the temperature values, Equation E.3, Appendix E.2), a correction was necessary to the calculated temperature data to account for the changing resistance in the AD590 circuits. In order to make the correction to the previously collected VIEW-CPL temperature data, the raw voltage data was first recovered from the temperature values using the original resistance values from Table G.1

in Eq. G.1. The correct values of the resistors was determined for each test by comparison with the panel meter readings. Since there was a gradual change in the resistors, a curve fit of resistance with powered usage time was used. Once the corrected resistance values were determined for each test, the raw voltage was divided by the resistance to obtain the temperature.

The original calibration of the temperature sensors, made using ambient air conditions and an elevated temperature of 40 °C in an oven (see Section G.2), were performed in August 1996. After that, the only check on the VIEW-CPL temperature measurements during the testing are comparisons of the temperature measurement on the reservoir (T8) and the panel meter measurement, also on the reservoir. The panel meter temperature measurement is the only AD590 circuit with a precision resistor, and this temperature measurement was still correct in May 1997 when verified after the shuttle flight. To make the corrections, the T8 measurements were converted to raw voltages using the calibration factors in the data acquisition software (Table G.1). Assuming the panel meter reading is the correct temperature measurement, the expected resistance, R_{T8} is then a function of the raw voltage, V , and the measured temperature, T_{panel} .

$$R_{T8} = \frac{V}{T_{panel}} \quad (G.2)$$

A new slope calibration was essentially performed for each test using the panel meter as the basis of the calibration according to Eq. G.2. A curve-fit of the R_{T8} data provided the new slope calibration required to correct the temperature data.

The measurements used to fit a curve to the resistance were collected from data sheets and grouped into three distinct time periods: pre-flight (152 samples), flight (82 samples), and post-flight (39 samples). The three data sets are plotted versus usage time in Figure G.2. The periods in between the three main groups were times that the CPL was not tested and no power was applied to the resistors in the AD590 circuits for an extended period of time (~2 months). Since there was no usage of the AD590 resistors during these down times, the groups of data appear one after the other on Figure G.2. Approximations of non-powered periods, in-between the individual tests, were made in order to determine the actual usage time of the resistors. The usage time, that is the time that the resistors received power, is the main independent variable for the resistance curve-fit since it is known that resistors can decrease value over the period they are powered [Wellard, 1960]. The breakdown of the data into the three ranges resulted from the resistor values partially correcting themselves toward their original resistance values during the extended non-use times. In the time period between the end of pre-flight testing and the start of flight testing, as well as during the time period between the end of flight testing and the start of post-flight testing, the resistance values increased 0.8% in each period.

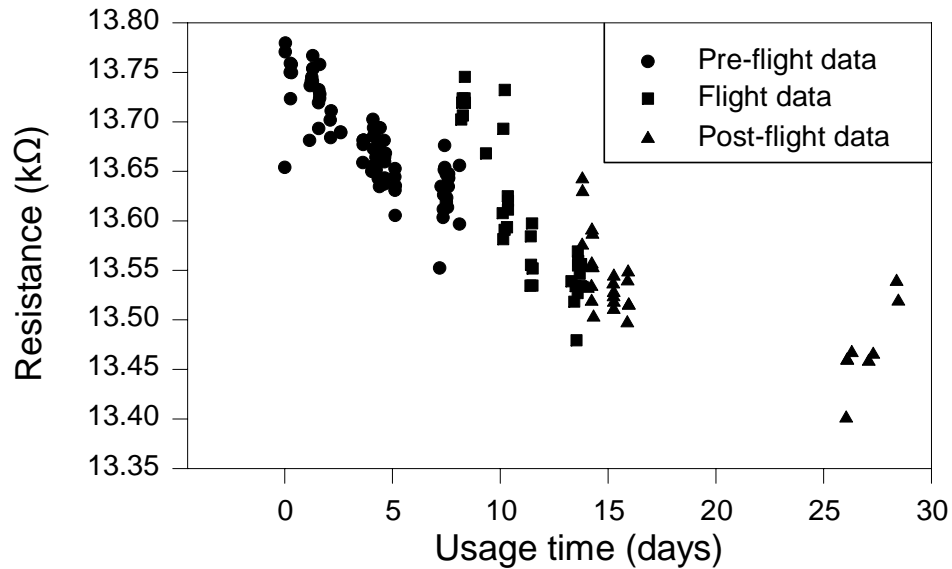


Figure G.2 Steady VIEW-CPL resistance calculations from the reservoir AD590 panel meter and T8 temperature measurement.

Depending upon the conditions in the CPL and the speed with which the data is manually recorded, the time lag between the recording of the T8 temperature value and the panel meter value could allow the T8 value to change before the panel meter is actually recorded. Any transient panel meter or T8 data points could adversely affect the accuracy of the resistance curve-fit, therefore only data collected during steady state conditions were included in the data set used for the curve-fit. Since the panel meter measurement was recorded immediately following the manual recording of the time on the data sheet, it is assumed that the panel meter was manually recorded very close to the recorded time. The data is considered steady if the difference between T8 on the data sheet and T8 obtained from the computer collected data file, at the time the panel meter reading was recorded, is less than or equal to ± 0.1 °C. All data not

meeting this criteria, 124 samples out of 273 total, were rejected from the samples used for the curve-fit.

Panel meter and T8 measurements below 40 °C were also eliminated from the curve-fit data samples in order to reduce temperature effects and focus on the resistance-time variations. The 40 °C threshold was chosen because the reservoir typically operated in the 40 to 50 °C range. The data below 40 °C accounted for 20 out of 149 samples.

A non-linear least squares curve-fit of the data was performed for each range of data: pre-flight, flight, and post-flight. The function expresses the resistance, R , as a function of the usage time, t , as

$$R = C_1(t-t_0)^{C_2} e^{C_3(t-t_0)} \quad (3)$$

A time offset, t_0 , which is a different value for the pre-flight, flight, and post-flight data, is required to shift the data in time. The offset was chosen in an iterative manner to reduce the sensitivity of the resistance calculation for t near the lower bounds of the time range. The results from the three curve-fits are summarized in Table G.2 and the curves with the data points used in the correlation are plotted in Figure G.3.

The standard error of estimate, S_e , is a measure of the ability of the model to predict data values. A value of S_e lower than the standard deviation of the values of the random variable about the mean, S_y , indicates an improvement in the prediction capability of the model over the prediction capability of just using

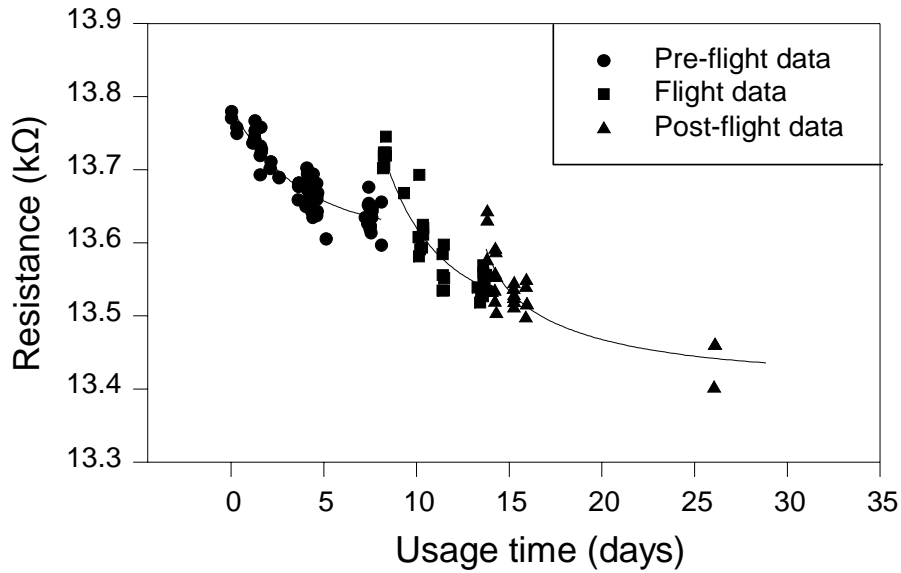


Figure G.3. Pre-flight, flight, and post-flight curve-fits to VIEW-CPL resistance data from the reservoir T8 AD590 circuit.

Table G.2 VIEW-CPL T8 resistance curve-fit coefficients and goodness-of-fit statistics.

Data set:	Pre-Flight	Flight	Post-Flight
Data range, days	$0.00 \leq t < 8.15$	$8.15 \leq t < 13.76$	$13.76 \leq t < 29.00$
Sample size	70	33	26
Offset: t_0 , days	-3.00	6.00	13.00
C_1 (kΩ/days)	13.96943	13.8662	13.5732
C_2	-0.0144688	-0.0168156	-0.0045452
C_3 (days ⁻¹)	0.0009376	0.0013620	0.0001502
Standard error of estimate (S_e), kΩ	0.01854	0.02503	0.02900
S_e/S_y	0.4194	0.3489	0.5770
Explained variance (R^2)	0.8292	0.8858	0.6937
Correlation coefficient (R)	0.9106	0.9412	0.8329
Critical R value for 0.0005 level of significance (McCuen, 1985)	0.3927	0.5477	0.6073

the mean value of the data [McCuen, 1993]. Therefore, the lower the S_e/S_y ratio, the better the prediction capability achieved with the model. The explained variance, R^2 , is the square of the correlation coefficient and is equal to the percentage of the variation in the data that is explained by the model. Critical R^2 values for the data sample sizes used in the pre-flight, flight, and post-flight curve-fits are determined using the 0.05% one-tailed Pearson test for correlation significance [McCuen, 1985]. The Pearson correlation test determines that the correlation is significant (in a statistical sense) for any R^2 values larger than the critical value. Since the R^2 for all three sets of data are larger than the critical R^2 values, statistical analyses suggest that the curve-fits are reasonable models for determining the resistance values as a function of usage time (as can be seen by examining Figure G.3).

Some of the spread between groups of data at close time periods can be explained from the panel meter reading resolution of only 1 °C. Using the methods in Appendix E, a ± 1 °C change in the panel meter reading results in a change of ± 0.04 k Ω in the calculated resistance value or a spread in the data of 0.08 k Ω . From Figure G.3, the maximum spread in the data is 0.1 k Ω , occurring at 10.2 days. The most probable error between the data and the predicted values is $S_e = 0.029$ k Ω (0.21% relative error in resistance). With the new resistance uncertainty of 0.21%, the resulting temperature uncertainty is 0.7 °C, rather than the 15 °C uncertainty from the 5% resistance uncertainty (Appendix E.2). The

uncertainty of the temperature measurements are greatly reduced when the resistance curve-fits are used to calculate the temperatures from the AD590 sensors.

G.4 Temperature correction routine

Based on Ohm's law and the definition of a current source, when the resistance in the AD590 circuit differs while at constant temperature, the voltage measured across the resistor will also change. Since the resistance values for the software conversion from voltage to temperature (Eq. G.1) were coded into the VIEW-CPL data acquisition routines, an error was introduced in the recorded temperatures. In order to correct the temperatures, new resistance values were calculated using the T8 resistor curve fits from Eq. G.3.

The resistors in each AD590 circuit must be corrected using Eq. G.3, but this equation only calculates the resistance value of the T8 AD590 circuit. In order to correct all of the temperature measurements and since the resistors were purchased from the same lot and manufacturer, it is assumed that all of the resistors changed at the same rate and in the same magnitude. This assumption was supported by a comparison of resistance measurements on different days. The value of three resistors were measured in May 1997, corresponding to a usage time of 28.47 days, and in August 1996 (during temperature calibration). The changes from the original resistance values (recorded in the data acquisition software) to the values measured after flight are listed in Table G.3 along with the original T8 resistance value and the value from Eq. G.3 at 28.47 days. Since the

Table G.3 Comparison of resistance values from the VIEW-CPL AD590 circuits.

AD590 circuit:	T2	T6	T10	T8
Original Resistance value, August 1996, kΩ	13.76 ^D	13.55 ^D	13.97 ^D	13.73 ^D
Resistance value on May 13, 1997, kΩ	13.45 ^M	13.25 ^M	13.66 ^M	13.44 ^c
Difference, kΩ	0.31	0.30	0.31	0.29

^Dderived from isothermal calibration^Mmeasured value^ccalculated value (Eq. C.3)

resistances varied by nearly the same amount, the assumption that all resistors changed in a similar manner is partially verified.

With the model of the T8 resistance correction, the difference between the original resistance, R_o , and the corrected resistance during any other test, R_c , can be obtained as follows

$$R_c = R_o + (C_1(t-t_0)^{C_2} e^{C_3(t-t_0)} - R_{o,T8}) \quad (G.4)$$

The constants, C_1 , C_2 , C_3 , and t_0 , are listed in Table G.2 for each of the three ranges of usage time, t . The resistance $R_{o,T8}$ is the original resistance of the T8 circuit as in Table G.1 ($R_{o,T8}=13.73$ kΩ).

The temperatures were corrected for each VIEW-CPL data file collected during tests performed between August 16, 1996 and May 13, 1997. The correction involved determining the usage time, t , according to the time at the start of the test and then correcting the resistance, R_c , for each AD590 circuit (T1 through T10) using Eq. G.4. The corrected temperature was found using R_c for the resistance value in Eq. G.1.

APPENDIX H: VIEW-CPL Data Acquisition Software

H.1 Pseudo-code

Display VIEW-CPL logo, and data acquisition version number

Initialization block - Start:

- Initialize board with INITIALIZE, Set-up logical channels with SEL1050

- Configure Ch 0 and Ch 1 as differential analog input channels for voltage and heater power measurements using AITYPE and AING

- Configure Ch 12 and Ch 13 for the absolute pressure and differential pressure transducers, respectively, using AITYPE and AING

- Configure Ch 14 through 23 for the AD590 temperature sensors using AITYPE and AING

- Configure Ch 60 for the mMAC-1050 board temperature sensor using AITYPE and AING

Main menu block - mmenu:

- Option 1 - Sample one channel

 - Select channel number

 - Call chan1(Num%, Store)

 - List conversion factors

 - Start Loop

 - If Store =1 call DASC every 10 seconds - call DASC:

 - Call DAS: Sample channels, Write physical data to file

 - Call chan1 again

 - If reading VIEW-CPL data channels (i.e. voltage, power, absolute or differential pressure transducer, AD590 temperature sensors), call XAING to read input channel voltage

 - If reading board temperature channel, call XAIN to read input

 - Convert input voltages to physical quantities, Print to screen

 - Loop until ^C is entered, then return to Main menu

- Option 2 - Sample all channels

 - Call nchan(Store)

 - List conversion factors

 - Read initial time

 - Start loop

 - Sample channels, convert data, write physical data to screen

 - If Store=1 and if current time is 10 seconds greater than initial time, write physical data output to a binary file

 - Check if temperatures are greater than 60°C and call WARN if true

 - Loop until ^C is entered, then return to Main Menu

- Option 3 - Data plot

 - Call plott(timescale, store)

 - Clear screen and color plot area

 - List calibration factors

 - Print data, and exit instructions to screen

 - Plot axes on screen using pixel locations

 - Begin loop

 - Record current time

 - Read channels and convert to physical values

 - Calculate plotting points using pixel locations (LX,LY) with (0,0) in upper left corner of screen

 - $LX = XO + (TN - TI) * R / Tscale$

 - LX = x pixel location (with 0 at left of screen)

 - XO = offset for axis text (30 pixels)

 - TN = current time

 - TI = initial start time

 - R = range of pixels for plotting (500 pixels)

 - Tscale = time scale in seconds

```

        Select appropriate range for x value
        Plot area broken into 4 plotting ranges to allow
        continuous plotting by overwriting old data when
        reaching the end of the screen. Current plotting
        region is cleared of old data to clearly mark current
        plotting location. A vertical bar is plotted to separate
        the old data from current data.
        LY = BPL - PRP/(HV-LV)*(V-LV)
        LY = y pixel location (with 0 at top of screen)
        LPL = Bottom pixel limit for selected data
        PRP = Plot range height in number of pixels
        UV = Expected highest data value
        LV = Expected lowest data value
        V = Converted data value
        If LY out of range, set to upper or lower limit
        Write axis information on screen
        Plot points on screen using pixel location and selected color
        Print data on screen to right of plot
        If Store=1 and if current time is 4 seconds greater than initial time,
            Write physical data output to a binary file
        Go to top of loop is temperature warning disabled
        Check if temperatures are greater than 60°C and call WARN if true
        Loop until ^C is entered, return to main menu
Option 4 - CPL Schematic
    Call schem(store)
    List calibration factors
    Draw CPL schematic with lines
    Start loop
        Print time to screen
        Sample channels and convert data
        Locate data location on CPL schematic and print data
        If Store=1 and if current time is 4 seconds greater than initial time,
            write physical data output to a binary file
        Go to top of loop is temperature warning disabled
        Check if temperatures are greater than 60°C and call WARN if true
        Loop until ^C is entered, return to main menu
Option 5 - Start/stop acquisition of data
    Check and print current status of writing data to file
    Print options: Return to toggle to or from storing data, 1 to store data, 0 to stop
    storing data, S to exit without changing
    If storing data, set store=1
        Call dirsub to check if file already exists; dirsub (filen$,exist):
        Shell to DOS
        Issue DOS directory command and write output to file
        a:xyzdir.txt
        Search a:xyzdir.txt file for file with same name as filen$
        If file already exists, exist!=1, else exist!=0
        If file already exists, give option to overwrite
        Open data file for binary access as unit #2
    If not storing data, set store=0
    Return to Main menu
Option 6 - Change plot defaults
    Print current plot default time scale
    Ask for new plot default time scale
    Store new plot default time scale
    Return to Main menu
Option 7 - Reset data acquisition board

```

- Call RST1050 to reset board
- Print error code
- Hit return to continue
- Go to Start to re-initialize channels
- Option 8 - Disk directory
 - Clear screen
 - Ask for DOS command
 - Shell to DOS, issue command
 - Return to Main menu
- Option 9 - Exit
 - Exit to DOS by issuing "System" command

User functions and other subroutines

- time - timestamp routine
 - Find year, month, and day from DATE string value
 - Find hour, minute and second from TIME string value
 - Create time stamp in number of seconds elapsed since 0 A.D.
 - Sum number of days in previous months (i.e. if month = 2, previous days = 31) by calling function "days(month)"
 - Add current number of days in month to sum of days
 - time# = yr * 31536000 + dday * 86400 + hr * 3600 + min * 60 + sec
- days(month) - lookup table for number of days in previous month
 - Set Days = 0 for Month = 1
 - Set Days = 31 for Month = 2, 4, 6, 8, and 9
 - Set Days = 28 for Month = 3 (does not handle leap years)
 - Set Days = 30 for Month = 5, 7, 10, and 12
- warn - high temperature warning
 - Clear screen
 - Print warning to remove power from all heaters because a sensor had registered a temperature above 60°C
 - Input ^C to continue, or enter "Kolos" to continue testing without warning again

H.2 Subroutine definitions

USER WRITTEN SUBROUTINES:

CHAN1 (Num%, store)
 Reads channel number Num% using XAIN for differential channel input and XAIN for single-ended input. Data is converted from input voltage (+/-10V) to physical quantities and displayed on the computer screen. All data is written to the output file if Store = 1 by calling subroutine DAS and returning to subroutine CHAN1 after writing output. Hitting ^C exits to the main menu.

DAS ()
 Samples all channels and writes physical data (converted from voltage output) to both an ascii file and a binary file for a single time step.

DASC ()
 Calls subroutine DAS to print output to file and then calls CHAN1 to continue sampling a single channel.

dirsub (filen\$, Exist!)
 Checks if the inputted filename (filen\$) for storing data already exists. Returns Exist!=1 if the file is found, or Exist!=0 if the file is not found.

logo (x!, y!, C!) Displays "VIEW-CPL" logo, and the data acquisition software version number.

logo1 () First subroutine called. Calls subrouting logo to display "VIEW-CPL" logo in block form. Pauses after displaying information; return required to continue with program.

nchan (store) Samples all channels and writes raw voltage output to both an ascii file and a binary file every 10 seconds if Store=1. Prints physical data values to screen in the form of converted voltages for voltage, power, pressure data, and temperature data.

plott (Tscale, store)
 Samples all channels. Plots data on screen and lists numerical data to right of plot. Plotting has scrolling capability by dividing screen into four regions and only clearing regions on the screen of old data and plotting new data when the specific region is entered (i.e. when plot reaches the end of the screen at x=timescale, it returns to the start of the plot x=0 and clears data from one-fourth of the screen before beginning to plot points again). Writes physical output to a binary file every 4 seconds if store=1.

schem (store) Samples all channels. Draws a CPL schematic and prints data on locations of the schematic according physical location on experiment. Writes physical output to a binary file every 4 seconds if store=1.

warn () Changes the screen to display a warning to stop the test because a temperature sensor has returned a reading above 60°C. Allows an override by typing "Kolos" to prevent the warning from showing again.

USER DEFINED FUNCTIONS:

time# () - creates a time stamp by converting date and time to the number of elapsed seconds since 0 A.D.

days! (mon!) - Look up table for the number of days in the previous month (i.e. Jan = 0 , Feb = 31, Mar = 28, ...). Does not account for a leap year

μMAC1050 (Host Software) SUBROUTINES (located in library QB1050.QLB):

SEG - is a value returned from the subroutine

BYVAL - is a value required by the subroutine

AIN1050 (BYVAL a%, BYVAL b%, BYVAL C%, SEG er%)
 Performs same function as AING1050, except for a single channel

AING1050 (BYVAL Lchann%, BYVAL Unit%, BYVAL Pchan%, BYVAL NNchan%, SEG Erstat%)
 Sets up one or more (number determined from Pchan%) logical channels (Lchann%) for the XAING subroutine that returns scaled analog input values. Unit% is set on the μMAC-1050 hardware and Pchan% is the first physical analog channel to be read.

AITYPE1050 (BYVAL Lchan1%, BYVAL Pchan%, BYVAL Nnchan%, BYVAL Modtype%, SEG Erstat%)

Configures and activates one or more (number determined by Nnchan%) consecutive analog input channels (starting with Pchan%) and stores the configuration data in the mMAC-1050 RAM.

Lchan1% is the same logical channel number used in setting up the channel with the SEL1050 subroutine.

Pchan% selections are as follows:

Channels 0 to 7 are differential channels

Channels 8 to 23 are single-ended channels

Channels 24 to 55 are for expansion panels

Channels 56 to 59 are for CJC sensors

Channel 60 is for the temperature sensor on the mMAC-1050 unit

Channel 61 is for monitoring the power supply to the mMAC-1050 unit

Modtype% is for specifying the type of input to the channel, a value of 255 deactivates the channel, 128 is for +/-10V or power supply monitor, 144 is for +/- 40 mA, and 240 is for the mMAC-1050 board temperature sensor.

INITIALIZE (SEG Erstat%)

Initializes the PIU; this is the first step before calling any other mMAC1050 subroutines. The routine reads the hardware configuration in the CONFIGB.DAT file and performs other initialization steps. Erstat% is an integer variable for returning an error code if one is detected during the initialization step.

RST1050 (BYVAL a%, SEG er%)

Resets mMAC-1050 hardware.

SEL1050 (BYVAL Lchan1%, BYVAL Unit%, SEG ISTATUS%, SEG Erstat%)

Used to setup logical channels (Lchan1%) for the AITYPE1050 subroutine that sets up the analog input channels. Unit% is set on the mMAC-1050 hardware.

XAING (BYVAL Lchann%, SEG d!(n%), SEG Erstat%)

Returns multiple scaled values from a consecutive group of analog input channels, where Lchann% is the first channel read corresponding to the logical channels setup with the AING1050 subroutine. Array d!(n%) is returned with the values, in engineering units specified for with an AITYPE1050 channel configuration routine, from the number of channels specified in the AING1050 routine.

XAIN (BYVAL a%, SEG b!, SEG er%)

Performs same function as XAING1050, except for a single channel

H.3 QuickBasic code for VIEW-CPL data acquisition

Main Program:

```
DECLARE SUB dirsub (filen$, Exist!)
DECLARE SUB warn ()
DECLARE SUB das ()
```

```

DECLARE SUB plott (Tscale, store)
DECLARE SUB schem (store)
DECLARE FUNCTION ttime# ()
DECLARE FUNCTION days! (mon!)
DECLARE SUB nchan (store)
DECLARE SUB chan1 (Num%, store)
DECLARE SUB initialize CDECL (SEG Erstat%)
DECLARE SUB sel1050 CDECL (BYVAL a%, BYVAL b%, SEG C%, SEG Erstat%)
DECLARE SUB AITYPE1050 CDECL (BYVAL a%, BYVAL b%, BYVAL C%, BYVAL d%, SEG
Erstat%)
DECLARE SUB AING1050 CDECL (BYVAL a%, BYVAL b%, BYVAL C%, BYVAL d%, SEG
Erstat%)
DECLARE SUB xaing CDECL (BYVAL a%, SEG b!, SEG Erstat%)
DECLARE SUB logo1 ()
DECLARE SUB logo (x!, y!, C!)
DECLARE SUB ain1050 CDECL (BYVAL a%, BYVAL b%, BYVAL C%, SEG er%)
DECLARE SUB xain CDECL (BYVAL a%, SEG b!, SEG er%)
DECLARE SUB RST1050 CDECL (BYVAL a%, SEG er%)

```

```

DIM SHARED StopVar%
DIM SHARED Warn1$

```

'VIEW-CPL DAS Software Change Log

'Upgrade from V 1.83 to 1.84 7 May 1996 K.E. Herold
'Added warning message for temperatures above 60°C to 3 routines (nchan,
'plott and schem. Also added subroutine warn to print the message.
'Added ".dat" to both file names

'Upgrade from 1.84 to 1.85 9 May 1996 K.E. Herold
'Fixed data write in options 1,3 and 4 - problem with format of PUT statement
'Fixed temp conversion to match calibration - all routines
'Added sensing of RDAS-1050 temp sensor

'Upgrade from 1.85 to 1.86 4 June 1996 K.E. Herold
'Added sensing of on-board temp sensor on DAS board
'Cleaned up various inconsistencies and tested all basic functions
'Added data display on schematic

'Upgrade from 1.86 to 1.87 14 June 1996 K.E. Herold
'Added temp calibration factors

'Upgrade from 1.87 to 1.88 15 June 1996 K.E. Herold
'Restructured board calls to main routine so they are called only once
'This eliminates the problem of the board failing after 100 samples

'Upgrade from 1.88 to 1.89 16 June 1996 K.E. Herold
'Added location numbers to schematic
'Added Tdas to data storage
'Fixed units on data disk to engineering units
'Added software reset of DAS board
'Fixed problem with Stack overflow by making CTRL-C exit more gracefull

'Upgrade from 1.89 to 1.90 17 June 1996 K.E. Herold
 'Fixed RDAS reset function, needed to re-initialize software after reset
 'Fixed option 1 flicker

'Upgrade from 1.90 to 1.91 26 June 1996 K.R. Kolos
 'Corrected voltage measurement constant from 4.39 to 3.5

'Upgrade from 1.91 to 1.92 28 June 1996 K.R. Kolos
 'Increased plotting temperature scale from 20-60°C to 0-60°C

'Upgrade from 1.92 to 1.93 07 July 1996 K.R. Kolos
 'Added file protection to prevent over-writing data files
 'Corrected time stamp to include month information
 'Print heater power in watts instead of amps
 'Replaced temperature constants with measured resistive values
 'Checked Differential pressure calculation
 'Modified plot screen

'Upgrade from 1.93 to 1.94 22 July 1996 K.E. Herold
 'Fixed plot screen to automatically wrap the plot after window
 ' fills up.
 ' 24 July 1996 K.R. Kolos
 'Modified overwrite command
 'Removed writing to ASCII file #1
 'Corrected time stamp error of still not including month information
 '

'Upgrade from 1.94 to 1.95 02 Aug 1996 K.R. Kolos
 'Re-calibrated AD590 temperature sensors
 '

'Upgrade from 1.95 to 1.96 10 Aug 1996 K.R. Kolos
 'Changed data storage variable to 1 second storage in the plott subroutine
 '

'Upgrade from 1.96 to 1.97 11 Aug 1996 K.R. Kolos
 'Changed data storage variable to 4 second storage in all subroutines
 'Modified calibration for temperature sensors
 '

'Upgrade from 1.97 to 1.98 20 Aug 1996 K.R. Kolos
 'Corrected time stamp in statement "dday = dday + days(mon)" to read
 "'dday = dday + days(i)"

'These lines give ctrl-c sensitivity
 KEY 15, CHR\$(&H4) + CHR\$(&H2E)
 ON KEY(15) GOSUB ctrlc
 KEY(15) ON

'These lines give ctrl-c sensitivity with Num Lock on
 KEY 16, CHR\$(&H24) + CHR\$(&H2E)
 ON KEY(16) GOSUB ctrlc
 KEY(16) ON

'These lines give ctrl-c sensitivity with Caps Lock on
 KEY 17, CHR\$(&H44) + CHR\$(&H2E)
 ON KEY(17) GOSUB ctrlc
 KEY(17) ON

'These lines give ctrl-c sensitivity with both Num and Caps Lock on

```

    KEY 18, CHR$(&H64) + CHR$(&H2E)
    ON KEY(18) GOSUB ctrlc
    KEY(18) ON

SCREEN 12
CALL logo1
INPUT a

Start:
'Board initialization
  CALL initialize(Erstat%)
  Lchan1% = 1    'Logical channel number
  Lchan2% = 2
  Lchan3% = 3
  Lchan4% = 4
  Lchan5% = 5
  Unit% = 1     'Set in hardware on RDAS-1050
  CALL sel1050(Lchan1%, Unit%, ISTATUS%, Erstat%)
'Configure and setup 2 differential channels
  Pchan% = 0
  NNchan% = 2
  CALL AITYPE1050(Lchan1%, Pchan%, NNchan%, 128, Erstat%)
  CALL AING1050(Lchan2%, Unit%, Pchan%, NNchan%, Erstat%)
'Configure and setup 2 pressure channels
  Pchan% = 12
  NNchan% = 2
  CALL AITYPE1050(Lchan1%, Pchan%, NNchan%, 128, Erstat%)
  CALL AING1050(Lchan3%, Unit%, Pchan%, NNchan%, Erstat%)
'Configure and setup 10 temperature channels
  Pchan% = 14
  NNchan% = 10
  CALL AITYPE1050(Lchan1%, Pchan%, NNchan%, 128, Erstat%)
  CALL AING1050(Lchan4%, Unit%, Pchan%, NNchan%, Erstat%)
'Configure and setup onboard temp sensor
  Pchan% = 60
  NNchan% = 1
  CALL AITYPE1050(Lchan1%, Pchan%, NNchan%, 240, Erstat%)
  CALL ain1050(Lchan5%, Unit%, Pchan%, Erstat%)

Tscale = 600

mmenu:

CLS 0
FOR i = 1 TO 600 STEP 20
  LINE (1 + i, 1)-(10 + i, 10), 11, BF
  LINE (1 + i, 450)-(10 + i, 460), 11, BF
NEXT

LOCATE 3, 1
PRINT "Welcome to the VIEW-CPL DAS Program - MAIN MENU"
PRINT
PRINT "Options:"

```

```

PRINT "1 - Sample one channel "
PRINT "2 - Sample all channels"
PRINT "3 - Data plot"
PRINT "4 - CPL Schematic"
PRINT "5 - Start/stop acquisition of data"
PRINT "6 - Change plot defaults"
PRINT "7 - Reset data acquisition board"
PRINT "8 - Disk directory"
PRINT "9 - Exit"
PRINT
PRINT "Hit CRTL-C at any time to return to this menu"
PRINT
PRINT
INPUT choice

SELECT CASE choice
CASE 1
    PRINT
    PRINT "Which Channel do you want to sample:"
    PRINT "8(9)  Differential line voltage"
    PRINT "10(11) Differential line voltage"
    PRINT "12   Absolute pressure transducer"
    PRINT "13   Differential pressure transducer"
    PRINT "14-23 Temperatures"
    PRINT "60   RDAS-1050 Temperature Sensor"
    INPUT "Enter Channel number "; Num%
    CALL chan1(Num%, store)
CASE 2
    CALL nchan(store)
CASE 3
    CALL plott(Tscale, store)
CASE 4
    CALL schem(store)
CASE 5
    CLS
    PRINT "This option allows the user to stop or start"
    PRINT "the process of storing data to the floppy disk"
    PRINT
    IF store = 1 THEN
        PRINT "The program is currently storing data"
    ELSE
        PRINT "The program is not storing data currently"
    END IF
    PRINT
    PRINT "Enter one of the following:"
    PRINT "(CR) to toggle the storage variable"
    PRINT "1 - to set the storage variable to begin storing data"
    PRINT "0 - to set the storage variable to end storing data"
    PRINT "S - to exit option without changing anything"
    INPUT store1$
    IF store1$ = "S" OR store1$ = "s" THEN
        GOTO mmenu
    ELSEIF LEN(store1$) = 0 THEN

```

```

        IF store = 1 THEN
            store = 0
        ELSE
            store = 1
        END IF
    ELSE
        store = VAL(MID$(store1$, 1, 1))
    END IF
store1:
IF store = 1 THEN
    CLOSE
    INPUT "Enter data file name (.DAT automatically included)"; filen$
    fileb$ = "a:b" + filen$ + ".dat"
    PRINT "Please wait..."
    PRINT "Searching for pre-existing files with the same file name"
    CALL dirsuf(fileb$, Exist)
    IF Exist = 1 THEN
        PRINT
        PRINT "Binary file already exists"
        PRINT
        PRINT "Enter 'OK' to overwrite and continue, anything else to enter new file"
        INPUT Over$
        IF ((Over$ <> "OK") AND (Over$ <> "Ok") AND (Over$ <> "ok")) GOTO store1
    END IF
    IF Exist = 0 THEN
        PRINT
        PRINT "Data stored in ", fileb$
    END IF

    OPEN "a:b" + filen$ + ".dat" FOR BINARY ACCESS WRITE AS #2
ELSE
    TIMER OFF
    CLOSE 2
END IF

CASE 6
CLS
PRINT "Plot Defaults"
PRINT
PRINT "Current time scale is "; Tscale; " sec"
PRINT
Tsave = Tscale
INPUT "Enter new value of time scale in sec"; Tscale
IF Tscale = 0 THEN
    Tscale = Tsave
END IF

CASE 7
CALL RST1050(Lchan1%, Erstat%)
SLEEP 1
CLS
PRINT "RDAS-1050 Board Reset"
PRINT

```

```

IF Erstat% = 0 THEN
    PRINT "Successful reset - hit CR to continue"
    INPUT a
ELSE
    PRINT "Error code = "; Erstat%
    PRINT "hit CR to continue"
    INPUT a
END IF
GOTO Start

CASE 8
    CLS
    INPUT "Enter directory command"; aa$
    SHELL aa$
    INPUT aa

CASE 9
    SYSTEM

END SELECT
GOTO mmenu

ctrlc:
' This is the ctrl-c processing routine
GOTO mmenu
END

dasc:
CALL das
'CALL chan1(Num%, store)
RETURN
END

ctrlc1:
'This is the more gracefull CTRL-C processing routine
StopVar% = 1
RETURN

```

SUB chan1 (Num%, store)

```

DIM d!(10), CT!(10), V!(2), P!(2), T!(10), CTI!(10)

```

```

CLS 0
StopVar% = 0
ON KEY(15) GOSUB ctrlc1
KEY(15) ON
ON KEY(16) GOSUB ctrlc1
KEY(16) ON
ON KEY(17) GOSUB ctrlc1
KEY(17) ON
ON KEY(18) GOSUB ctrlc1
KEY(18) ON
ON TIMER(10) GOSUB dasc

```

```

IF store = 1 THEN
    TIMER ON
ELSEIF store = 0 THEN
    TIMER OFF
END IF

```

'Temp cal factors

'Temp. calibration factors based two points 15 AUG 1996 KRK

```

CT!(1) = 72.26 'KRK 11aug96 70.893 'KRK 2aug96 72.254 - KRK 7jul96 71.685 - KEH 72.123
CT!(2) = 72.66 'KRK 11aug96 72.292 'KRK 2aug96 72.727 'KRK 7jul96 72.307 - KEH 72.622
CT!(3) = 73.43 'KRK 11aug96 71.206 'KRK 2aug96 73.421 'KRK 7jul96 72.939 - KEH 73.346
CT!(4) = 73.3 'KRK 11aug96 73.139 'KRK 11aug96 73.139 'KRK 2aug96 73.153 'KRK 7jul96
72.674 - KEH 73.258
CT!(5) = 71.09 'KRK 11aug96 70.457 'KRK 2aug96 70.922 'KRK 7jul96 70.274 - KEH 70.913
CT!(6) = 73.8 'KRK 11aug96 71.917 'KRK 2aug96 73.746 'KRK 7jul96 73.314 - KEH 73.802
CT!(7) = 71.89 'KRK 11aug96 70.316 'KRK 2aug96 71.891 'KRK 7jul96 71.429 - KEH 71.862
CT!(8) = 72.81 'KRK 11aug96 72.820 'KRK 2aug96 72.993 'KRK 7jul96 72.046 - KEH 72.243
CT!(9) = 70.91 'KRK 11aug96 71.206 'KRK 2aug96 71.124 'KRK 7jul96 70.622 - KEH 70.838
CT!(10) = 71.6 'KRK 11aug96 70.207 'KRK 2aug96 71.685 'KRK 7jul96 71.276 - KEH 71.603

```

```

CTI!(1) = -273.15 'KRK 11aug96 -267.255
CTI!(2) = -273.15 'KRK 11aug96 -271.61
CTI!(3) = -273.15 'KRK 11aug96 -263.891
CTI!(4) = -273.15 'KRK 11aug96 -272.484
CTI!(5) = -273.15 'KRK 11aug96 -270.413
CTI!(6) = -273.15 'KRK 11aug96 -265.276
CTI!(7) = -273.15 'KRK 11aug96 -266.343
CTI!(8) = -273.15 'KRK 11aug96 -273.189
CTI!(9) = -273.15 'KRK 11aug96 -274.39
CTI!(10) = -273.15 'KRK 11aug96 -267.281

```

'CV1 = 4.39

CV1 = 3.5 'corrected from 4.39, 26 June 1996 KRK

CV2 = 10!

CP1 = 34.44

CP2 = 6.8822 'increased significant digits from 6.8, 07 JULY 1996 KRK

'Set logical channel numbers

```

Lchan1% = 1 'Logical channel number
Lchan2% = 2
Lchan3% = 3
Lchan4% = 4
Lchan5% = 5

```

IF Num% = 8 OR Num% = 10 THEN

Vloop:

IF StopVar% = 1 THEN EXIT SUB

LOCATE 1, 1

' CLS

J = J + 1

PRINT "VIEW-CPL Data Display"

PRINT

```

PRINT "J = "; J; " Hit CTRL-C to return to Main Menu"
n% = 1 'dummy parameter
CALL xaing(Lchan2%, d!(n%), Erstat%)
V!(1) = d!(1) * CV1
V!(2) = d!(2) * CV2
IF Num% = 8 THEN
    PRINT
    PRINT "Channel 8: Line Voltage ";
    PRINT USING "###.### V"; V!(1)
ELSE
    PRINT
    PRINT "Channel 10: Heater Current ";
    PRINT USING "###.### A"; V!(2)
END IF
PRINT
PRINT "erstat = "; Erstat%
SLEEP 1
GOTO Vloop
END IF

IF Num% = 12 OR Num% = 13 THEN
Ploop:
    IF StopVar% = 1 THEN EXIT SUB
    LOCATE 1, 1
    CLS
    J = J + 1
    PRINT "VIEW-CPL Data Display"
    PRINT
    PRINT "J = "; J; " Hit CTRL-C to return to Main Menu"
    n% = 1 'dummy parameter
    CALL xaing(Lchan3%, d!(n%), Erstat%)
    P!(1) = (d!(1) + 1) * 23.31
    P!(1) = (d!(1) + 1) * CP1
    P!(2) = (d!(2) + .00725) * CP2
    IF Num% = 12 THEN
        PRINT
        PRINT "Channel 12: Loop Pressure ";
        PRINT USING "###.### kPa"; P!(1)
    ELSE
        PRINT
        PRINT "Channel 13: Diff. Pressure Across Evap ";
        PRINT USING "###.### kPa"; P!(2)
    END IF
    PRINT
    PRINT "erstat = "; Erstat%
    SLEEP 1
    GOTO Ploop
END IF

IF Num% >= 14 AND Num% <= 23 THEN
Tloop:
    IF StopVar% = 1 THEN EXIT SUB
    LOCATE 1, 1

```

```

'   CLS
   J = J + 1
   PRINT "VIEW-CPL Data Display"
   PRINT
   PRINT "J = "; J; " Hit CTRL-C to return to Main Menu"
   n% = 1 'dummy parameter
   CALL xaing(Lchan4%, d!(n%), Erstat%)
   T!(Num% - 13) = d!(Num% - 13) * CT!(Num% - 13) + CTI!(Num% - 13)
   PRINT
   PRINT "Channel "; Num%; ": ";
   PRINT USING "###.### °C "; T!(Num% - 13)
   PRINT
   PRINT "erstat = "; Erstat%
   SLEEP 1
   GOTO Tloop
ELSEIF Num% = 60 THEN
'   PRINT "erstat"; erstat%
'   INPUT aa
TTloop:
   IF StopVar% = 1 THEN EXIT SUB
   LOCATE 1, 1
'   CLS
   J = J + 1
   PRINT "VIEW-CPL Data Display"
   PRINT
   PRINT "J = "; J; " Hit CTRL-C to return to Main Menu"
   CALL xain(Lchan5%, Tdas!, Erstat%)
   PRINT
   PRINT "Channel "; Num%; ": ";
   PRINT USING "###.### °C "; Tdas!
'   PRINT Tdas; " °C"
   PRINT
   PRINT "erstat = "; Erstat%
   SLEEP 1
   GOTO TTloop
END IF
END SUB

```

SUB das

DIM d!(10), V!(2), P!(2), T!(10), CT!(10), CTI!(10)

'Temp cal factors

'Temp. calibration factors based two points 15 AUG 1996 KRK

CT!(1) = 72.26 'KRK 11aug96 70.893 'KRK 2aug96 72.254 - KRK 7jul96 71.685 - KEH 72.123

CT!(2) = 72.66 'KRK 11aug96 72.292 'KRK 2aug96 72.727 'KRK 7jul96 72.307 - KEH 72.622

CT!(3) = 73.43 'KRK 11aug96 71.206 'KRK 2aug96 73.421 'KRK 7jul96 72.939 - KEH 73.346

CT!(4) = 73.3 'KRK 11aug96 73.139 'KRK 11aug96 73.139 'KRK 2aug96 73.153 'KRK 7jul96 72.674 - KEH 73.258

CT!(5) = 71.09 'KRK 11aug96 70.457 'KRK 2aug96 70.922 'KRK 7jul96 70.274 - KEH 70.913

CT!(6) = 73.8 'KRK 11aug96 71.917 'KRK 2aug96 73.746 'KRK 7jul96 73.314 - KEH 73.802

CT!(7) = 71.89 'KRK 11aug96 70.316 'KRK 2aug96 71.891 'KRK 7jul96 71.429 - KEH 71.862

CT!(8) = 72.81 'KRK 11aug96 72.820 'KRK 2aug96 72.993 'KRK 7jul96 72.046 - KEH 72.243

CTI!(9) = 70.91'KRK 11aug96 71.206 'KRK 2aug96 71.124 'KRK 7jul96 70.622 - KEH 70.838
 CTI!(10) = 71.6 'KRK 11aug96 70.207 'KRK 2aug96 71.685 'KRK 7jul96 71.276 - KEH 71.603

CTI!(1) = -273.15 'KRK 11aug96 -267.255
 CTI!(2) = -273.15 'KRK 11aug96 -271.61
 CTI!(3) = -273.15 'KRK 11aug96 -263.891
 CTI!(4) = -273.15 'KRK 11aug96 -272.484
 CTI!(5) = -273.15 'KRK 11aug96 -270.413
 CTI!(6) = -273.15 'KRK 11aug96 -265.276
 CTI!(7) = -273.15 'KRK 11aug96 -266.343
 CTI!(8) = -273.15 'KRK 11aug96 -273.189
 CTI!(9) = -273.15 'KRK 11aug96 -274.39
 CTI!(10) = -273.15'KRK 11aug96 -267.281

'CV1 = 4.39

CV1 = 3.5

CV2 = 10!

CP2 = 6.8822 'increased significant digits from 6.8, 07 JULY 1996 KRK

'Set logical channel numbers

Lchan1% = 1

Lchan2% = 2

Lchan3% = 3

Lchan4% = 4

Lchan5% = 5

'Sample voltages

n% = 1 'dummy parameter

CALL xaing(Lchan2%, d!(n%), Erstat%)

V!(1) = d!(1) * CV1

V!(2) = d!(2) * CV2

WATTS! = V!(1) * V!(2)

' PRINT #1, ttime; V!(1); WATTS!;

PRINT ttime

ts# = ttime

PUT 2, , ts#

PUT 2, , V!(1)

PUT 2, , WATTS!

'Sample pressures

CALL xaing(Lchan3%, d!(n%), Erstat%)

' P!(1) = (d!(1) - 1) * 23.31

P!(1) = (d!(1) + 1) * 34.44

P!(2) = (d!(2) + .00725) * CP2

' PRINT #1, P!(1); P!(2);

PUT 2, , P!(1)

PUT 2, , P!(2)

'Sample temps

CALL xaing(Lchan4%, d!(n%), Erstat%)

FOR i = 1 TO 10: T!(i) = d!(i) * CTI!(i) + CTI!(i): NEXT

' FOR i = 1 TO 10: PRINT #1, T!(i); : NEXT

FOR i = 1 TO 10: PUT 2, , T!(i): NEXT

CALL xain(Lchan5%, Tdas!, Erstat%)

```
' PRINT #1, Tdas!  
PUT 2, , Tdas!
```

```
END SUB
```

FUNCTION days (mon)

```
SELECT CASE mon  
CASE 1  
    days = 0  
'CASE 1, 3, 5, 7, 8, 10, 12  
CASE 2, 4, 6, 8, 9, 11  
    days = 31  
'CASE 2  
CASE 3  
    days = 28  
'CASE 4, 6, 9, 11  
CASE 5, 7, 10, 12  
    days = 30  
END SELECT  
END FUNCTION
```

SUB dirs (filen\$, Exist)

```
Exist = 0  
SHELL "dir " + filen$ + " > a:xyzdir.txt"  
SHELL "Type a:xyzdir.txt"  
OPEN "a:xyzdir.txt" FOR INPUT AS #10  
FOR i = 1 TO 5  
    LINE INPUT #10, a$  
NEXT  
IF EOF(10) THEN  
    CLOSE 10  
    EXIT SUB  
END IF  
LINE INPUT #10, a$  
CLOSE 10  
b$ = RTRIM$(MID$(a$, 1, 8))  
'PRINT "Here it is";b$  
C$ = "a:" + b$ + ".dat"  
IF UCASE$(C$) = UCASE$(filen$) THEN  
' PRINT "File exists"  
    Exist = 1  
' PRINT "Filen$"; filen$  
' PRINT "C$"; C$  
END IF  
END SUB
```

SUB logo (x, y, C)

```
LINE (x + 1, y + 1)-(x + 15, y + 50), C  
LINE (x + 15, y + 50)-(x + 29, y + 1), C  
  
LINE (x + 45, y + 1)-(x + 45, y + 50), C
```

```

LINE (x + 60, y + 1)-(x + 60, y + 50), C
LINE (x + 60, y + 1)-(x + 75, y + 1), C
LINE (x + 60, y + 25)-(x + 70, y + 25), C
LINE (x + 60, y + 50)-(x + 75, y + 50), C

LINE (x + 90, y + 1)-(x + 100, y + 50), C
LINE (x + 100, y + 50)-(x + 110, y + 1), C
LINE (x + 110, y + 1)-(x + 120, y + 50), C
LINE (x + 120, y + 50)-(x + 130, y + 1), C

LINE (x + 140, y + 25)-(x + 155, y + 25), C

CIRCLE (x + 195, y + 25), 25, C, 1.5, 4.8

LINE (x + 210, y + 1)-(x + 210, y + 50), C
CIRCLE (x + 220, y + 12), 11, C, 4.8, 1.5
LINE (x + 210, y + 1)-(x + 220, y + 1), C
LINE (x + 210, y + 23)-(x + 220, y + 23), C

LINE (x + 245, y + 1)-(x + 245, y + 50), C
LINE (x + 245, y + 50)-(x + 260, y + 50), C

LOCATE 20, 30
PRINT "Data Acquisition Program"
LOCATE 22, 36
PRINT "Version 1.98"
LOCATE 26, 25
PRINT "UNIVERSITY OF MARYLAND - COLLEGE PARK"
END SUB

```

SUB logo1

```

CALL logo(190, 150, 4)
CALL logo(191, 150, 4)
CALL logo(190, 151, 4)

LINE (170, 145)-(475, 215), 3, B
LINE (171, 144)-(476, 216), 3, B

CALL logo(191, 151, 1)
CALL logo(192, 152, 2)
CALL logo(193, 153, 9)
CALL logo(194, 154, 10)

CALL logo(195, 155, 4)
CALL logo(196, 155, 4)
CALL logo(195, 156, 4)

PRINT "Hit <ENTER> to continue"

END SUB

```

SUB nchan (store)

DIM d!(10), V!(2), P!(2), CT!(10), T!(10), CTI!(10)

CLS 0

StopVar% = 0

ON KEY(15) GOSUB ctrlc1

KEY(15) ON

ON KEY(16) GOSUB ctrlc1

KEY(16) ON

ON KEY(17) GOSUB ctrlc1

KEY(17) ON

ON KEY(18) GOSUB ctrlc1

KEY(18) ON

ts# = ttime

'Temp cal factors

'Temp. calibration factors based two points 15 AUG 1996 KRK

CT!(1) = 72.26 'KRK 11aug96 70.893 'KRK 2aug96 72.254 - KRK 7jul96 71.685 - KEH 72.123

CT!(2) = 72.66 'KRK 11aug96 72.292 'KRK 2aug96 72.727 'KRK 7jul96 72.307 - KEH 72.622

CT!(3) = 73.43 'KRK 11aug96 71.206 'KRK 2aug96 73.421 'KRK 7jul96 72.939 - KEH 73.346

CT!(4) = 73.3 'KRK 11aug96 73.139 'KRK 11aug96 73.139 'KRK 2aug96 73.153 'KRK 7jul96 72.674 - KEH 73.258

CT!(5) = 71.09 'KRK 11aug96 70.457 'KRK 2aug96 70.922 'KRK 7jul96 70.274 - KEH 70.913

CT!(6) = 73.8 'KRK 11aug96 71.917 'KRK 2aug96 73.746 'KRK 7jul96 73.314 - KEH 73.802

CT!(7) = 71.89 'KRK 11aug96 70.316 'KRK 2aug96 71.891 'KRK 7jul96 71.429 - KEH 71.862

CT!(8) = 72.81 'KRK 11aug96 72.820 'KRK 2aug96 72.993 'KRK 7jul96 72.046 - KEH 72.243

CT!(9) = 70.91 'KRK 11aug96 71.206 'KRK 2aug96 71.124 'KRK 7jul96 70.622 - KEH 70.838

CT!(10) = 71.6 'KRK 11aug96 70.207 'KRK 2aug96 71.685 'KRK 7jul96 71.276 - KEH 71.603

CTI!(1) = -273.15 'KRK 11aug96 -267.255

CTI!(2) = -273.15 'KRK 11aug96 -271.61

CTI!(3) = -273.15 'KRK 11aug96 -263.891

CTI!(4) = -273.15 'KRK 11aug96 -272.484

CTI!(5) = -273.15 'KRK 11aug96 -270.413

CTI!(6) = -273.15 'KRK 11aug96 -265.276

CTI!(7) = -273.15 'KRK 11aug96 -266.343

CTI!(8) = -273.15 'KRK 11aug96 -273.189

CTI!(9) = -273.15 'KRK 11aug96 -274.39

CTI!(10) = -273.15 'KRK 11aug96 -267.281

'CV1 = 4.39

CV1 = 3.5

CV2 = 10!

CP2 = 6.8822 'increased significant digits from 6.8, 07 JULY 1996 KRK

'Set logical channel numbers

Lchan1% = 1

Lchan2% = 2

Lchan3% = 3

```

Lchan4% = 4
Lchan5% = 5

Nloop:
IF StopVar% = 1 THEN EXIT SUB
'CLS 0
LOCATE 1, 1
J = J + 1
PRINT "VIEW-CPL Data Display "; DATE$; "    "; TIME$
PRINT
PRINT "J = "; J; "  Hit CTRL-C to return to Main Menu"
PRINT
'Read voltages
  n% = 1 'dummy parameter
  CALL xaing(Lchan2%, d!(n%), Erstat%)
  V!(1) = d!(1) * CV1
  V!(2) = d!(2) * CV2
  WATTS! = V!(1) * V!(2)
  PRINT "Channel 8 : "; : PRINT USING "###.### V"; V!(1);
  PRINT "      Line Voltage"
  PRINT "Channel 10 : "; : PRINT USING "###.### W"; WATTS!;
  PRINT "      Heater Power"
'Read pressures
  CALL xaing(Lchan3%, d!(n%), Erstat%)
  P!(1) = (d!(1) + 1) * 23.31
  P!(1) = (d!(1) + 1) * 34.44
  P!(2) = (d!(2) + .00725) * CP2
  PRINT "Channel 12 : "; : PRINT USING "###.### kPa"; P!(1);
  PRINT "      Loop Pressure"
  PRINT "Channel 13 : "; : PRINT USING "###.### kPa"; P!(2);
  PRINT "      Diff. Pressure Across Evap."
'Read temperatures
  CALL xaing(Lchan4%, d!(n%), Erstat%)
  PRINT "erstat"; erstat%
  FOR i = 1 TO 9
    PRINT "Channel "; i + 13; ": ";
    T!(i) = d!(i) * CT!(i) + CTI!(i)
    PRINT USING " ###.### °C    Temp. ## "; T!(i); i
  NEXT
  T!(10) = d!(10) * CT!(10) + CTI!(i)
  PRINT USING "Channel 23 : ###.### °C    Temp. 10"; T!(10)
'Read DAS board temp
  CALL xain(Lchan5%, Tdas!, Erstat%)
  PRINT "Channel 60 : ";
  PRINT USING "###.### °C    DAS Board Temp. "; Tdas!
  PRINT Tdas; " °C"

SLEEP 1

IF store = 1 THEN
  IF ttime - ts# > 4 THEN
    ts# = ttime
  PRINT #1, ttime; V!(1); WATTS!; P!(1); P!(2);

```

```

'   FOR i = 1 TO 10: PRINT #1, T!(i); : NEXT
'   PRINT #1, Tdas!
    ts# = ttime
    PUT 2, , ts#
    PUT 2, , V!(1)
    PUT 2, , WATTS!
    PUT 2, , P!(1)
    PUT 2, , P!(2)
    FOR i = 1 TO 10: PUT #2, , T!(i): NEXT
    PUT #2, , Tdas!
  END IF
END IF

```

```

IF Warn1$ = "Kolos" GOTO Nloop
FOR i = 1 TO 10

```

```

    IF T!(i) > 60 THEN CALL warn
NEXT
IF Tdas! > 60 THEN CALL warn

```

```

GOTO Nloop

```

```

END SUB

```

SUB plott (Tscale, store)

```

DIM V!(10), T!(10), P!(10), TT!(10), PP!(2), CT!(10), d!(10), CTI!(10)

```

```

ts# = ttime
StopVar% = 0
lregion = -1

```

```

CLS 2
SCREEN 12
LINE (1, 1)-(639, 479), 1, BF

```

```

ON KEY(15) GOSUB ctrlc1
KEY(15) ON
ON KEY(16) GOSUB ctrlc1
KEY(16) ON
ON KEY(17) GOSUB ctrlc1
KEY(17) ON
ON KEY(18) GOSUB ctrlc1
KEY(18) ON

```

```

'Temp cal factors

```

```

'Temp. calibration factors based two points 15 AUG 1996 KRK

```

```

CT!(1) = 72.26 'KRK 11aug96 70.893 'KRK 2aug96 72.254 - KRK 7jul96 71.685 - KEH 72.123
CT!(2) = 72.66 'KRK 11aug96 72.292 'KRK 2aug96 72.727 'KRK 7jul96 72.307 - KEH 72.622
CT!(3) = 73.43 'KRK 11aug96 71.206 'KRK 2aug96 73.421 'KRK 7jul96 72.939 - KEH 73.346
CT!(4) = 73.3 'KRK 11aug96 73.139 'KRK 11aug96 73.139 'KRK 2aug96 73.153 'KRK 7jul96
72.674 - KEH 73.258
CT!(5) = 71.09 'KRK 11aug96 70.457 'KRK 2aug96 70.922 'KRK 7jul96 70.274 - KEH 70.913

```

CTI(6) = 73.8'KRK 11aug96 71.917 'KRK 2aug96 73.746 'KRK 7jul96 73.314 - KEH 73.802
 CTI(7) = 71.89'KRK 11aug96 70.316 'KRK 2aug96 71.891 'KRK 7jul96 71.429 - KEH 71.862
 CTI(8) = 72.81 'KRK 11aug96 72.820 'KRK 2aug96 72.993 'KRK 7jul96 72.046 - KEH 72.243
 CTI(9) = 70.91'KRK 11aug96 71.206 'KRK 2aug96 71.124 'KRK 7jul96 70.622 - KEH 70.838
 CTI(10) = 71.6 'KRK 11aug96 70.207 'KRK 2aug96 71.685 'KRK 7jul96 71.276 - KEH 71.603

CTI(1) = -273.15 'KRK 11aug96 -267.255
 CTI(2) = -273.15 'KRK 11aug96 -271.61
 CTI(3) = -273.15 'KRK 11aug96 -263.891
 CTI(4) = -273.15 'KRK 11aug96 -272.484
 CTI(5) = -273.15 'KRK 11aug96 -270.413
 CTI(6) = -273.15 'KRK 11aug96 -265.276
 CTI(7) = -273.15 'KRK 11aug96 -266.343
 CTI(8) = -273.15 'KRK 11aug96 -273.189
 CTI(9) = -273.15 'KRK 11aug96 -274.39
 CTI(10) = -273.15'KRK 11aug96 -267.281

'CV1 = 4.39

CV1 = 3.5

CV2 = 10!

CP2 = 6.8822 'increased significant digits from 6.8, 07 JULY 1996 KRK

PRINT " VIEW-CPL Data Plot - "; DATE\$

Tinit# = ttime#

'PRINT tinit#

'INPUT a

LOCATE 25, 68

PRINT "Hit CRTL-C "

LOCATE 26, 68

PRINT "to exit to "

LOCATE 27, 68

PRINT "MAIN MENU"

'Set logical channel numbers

Lchan1% = 1

Lchan2% = 2

Lchan3% = 3

Lchan4% = 4

Lchan5% = 5

LINE (30, 40)-(30, 440), 3

LINE (30, 440)-(530, 440), 3

LINE (30, 300)-(530, 300), 3

LINE (30, 370)-(530, 370), 3

LINE (30, 40)-(530, 40), 3

LINE (530, 40)-(530, 440), 3

LINE (28, 105)-(32, 105), 3

LINE (28, 170)-(32, 170), 3

LINE (28, 235)-(32, 235), 3

```

LINE (533, 25)-(545, 25), 7
LINE (533, 40)-(545, 40), 10
LINE (533, 55)-(545, 55), 6
LINE (533, 70)-(545, 70), 4
LINE (533, 85)-(545, 85), 6
LINE (533, 100)-(545, 100), 4
LINE (533, 115)-(545, 115), 4
LINE (533, 133)-(545, 133), 7
LINE (533, 148)-(545, 148), 9
LINE (533, 165)-(545, 165), 10
LINE (533, 180)-(545, 180), 9

```

```

'FOR j = 1 TO 100
Mainloop:
IF StopVar% = 1 THEN EXIT SUB
Tnow# = ttime#

```

```

    n% = 1 'dummy parameter
    CALL xaing(Lchan2%, d!(n%), Erstat%)
    V!(1) = d!(1) * CV1
    V!(2) = d!(2) * CV2
    WATTS! = V!(1) * V!(2)
    CALL xaing(Lchan3%, d!(n%), Erstat%)
'   P!(1) = (d!(1) + 1) * 23.31
    P!(1) = (d!(1) + 1) * 34.44
    P!(2) = (d!(2) + .00725) * CP2
    CALL xaing(Lchan4%, d!(n%), Erstat%)
    CALL xain(Lchan5%, Tdas!, Erstat%)

```

```

FOR i = 1 TO 10: T!(i) = d!(i) * CT!(i) + CT!!(i): NEXT

```

```

'Expecting temps between 0-60°C
LOCATE 9, 1
PRINT "T(°C)"
LOCATE 3, 2: PRINT "60"
LOCATE 7, 2: PRINT "45"
LOCATE 11, 2: PRINT "30"
LOCATE 15, 2: PRINT "15"
LOCATE 19, 2: PRINT "0"

```

```

T1x% = 30 + (Tnow# - Tinit#) * 500 / Tscale

```

```

IF T1x% > 530 THEN
    Tinit# = Tnow#
    LINE (31, 439)-(130, 41), 1, BF
    LINE (125, 439)-(130, 41), 3, BF
    LINE (525, 439)-(529, 41), 1, BF
    LINE (525, 300)-(530, 300), 3, BF
    LINE (525, 370)-(530, 370), 3, BF
    LINE (31, 300)-(130, 300), 3, BF
    LINE (31, 370)-(130, 370), 3, BF

```



```

Iregion = 0
T1x% = 0
END IF
IF T1x% > 130 AND Iregion = 0 THEN
  LINE (131, 439)-(230, 41), 1, BF
  LINE (225, 439)-(230, 41), 3, BF
  LINE (125, 439)-(130, 41), 1, BF
  LINE (31, 300)-(230, 300), 3, BF
  LINE (31, 370)-(230, 370), 3, BF
  Iregion = 1
END IF
IF T1x% > 230 AND Iregion = 1 THEN
  LINE (231, 439)-(330, 41), 1, BF
  LINE (325, 439)-(330, 41), 3, BF
  LINE (225, 439)-(230, 41), 1, BF
  LINE (31, 300)-(330, 300), 3, BF
  LINE (31, 370)-(330, 370), 3, BF
  Iregion = 2
END IF
IF T1x% > 330 AND Iregion = 2 THEN
  LINE (331, 439)-(430, 41), 1, BF
  LINE (425, 439)-(430, 41), 3, BF
  LINE (325, 439)-(330, 41), 1, BF
  LINE (31, 300)-(430, 300), 3, BF
  LINE (31, 370)-(430, 370), 3, BF
  Iregion = 3
END IF
IF T1x% > 430 AND Iregion = 3 THEN
  LINE (431, 439)-(530, 41), 1, BF
  LINE (525, 439)-(530, 41), 3, BF
  LINE (425, 439)-(430, 41), 1, BF
  LINE (31, 300)-(530, 300), 3, BF
  LINE (31, 370)-(530, 370), 3, BF
  Iregion = 4
END IF

'Scaling over 260 pixels in the y direction
T1y% = 300 - 260 / 60 * (T!(1) - 0)
IF T1y% < 40 THEN T1y% = 40
IF T1y% > 300 THEN T1y% = 300
T2y% = 300 - 260 / 60 * (T!(2) - 0)
IF T2y% < 40 THEN T2y% = 40
IF T2y% > 300 THEN T2y% = 300
T3y% = 300 - 260 / 60 * (T!(3) - 0)
IF T3y% < 40 THEN T3y% = 40
IF T3y% > 300 THEN T3y% = 300
T4y% = 300 - 260 / 60 * (T!(4) - 0)
IF T4y% < 40 THEN T4y% = 40
IF T4y% > 300 THEN T4y% = 300
T5y% = 300 - 260 / 60 * (T!(5) - 0)
IF T5y% < 40 THEN T5y% = 40
IF T5y% > 300 THEN T5y% = 300
T6y% = 300 - 260 / 60 * (T!(6) - 0)

```

```

IF T6y% < 40 THEN T6y% = 40
IF T6y% > 300 THEN T6y% = 300
T7y% = 300 - 260 / 60 * (T!(7) - 0)
IF T7y% < 40 THEN T7y% = 40
IF T7y% > 300 THEN T7y% = 300
T8y% = 300 - 260 / 60 * (T!(8) - 0)
IF T8y% < 40 THEN T8y% = 40
IF T8y% > 300 THEN T8y% = 300
T9y% = 300 - 260 / 60 * (T!(9) - 0)
IF T9y% < 40 THEN T9y% = 40
IF T9y% > 300 THEN T9y% = 300
T10y% = 300 - 260 / 60 * (T!(10) - 0)
IF T10y% < 40 THEN T10y% = 40
IF T10y% > 300 THEN T10y% = 300
T11y% = 300 - 260 / 60 * (Tdas! - 0)
IF T11y% < 40 THEN T11y% = 40
IF T11y% > 300 THEN T11y% = 300

```

'Expecting pressures in the range of 0-15 kPa

```

LOCATE 21, 1
PRINT "P(kPa)"
LOCATE 2, 5: PRINT "Pres Scale:0-15 kPa"
'Scaling over 70 pixels in y direction
P1y% = 370 - 70 / 15 * P!(1)
IF P1y% < 300 THEN P1y% = 300
IF P1y% > 370 THEN P1y% = 370
P2y% = 370 - 70 / 15 * P!(2)
IF P2y% < 300 THEN P2y% = 300
IF P2y% > 370 THEN P2y% = 370

```

'Expecting voltages in the range 0-30 V

```

LOCATE 25, 1
PRINT "V,W"
LOCATE 2, 28: PRINT "Volt Scale:0-30 V, Power Scale:0-80 W"
V1y% = 440 - 70 / 30 * V!(1)
IF V1y% < 370 THEN V1y% = 370
IF V1y% > 440 THEN V1y% = 440
V2y% = 440 - 70 / 2 * V!(2)
IF V2y% < 370 THEN V2y% = 370
IF V2y% > 440 THEN V2y% = 440
WATTSy% = 440 - 70 / 80 * WATTS!
IF WATTSy% < 370 THEN WATTSy% = 370
IF WATTSy% > 440 THEN WATTSy% = 370

```

'Color codes 2 - Green

```

'      3 - Aqua
'      4 - Red (EVAPORATOR)
'      5 - Pink
'      6 - Orange(VAPOR LINE)
'      7 - White (RESERVOIR)
'      8 - Brown
'      9 - Grey (AIR, DAS BOARD)
'     10 - Green (LIQUID LINE)

```

```

PRESET (T1x%, T1y%), 7
  PRESET (T1x%, T2y%), 10
  PRESET (T1x%, T3y%), 6
  PRESET (T1x%, T4y%), 4
  PRESET (T1x%, T5y%), 6
  PRESET (T1x%, T6y%), 4
  PRESET (T1x%, T7y%), 4
  PRESET (T1x%, T8y%), 7
  PRESET (T1x%, T9y%), 9
  PRESET (T1x%, T10y%), 10
  PRESET (T1x%, T11y%), 9
  PRESET (T1x%, P1y%), 4
  PRESET (T1x%, P2y%), 10
  PRESET (T1x%, V1y%), 4
  PRESET (T1x%, WATTSy%), 10
SLEEP 1

```

```

LOCATE 1, 50
PRINT TIMES$
LOCATE 1, 68
PRINT "Temps (°C)"
LOCATE 2, 70
PRINT USING "1:###.#"; T!(1)
LOCATE 3, 70
PRINT USING "2:###.#"; T!(2)
LOCATE 4, 70
PRINT USING "3:###.#"; T!(3)
LOCATE 5, 70
PRINT USING "4:###.#"; T!(4)
LOCATE 6, 70
PRINT USING "5:###.#"; T!(5)
LOCATE 7, 70
PRINT USING "6:###.#"; T!(6)
LOCATE 8, 70
PRINT USING "7:###.#"; T!(7)
LOCATE 9, 70
PRINT USING "8:###.#"; T!(8)
LOCATE 10, 70
PRINT USING "9:###.#"; T!(9)
LOCATE 11, 70
PRINT USING "10:###.#"; T!(10)
LOCATE 12, 70
PRINT USING "Tdas: ##.#"; Tdas!

```

```

LOCATE 14, 68
PRINT "Pres(kPa)"
LOCATE 15, 68
PRINT USING "Pa: ###.#"; P!(1)
LOCATE 16, 68
PRINT USING "dP: ###.###"; P!(2)
LOCATE 18, 68
PRINT "Voltage (V)"
LOCATE 19, 68

```

```

PRINT USING "V1: ###.##"; V!(1)
LOCATE 21, 68
PRINT "Power (W)"
LOCATE 22, 68
PRINT USING "W : ###.##"; WATTS!

```

```

IF store = 1 THEN
  IF ttime - ts# > 4 THEN
    ts# = ttime
    PUT 2, , ts#
    PUT 2, , V!(1)
    PUT 2, , WATTS!
    PUT 2, , P!(1)
    PUT 2, , P!(2)
    FOR i = 1 TO 10: PUT #2, , T!(i): NEXT
    PUT 2, , Tdas!
  END IF
END IF

```

```

IF Warn1$ = "Kolos" GOTO Mainloop
FOR i = 1 TO 10
  IF T!(i) > 60 THEN CALL warn
NEXT
IF Tdas! > 60 THEN CALL warn
GOTO Mainloop

```

```

END SUB

```

SUB schem (store)

```

DIM d!(10), T!(10), V!(2), P!(2), CT!(10), CTI!(10)

```

```

ts# = ttime
StopVar% = 0

```

```

CLS 0

```

```

  ON KEY(15) GOSUB ctrlc1
  KEY(15) ON
  ON KEY(16) GOSUB ctrlc1
  KEY(16) ON
  ON KEY(17) GOSUB ctrlc1
  KEY(17) ON
  ON KEY(18) GOSUB ctrlc1
  KEY(18) ON

```

```

CLS 2
SCREEN 12
LINE (1, 1)-(639, 479), 1, BF

```

'Temp cal factors

'Temp. calibration factors based two points 15 AUG 1996 KRK

CT!(1) = 72.26 'KRK 11aug96 70.893 'KRK 2aug96 72.254 - KRK 7jul96 71.685 - KEH 72.123

CT!(2) = 72.66'KRK 11aug96 72.292 'KRK 2aug96 72.727 'KRK 7jul96 72.307 - KEH 72.622
 CT!(3) = 73.43'KRK 11aug96 71.206 'KRK 2aug96 73.421 'KRK 7jul96 72.939 - KEH 73.346
 CT!(4) = 73.3 'KRK 11aug96 73.139 'KRK 11aug96 73.139 'KRK 2aug96 73.153 'KRK 7jul96
 72.674 - KEH 73.258
 CT!(5) = 71.09'KRK 11aug96 70.457 'KRK 2aug96 70.922 'KRK 7jul96 70.274 - KEH 70.913
 CT!(6) = 73.8'KRK 11aug96 71.917 'KRK 2aug96 73.746 'KRK 7jul96 73.314 - KEH 73.802
 CT!(7) = 71.89'KRK 11aug96 70.316 'KRK 2aug96 71.891 'KRK 7jul96 71.429 - KEH 71.862
 CT!(8) = 72.81 'KRK 11aug96 72.820 'KRK 2aug96 72.993 'KRK 7jul96 72.046 - KEH 72.243
 CT!(9) = 70.91'KRK 11aug96 71.206 'KRK 2aug96 71.124 'KRK 7jul96 70.622 - KEH 70.838
 CT!(10) = 71.6 'KRK 11aug96 70.207 'KRK 2aug96 71.685 'KRK 7jul96 71.276 - KEH 71.603

CTI!(1) = -273.15 'KRK 11aug96 -267.255
 CTI!(2) = -273.15 'KRK 11aug96 -271.61
 CTI!(3) = -273.15 'KRK 11aug96 -263.891
 CTI!(4) = -273.15 'KRK 11aug96 -272.484
 CTI!(5) = -273.15 'KRK 11aug96 -270.413
 CTI!(6) = -273.15 'KRK 11aug96 -265.276
 CTI!(7) = -273.15 'KRK 11aug96 -266.343
 CTI!(8) = -273.15 'KRK 11aug96 -273.189
 CTI!(9) = -273.15 'KRK 11aug96 -274.39
 CTI!(10) = -273.15'KRK 11aug96 -267.281

'CV1 = 4.39

CV1 = 3.5

CV2 = 10!

CP2 = 6.8822 'increased significant digits from 6.8, 07 JULY 1996 KRK

PRINT "VIEW-CPL Data Display Schematic "; DATE\$

PRINT

PRINT "Hit CRTL-C to exit to MAIN MENU"

LINE (100, 50)-(500, 50), 3

LINE (500, 50)-(500, 100), 3

LINE (480, 100)-(520, 100), 3

LINE (480, 300)-(520, 300), 3

LINE (480, 100)-(480, 300), 3

LINE (520, 100)-(520, 300), 3

LINE (500, 300)-(500, 400), 3

LINE (500, 400)-(100, 400), 3

LINE (100, 50)-(100, 100), 3

LINE (80, 100)-(120, 100), 3

LINE (80, 300)-(120, 300), 3

LINE (80, 100)-(80, 300), 3

LINE (120, 100)-(120, 300), 3

LINE (100, 300)-(100, 400), 3

LINE (230, 100)-(270, 100), 3

LINE (230, 300)-(270, 300), 3

LINE (230, 100)-(230, 300), 3

LINE (270, 100)-(270, 300), 3

LINE (250, 300)-(250, 400), 3

Mainloops:

IF StopVar% = 1 THEN EXIT SUB

LOCATE 1, 50

PRINT TIME\$

'Set logical channel numbers

Lchan1% = 1

Lchan2% = 2

Lchan3% = 3

Lchan4% = 4

Lchan5% = 5

'Sample voltages

n% = 1 'dummy parameter

CALL xaing(Lchan2%, d!(n%), Erstat%)

V!(1) = d!(1) * CV1

V!(2) = d!(2) * CV2

WATTS! = V!(1) * V!(2)

'Sample pressure

CALL xaing(Lchan3%, d!(n%), Erstat%)

' P!(1) = (d!(1) + 1) * 23.31

P!(1) = (d!(1) + 1) * 34.44

P!(2) = (d!(2) + .00725) * CP2

'Sample temps

CALL xaing(Lchan4%, d!(n%), Erstat%)

CALL xain(Lchan5%, Tdas!, Erstat%)

FOR i = 1 TO 10: T!(i) = d!(i) * CT!(i) + CT!!(i): NEXT

LOCATE 14, 30

PRINT USING "8: ###.##°C"; T(8)

LOCATE 22, 29

PRINT USING "1: ###.##°C"; T!(1)

LOCATE 22, 60

PRINT USING "2: ###.##°C"; T!(2)

LOCATE 22, 10

PRINT USING "10: ###.##°C"; T!(10)

LOCATE 18, 10

PRINT USING "7: ###.##°C"; T!(7)

LOCATE 15, 10

PRINT USING "4: ###.##°C"; T!(4)

LOCATE 11, 14

PRINT USING "6: ###.##°C"; T!(6)

LOCATE 5, 10

PRINT USING "5: ###.##°C"; T!(5)

LOCATE 5, 60

PRINT USING "3: ###.##°C"; T!(3)

LOCATE 15, 65

PRINT USING "9: ###.##°C"; T!(9)

LOCATE 27, 10

PRINT USING "P: ###.# kPa"; P!(1)

```

LOCATE 28, 10
PRINT USING "dP: ###.## kPa"; P!(2)

LOCATE 27, 30
PRINT USING "Input Power Supply: ###.## V"; V!(1)
LOCATE 28, 30
PRINT USING "Heater Power: ###.## W"; WATTS!

LOCATE 1, 64
PRINT USING "Tdas = ###.##°C"; Tdas!

SLEEP 1

IF store = 1 THEN
  IF ttime - ts# > 4 THEN
    ts# = ttime
    PUT 2, , ts#
    PUT 2, , V!(1)
    PUT 2, , WATTS!
    PUT 2, , P!(1)
    PUT 2, , P!(2)
    FOR i = 1 TO 10: PUT #2, , T!(i): NEXT
    PUT 2, , Tdas!
  ' PRINT "Schem"
  END IF
END IF

IF Warn1$ = "Kolos" GOTO Mainloops
FOR i = 1 TO 10
  IF T!(i) > 60 THEN CALL warn
NEXT
IF Tdas! > 60 THEN CALL warn
GOTO Mainloops

END SUB

```

FUNCTION ttime#

```

yr = VAL(MID$(DATE$, 7, 4))
mon = VAL(MID$(DATE$, 4, 2))
day = VAL(MID$(DATE$, 1, 2))

hr = VAL(MID$(TIME$, 1, 2))
min = VAL(MID$(TIME$, 4, 2))
sec = VAL(MID$(TIME$, 7, 2))

FOR i = 1 TO mon
  dday = dday + days(i)
NEXT
dday = dday + day

'ttime# = yr * 31536000 + day * 86400 + hr * 3600 + min * 60 + sec

```

```
ttime# = yr * 31536000 + dday * 86400 + hr * 3600 + min * 60 + sec  
END FUNCTION
```

```
SUB warn  
CLS  
LOCATE 8, 1  
PRINT "*****"  
PRINT  
PRINT "A temperature sensor has registered a reading above 60°."  
PRINT  
PRINT "End the current test immediately and verify that power is"  
PRINT "removed from the evaporator heaters, and line heaters:"  
PRINT "  MH1-40W"  
PRINT "  MH2-25W"  
PRINT "  MH3-10W"  
PRINT "  LH1-LIQUID"  
PRINT "  LH2-VAPOR"  
PRINT "  LH3-LIQUID"  
PRINT "  LH4-VAPOR"  
PRINT  
PRINT "*****"  
INPUT "Press <CTRL> C then <ENTER> to continue"; Warn1$  
END SUB
```

H.4 VIEW-CPL data acquisition user's manual (NSTS21343 Annex3, 1996)

Version 1.84 (instructions are similar for Version 1.98)

8 May 1996

Written by Keith E. Herold and Kimberly R. Kolos

Center for Environmental Energy Engineering

College Park, Maryland

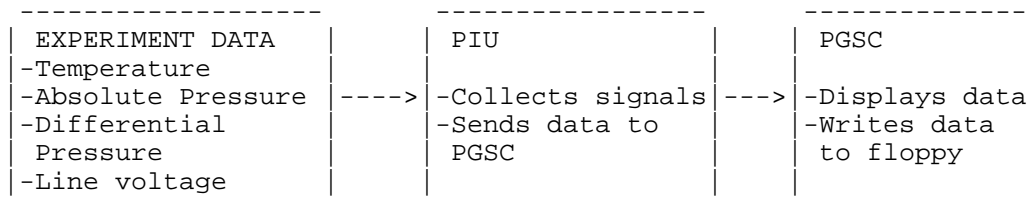
1. Introduction

The VIEW-CPL Data Acquisition Software (DAS) was written to support the VIEW-CPL middeck flight experiment which will fly on STS-80 in November 1996. The experiment is a modest budget student experiment and, as such, the experiment and the software are highly efficient. The software is strictly for data collection and has no control function. However, effective monitoring of the experiment will require that the astronaut observe the screen displays so that it is known whether or not the experiment is working. The choice of tests and the test sequence depends somewhat on observations taken during operation. Because of the minimum number of user options, the software is quite simple and straightforward.

The software is written in QuickBasic and is compiled into a stand-alone executable which runs under DOS. The software has several text mode screens and several graphic screens. All of these screens are designed to support the data acquisition objective.

2. PGSC Operations Flow

The PGSC communicates with the experiment via an RS-232 serial link. The software is designed to interrogate the DAS system periodically and to automatically store the data on floppy disk as well as to display it on the PGSC screen. There are several screen display modes available and the choice of which mode to use depends somewhat on user preference. The similarities and difference between these screen display modes are discussed in Section 3.



3. Windows, menus, and forms

The display screens of the VIEW-CPL DAS software are discussed in this section. The software was designed for simplicity and thus has a minimum number of screens. It should be noted that CTRL-C should be used to escape from any of the data acquisition modes and to return to the Main Menu from anywhere in the program.

3.1 Title Screen

The title screen has a graphic VIEW-CPL logo and the following text. The screen displays until the user hits a carriage return.

```
*****  
Data Acquisition Program  
Version 1.84  
UNIVERSITY OF MARYLAND - COLLEGE PARK  
*****
```

3.2 Main Menu

The Main Menu is shown below. It includes 7 choices. Each of these choices is described more fully in the following material.

```
*****  
Welcome to the VIEW-CPL DAS Program - MAIN MENU  
  
Options:  
1 - Sample one channel  
2 - Sample all channels  
3 - Data plot  
4 - CPL Schematic  
5 - Start/stop acquisition of data  
6 - Change plot defaults  
9 - Exit  
*****
```

3.2.1 Main Menu - Option 1

The first option under the Main Menu is for monitoring a single channel. This feature was useful during debugging and it is included here for completeness. It is not anticipated that this option would be used during the flight experiment.

When Option 1 is selected, the user is asked to specify which channel is to be monitored and the following screen appears:

```
*****
Which Channel do you want to sample:
8(9)  Differential line voltage
10(11) Differential line voltage
12    Absolute pressure transducer
13    Differential pressure transducer
14-23 Temperatures
Enter Channel number ? 8
*****
```

Once the user has specified a channel to monitor, a screen appears that prints out the value of the data channel along with information about the error variable obtained from the DAS system. For normal operation, the error variable will be zero. A counter, J, indicates the number of display iterations. The screen display for channel 8 is shown next.

```
*****
VIEW-CPL Data Display

J = 1  Hit CTRL-C to return to Main Menu

Channel 8:  0.000 V

erstat = 0
*****
```

3.2.2 Main Menu - Option 2

Main Menu Option 2 allows a simple text display of all data channels as shown next. This screen may be used during experiment monitoring (however, Options 3 and 4 are designed to provide even more information).

```
*****
VIEW-CPL Data Display

J = 1  Hit CTRL-C to return to Main Menu

Channel 8 :  0.000 V
Channel 10 : 0.000 V
Channel 12 : 0.000 kPa
Channel 13 : 0.000 kPa
```

```
Channel 14 : %-273.150 C
Channel 15 : %-273.150 C
Channel 16 : %-273.150 C
Channel 17 : %-273.150 C
Channel 18 : %-273.150 C
Channel 19 : %-273.150 C
Channel 20 : %-273.150 C
Channel 21 : %-273.150 C
Channel 22 : %-273.150 C
Channel 23 : %-273.150 C
*****
```

3.2.3 Main Menu - Option 3

Main Menu Option 3 provides a plot of all data channels versus time. In addition, a text display of the data is also provided. This screen is one of the primary tools provided for experiment monitoring. The user can select the time scale by utilizing Option 6 from the Main Menu. The essentially graphic screen is not reproduced here.

3.2.4 Main Menu - Option 4

Main Menu Option 4 provides a schematic of the experiment with the data superimposed close to the transducer location. This display allows the user to associate the data with the physical locations in the experiment. The essentially graphic screen is not reproduced here.

3.2.5 Main Menu - Option 5

Main Menu Option 5 allows the user to start and stop the recording of the data. The main function of this option is to set a variable in the program that tells it whether to store the data. When the storage variable is turned on, the user is then asked to specify a file name. Since DOS file names are limited to 8 characters, the user should enter a name of the form vcpl-xyy where xx is the test number and y is a code that allows a test to be restarted without over-writing a file. The Option 5 screen show up as:

```
*****
```

This option allows the user to stop or start
the process of storing data to the floppy disk

The program is not storing data currently

Enter one of the following:
(CR) to toggle the storage variable
1 - to set the storage variable to begin storing data
0 - to set the storage variable to end storing data
S - to exit option without changing anything
?

If the user toggles the storage variable or sets it to 1, then the software asks the user for the file name as

Please enter the filename

The filename is automatically assigned to the floppy drive and an extension of DAT is appended.

3.2.6 Main Menu - Option 6

Main Menu Option 6 allows the user to set the maximum time scale for the plot in Main Menu Option 3. This is set as a Main Menu Option so that the user does not have to reset it each time Option 3 is entered.

Plot Defaults

Current time scale is 600 sec

Enter new value of time scale in sec? 10

4. Messages

The only message issued to the crew through the DAS interface is a warning to end a test if a temperature of 60°C is measured by the DAS. The warning is displayed over the PGSC display with the following text.

A temperature sensor has registered a reading above 60°C,

End the current test immediately and verify that power is removed from the evaporator heaters, and line heaters:

MH1-40W
MH2-25W
MH3-10W
LH1-LIQUID
LH2-VAPOR
LH3-LIQUID
LH4-VAPOR

Hit (CR) to continue?

Directory Listing for VIEW-CPL DAS

Volume in drive B is VIEW-CPL

Volume Serial Number is 13EF-1643

Directory of B:\

COMMAND	COM	92,870	07-06-96	12:35p
CONFIGB	DAT	106	01-04-96	3:58p
80VCPL	EXE	103,800	07-07-96	5:09p
3 file(s)		196,776 bytes		
		965,120 bytes free		

APPENDIX I: EXPLANATION OF VOLTAGE DROPS IN DATA

The magnitude of the voltage drop measured during the flight testing is different than that measured during ground testing because different power supplies were used to provide power to the experiment. When VIEW-CPL was operated on power from the Space Shuttle fuel cells, a drop of 0.023 to 0.027 V was observed for every watt of power consumed by the experiment. Using the Acme Electric Corporation power supply (Model SPS/CPS 220) during ground testing, the typical drop was 0.0075 V/W.

The voltage drop measured from the Space Shuttle operations, along with some audio notes on the video tapes, were used to determine the exact times the astronauts executed steps in the procedures and turned on various electrical components. By checking the voltage difference between consecutive time periods and following along with the procedures, the order in which switches were toggled on and off was determined. Table I.1 contains the voltage drop observed when the corresponding component is switched on during flight testing.

A Keithley 197 Autoranging microvolt digital multimeter (DMM) was used to check the current draw of the VIEW-CPL components. Table I.2 provides the power consumed by each component as calculated by multiplying the voltage read from the VIEW-CPL data acquisition system and the current measured from the DMM, and subtracting the power consumed by having the Main PWR, 5VDC, and PIU switched on.

Table I.1 Voltage drop associated with powered components.

Component	Measured power on ground (W)	Power draw on shuttle during typical operation (W)	Observed Voltage drop (V)
TC2	5.0 to 5.4	4.6 + 0.084	0.12 to 0.16
TC1	22.7 to 27.5	20.6 + 0.084	0.40 to 0.45
Fans (3 @ 4.45W each)	11.5 to 12.7	13.35	0.36
TEC	24.5 to 23.8		0.44
MH1	46.9	40.4	0.9
MH2	29.1	25.7	0.5625
MH3	11.0	9.3	0.225

Table I.2 Measured voltage drop during ground operations.

			Total	Component
Switch	Volts	Amps	Power (W)	Power
MAIN PWR	29.9	0.014	0.4	0.4
5VDC	29.9	0.147	4.4	4.0
* PIU	29.9	0.304	9.1	4.7
* TEC	29.8	1.131	33.7	24.6
* FAN1	29.9	0.457	13.7	4.6
* FAN1, FAN2	29.9	0.587	17.5	8.4
* FAN1, FAN2, FAN3	29.8	0.734	21.9	12.8
* MH1	29.6	1.896	56.1	47.0
* MH2	29.7	1.288	38.3	29.2
* MH3	29.8	0.675	20.1	11.0
* TC1	29.8	1.070	31.8	22.7
* TC2	29.9	0.489	14.6	5.5
* LH1	29.9	0.427	12.8	3.7
* LH2	29.9	0.427	12.8	3.7
* LH3	29.9	0.426	12.7	3.6
* LH4	29.9	0.428	12.8	3.7

*indicates that the MAIN PWR, 5VDC, and PIU are switched ON.

The voltage drops and rises were measured from the data collected and

voltage changes above a threshold of 0.095V were printed to a file for assignment to component switching. When matched to the switching sequence in the procedures, the voltage changes give an excellent record of the sequence and timing of the manual switching controls. Beginning with the initial pressure prime, Astronaut Kent Rominger gave audio comments on the video tape detailing which components were turned on at various times. These comments were used to determine the magnitude of the voltage changes associated with various components.

Since the data acquisition system records the data every 5 seconds, there is the possibility of a data point being collected during the transient voltage change; if this happens, the voltage change reads lower than expected. When voltage changes are misleading or large same sign voltage changes occur back-to-back, taking the voltage change over two data points gives more accurate results.

Small temperature changes are observed as large power drawing components are turned on. A 0.1 K temperature drop in all temperatures is noted when the TEC is turned on; temperatures rise when the TEC is turned off (the TEC is powered from a DC/DC converter that is separated electrically from the other DC/DC converter supplying voltage to the temperature sensors). A 0.01 K temperature rise is observed in some of the temperatures when TC1 and TC2 are turned on. None of these variations have a major impact on the conclusions drawn from the VIEW-CPL temperature data.

APPENDIX J: INFORMATION ABOUT ON-ORBIT TESTING

Table J.1 Summary of on-orbit testing of VIEW-CPL on STS-80.

Test #	Test Title	Date performed	Start Time	Stop Time	MET start time	Previous Procedure
*	PRIME-1	11-20-1996	22:03:01	23:23:51	01/03:47	UNSTOW
1	S40-1	11-20-1996	00:00:40	01:46:49	01/05:23	PPRIME
2	S25-1	11-22-1996	02:34:36	04:06:52	01/08:00	COOL
3	S75-1	11-21-1996	01:33:33	02:29:40	02/05:38	STANDBY
4	S65-1	11-21-1996	02:35:52	02:54:03	02/06:40	COOL
5	S10-1	11-22-1996	21:15:52	22:32:01	04/01:20	STANDBY
6	S50-1	11-22-1996	23:22:58	23:53:16	04/03:27	COOL
7	GRAD-1	11-23-1996	01:36:59	02:13:57	04/05:41	COOL
8	SS25-1	11-23-1996	02:58:11	03:37:11	04/07:03	COOL
9	S40R-1	11-24-1996	04:07:39	05:05:17	05/08:12	STANDBY
10	S35-1	11-24-1996	05:45:25	06:38:48	05/09:50	COOL
11	LOW-1	11-25-1996	23:39:45	00:31:03	07/03:44	STANDBY
12	LOW-2	11-26-1996	00:31:52	01:10:48	07/04:36	COOL
13	JUMP-1	11-26-1996	01:48:32	02:25:57	07/05:53	COOL
14	SC-1	11-26-1996	03:20:35	03:57:42	07/07:25	COOL
15	CV-1	11-26-1996	04:56:12	05:34:11	07/09:01	COOL
16	SC-2	11-26-1996	06:16:52	06:55:08	07/10:21	COOL
*	PRIME-2	11-30-1996	03:17:52	04:27:17	11/07:22	UNSTOW
17	S25-2	11-30-1996	04:30:25	05:57:15	11/08:35	PPRIME
18	S40-2	11-30-1996	06:01:56	07:02:05	11/10:06	COOL
19	S35-2	11-30-1996	07:42:08	08:33:42	11/11:47	COOL

UNSTOW - removal from Middeck locker and set-up in the Space Shuttle

PPRIME - Pressure prime

COOL - Evaporator cooldown and pressure prime (25W on reservoir temperature controlled heaters)

STANDBY - Standby mode with minimal power (5W on reservoir temperature controlled heaters)

- In test #4 the large bubble is located in the same location of the small clustered bubbles that were observed in tests #2, #3, #5, and #6.
- In test #5, the large bubble is just to the left of the location of the small clustered bubbles.
- During test #6, a bubble begins at the vapor plug and expands to combine with the bubbles in the middle of the core. After test #6, the core is filled with liquid with only one small bubble at the vapor plug.
- The following tests #7, #8, #9, #10, #11, #12, and #13 all start with a mostly liquid core and only one vapor bubble at the vapor plug.
- During test #13, the core fills with liquid with small vapor bubble through-out the core.
- Test #14 begins with four small bubbles in the last half length of the core.
- Tests #15, #16, and #17 begin with all liquid in the core.
- Test #17 ends with a vapor bubble at the vapor plug.
- Test #18 begins with a vapor bubble at the vapor plug and ends with small vapor bubbles scattered through-out the core.
- Test #19 begins with mostly liquid and only a few very small vapor bubbles in the core.

Table J.3 Initial state of the evaporator prior to start-up for on-orbit testing.

Test #	Test Title	Initial state inside core	% core volume	Evaporator Temperature, T6 (°C)	Reservoir Temperature, T8 (°C)
1	S40-1	Nearly 50% of core is filled with vapor	47.6%	26.1	46.2
2	S25-1	Core is nearly liquid filled with only four very small bubbles located midway between inlet	0.2%	27.5	47.0
3	S75-1	Core is nearly liquid filled with only two very small bubbles located midway between inlet and vapor plug	0.1%	26.1	45.0
4	S65-1	Cylindrical bubble located in middle of core	18.9%	28.0	46.8
5	S10-1	Cylindrical bubble located in middle of core and several very small bubbles	14.8%	28.6	46.4
6	S50-1	Small cluster of four bubbles at half the length of the core	1.2%	30.3	47.3
7	GRAD-1	Small bubble at the vapor plug	1.6%	27.2	44.6
8	SS25-1	One bubble at the vapor plug	1.2%	32.1	47.0
9	S40R-1	One bubble at the vapor plug	1.2%	28.0	45.5
10	S35-1	One bubble at the vapor plug	1.2%	29.9	47.0
11	LOW-1	One bubble at the vapor plug	1.2%	28.4	39.9
12	LOW-2	One bubble at the vapor plug	1.2%	30.3	43.0
13	JUMP-1	One bubble at the vapor plug	1.2%	30.4	47.0
14	SC-1	Four small bubbles in last half of the core	1.1%	30.3	46.0
15	CV-1	All liquid	0.0%	31.8	47.4
16	SC-2	All liquid	0.0%	29.4	45.2
17	S25-2	All liquid	0.0%	26.3	47.5
18	S40-2	One bubble at the vapor plug with droplets of condensation on the lexan above the bubble	2.6%	32.3	47.7
19	S35-2	A few very small vapor bubbles in the core	0.1%	31.4	46.4

Table J.4 Location of initial bubble growth for on-orbit testing (continued on next page).

Test #	Test Title	Boiling location and description	Elapsed Time from heater power on (sec)		
			Boiling or Bubble Growth	All vapor in plenum	All vapor in core
1	S40-1	Heater on at 1096 sec elapsed time 1) Core bubble expanding 2) Boiling in vapor groove	1) 34 2) 149	***	224
2	S25-1	Heater on at 735 sec elapsed time 1) Slow boiling from the vapor grooves 2) Core bubbles fed with vapor through the wick	1) 152 2) 369	*	677
3	S75-1	Heater on at 731 sec elapsed time 1) Bubbles forming in core 2) Boiling in plenum	1) 171 2) 183	271	*
4	S65-1	Heater on at 457 sec elapsed time 1) Core bubble expanding 2) Boiling in vapor plenum	1) 57 2) 201	262	951
5	S10-1	Heater on at 505 sec elapsed time 1) No boiling in vapor grooves 2) Core bubble expands	1) * 2) 245	*	*
6	S50-1	Heater on at 538 sec elapsed time 1) Slow boiling in plenum 2) Core bubble growth	1) 203 2) 334	364	630
7	GRAD-1	Heater on at 982 sec elapsed time 1) Boiling in vapor groove 2) Core bubble at vapor plug growing	1) 219 2) 313	***	663
8	SS25-1	Heater on at 460 sec elapsed time 1) Boiling not observable in the plenum 2) Core bubbles fed with vapor through the wick	1) *** 2) 262	665	1495*
9	S40R-1	Heater on at 929 sec elapsed time 1) Vapor groove clearing 2) Core bubble growing	1) 263 2) 353	408	773
10	S35-1	Heater on at 495 sec elapsed time 1) Boiling in plenum and bubble expanding in core at the same time	1) 97	439	655
11	LOW-1	Heater on at 289 sec elapsed time 1) Boiling in plenum 2) Core bubble expanding	1) 30 2) 180	310	420

Table J.4 Location of initial bubble growth for on-orbit testing (continued from previous page).

Test #	Test Title	Boiling location and description	Elapsed Time from heater power on (sec)		
			Boiling or Bubble Growth	All vapor in plenum	All vapor in core
12	LOW-2	Heater on at 227 sec elapsed time 1) Slow boiling in plenum 2) Core bubble growing	1) 70 2) 187	412	571
13	JUMP-1	Heater on at 501 sec elapsed time 1) Plenum not visible 2) Bubble expands in core	1) *** 2) 47	***	397
14	SC-1	Heater on at 880 sec elapsed time 1) Boiling in vapor plenum 2) Core bubble expanding	1) 243 2) 305	332	336
15	CV-1	Heater on at 551 sec elapsed time 1) No observation of boiling in the plenum 2) Small bubbles forming in the core	1) * 2) 713	982	1100
16	SC-2	Heater on at 463 sec elapsed time No video available	***	***	***
17	S25-2	Heater on at 455 sec elapsed time 1) Slow boiling from the vapor grooves 2) Bubble forms and grows in core	1) 975 2) 1020	1126	1037
18	S40-2	Heater on at 859 sec elapsed time 1) Expanding core bubble 2) Slowly boiling in vapor groove	1) 115 2) 195	535	405
19	S35-2	Heater on at 496 sec elapsed time 1) Core bubble growing 2) Boiling in vapor plenum	1) 521 2) 622	***	567

* Never during start-up

** Never during testing

*** Not visible

Table J.5 Initial start-up period for on-orbit testing.

Test #	Test Title	Initial power (W)	Initial power Interval (sec)	Ending mode	Duration of initial start-up (sec)
1	S40-1	43.46	926	VAPOR AT CONDENSER	632
2	S25-1	28.31	727	HEATERS OFF All vapor in the evaporator core; no vapor at condenser; boiling began in the vapor grooves first	727
3	S75-1	77.60	470	Vapor at condenser	319
4	S65-1	67.56	551	Vapor at condenser	333
5	S10-1	10.91	2213	INCREASE POWER Bubble in core expanding; no vapor in grooves	2213
6	S50-1	53.34	696	Vapor at condenser	495
7	GRAD-1	37.23	670		
8	SS25-1	28.15	899		
9	S40R-1	42.71	792	Vapor at condenser	617
10	S35-1	37.96	709	Vapor at condenser	693
11	LOW-1	75.60	367	Vapor at condenser	280
12	LOW-2	36.84	662		
13	JUMP-1	51.30	623	Vapor at condenser	526
14	SC-1	65.74	398	Vapor at condenser	392
15	CV-1	26.99	1080	HEATERS OFF: Mostly vapor in the evaporator core; no vapor at condenser	1080
16	SC-2	65.16	457	Vapor at condenser	398
17	S25-2	27.55	1196		
18	S40-2	42.64	772	Vapor at condenser	594
19	S35-2	36.59	713	Vapor at condenser	733

BIBLIOGRAPHY

Antoniuk, D., 1995, "An Investigation of the CAPL Flight Experiment Thermal Anomalies", SAE Paper 951717, 25th International Conference on Environmental Systems, San Diego, CA, July 10-13.

Antoniuk D., and Pohner, J., 1994, "Deleterious Effects of Non-Condensable Gas During Capillary Pumped Loop Startup", SAE Paper 941408, SAE 1994 Transactions, Journal of Aerospace, Sec. 1, Vol. 101, pp. 1000-1010.

Arpaci, V.S., and Larsen, P.S., 1984, Convection Heat Transfer, Prentice-Hall, Inc., Englewood Cliffs, New Jersey.

ASHRAE, 1997, ASHRAE Handbook: Fundamentals, American Society of Heating, Refrigerating and Air Conditioning Engineers, Inc., Atlanta, GA.

Askeland, D.R., 1989. The Science and Engineering of Materials, 2nd ed., PWS-KENT Publ. Co., Boston, MA.

Azonix Corp., 1995. μMAC-1050 User's Manual, Azonix Corporation, Billerica, MA.

Borodkin, A., Sasin, V., Fedorov, V., 1995, "Experimental Investigation and Analytical Modelling of an Autooscillation Two-Phase Loop", Proceedings of the 9th International Heat Pipe Conference, May 1-5, Albuquerque, NM.

Braun, C.E., 1990, "Capillary Pumped Loop Supporting Technology", Thermal-Hydraulics for Space Power Propulsion, and Thermal Management System Design, Progress in Astronautics and Aeronautics, Vol. 122, pp. 131-139.

Buchko, M., 1992, "Test Results of Prototype Two-Phase Reservoirs for the CAPL Flight Experiment", AIAA Paper 92-2888, AIAA 27th Thermophysics Conference, Nashville, Tennessee, July 6-8.

Buchko, M., Kaylor, M., and Ottenstein, L., 1999, "Flight Test Results for the HST Orbital Systems Test (HOST) Capillary Pumped Loop Cooling System", SAE Paper 1999-01-1980, Proceedings of the International Conference on Environmental Systems, Denver, Colorado

Bugby, D.C., Nguyen, T., Krolczek, E.J., Ku, J., Swanson, T., Kobel, M., Baumann, J.E., and Cullimore, B.A., 1998, "Development and Testing of a Cryogenic Capillary Pumped Loop Flight Experiment", Paper No. ICECEC-98-288, 33rd Intersociety Engineering Conference on Energy Conversion, Colorado Springs, August 2-6.

Butler, D., and Hoang, T., 1991, "The Enhanced Capillary Pumped Loop Flight Experiment: A Prototype of the EOS Platform Thermal Control System", AIAA Paper 91-1377, AIAA 26th Thermophysics Conference, Honolulu, Hawaii, June 24-26.

Butler, D., Ottenstein, L., and Ku, J., 1996, "Design Evolution of the Capillary Pumped Loop (CAPL 2) Flight Experiment", SAE 961431, 26th International Conference on Environmental Systems, Monterey, California, pp. 1-13.

Callister W.D., Jr., 1991, Materials Science and Engineering: An Introduction, 2nd ed., John Wiley & Sons, Inc, New York.

Carey, V.P., 1992, Liquid-Vapor Phase-Change Phenomena: An Introduction to the Thermophysics of Vaporization and Condensation Processes in Heat Transfer Equipment, Hemisphere Publishing Corp, Washington.

Chalmers, D.R., Pustay, J.J., Moy, C.B., and Kroliczek, E.J., 1986, "Application of Capillary Pumped Loop Heat Transport Systems to Large Spacecraft", AIAA Paper No. 86-1295, AIAA/ASME 4th Joint Thermophysics and Heat Transfer Conference, Boston, Massachusetts, pp. 1-12.

Clayton, S.R., Martin, D., and Baumann, J., 1997, "Mars Surveyor Thermal Management Using a Fixed Conductance Capillary Pumped Loop", SAE Paper No. 972467.

Conner, W.C., Jr., Lane, A.M., and Hoffman, A.J., 1984, "Measurement of the Morphology of High Surface Area Solids: Hysteresis in Mercury Porosimetry" J. Colloid Interface Science, Vol. 100, No. 1, pp. 185-193.

Cullimore, B.A., 1991, "Start-up Transients in Capillary Pumped Loops", AIAA Paper 91-1374, AIAA 26th Thermophysics Conference.

Cullimore, B.A., 1993, "Capillary Pumped Loop Application Guide", SAE Paper 932156, Proceedings of the 23rd International Conference on Environmental Systems, Colorado Springs, July 12-15.

Delil, A.A.M., Heemskerk, J.F., Mastenbroek, O., Dubois, M., van Oost, S., Coesel, M.J.N., Supper, W., and Aceti, R., 1995, "TPX for In-Orbit Demonstration of Two-Phase Heat Transport Technology-Evaluation of Flight and Post-Flight Experiment Results", SAE Paper 951510, 25th International Conference on Environmental Systems, San Diego, CA, July 10-13, pp. 1-20.

Doebelin, E.O., 1966, Measurement systems, McGraw-Hill Book Co., New York.

Douglas, D., Ku, J., and Schlager L, 1997, "Investigation of the Starter Pump Purge Superheat Observed in the CAPL1 Flight", AIAA Paper No. 97-3871, 1997 National Heat Transfer Conference, Baltimore, Maryland, pp. 1-10

F-Chart Software, 1996, Finite Element Analysis version 6.88, F-Chart Software, Middleton, WI.

Fox, R.W. and A.T. McDonald, 1985, Introduction to Fluid Mechanics, John Wiley & Sons, New York.

Fredley, J.E., and Braun, C.E., 1988, "A Low Pressure Drop Heat Exchanger with Integral Heat Pipe", ASME National Heat Transfer Conference, Houston, July 24-27.

Goncharov, K.A., Barantsevich, V.L., Orlov, A.A., 2003, "Experience of Development of Heat Pipes Applied in Russian Spacecrafts", 5th Minsk International Seminar on Heat Pipes, Heat Pumps, Refrigerators, Minsk, Belarus, Sept 8-11.

Goncharov, K.A., Nikitkin, M.N., Golovin, O.A., Fershtater, Yu.G., Maidanik, Yu.F., Piukov, S.A., 1995, "Loop Heat Pipes in Thermal Control Systems for "OBZOR" Spacecraft", SAE Paper 951555, 25th International Conference on Environmental Systems, San Diego, California, July 10-13.

Haar, L., Gallagher, J.S., and Kell, G.S., 1984, NBS/NRC Steam Tables: Thermodynamic and Transport Properties and Computer Programs for Vapor and Liquid States of Water in SI Units, Hemisphere Publishing Corp., New York.

Hoang, T.T., 1997, "Development of an Advanced Capillary Pumped Loop", SAE Paper No. 972325.

Hoang, T., and Ku, J., 1995, "Theory of Hydrodynamic Stability for Capillary Pumped Loops", 1995 National Heat Transfer Conference, Portland, Oregon.

Hoang, T., and Ku, J., 1996, "Hydrodynamic Aspects of Capillary Pumped Loops", SAE Paper No. 961435.

Incropera, F.P., and DeWitt, D.P., 1990, Fundamental's of Heat and Mass Transfer, John Wiley & Sons, New York.

Kaylor, M., Krolczek, E., and Fredley, J., 1993, "CPHTS Hardware Development of the EOS AM SPacecraft Instruments", SAE Paper No. 932239 Proceedings of the 23rd International Conference on Environmental Systems, Colorado Springs, July 12-15.

Kays, W.M., and Crawford, M.E., 1980, Convective Heat and Mass Transfer, 2nd edition, McGraw-Hill, Inc., New York.

Kiper, A.M., 1991, "Investigation of thermal-fluid mechanical characteristics of the capillary pumped loop", NASA CR-188730, Goddard Space Flight Center, pp. 1-59.

Kiper, A.M., Swanson, T.D., and McIntosh, R., 1988, "Exploratory Study of Temperature Oscillations Related to Transient Operation of a Capillary Pumped Loop Heat Pipe", Proc. of National Heat Transfer Conference, ASME HTD-96, Vol. 1, pp. 353-359.

Kim, J.H., Cheung, K., Butler, D., Ku, J., Haught, E., Kroliczek, E.J., Cullimore, B., and Baumann, J., 1997, "The Capillary Pumped Loop III (CAPL 3) Flight Demonstration Description and Status", Proceedings of the Space Technology and Applications International Forum, CONF970115, Albuquerque, New Mexico.

KOA Speer Electronics, Inc., 1997. Private Communication with Quality/Product Engineer, Mr. Brian Piscitelli on May 19, 1997.

Kolos, K.R., and Herold, K.E., 1997, "Low Temperature and Fluid Oscillations in Capillary Pumped Loops", Proceedings of the National Heat Transfer Conference, Baltimore, Maryland, Aug 10-12, pp. 1-8.

Kolos, K.R., Herold, K.E., Kroliczek, E.J., and Swanson, T.D., 1996, "Flow Visualization in Capillary Pumped Loop Systems", Proceedings of Space Technology and Applications International Forum, Part II, American Institute of Physics, Woodbury, New York, pp. 731-738.

Kroliczek, E.J., and Cullimore, B., 1996, "Development of a Cryogenic Capillary Pumped Loop", Proceedings of Space Technology and Applications International Forum, Part II, American Institute of Physics, Woodbury, New York, pp. 745-752.

Ku, J., 1993, "Overview of Capillary Pumped Loop Technology", HTD-Vol. 236, Heat Pipes and Capillary Pumped Loops, American Society of Mechanical Engineers, New York, HTD-Vol 236, pp. 1-17.

Ku, J., 1994, "Thermodynamic Aspects of Capillary Pumped Loop Operation", AIAA Paper 94-2059, 6th AIAA/ASME Joint Thermophysics and Heat Transfer Conference, Colorado Springs, June 20-23, pp. 1-11.

Ku, J., 1997, "Recent Advances in Capillary Pumped Loop Technology", AIAA 97-3870, 1997 National Heat Transfer Conference, August 10-12, Baltimore, Maryland.

Ku, J., and Hoang, T.T., 1997, "Testing of a Capillary Pumped Loop with Multiple Parallel Starter Pumps", SAE Paper No. 972329.

Ku, J., Kroliczek, E.J., Butler, D., Schweickart, R.B, and McIntosh, R., 1986a, "Capillary Pumped Loop GAS and Hitchhiker Flight Experiments", AIAA/ASME 4th Joint Thermophysics and Heat Transfer Conference, June 2-4, Boston, Massachusetts.

Ku, J., Kroliczek, E.J., McCabe, M.E., and Benner, S.M., 1988, "A High Power Spacecraft Thermal Management System", AIAA Paper 88-2702, AIAA Thermophysics, Plasmadynamics and Lasers Conf., San Antonio, June 27-29, pp. 1-11.

Ku, J., Kroliczek, E.J., Taylor, W.J., and McIntosh, R., 1986b, "Functional and Performance Tests of Two Capillary Pumped Loop Engineering Models," American Institute of Aeronautics and Astronautics, Washington, D.C., AIAA Paper 86-1248, pp. 1-11.

Ku, J., Swanson, T.D., Herold, K., and Kolos, K., 1993, "Flow Visualization within a Capillary Evaporator", SAE Paper No. 932236, Proceedings of the 23rd International Conference on Environmental Systems, July 12-15.

Lin, W.K., Wong, P.L., Wong, P.C., Cheng, P.C., and Wang, H.P., 1994, "A Design and Performance Test of the Visualization within a Capillary Pumped Loop," *Il Nuovo Climento*, Vol. 16D, No. 7, pp. 883-893.

Maidanik, Yu.F., Vershinin, S.V., Kholodov, V.F., and Dolgirev, Yu.F., 1985, "Heat Transfer Apparatus," United States Patent No. 4515209.

McCuen, R.H., 1985. Statistical methods for engineers, Prentice-Hall, Englewood Cliffs, NJ.

McCuen, R.H., 1993. Microcomputer applications in statistical hydrology, Prentice-Hall, Englewood Cliffs, NJ.

McKetta, J.J., and Cunningham, W.A., (eds.), 1985, "Pore Size and Size Distribution", Encyclopedia of Chemical Processing and Design, Vol. 41, Marcel Dekker, Inc., New York, pp. 113-129.

McMaster-Carr Catalog (1996).

Minco Products Inc, 1994, "Minco Heaterstat Sensorless Temperature Controller", Bulletin CT198, Minneapolis, Minnesota.

Minkowycz, W.J., and Sparrow, E.M., 1966, "Condensation Heat Transfer in the Presence of Noncondensables, Interfacial Resistance, Superheating, Variable Properties, and Diffusion", International Journal of Heat and Mass Transfer, Vol. 9, pp. 1125-1144.

Moran, M.J., and Shapiro, H.N., 1988. Fundamentals of Engineering Thermodynamics, John Wiley & Sons, Inc., New York, NY.

NASA Johnson Space Center, 1992, "Protection of Payload Electrical Power Circuits", JSC Letter TA-92-038.

NASA Goddard Space Flight Center, 1995, "Goddard Space Flight Center Preferred Part List PPL-21", Greenbelt, Maryland.

NASA JSC, 1995, "Visualization In An Experimental Water Capillary Pumped Loop Payload: Payload Integration Plan", Doc. No. NSTS 21343, Houston, Texas.

NASA JSC, 1996a, "Middeck Interface Definition Document", Doc. No. NSTS 21000-IDD-MDK, Rev B, Houston, Texas.

NASA JSC, 1996b, "Orbiter Crew Compartment Interface Control Annex: Visualization in Experimental Water - Capillary Pumped Loop", Doc. No. NSTS 21343 ICA, Houston, Texas.

NASA JSC, 1996c, "Payload Operations Checklist", Doc. No. PL OPS/80/FIN A, Houston, Texas.

NASA Office of Safety and Mission Quality, 1991, "Flammability, Odor, Offgassing, and Compatibility Requirements and Test Procedures for Materials in Environments that Support Combustion", Doc. No. NHB 8060.1C, Washington, D.C.

NHB 8060.1C, 1991, "Flammability, Odor, Offgassing, and Compatibility Requirements and Test Procedures for Materials in Environments that Support Combustion", Office of Safety and Mission Quality, NASA.

Nguyen, T., 1996, "View CPL Evaporator Pump Bubble Test Results", Memorandum 7108-MEM-101, Swales and Associates, Inc., Beltsville, Maryland.

O'Connell, T., Hoang, T., and Ku, J., 1995, "Investigation of power turn down transients in CAPL-1 flight experiment", AIAA Paper No. 95-2067, Proceedings of the 30th AIAA Thermophysics Conference, June 19-22, San Diego, CA, pp. 1-7.

Ohadi, M.M., Dessiatoun, S.V., Mo, B., Kim, J., Cheung, K., and Didion, J., 1997, "An Experimental Feasibility Study on EHD-Assisted Capillary Pumped Loop (CPL)", Proceedings of the Space Technology and Applications International Forum (STAIF-97), AIP Conference Proceeding 387, New York.

OMEGA, 1987. "AD590 Temperature Sensor - Operator's Manual", Omega Engineering, Inc., Stamford, Connecticut.

Ottenstein, L., Butler, D., Ku, J., Cheung, K., Baldauff, R., and Hoang, T., 2003, "Flight Testing of the Capillary Pumped Loop 3 Experiment", Proceedings of the Space Technology and Applications International Forum - STAIF-2003, American Institute of Physics, pp 55-64.

Ottenstein, L., Ku, J., and Butler, D., 1993, "Testing of Flight Components for the Capillary Pumped Loop Flight Experiment", SAE paper 932235, 23rd International Conference on Environmental Systems, Colorado Springs, Colorado, July 12-15. pp. 1-12.

Ottenstein, L., and Nienberg, J., 1998, "Flight Testing of the Two-Phase Flow Flight Experiment", Proceedings of the 28th International Conference on Environmental Systems, Danvers, Mass., July 13-16.

Ozisik, M.N., 1980, Heat Conduction, John Wiley & Sons, New York, pp. 276.

Papst, 1994, "PAPST Equipment Fans", Catalog L600a GB/D, Papst Mechatronic Corp., Newport, Rhode Island 02840.

Pohner, J., and Antoniuk, D., 1991, "Recent Enhancements to Capillary Pumped Loop Systems", AIAA Paper 91-1375, AIAA 26th Thermophysics Conf., Honolulu, June 24-26, pp. 1-6.

Porex Technologies Corp., 1989, Informational leaflet ID # 645330789, Porex Technologies, Fairburn, GA.

Roukis, S.L., Kroliczek, E., and Hall, G., 1992, "COMET Service Module Thermal Control System Design Using a Capillary Pumped Loop", SAE Paper 921367, 22nd International Conference on Environmental Systems, Seattle, Washington, pp. 1338-1347.

Schweickart, R.B., Neiswanger, L., and Ku, J., 1987, "Verification of an Analytical Modeler for Capillary Pump Loop Thermal Control Systems", AIAA 22nd Thermophysics Conference, June 8-10, Honolulu, Hawaii.

Sinclair, I.R., 1990. Passive components: A user's guide, Heinemann Newnes,

Oxford.

Stenger, F.J., 1966, "Experimental Feasibility Study of Water-Filled Capillary-Pumped Heat Transfer Loop", NASA TM X-1310, NASA Lewis Research Center, Cleveland, Ohio, pp. 1-32.

Stephan, K., 1992. Heat transfer in condensation and boiling, Springer-Verlag, Berlin, pp. 150-152.

Swales Aerospace, 2004, "Swales Aerospace Brochure: Heat Pipe Extrusions", 5050 Powder Mill Road, Beltsville, Maryland, 20705, pg 5.

Szymanski, F., 1932, "Quelques solutions exactes des équations de l'hydrodynamicque de fluide visqueux dans le cas d'un tube cylindrique," J. Math. Pures Appl., (9), Vol. 11, pg 67-107.

University of Maryland, 1996, ""Verification Plan for VIEW-CPL", Report Number UMCP-PLAN-006-VCPL, College Park, Maryland.

Wang, C.Y and Tu, C.J., 1988, "Effects of non-condensable gas on laminar film condensation in a vertical tube", International Journal of Heat and Mass Transfer, Vol. 31, no. 11, pp. 2399-2345.

Webb, R.L., 1980, "Air-Side Heat Transfer in Finned Tube Heat Exchangers", Heat Transfer Engineering, Vol. 1, no. 3, pp. 33-49.

Wellard, C.L., 1960. Resistance and resistors. McGraw-Hill Book Company, Inc., New York.

White, F.M., 1991, Viscous Fluid Flow, 2nd edition, McGraw-Hill, Inc., New York.

White Sands Test Facility, 1996, Report #96-30149, "Offgas Test for VIEW-CPL Experiment", New Mexico.

Wolf, D.A., 2004, Personal Communication, March 10.

Wolf, D.A., Ernst, D.M., and Phillips, A.L., 1994, "Loop Heat Pipes - Their Performance and Potential", Proceedings of the 24th International Conference on Environmental Systems, Friedrichshafen, Germany, June 20-23.

Wrenn, K.R., 2002a, "Thermal Analysis for the INMARSAT-4 Loop Heat Pipes", SAI-RPT-391, Rev A, Swales Aerospace, Beltsville, Maryland.

Wrenn, K.R., 2002b, "End Item Data Package for INMARSAT-4 Loop Heat Pipes

Shipset #1, Upper Loop Heat Pipes”, SAI-EIDP-0887, Rev A, Swales Aerospace, Beltsville, Maryland.

Wrenn, K.R, Wolf, D.A, and Kroliczek, E.J., 2000, “Effect of Noncondensable Gas and Evaporator Mass on Loop Heat Pipe Performance”, SAE Paper 2000-01-2409.

YSI Precision Thermistor, 1995, “YSI 44006 Resistance 10,000 Ohms @ 25°C”, Document Item No.003240, Yellow Springs Instrument Co., Yellow Springs, Ohio.

Yun, S., Nguyen, T., and Kroliczek, E., 1996, “Design and Ambient Testing of the Flight Starter Pump Cold Plate”, SAE Paper 961433.